THE MESOZOIC GEOLOGY OF THE MT SOMERS AREA, CANTERBURY including Geochemical and Paleomagnetic studies of the Cretaceous calc-alkaline Mt Somers Volcanics.

With 3 separate maps

A thesis
submitted for the Degree
of
Doctor of Philosophy
in the
University of Canterbury

by

P. J. Oliver

University of Canterbury
April, 1977.

ABSTRACT

The Mesozoic rocks of the Mt Somers area consist of Triassic-Jurassic sedimentary rocks (Torlesse Supergroup) and Upper Cretaceous calc-alkaline volcanics (Mt Somers Volcanics). These are described, and geological maps presented.

The Torlesse rocks are subdivided into Mt Taylor Group, consisting of the Fingers Formation (Middle Triassic) and Pudding Hill Formation (?Upper Triassic), and the Clent Hills Group (?Middle to Upper Jurassic). Undifferentiated Torlesse rocks are also described which may range from Permian to Upper Jurassic in age.

The Fingers Formation is composed of a coarse white micaceous sandstone with "cannon-ball" concretions, and interbedded black siltstone. Key fossils are *Spiriferina* cf. *abichi* and *Daonella* sp. The age range is from Kaihikuan to Oretian.

The Pudding Hill Formation is alternating fine sandstone and siltstone of probable turbidite origin, and contains *Torlessia mackayi* both *in situ* and redeposited on bedding planes.

The Clent Hills Group consists of sandstone and siltstone with thick channel conglomerate and richly fossiliferous plant beds. Key fossils are *Inoceramus* sp. cf. *gracilis* and *Buchia* sp. Both shallow-marine and non-marine environments can be recognised. The age range is Temaikan to Puaroan.

The undifferentiated Torlesse rocks range from moderately indurated to highly indurated quartz-veined subschistose sandstone and siltstone.

The Clent Hills Group forms an arcuate structure and is overthrust by the Fingers Formation. A low angle thrust also occurs on the Winterslow Range where subschistose rocks overlie Clent Hills Group rocks. The age of the thrust faults is early Cretaceous and they are the result of the Rangitata Orogeny. The uplift that has resulted in the present block-faulted mountain ranges in the area, of both Torlesse rocks and Mt Somers Volcanics, commenced in the late Tertiary as part of the Kaikoura Orogeny, and active fault traces indicate the process is still continuing.

The Mt Somers Volcanics form a single complex with three main eruptive centres known: the Rangitata Gorge, Mt Somers, and the Malvern Hills. The following volcanic units are described: Somers Rhyolite, Barrosa Andesite, Hinds River Dacite, Surrey Hills Tuff, Alford Rhyolite, Graham Dolerite, Rata Peaks Rhyolite, Stew Point Andesite, and the rhyolite and andesite of the Malvern Hills.

The rhyolites generally contain sanidine, plagioclase and bipyramidal quartz phenocrysts, with minor biotite and almandine garnet. However the Alford Rhyolite contains no biotite or garnet, and the Rata Peaks Rhyolite contains no biotite, garnet or quartz. The dacite contains plagioclase with some hypersthene phenocrysts. Xenoliths of sedimentary origin enclosing almandine are ubiquitous. The andesites have a similar mineralogy to the dacite but contain no

garnet. The andesites and dacites have quartz-hypersthene normative compositions. Eruptions of the volcanics were predominantly flows from fissures. The rhyolites also form domes and ignimbrite sheets.

The major and trace element chemistry shows that the volcanics are genetically related, and they formed a continuous sequence of differentiated volcanics ranging from high-alumina basalt to silica-rich rhyolite. The only petrogenetic model consistent with the geochemistry is one involving fractional crystallisation of the high-Al basalt. The volcanics contain low and constant K/Rb and Ba/Rb ratios, high Rb/Sr and Ba/Rb ratios, high abundances of Th, Zr, Ba, Pb, Rb, and K, and low abundances of V and Sr, compared to other calc-alkaline volcanics. The depth of magma generation, above a westward dipping Benioff Zone, is calculated to be 190 km.

The K/Ar dates for the Mt Somers Volcanics give an upper limit of 98.1±0.7 Ma. The age range is probably less than 10 Ma. The eruptions coincide with the final stages of the Rangitata Orogeny.

Paleomagnetic measurements on the Mt Somers Volcanics give consistent normal magnetic directions with no reversals. The paleo-pole position determined is 57°S 174°E (α_{95} = 6.4; K = 11.9). This position is consistent with that from Cretaceous volcanics in Australia, when the opening of the Tasman Sea and movement along the Alpine Fault is allowed for. The results indicate no significant rotation of the eastern South-Island has occurred since the late Cretaceous.

ACKNOWLEDGEMENTS

Many people have assisted me in the course of this thesis. In particular I would like to thank the following:

Drs D. Shelley and J. Bradshaw - for advice and helpful criticism of the thesis.

Mr H. W. Keene - for helpful discussions and complete cooperation with the field mapping.

Dr D. Lewis - for stimulating discussions and encouragement.

Dr R. P. Suggate - for advice, help, and providing material assistance.

Dr G. W. Grindley and Professor P. Vella - for assistance with the paleomagnetic study.

Mr T. Mumme - for assistance with the paleomagnetic measurements, and computer processing of the data.

Dr C. Adams - for K/Ar age determinations.

Mr F. Schaffer - for technical assistance with XRF analyses.

Mr T. Crippon - for his enthusiastic help with field work in difficult terrain.

Mrs P. Riddolls and Mr B. W. Collins - for assistance with editing the manuscript.

Mr B. Scott - for the considerable amount of excellent photographic processing.

Dr J. Cole, Messrs E. Nicol and P. Luckman, and Drs P. and R. Kyle - for many helpful discussions.

Dr I. Speden, Professor J. D. Campbell and Dr D. Mildenhall - for fossil identifications.

Dr C. P. Wood - for helpful discussions of the geochemistry.

In addition I wish to acknowledge the helpful and stimulating discussions of the staff of Canterbury University Department of Geology, the N.Z. Geological Survey staff at Christchurch and Lower Hutt, and the staff at Victoria University of Wellington Department of Geology who also made their analytical facilities so freely available

I thank my wife, Olga, for typing the draft copy, and the many tables in this thesis, and Mrs R. J. Singleton who typed the final copy so expertly.

Many farmers generously allowed me to use their huts and shearers' quarters for which I am grateful. In particular I wish to thank Mr and Mrs J. Kerr for their hospitality.

This study was financially supported by a Post-Graduate Research Fellowship generously provided by the New Zealand Geological Survey, who also assisted materially with the mapping project.

CONTENTS

LIST OF TABLES

LIST OF FIGURES

Maps

0. INTRODUCTION

0.1 Location of Area Studied

The area studied for this thesis is that covered by the NZMS 1, Mt Somers (S81), 1:63,360 topographic map. The Mt Somers area is located in Mid-Canterbury, in the South Island of New Zealand. A locality map is shown in Figure 1.

The study of the Mt Somers Volcanics included the collection of samples from the Rakaia Gorge and Malvern Hills; areas which are north-east of the Mt Somers area.

The Mt Somers area consists of mountain ranges from 1,000 to 2,300 m in height above sea level that form part of the "Foothills" of the Southern Alps. The area is dissected by wide glacial-cut valleys that open out onto the Canterbury Plains in the south-east corner of the area.

0.2 Purpose and Scope of the Study

The geology of the Mt Somers area was jointly mapped by the author and H. W. Keene, as a condition of a Postgraduate Fellowship granted by the New Zealand Geological Survey. The mapping was subdivided into three parts. The Qua ternary geology was mapped by H. W. Keene; the Cretaceous Volcanics were mapped by the author; and the remaining Tertiary and Mesozoic Torlesse sediments were divided, for the purpose of mapping, between the author and H. W. Keene.

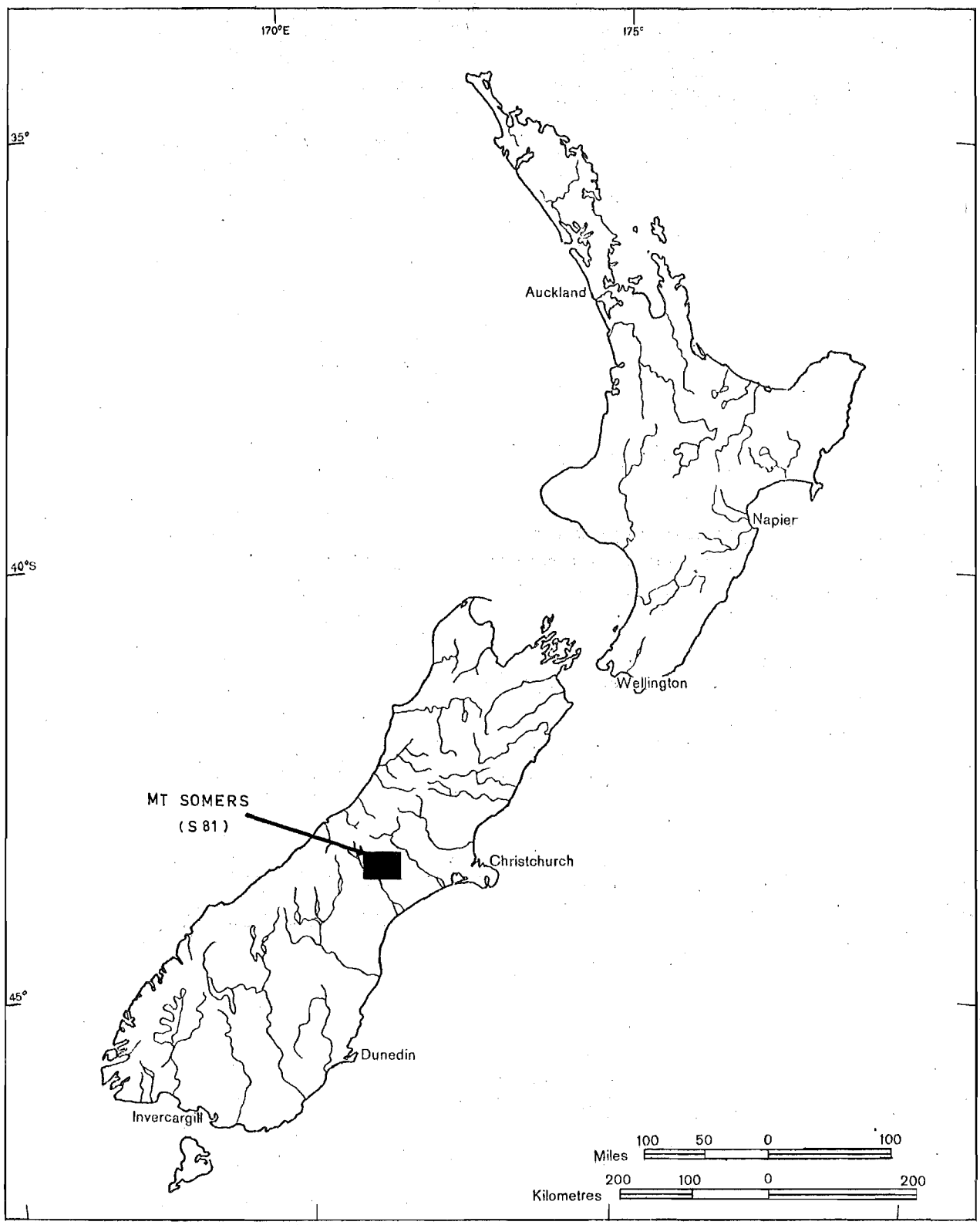

Figure 1. Locality map of the Mt Somers area (Sheet S81).

The primary aim of this study has been to produce a reliable geological map of the Mt Somers area. For this reason the studies of the geochemistry and petrology of the Mt Somers Volcanics have been made with the emphasis biased to the elucidation of the field work, by solving such problems as the genetic relationships, and eruptive forms.

The study of the Torlesse Supergroup has been confined to facts and observations that have arisen from the field mapping. As over half of the 1,100 km^2 area of the Mt Somers sheet (S81) is Torlesse rocks, a detailed study of the structures and composition of these rocks would require considerably more time to be spent on both field work and laboratory studies. From the field mapping of the Torlesse rocks, significant new information has arisen and this has therefore been described briefly in Part I of this thesis.

The paleomagnetic study of the Mt Somers Volcanics was made as a contribution to the theories of plate tectonics as they affect New Zealand. As the Cretaceous volcanics of Mt Somers are of "pre-drift" age, they are ideally suited to a study of the position of New Zealand relative to other Gondwanaland countries. This study is essentially a pilot study of Cretaceous paleomagnetism in New Zealand, and it is not intended to draw wide ranging conclusions from the results presented until further work has been carried out.

0.3 Previous Work

Intensive field studies of the Mt Somers area were carried out by Haast in 1861, 1864, and 1873 (Haast, 1877). During these expeditions Haast made a general geological map of the area that included the "melaphyre" (andesite and dacite) and "quartziferous porphyry" (rhyolite). Haast also collected plant fossils from Haast Stream and made a field study of the Torlesse rocks of the area. He located many of the Tertiary outcrops of the area. As a preliminary study his work was good, although detail in his mapping and his descriptions of structural forms and cross sections often relied heavily on interpolation of the field data.

A series of investigations into the geology of the Mt Somers area was made by S. H. Cox in 1876 and 1883 (Cox, 1877, 1884a). These contributed a little to the geological knowledge of the area, but his geological map (Cox, 1884a) was even more general and less accurate than that of Haast (Haast, 1877). Most of these early investigations were orientated to finding economic deposits of coal and limestone. An old coal mine near the Ashburton Gorge Rd (GR 813433*) has been worked since 1866, and is the third oldest coal mine in New Zealand (Speight, 1938, p75).

*Note - All grid references in this thesis refer to NZMS 1 Sheet S81, Mt Somers, 1:63,360, 2nd Edition 1970, unless otherwise specified.

Arber (1917) published a bulletin on the Mesozoic floras of New Zealand in which plant fossils from Haast Stream were formally described.

Speight (1938) published a Geological Memoir on the Mt Somers District. This memoir was the result of mapping of the foothills of the Southern Alps between the South Branch of the Hinds River and the North Branch of the Ashburton River. The Torlesse rocks were not differentiated and the Cretaceous volcanics were divided simply into andesite, rhyolite, and dolerite, with some rhyolite tuff also mapped. The text examined various possibilities to explain the geological complexity of the volcanics, but did not solve these problems, and is generally confusing for anyone not familiar with details of the area. Part of the problem in interpreting Speight's text lay in the absence of a grid co-ordinate system by which the location of rocks under discussion could be found. Speight's map of the Mt Somers district was the first reasonably accurate map with respect to lithological boundaries but little detailed geology was shown. Also Speight (1938) identified the rhyolite tuffs as a "First Stage Rhyolite" for all areas except the Alford Range where the same tuffs were incorporated with the "Second Stage Rhyolite" (Speight, 1938). The Creek shown as Chapman Creek on Speight's map is now known as Woolshed Creek, and the adjacent creek, shown as Quarry Creek on Speight's map, is now known as Chapman Creek. This important change of nomenclature has resulted in much confusion and should

be noted when reference is made to Speight's (1938) memoir.

The Mt Somers area is part of the 4 miles:1 inch geological map of Mt Cook, Sheet 20 (Gair 1967), in which the volcanics on the south bank of the Rangitata Gorge were shown as belonging to the Mt Somers Volcanics. Haast had first observed the andesite in this area in 1861 (Haast, 1879, p282).

Wood (1974) published a paper on the petrogenesis of the rhyolite from the Mt Somers and Mt Misery areas. This study was based on petrographic and electron microprobe analyses of the constituent minerals of the rhyolites. It included pressure and temperature determinations for the magmas.

PART I

TORLESSE SUPERGROUP

1.1 NOMENCLATURE

The term "Torlesse Supergroup" has been used for the "greywacke"-type sedimentary rocks, that make up the Southern Alps, by many authors (e.g. Campbell and Coombs, 1966; Warren, 1967; Bradshaw, 1972(a); Andrews, 1974; Spörli *et al.*, 1974). The Torlesse Supergroup has also been referred to as the "Torlesse Group" (Suggate, 1961; Campbell and Warren, 1965); the "Torlesse facies" (Fleming, 1970); and as the "Alpine facies" (Wellman, 1956).

Carter *et al* (1974) suggested a complete revision of the nomenclature of the sedimentary rocks of the New Zealand Geosyncline in which the "greywacke" rocks became the "Torlesse Zone" which, together with the "Haast Schist Zone" was included in the "Alpine Assemblage". The basis for this nomenclature was that the Torlesse and Haast Schist rocks are textural zones, and transgress stratigraphic subdivisions. This nomenclature is not in general use at present, and the use of the term Torlesse Supergroup is retained in this thesis.

The Torlesse rocks of the Mt Somers area (S81) have been subdivided into Groups and Formations. The range of lithologies is limited and the differences are subtle. The fossils provide the key to the recognition of these units, especially in isolated areas.

Two groups can be recognised; the Clent Hills Group and the Mt Taylor Group. An unfossiliferous undifferentiated formation also exists which may or may not belong to either

of these Groups. The Mt Taylor Group is subdivided into two formations: the Pudding Hill Formation, and the Fingers Formation.

1.2 MT TAYLOR GROUP

The Mt Taylor Group is named after Mt Taylor, the highest mountain in the Mt Somers area, and the main peak joining the Mt Somers Range to the Old Man Range.

The Mt Taylor Group contains two formations: the Fingers Formation and the Pudding Hill Formation. From the field relations, it is possible that these two formations are lateral equivalents.

1.2.1 Fingers Formation

This formation is named after the ridge on the Mt Somers Range known as "The Fingers".

1.2.1.1 Definition

The Fingers Formation consists of well bedded very coarse sandstone with minor interbedded fine sandstone to siltstone. The thickness is not less than 3,000 m in the area covered by the Mt Somers Sheet (S81). It is possible that the total thickness could be several times this value.

The sandstone is characteristically micaceous, white in colour, sparsely jointed, with spherical calcareous

concretions. The siltstone is dark grey to black and thin bedded, often convoluted, and characteristically contains thin calcareous concretionary beds or boudins.

A reference locality is designated west of Quaker Saddle near the upper reaches of the west branch of the Stour River, at GR 810557.

1.2.1.2 Distribution

This formation has only been mapped in the north-east quarter of the Mt Somers sheet (S81) (Maps 1,2). It makes up the Mt Somers Range from Trig TT to Mt Taylor, and the Old Man Range from Mt Taylor to Old Man Peak. The northern limit of this formation has not been mapped.

1.2.1.3 Lithology

The sandstone is very coarse grained, and white to light grey in colour. Finer dark green-grey to black sandstone is occasionally interbedded with the white variety, and in places the two types interdigitate. The white sandstone is generally unjointed and unveined, although individual beds were observed to be veined with quartz, with the adjacent beds unveined. The sandstone beds occasionally contain gritty bands of quartz, but true conglomerate was not found. A characteristic feature of this white sandstone is the presence of dark grey spherical calcareous concretions, which develops a ferruginous "rind" when

weathered. The size of these concretions is variable but they commonly occur in sizes of 10 to 20 cm diameter. No sandstone of the other Torlesse formations in the area were observed to have these "cannonball" concretions. The sandstone appears to lack graded bedding or internal structures.

The siltstone, that is interbedded with the sandstone just described, forms thin (1 to 10 cm) beds, graded from siltstone to very fine sandstone. It is dark grey to black and is generally sheared and contorted. Graded bedding and cross lamination are common. These features can be most readily observed on weathered surfaces. Thin calcareous concretionary beds are common within the siltstone and range in thickness from a few millimeters to 5 cm. Thicker concretionary bands are occasionally drawn out into boudinage structures.

The bedding planes between siltstone and sandstone are generally featureless, but flute casts are occasionally found.

At GR 854570 an intraformational conglomerate was found. This conglomerate consisted of angular clasts of grey siltstone with jagged ends, in a matrix of a gritty sandstone. When fresh it is very indurated and almost concretionary, but it weathers to a relatively friable state. The average size range of the siltstone clasts is very approximately 1.5 cm. The coarse sandstone matrix contained the calcareous remains of many macro-fossils (S81/f559). These weathered out to leave excellent casts of the fossils. This conglomerate bed could be traced south down the crest of the ridge for about 100 m.

1.2.1.4 Fossil Content

Only two fossil localities have been found in the Fingers Formation (S81/f558 and S81/f559, Table 1). Locality S81/f558 is in a bedded sequence of medium grained dark-grey sandstone, which locally interbeds with the coarser white sandstone more typical of the formation. An adjacent lithology is a conspicuously thick siltstone sequence which can be traced over Quaker Saddle into Saddle Creek. The fossiliferous sandstone yielded a variety of Bivalvia, Brachiopoda, Gastropoda, and Echinoidea (Table 1). The most significant of these for age determination are *Spiriferina* cf. *abichi* Oppel, and *Daonella* sp. The fossil assemblage was sparsely distributed within the sandstone beds. The only fossils found in the adjacent siltstone were echinoid fragments.

The fossil locality (S81/f559) is an intraformational conglomerate (described in section 1.2.1.3). This fossil locality contains a large number and variety of macrofauna including Bivalvia, Brachiopoda, Gastropoda, Bryozoa, and Echinoidea (Table 1). The structural relation of this locality to the beds of the main mass of the Old Man Range is not certain, as this conglomerate bed strikes at right angles to the main trend and appears to be part of a steeply plunging tight fold in a region of over-thrusting. Further field work would be necessary to clarify the structure in this area.

Figure 2 is a map of all the fossil localities in the Torlesse rocks.

TABLE 1: Details of new fossil localities in Torlesse rocks of the Mt Somers area (S81) found since 1973.

Fossil Record No.	Grid Reference (S81)	Locality	Collector	In Place	Fossils Identified	Fossils Identified By:	Age Range of Fossil Assemblage
S81/f546	937468	Stavely Stream	H.W.K.	No	Annulispora sp. Araucariacites cf. australis Cookson. Classopollis aff. torosus Couper. Cyathiidites minor Couper. Osmundacidites wellmanii Couper. Baculatisporites sp. Lycopodiumsporites cf. austroclavatidites (Cookson). Lycopodiumsporites sp. Leptolepidites sp. Podocarpidites cf. major Couper. Vitreisporites pallidus (Reissinger). Tancredia sp.	G.J.W. I.G.S.	Middle-Upper Jurassic Temaikan to Puaroan
S81/f547	662362	Harper Range	H.W.K.	Yes	Cladophlebis sp. Sphenopteris sp. ?Thinnfeldia sp.	D.C.M.	Jurassic
S81/f548	937468	Stavely Stream	H.W.K.	No	Cladophlebis sp. Plant fragments	D.C.M.	Jurassic
S81/f549	898487	Bowyers Stream	P.J.O.	Yes	Taeniopteris sp.	D.C.M.	Jurassic
S81/f550	909482	Pony Knob	P.J.O.	Yes	Cladophlebis sp. ?Matia sp. Taeniopteris sp. pteridosperm fragments	D.C.M.	Jurassic
S81/f551	885489	Bowyers Stream	P.J.O.	Yes	Taeniopteris sp. Tree stems and branches	D.C.M.	Jurassic
S81/f552	880543	Isaac Stream	H.W.K.	No	Entolium sp. Tancredia sp. ?Grammotodon sp. ?Cyrithinella sp.	I.G.S.	Ururoan - Puaruoan
S81/f553	880543	Isaac Stream	H.W.K.	Yes	Pachymya (p) sp. ?Certomya sp. Camptonectes sp. indet. ?Isocyprina sp. ?Serpula sp. echinoid spines plant stems and fragments.	I.G.S.	Arataouran to Puaroan
S81/f554	881542	Isaac Stream	H.W.K.	No	Inoceramus sp. cf. gracilis Holdhaus. ?Aoesta sp. ?Pacryomya sp.	I.G.S.	?Puaroan

TABLE 1 (continued)

Fossil Record No.	Grid Reference (S81)	Locality	Collector	In Place	Fossils Identified	Fossils Identified By:	Age Range of Fossil Assemblage
S81/f555	947508	Hutt Creek	D.G.T.	No	Tancredia sp. ?Pleuromya sp. ?Astarte sp. Rhynchonella sp.	I.G.S.	Temaikan to Puaroan
S81/f556	943502	Hutt Creek	D.G.T. Recollected: P.J.O, J.D.C, & J.G.B.	Yes	Pachymya sp. ?Ceratomya sp.	I.G.S.	?Aratauran to Puaroan
S81/f557	660350	Low Hills	P.J.O.	Yes	Tancredia sp. Coprolites	I.G.S.	Temaikan to Puaroan
S81/f558	809557	Mt.Somers Range	T.F.C. & P.J.O. Recollected: P.J.O, J.D.C, & J.G.B.	Yes	Spiriferina cf. abichi Oppel aff. Modiolus sp. ?aff. Tancredia sp. ?Myalinid gen. et sp. ind. Daonella sp. Nuculana cf. semicrenulata (Trechmann). Poroa cf. arata (Trechmann) ?Pleurotomariid Cidaroida aff. Dicyclocidaris sp. Minute Plant Fragments	J.D.C.	Kaihikuan (Landinian)
S81/f559	854570	Old Man Range	P.J.O'S, P.J.O, H.W.K. Recollected: P.J.O, J.D.C, N.F.	Yes	Pliculata sp. Ostreacean ?Liostrea sp. Pteriacean ?Caesianellidae Pteria sp. cf. spedeni Waterhouse. aff. Triaphorus sp. Limatulid. Trigonid. Patella cf. nelsonensis Trechmann. Poroa sp. Pleurotomaria aff. hokonuiensis Trechmann. Mentzeliopsis sp. Mentzelia sp. Rhynchonellacean Rhynchonella cf. zelandica (Trechmann). Athyris cf. wreyi (Suess). Spiriferina cf. abichi Oppel. Spiriferina sp. Lingula sp. ?Monotrypella sp. Cidaroida. Columals.	J.D.C.	Gore to Balfour (Kaihikuan to Oretian)

TABLE 1 (continued)

Fossil Record No.	Grid Reference (S81)	Locality	Collector	In Place	Fossils Identified	Fossils Identified By:	Age Range of Fossil Assemblage
S81/f560	948514	Hutt Creek	D.G.T.	No	Tancredia sp. ?Ceratomya sp.	I.G.S.	Temaikan to Puaroan
S81/f561	948512	Hutt Creek	D.G.T.	No	?Tancredia sp. ?Pachymya sp.	I.G.S.	?Temaikan to Puaroan
S81/f562	945505	Hutt Creek	D.G.T.	No	?Tancredia sp.	I.G.S.	Arataauran to Puaroan
S81/f563	947574	Nth Branch Ashburton River	H.W.K.	Yes	Torleesia mackayi (Bather)	H.W.K.	?Upper Triassic
S81/f564	977551	Campbells Stream	H.W.K.	No	Torlessia mackayi (Bather)	H.W.K.	?Upper Triassic
S81/f565	985598	Mt Bruce	P.J.O.	Yes	Torlessia mackayi (Bather)	P.J.O.	?Upper Triassic
S81/f556	910484	Pony Knob	P.J.O.	Yes	Taeniopteris sp. Leaf fragments and stems.	D.C.M.	Jurassic
S81/f567	897490	Mt Winterslow	P.J.O.	Yes	Large tree trunk, stems, branches, plant fragments.		
S81/f570	887479	Upper Bowyers Stream	P.J.O.	Yes	Plant stems, leaves & plant fragments		
S81/f571	891481	Upper Bowyers Stream	P.J.O.	Yes	Plant stems, leaves & plant fragments		
S81/f572	843493	Woolshed Creek	P.J.O.	Yes	Large tree trunk & stems, and plant fragments.		
S81/f573	862528	Peache Saddle	P.J.O.	Yes	Plant stems & fragments		
S81/f574	874527	Mt Winterslow	P.J.O.	Yes	?Buchia sp. indet. plant fragments.	I.G.S.	?Heterian to Puaroan
S81/f575	884527	Mt Winterslow	P.J.O.	Yes	Plant stems & leaf fragments		
S81/f576	894527	Mt Winterslow	P.J.O.	Yes	Plant stems & leaf fragments		
S81/f577	904530	Mt Winterslow	P.J.O.	Yes	Plant stems & leaf fragments		
S81/f578	930523	Diggers Creek	T.F.C.	Yes	Plant leaves & fragments		
S81/579	902534	Taylors Stream	T.F.C.	Yes	Plant stem & leaves		
S81/f580	913544	Taylors Stream	H.W.K.	No	Plant leaves, fragments, and stems. Cladophlebis sp.	P.J.O.	Jurassic
S81/f581	916546	Taylors Stream	H.W.K.	Yes	Tree trunks, stems & plant fragments.		

TABLE 1 (continued)

Fossil Record No.	Grid Reference (S81)	Locality	Collector	In Place	Fossils Identified	Fossils Identified By:	Age Range of Fossil Assemblage
S81/f582	920540	Taylors Stream	H.W.K.	Yes	Tree trunks, branches & stems.		
S81/f586	939520	Confluence Diggers Creek and Taylors Stream	P.J.O.	Yes	Torlessia mackayi (Bather)	P.J.O.	?Upper Triassic
S81/587	932519	Diggers Creek	P.J.O.	Yes	Large tree trunk.		
S81/588	948515	Taylors Stream	P.J.O.	Yes	Torlessia mackayi (Bather)	P.J.O.	?Upper Triassic
S81/589	949517	Grahams Creek	P.J.O.	Yes	Torlessia mackayi (Bather)	P.J.O.	?Upper Triassic
S81/f590	987519	North Branch Ashburton River	P.J.O.	Yes	Torlessia mackayi (Bather)	P.J.O.	?Upper Triassic
S81/f591	987517	North Branch Ashburton River	P.J.O.	Yes	Torlessia mackayi (Bather)	P.J.O.	?Upper Triassic

Initials used in table: J.G.B. = J.G.Begg; J.D.C. = J.D.Campbell; T.F.C. = T.F.Crippen; H.W.K. = H.W.Keene; D.C.M. = D.C.Mildenhall; P.J.O. = P.J.Oliver; P.J.O'S = P.J.O'Shea; D.G.T. = D.G.Titheridge. I.G.S. = I.G.Speden; G.J.W. = G.J.Wilson.

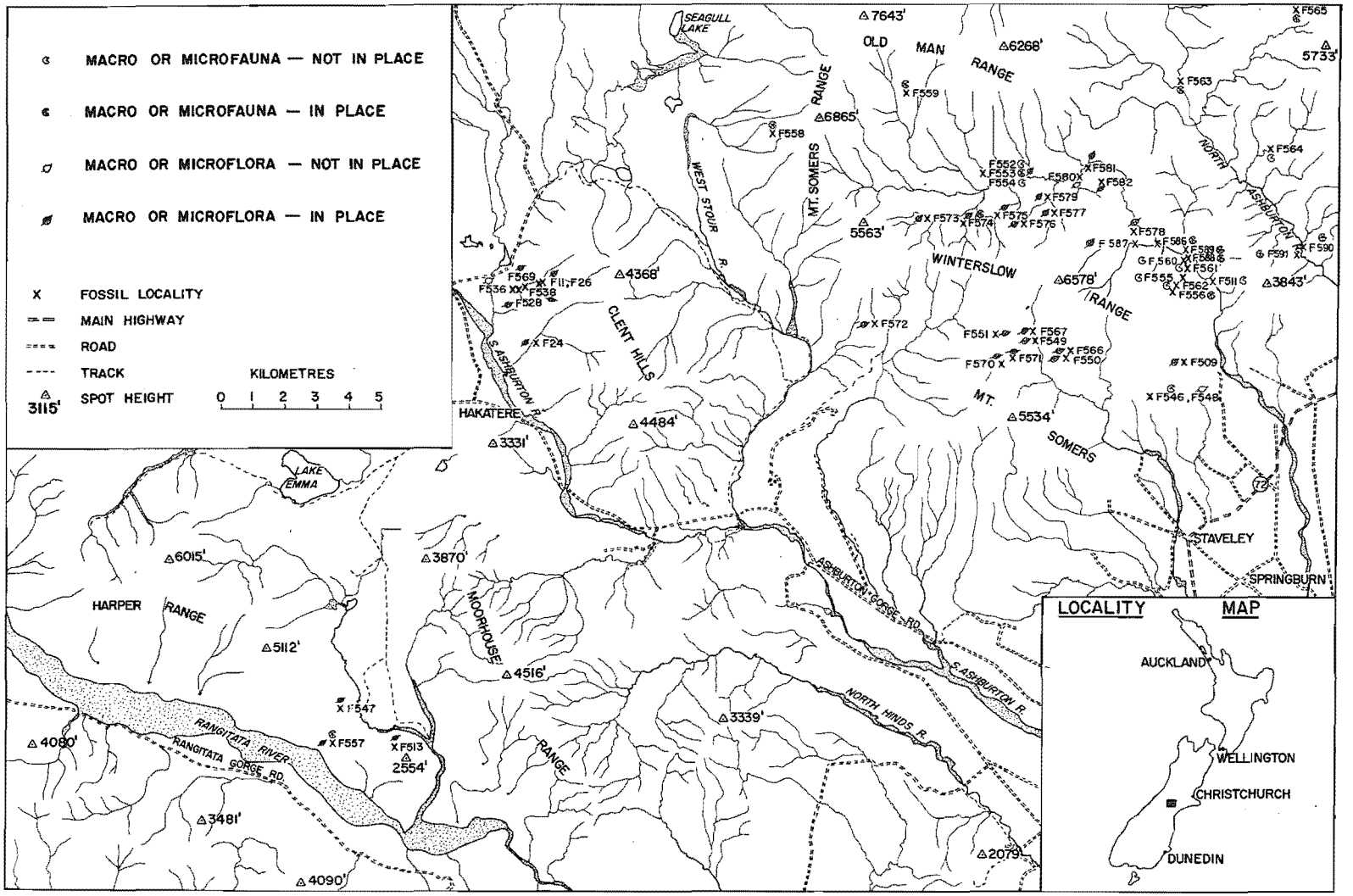

Figure 2. Fossil locality map of the Mt Somers area (S81).

1.2.1.5 Age

The age control for this formation is based solely on the fossils from two localities. Locality S81/f558 gave a definite Kaihikuan to Oretian age on the fossil assemblage collected (J. D. Campbell, pers. comm.).

1.2.1.6 Petrography and Metamorphism

The sandstone of the Fingers Formation is moderately sorted, medium to coarse grained feldsarenites. The major minerals are quartz, and alkali feldspar with minor plagioclase. These are sub-angular to sub-rounded in shape. The feldspar typically shows slight to moderate serucitisation. Minor minerals include muscovite, biotite and zircon. The muscovite is particularly characteristic as it occurs in large (up to 2 mm) flakes and can be easily seen in hand specimens. Lithic fragments are rare to absent. The petrography clearly indicates a granitic provenance.

The dark grey sandstone differs from the white sandstone in having a slightly smaller grain size (medium sand), is less sorted, and has more clay minerals in the matrix.

Metamorphism is slight with only occasional quartz veins which are confined to individual beds.

1.2.1.7 Depositional Environment

In general the thick, medium to coarse-grained sandstone beds are interbedded with graded siltstone beds

in a parallel-bedded sequence. In places, however, the siltstone beds are wedge-shaped and thicken to become the dominant lithology. The sandstone could thus be interpreted as a proximal facies and the siltstone as a distal facies, with overlap of these two dominant types.

There is no direct evidence for the depth of deposition of these beds, although indirect evidence from the fossils tends to favour a shallow to medium depth. Echinoid spines with delicate basal plates still attached (S81/f558) provide evidence of limited transport (J. D. Campbell pers. comm.), and the completely unsorted nature of the richly fossiliferous thin bed of intraformational conglomerate (S81/f559) is also consistent with limited transport. The taxonomic diversity of the fossil-fauna (Table 1) is consistent with a near shore origin of the fauna, which, if transported only a short distance, would imply a continental shelf environment of (re-)deposition.

The general sparcity of plant fragments does not rule out the possibility that the formation is of deltaic origin (Andrews, 1974) but this, together with the lateral extent and uniformity of the beds and the absence of channel deposits such as conglomerates, seems more consistent with a shelf environment.

1.2.1.8 Associated Volcanics

The only volcanic rocks associated with the Fingers Formation are basalts located near the summit of Trig TT

on the Mt Somers Range. The basalt outcrops possibly form a single dike but as exposure is not continuous, this is not certain.

The chemistry and petrography of this basalt is discussed in detail in Part II, from which it appears that it is associated with the Tertiary tholeiitic basalts of the area.

1.2.2 Pudding Hill Formation

This formation is named after the Pudding Hill Range which forms the north-eastern boundary of the Mt Somers area (S81).

1.2.2.1 Definition

The Pudding Hill Formation is a thin bedded sequence of medium to fine sandstone and siltstone. The sandstone is medium to dark grey, and the siltstone is dark grey. The total thickness of the formation is unknown as it extends to the west and north incorporating the Mt Hutt area which has not been mapped.

This thin bedded formation is characterised by the intermittent presence of the fossil *Torlessia mackayi*.

1.2.2.2 Distribution

In the Mt Somers area (S81) the distribution of the Pudding Hill Formation is confined to the Pudding Hill Range, Alford Range, and the area east of Taylors Stream in the region of Centre Spur (see Map 1). The formation is known to extend north and east of sheet S81.

1.2.2.3 Lithology

This formation is composed of a monotonous repetition of thin-bedded (usually less than 1 m) fine sandstone to medium grained siltstone. The beds are invariably graded and frequently show cross lamination in the upper part of the bed. The colour varies from light to dark grey. Induration is moderate.

Conglomerate beds are not common. Two types of conglomerate beds occur in close proximity in Grahams Creek near the confluence of Taylors Stream. One of these is composed of well-rounded sandstone and siltstone pebbles with scattered well-rounded dark-grey marble pebbles (which contain minute cubic pyrite crystals). The second type of conglomerate is composed only of pebbles of a light grey to fine siltstone. These vary in size from 2 to 30 cm, and are elongated in the direction of the bedding. This penecontemporaneous conglomerate was formed by a siltstone bed being torn apart.

Thick, coarse grained, white sandstone beds, containing occasional concretions, crop out in the North Branch of the

Ashburton River opposite the confluences of Waterfall Creek, Campbells Stream, and Five Mile Creek, with the Ashburton River.

The white sandstone is similar to that of the Fingers Formation, and may in fact belong to that formation. It is apparently interbedded with the *Torlessia*-bearing beds. No contact between the Fingers Formation and the Pudding Hill Formation has been found and if the two interdigitate then an age restraint can be applied to the *Torlessia*-bearing beds.

1.2.2.4 Fossil Content

The only fossils found in this formation are *Torlessia mackayi* (Table 1 and Figure 2). In one locality (S81/f563), in addition to the *Torlessia*, there were sinuous and bifurcating burrows 1 cm in diameter and up to 1 m in length (H. W. Keene, pers. comm.) found in the sandstone beds.

In the north eastern corner of the area, on the ridges extending down from Mt Bruce, the *Torlessia* always occur on bedding planes and stand out in relief on the exposed sandstone surface. Near the summit of Mt Bruce the shallow dipping beds have a weathered red oxidised coating on their exposed surface against which the white *Torlessia* are conspicuously contrasted. At this locality (S81/f565) the *Torlessia* tubes show a pronounced orientation in one direction, with fragments of tubes locally concentrated in clusters. They have obviously been redeposited on the

bedding planes. The specimens of *Torlessia* from this locality are commonly 2 to 3 cm in length (maximum 4 cm), and 1.5 to 2 mm in width (maximum 3 mm). Some are slightly tapered but most have parallel sides. They are always flattened and have a lateral indentation as a result of this. Some tubes are perpendicular to the bedding plane, and these are oval in shape with a wall thickness of less than 0.5 mm. Some specimens show fine lateral striations.

At all other *Torlessia* localities, notably those in the region of the confluence of Grahams Creek and Taylors Stream (Figure 2), the tubes are *in situ*, and generally are to be found randomly oriented within the upper 10 cm of each bed.

Marble pebbles present in a conglomerate were dissolved in an attempt to isolate conodonts, but none were found.

1.2.2.5 Age

Torlessia mackayi (Bather) (=*Terebellina mackayi* Ulrich) is generally thought to be restricted to the Upper Triassic (Campbell *et al.*, 1960; Campbell and Warren, 1965; Webby, 1967; Campbell and Campbell, 1970; Landis and Bishop, 1972). Both Stevens (1972) and Speden (1975) place *Torlessia mackayi* in the Late Triassic, with a possible age range of ?Oretian-Otamitian.

1.2.2.6 Petrography and Metamorphism

The beds of this formation are moderately to well sorted, and composed of quartz and feldspar with a clay matrix. Carbonaceous fragments are visible in thin section, and appear to contribute to the fine colour banding of the cross-bedding.

Some thick sandstone beds of this area are quartz veined, but these are conformable with beds with no quartz veins. Quartz/prehnite veins also occur in some sandstone beds. Calcite veining is confined to fault zones.

In general the beds of this formation are only slightly more indurated than those of the Clent Hills Group.

1.2.2.7 Depositional Environment

The thin alternating beds of this formation generally correspond to that of a turbidite sequence (Bouma, 1962) however this cannot be correlated with a specific environmental setting. The presence of *Torlessia* gives no indication of the depth, but probably indicates soft muddy sediment (Stevens, 1972).

1.2.2.8 Associated Volcanics

There are several dikes of tholeiitic basalt intruded into the beds of this formation (Map 1). Basalt boulders were observed in Ribbonwood Stream but their source was not found.

1.3 CLENT HILLS GROUP

The Clent Hills Group is named after the Clent Hills where plant fossils were first found in 1861 by Haast (1877).

1.3.1 Definition

The Clent Hills Group consists of the Jurassic sandstone, siltstone, and conglomerate of the Mt Somers area. The Group consists of at least two (unnamed) Formations, one is composed of what is probably a non-marine facies, and the other marine, with possible gradations between these.

The lithologies of this group are predominantly of dark-grey to green-grey sandstones. Conglomerate beds, predominantly composed of sandstone boulders, are a characteristic feature of this Group. Induration is only moderate, and veining is uncommon. An exception is a distinctive and characteristic zeolite-veined, blocky to crumbly, sandstone bed that can be recognised in the Group. This veined sandstone bed is in a sequence that includes red and green siltstone and thick conglomerate.

The siltstone, conglomerate, and less commonly the sandstone, of the Clent Hills Group characteristically contain plant fragments, leaves, stems, and large tree trunks.

A reference section at Haast Stream (GR 720505 to 732509) is typical of the "non-marine" facies and contains thick conglomerates. The siltstone beds typically contain

excellent impressions of plants preserved along laminae bedding planes. Large tree trunk remains are not uncommon.

Two localities at GR 880543 (Isaac Stream) and GR 943502 (Hutt Creek) are designated as reference localities for the marine facies. Both localities contain diverse fossil assemblages (Table 1). The Isaac Stream locality is adjacent to pale-red to pale-purplish sandstone, interbedded with black siltstone, which is characteristic of the Three Creeks area. The Hutt Creek locality consists of dark grey sandstone and siltstone beds containing marine fossils, and thick conglomerate beds with plant fragments.

1.3.2 Distribution

The rocks of this group occupy the valleys of Taylors Stream between the Old Man Range and the Winterslow Range; the Alford Range and Winterslow Range; and in the valley of Bowyers Stream between Mt Somers and Mt Winterslow. They also occur on the west side of the Clent Hills, and on the eastern side of the Harper Range facing Pudding Valley. The Low Hills are composed of rocks of this group. (Map 1).

1.3.2 Lithology

The Clent Hills Group is composed of alternating siltstone and sandstone beds with conglomerate beds and lenses.

The sandstone is predominantly light grey to grey-green but in the valley of Taylors Stream in the area around and south of Three Creeks Hutt (GR 876538) the sandstone has a distinctive red tinge and weathers to a characteristic purplish colour. Purple weathered sandstone was not observed at any other locality in the Mt Somers area, although a pinkish sandstone at GR 815518 may be related. Where sandstone beds are adjacent to siltstone beds rich in plant fossils they are often weathered brown by iron oxide, these mainly crop out between Diggers Creek and Hutt Creek (GR 927522 to 945503). The siltstone is typically dark-grey to black but red and green siltstone occurs in Diamond Creek, Bowyers Stream, Woolshed Creek, Weta Stream, and the East Branch Stour River.

The conglomerates are predominantly composed of Torlesse sandstone boulders and pebbles. The largest boulder observed was 1 m in diameter but generally the size range is 2 to 10 cm. The sandstone boulders are not quartz veined, and are in a coarse sandstone matrix (Figure 3). Occasional well-rounded pebbles of jasper, vein quartz, quartzite, aplitic granite, granodiorite, and rhyolite occur. The igneous pebbles appear to be most common in the conglomerates of Pudding Valley and in a conglomerate bed on the east side of Mt Alford.

Parallel to the major conglomerate bed in Bowyers Stream is a thin bed of conglomerate, composed only of small (less than 1 cm) well rounded pebbles of quartz and jasper. The two conglomerates are separated by a sandstone

Figure 3. Typical sandstone conglomerate of Clent Hills Group.

Figure 4. Large lithified tree trunk in Haast Stream.

bed of variable thickness but generally of less than 10 m.

The association of a crumbly zeolitised sandstone bed with red beds and conglomerate occurs in all the Jurassic beds except those at Haast Stream. The nature of this assemblage of lithologies is characteristic enough to suggest that the Jurassic beds of the Low Hills are the stratigraphic equivalent to those in the basins of Bowyers and Taylors Streams, and all three localities could once have been continuous.

On the north east side of Mt Alford, the beds in the vicinity of GR 986504 have the same appearance as those of the Clent Hills Group. A conglomerate at this locality, near to the contact with the rhyolite, could belong to the Jurassic beds, although the plant material normally associated with the Jurassic conglomerates was not present. A very characteristic pink to white chert bed at GR 983512 corresponds to exactly the same lithology on the west side of Mt Alford at GR 965495. To the north of this pink chert bed, at GR 983522, a moderately indurated dark grey siltstone, similar in character to the *Tancredia*-bearing Jurassic siltstones, was found which contained bulbous copralites similar to those in S81/f557. There is no definite proof that these beds are Jurassic at present, but if they are, then they unconformably overlie quartz veined sandstones and the thin bedded sequence containing *Torlessia* that has been found near the north branch of the Ashburton River.

1.3.4 Fossil Content

Until 1961 the only known fossil localities in the Clent Hills Group were the plant fossil localities found by Haast. (Fossil Record No. S81/f11; GS 405), and by Mackay (S81/f24; GS 546). Haast found these plant fossils in 1861 (Haast 1864, 1872, 1877) in Haast Stream (referred to in various publications as Fossil Gully; Plant Fossil Gully; Fern Gully; Haast Gully; or Haast Creek) which is a small tributary to the South Branch of the Ashburton River situated on the Western side of the Clent Hills. Haast also found similar plant fossils on the south-eastern slopes of the Harper Range (Haast, 1864, 1872). Mackay, in 1877, collected plant fossils from Potato Stream (a stream adjacent to Haast Stream).

Haast sent his fossil collection from Mt Somers to McCoy, in Melbourne, who assigned a Jurassic age to the plant beds (Haast, 1879, p268). Haast also sent collections to Ettingshausen, in Austria, who considered most of the species analogous to Triassic flora (Haast, 1887; Ettingshausen, 1887, 1891). Ten species were listed by Ettingshausen, which were subsequently discredited (Arber, 1917; Mildenhall, 1970) as invalid *nomina nuda*. Plant fossils from Haast Stream were listed by Hector (1886, 1870) but his lists are also regarded as invalid *nomina nuda* by the rules of the *International Code of Botanical Nomenclature*, (Mildenhall, 1970).

R. Speight and D. G. Lillie collected fossils from Haast Stream that were subsequently sent to, and described

by Arber (Speight, 1938, pl4). Townrow (1967) also collected and described specimens from this stream.

Arber (1917) was critical of previous records of the plant fossils and revised the list. Table 2 is a list of the plant fossils that occur in the Clent Hills that were described by Arber (1917) and which are currently accepted as valid species (Mildenhall, 1970). Table 2 also lists the ages given to these plant fossils by Mildenhall (1970). Arber had ascribed a Rhaetian (Otapirian) age to the Plant Beds (Arber, 1917).

TABLE 2. Fossils of the Clent Hills described by Arber (1917)

Fossil	Age Range
Phyllotheca minuta Arber	Otapirian (Rhaetian)
Thinnfeldia odontopteroides (Morris)	Upper Temaikan (Callovian)
T. sp. cf. *T. argentinica* (Geinitz)	Temaikan to Heterian (Callovian to Kimmeridgian)
Cladophlebis australis (Morris)	Jurassic to Cretaceous
Dictyophyllum acutilobum (Braun)	Otapirian to Temaikan (Rhaetian to Callovian)
Taeniopteris daintreei McCoy	Temaikan to Heterian (Callovian to Kimmeridgian)
T. thomsoniana (Arber)	Otapirian (Rhaetian)
Elatocladus conferta (Oldham & Morris)	Jurassic

Edwards (1934, p97) criticized Arber's use of *Taeniopteris daintreei* McCoy 1860, on the grounds that *T. spatulata* McCelland 1850 had priority; a situation of which Arber had been fully aware (Arber 1917, p46). Arber gave no explanation for his choice of name.

A podocarp from Haast Stream, *Mataia podocarpoides* (Ettingshausen) Townrow, was described by Townrow (1967) who considered this species the only conifer present in the Clent Hills plant beds, and therefore that Arber's (1917) identification of *Elatocladus conferta* was incorrect. Townrow assigned an age of Middle Jurassic to the plant beds.

A study of the genus *Taeniopteris* Brongniart, from Haast Stream, has been made by P. M. Blashke, who concluded that *T. daintreei* is not present in the Clent Hills plant beds (P. M. Blashke, pers. comm.).

The two problems associated with the plant fossils are firstly the confusion that exists over their identification and secondly the lack of precise time ranges for the species. The first problem is due mainly to the lack of preservation of cuticles caused by post-depositional oxidation of the plant beds. Only the plant beds of Haast Stream have been properly investigated and as there are now many other plant-bed localities in the area, a comprehensive paleobotanical study of all of them is needed to re-assess the situation. At the present time the extensive plant beds of the Mt Somers area provide no better age control than that they are of Jurassic age.

In 1961, G. Warren & D. R. Gregg collected (in place), in Picnic Creek, Alford Forest, a carbonaceous siltstone that yielded spores (S81/f509, L2808, GR 989480). Norris (*in* Campbell and Warren, 1965) identified the spores (listed in Table 3) and tentatively assigned it to the Lower Jurassic. According to G. J. Wilson (N.Z. Geological Survey Palynological Report, August, 1973) the palynological evidence itself suggests an age range from Lower Jurassic to Lower Cretaceous, and it is not known on what evidence Norris based his age determination of Lower Jurassic.

The geological mapping of the Mt Somers (S81) area (1972-4) by the author and Mr H. W. Keene has resulted in many new fossil localities being found. Details of fossil localities are given in Table 1.

Fossil localities in Table 1 belonging to the Clent Hills Group are: S81/f546-f557, f560-f562, f566-f567, f570-f582. Most of these are plant fossil localities many of which have unidentified tree trunks, stems, and leaf fragments.

The plant fossils are preserved along bedding planes, or parallel to fine lamellar planes within the siltstone beds. While most of the plant fossil leaves occur as individual leaves, some localities have particularly good preservation of complete frond specimens. Fronds of *Cladophlebis* sp. up to 0.3 m across were collected by the author from Haast Stream. Smaller branches of *Elatocladus conferta (Mataia podocarpoides)* also occur intact with their slender leaves

TABLE 3. Microflora present in Picnic Creek siltstone, (S81/f509) (after Campbell & Warren, 1965)

Microflora identified
Cyathidites minor Couper
Cyathidites australis Couper
Todisporites sp.
Osmundacdites wellmanii Couper
Lycopodiumsporites austroclavatidites (Cookson)
Callialasporites segmentatus (Balme)
Araucariacites australis Cookson
Monosulcites aff. minimus Cookson
Ginkgocycadophytus nitidus (Balme)
Vitreisporites pallidus (Reissinger)
Classopollis reclusus (Thiergart)

still attached, in Haast Stream beds. *Taeniopteris* sp. invariably occur as individual leaf impressions. The plant beds of Haast Stream have in general only one species of macroflora to a bed or bedded sequence, and therefore sampling throughout the exposed section is necessary to obtain a complete representative sample of all species. The plant fossils show excellent structural impressions but their organic matter has been carbonised. Small seams of bituminous grade "coal" are occasionally interbedded with the plant beds in Haast Stream and in exposures on the Winterslow track (GR 954497). Speight (1938, p18) reported that a 15 cm seam of coal in the Torlesse rocks

in Picnic Creek was used as fuel for the nearby Winterslow Homestead. A search did not reveal this seam, although carbonaceous seams like those on the Winterslow track are to be found in the streams along the eastern flank of Mt Winterslow.

Fossil locality S81/f546 contained the bivalve *Tancredia* sp. and a pollen assemblage (Table 1). The nearby locality S81/f509 contained many pollens in common with S81/f546.

The lithology of the Torlesse rocks near S81/f546 is of carbonaceous siltstones and sandstones with occasional thin coal bands and thin beds of pebble conglomerates. The nature of the thick bush at this locality prevents tracing the beds for any distance but they appear to be similar to those in Hutt Creek which have a varied macroflora assemblage (S81/f555, f556, f560-f562) which includes the same species (undescribed) of *Tancredia* as in S81/f546.

The plant beds of Haast Stream have not been found to contain either spores or pollen, or macrofauna.

The bivalve *Tancredia* sp. was found in the Low Hills (S81/f557) where it is again associated with carbonaceous sandstones and thick conglomerate beds similar to those in Hutt Creek. *Tancredia* sp. is always found in a well sorted dark grey, non-calcareous, coarse siltstone of moderate induration. It is frequently accompanied by bulbous coprolites, which are sometimes associated with a yellow sulphurous mineral (possibly jarosite).

The macrofauna fossil localities of Isaac Stream (S81/f552-f554, Table 1) yield a diverse fauna which included *Inoceramus* sp. cf. *gracilis* Holdhaus, which indicates the probable age of the beds is Puaroan (I. G. Speden, pers. comm.). On the south side of the Taylor Stream Valley, opposite to Isaac Stream, a specimen of *Buchia* sp. was found (S81/f574). Although the specimen was not well preserved, I. G. Speden (pers. comm.) considered the specimen had similarities to the *plicata-hochstetteri* species group, and if this is correct then a Puaroan age is also indicated. The specimen of *Buchia* was found incorporated into a flute cast on a bedding plane, together with many other flute casts some of which had transverse ridges crossing them indicating that they too may have formed by eddy erosion around shells lying on the bottom. The matrix of S81/f574 was a coarse sandstone with many fragments of carbonised plant material.

The conglomerate associated with the Clent Hills Group contain lenses of sandstone rich in plant remains. These conglomerates also contain large tree trunks up to 1 m in diameter which have been lithified by infilling of sandstone, or have been carbonised together with calcite infilling cracks formed in the trunks. An excellent specimen of an infilled tree trunk crops out in Haast Stream (Figure 4). Large carbonised and calcified tree trunks with excellent preservation of internal structure are found in Diggers Creek and in the conglomerates of Bowyers Stream valley, with smaller tree trunks and branches being found in most of the other occurrences of the Clent Hills Group conglomerates.

1.3.5 Age

This group unconformably underlies the Mt Somers Volcanics which have been dated (section 2.19) as Turonian to Albian.

The plant fossils indicate only a Jurassic age and at this stage no importance can be placed on them other than their use as indicators of the presence of Clent Hills Group sediments.

The best indicators of age are the *Inoceramus* and *Buchia* neither of which have positive species determinations, but when taken together, and with the other macrofauna and microflora, provide strong evidence for a Puraroan age for at least some of the beds of this group. In general the Clent Hills Group can be assigned an age range of Temaikan to Puaroan.

1.3.6 Petrography and Metamorphism

The sandstones of the Clent Hills Group are typically poorly to moderately sorted, medium-grained, feldsarenites (using the classification of Folk *et al.*, 1970) with subangular to subrounded quartz and alkali feldspar with occasional plagioclase. Minor mineral phases present include muscovite, biotite, and chlorite. Carbonised plant fragments are ubiquitous. The grains of feldspar are commonly sericitised and are sometimes difficult to distinguish from the very fine siltstone grains that are often present. Most of the sandstones examined were feldsarenites but lithic-feldsarenites were also represented.

The siltstones of this group are poorly to moderately sorted, fine to medium feldsarenites. The feldspars generally show sericitisation. Carbonaceous material was present in all samples examined.

Metamorphism of these rocks is very slight with only rare, very fine, quartz veins. Adjacent to the main conglomerate beds in this formation is a thick sandstone bed that is entirely fractured with a very fine network of zeolite veins, giving the outcrop a characteristic blocky to crumbly texture, with a white powdery coating of zeolite. This veining is intraformational and has formed during diagenesis.

1.3.7 Depositional environment

The sandstone and siltstone beds of the Clent Hills Group are typically ungraded with an almost total absence of current lamination.

The conglomerates generally show lensoid shapes when exposed in cross section. Excellent examples of this can be found in the valley of Bowyers Stream where a conglomerate lens has an apparent length of 3.5 km and maximum thickness of 1 km. The thickness is however accentuated slightly by a north-west plunging fold in this conglomerate. At the extremeties, the conglomerate is seen to taper out into a number of thin conglomerate beds each interbedded with sandstone and some siltstone beds. This sequence is particularly well exposed on the ridge that runs between Pony Knob and

Mt Winterslow. Parallel to one margin of the conglomerate, and separated from it by a thick sandstone bed, are red and green siltstone beds. The shape of the conglomerate in Bowyers Stream is consistent with its formation as a channel deposit. The edges of the channel being represented by the interdigitating sandstone and siltstone beds.

There are no macrofaunal fossil localities associated with the Bowyers Stream conglomerate and there is a possibility that it represents a non-marine sedimentary environment, in which case the associated red beds could represent river silts that were seasonally above the water table. At present there is not sufficient evidence to support a completely non-marine environment for this conglomerate. The proximity and gross similarity of the Bowyers Stream conglomerate to those on the east and north flanks of Mt Winterslow, which are associated with shallow marine or marginal marine fossil fauna, indicates that the Bowyers Stream conglomerate was most probably formed in the same environment. The absence of pollens and leaf cuticles in these beds indicates an oxidising environment which is consistent with the presence of associated red-beds. There is also the possibility that the red-beds are redeposited red-oxidised (hematite bearing) sediments or volcanics.

The conglomerate beds in Taylors Stream are thinner than those of Bowyers Stream and tend to have a greater lateral extent. The conglomerate exposed in Hutt Creek near the Winterslow Track also lenses out rapidly at its extremities, but the structure of this locality is locally complicated by extensive faulting.

The conglomerates of Low Hills can be traced along the eastern slopes of the Harper Range above Pudding Valley Creek. They are locally rich in plant fossils and their interbedded sandstone and siltstone also contain *Tancredia* sp. like those on the east flanks of Mt Winterslow, and they were probably formed in a similar depositional environment.

The beds in Haast Stream are similar in appearance to others of the Clent Hills Group. Thick conglomerate beds in this sequence also appear to be lensoid as they cannot be followed for any distance laterally from Haast Stream. The geology is complicated by the deposits of glacial outwash gravels on the glacial scoured surface on the west side of the Clent Hills. The Haast Stream beds appear to be deposited in either a non-marine or deltaic environment as the large complete fern fronds preserved along bedding planes indicate non-turbulent low energy conditions of sedimentation, possibly with alternate high energy conditions. It is doubtful if the large delicate fern fronds could survive transport over great distances from their source. The absence of macrofaunal fossils, in spite of diligent searches by H. W. Keene and the author, and by Haast (1877), is consistent with this interpretation.

The size of the boulders in the conglomerate (commonly 10 cm diameter, but also up to 1 m), is also consistent with the non-marine to marginal marine range of depositional environments for the Clent Hills Group sediments.

There is much paleomagnetic evidence to show that the Mid-Mesozoic pole lay close to New Zealand when the

Gondwana countries are fitted back together (Creer, 1970, 1973; Schmidt 1976; McElhinny and Embleton, 1974; McElhinny, 1973), and even in the Late Jurassic the pole lay within 20° of latitude of the South Island. The size of the tree trunks, and abundance of plant fossils in the Clent Hills Group indicates that the climate that the plants grew in was at least temperate, and therefore totally different from present day polar climates, as the latitude of 70° represents the present day limit of tree growth and above which the mean summer temperature is zero (Irving, 1964; Blackett, 1961).

Hallam (1975, p196) reviewed the various paleoclimatic indicators of the Jurassic, and showed that the tropical and subtropical zones were wider than the present day, and that the polar regions had no ice caps but had temperate conditions, with an approximate temperature difference between polar and equatorial zones of 22°C (compared to 42°C at the present day). The presence of thin coal measures in the Clent Hills beds does not indicate any temperature but does indicate the climate was humid. Barnard (1973) has used the distribution of *Dictyophyllum* (from 50°N to 60°S), to show that the world climate was warm and highly equable in the Jurassic. However Arber (1917) lists *Dictyophyllum* among the fossil flora from Haast Stream (which must have been at a latitude of greater than 70°S).

The large tree trunks found in the conglomerate beds have distinct seasonal growth-ring structures. Studies by Chaloner and Creeber (1973) of tree growth patterns in various

climates have shown that the *onset* of seasonal xylem growth in trees is primarily controlled by photoperiodism (day length). Ambient temperature, water availability, and rate of photosynthesis control the thickness of tree rings. Tree rings from hot dry climates are indistinguishable from those formed in cold, wet climates (Chaloner and Creeber, 1973), but do indicate a distinct seasonal climatic periodicity.

The presence of abundant fossil floras from the New Zealand Jurassic sediments present the problem of plant growth, or even survival, during the winter months of complete darkness, this problem is not confined to New Zealand, e.g. early Triassic floras in Siberia, and Cretaceous floras in Alaska were also at latitudes greater than 70° (Barnard, 1973). The Permo-Triassic floras of Antarctica must also have lived through seasonal darkness, and these also exhibit good seasonal growth rings (Chaloner and Creeber, 1973). It is evident that some plants can survive seasonal periods of darkness, but presumably growth during this time would be minor, or possibly non-existent.

1.3.8 Associated Volcanics

No contemporaneous volcanic rock types have been found in the Clent Hills Group. Only two post-depositional dikes were found. One is in Taylors Stream at GR 916546. This is a basalt dike that has been intruded along a major fault zone that strikes south-east in this area. The age of this dike is not known and it may be related to the Mt Somers

Volcanics, but more likely to the Tertiary basalts. The other basalt dike cuts Jurassic(?) sediments in a stream on the south west side of the Clent Hills at GR 738478. The age of this dike is also unknown but it could have been a feeder dike for the Mt Somers Volcanics in this area. This is discussed further in section 2.2.11.

1.4 UNDIFFERENTIATED TORLESSE ROCKS

Rocks of unknown age make up the major part of the Torlesse Supergroup exposed in the Mt Somers area (S81). The Torlesse rocks that cap the Winterslow Range are distinctly different to the Jurassic Clent Hills Group rocks. The uppermost 500-600 m of Mt Winterslow is composed of well indurated, quartz veined, sandstone and siltstone. The sandstone is a pale grey-green colour and the siltstone is a very pale grey. Red argillite beds also occur. These rocks are composed of poorly sorted quartz and feldspar with the feldspar extensively altered and difficult to distinguish from lithic fragments, in thin section. The grains of the sandstones and siltstones are distinctly elongated giving a subschistose texture. Quartz veining is ubiquitous in the sandstones, but often too fine to be seen in hand specimens. These extremely indurated sandstones have a rounded scree covered form with few outcrops on the Winterslow Range. This contrasts with the rugged mountainous, well exposed, form of the less indurated Fingers Formation rocks and the subdued valley topography of the moderately indurated Clent Hills beds. The contact between these highly indurated beds of the Winterslow Range and the Clent Hills beds can be traced, in the form of an abrupt change in topography,

on the north, and to a less extent the south, flanks of the Winterslow Range. The structural relations will be discussed in a following section.

A similar lithology to that of the Winterslow Range just described, is found on the upper 300 m of the Clent Hills, north of the contact with the Barossa Andesite. There is also a change in topography that accompanies the change in induration, but the effect is masked by glacial gravels on the ice scoured west surface of the Clent Hills.

Two other areas of highly indurated quartz veined light grey-green sandstone and light grey siltstone also occur in the Mt Somers area (S81). These may in fact be identical to the beds that cap the Winterslow Range but further detailed work would be necessary to establish a positive relation. One of these is the area in the north west corner of the Mt Somers sheet (S81) in the region of Paddle Hill Creek, and the second area is on the south side of the Rangitata Gorge.

The area around Paddle Hill Creek was mapped as Haast Schist Group (petrographically of Chlorite II rank), by Gair (1967). The lateral extent of this rock type is undefined, as exposure in the north-west corner of the Mt Somers sheet (S81) is limited by a cover of glacial outwash gravels and moraines, and also because distinction in the field between the "subschistose" sandstones and

siltstones, and the adjacent indurated Torlesse rocks, is not always easy. This is true particularly for the sandstone as this does not show visible schistosity in hand specimen. The light grey siltstone shows a texture resembling schistosity but this is actually a result of parallel shear within the beds. Quartz and pumpellyite veins, also parallel to this very fine shearing, add to the visual appearance of schistosity.

A similar rock type occurs in the south of the Mt Somers area on the south bank of the Rangitata Gorge. Exposures of this rock are predominantly located on the border of S81 with the Mt Peel sheet (S91) in the region of the headwaters of Soup Stream through to Coal Hill. On the east side of Mt Peel (which is adjacent to Coal Hill) *Atomodesma* fragments have been found (Campbell & Warren, 1965; Gair, 1967) and it is therefore remotely possible that these beds at Coal Hill are also Permian, and if so then the Paddle Hill Creek beds (and possibly also those of the upper surface of the Clent Hills and the Winterslow Range) are also Permian in age.

The Torlesse rocks of the Harper Range are of unknown age and association. At the east end of Harper Range are the Low Hills which belong to the Clent Hills Group. These Jurassic conglomerates and plant beds can be traced north along the lower eastern slopes of the Harper Range. The remainder of the Harper Range consists of unfossiliferous Torlesse rock of apparently greater induration, and possibly

of different age. The rocks of the Harper Range are not generally quartz veined, and are of medium- to dark-grey sandstone and dark-grey to black siltstone. Sandstone predominates over the siltstone. Red argillite beds are not common but do occur. Thin conglomerate beds are relatively common but cannot be traced for any distance (Map 1) and it is possible they are channel deposits that lense out rapidly. Plant fragments are scarce in these rocks. Volcanic dikes have been found intruding beds of the Harper Hills (H. W. Keene, pers. comm.) but it is not known whether these are of the same tholeiitic basalt that is found in the dikes in the north-east part of the Mt Somers area. Haast (1879) described a small area of "melaphyre" on Mt Harper. This was not found during the mapping for this study, and it is not therefore known if Haast was referring to a basalt dike, or to andesite flows belonging to the Mt Somers Volcanics.

In the south-west corner of the Mt Somers Sheet (S81) between the Hewson River and the Rangitata River, the ridges that descend from Ben McLeod are composed of Torlesse rocks similar to those of the Harper Range. A good exposure of these is provided by the roche moutonée of Rawtor in which parallel, thin, alternating sandstone and siltstone beds dip steeply to the south. These beds are very sheared. No fossils were found, and the beds may belong either to the same formation as the beds at Coal Hill, or to the same formation as the beds of the Harper Range.

The valley of Power House Stream has conspicuously few outcrops of Torlesse rocks. The sandstones are a greenish-grey colour generally with quartz veins. In thin section their constituent feldspar grains are considerably altered, similar to those of the sandstones of the Winterslow Range. The interbedded light grey siltstones occasionally have current laminations. Flute casts are only occasionally found on the bedding planes. An intraformational conglomerate, consisting of siltstone from a penecontemporaneous disturbed bed, was observed in one sandstone bed.

The remaining areas of Torlesse rocks in the Mt Somers Sheet (S81) are those of the Moorehouse Range, Trinity Hill, and Peter Range. No fossils have been found in these rocks. The lithologies are generally similar to those of the Harper Range. Conglomerate beds are moderately common but do not contain the plant fossils typical of the Clent Hills Group. These conglomerates, like those of the Harper Range, are generally in beds less than 2 m in thickness and consist of small pebbles and boulders (generally less than 10 cm in diameter) of sandstone and siltstone with minor igneous and metamorphic pebbles. Red and green siltstone beds are occasionally present. Less commonly these form very thin-bedded alternating sequences of red and green silts.

The Torlesse rocks underlying the andesite at Mt Barrosa appear to belong to the same formation as those of Trinity Hill.

1.5 STRUCTURE

Structural interpretations of the Torlesse Supergroup in the Mt Somers area are only of a preliminary nature as much more detailed work is needed in all aspects of Torlesse geology in this area in order to unravel the complex relations.

Faulting is widespread and is most frequently observed as isolated crush zones, most of which are veined with calcite. The crush zones give little information about the tectonic events, or even the strike of the fault plane as only rarely can a fault be traced beyond the crush zone.

The timing of the tectonic uplift in the Mt Somers area is shown by outliers of Tertiary deposits that occur in fault-angle depressions, and by the faulted contacts of many of the Late Cretaceous Volcanics. In the Clent Hills Saddle, just north of Mt Taylor, a Tertiary sequence is exposed in a saddle at an elevation of 1600 m. The field evidence suggests that thrust faulting within the Torlesse Supergroup was probably pre-late Cretaceous and therefore part of Rangitata Orogeny, while the uplift and block faulting of the present Mountain ranges commenced in the late Tertiary as part of the Kaikoura Orogeny, and is still active at the present time as evidenced by active fault traces in the Mt Somers area.

1.5.1 Structural Outline

Figure 5 is an interpretive map of the Torlesse rocks in the Mt Somers area (S81) showing generalised structural form lines, major faults and possible thrust surfaces. Each of the main mountain ranges is probably a fault bound block but scree and a surface covering of glacial outwash gravel obscure the faulting. Recent fault traces in the main valley between Hakatere and Lake Heron are parallel to the valley sides. Other major faults are found along contacts between the Torlesse rocks and younger volcanics or sedimentary rocks.

The Jurassic Clent Hills Group form an arcuate belt truncated in the south by a faulted outlier of Tertiary and Cretaceous sediments on the south bank of the Rangitata River. The eastern extremity of the Jurassic beds is truncated by one of a number of faults that follow the line where the foothills meet the Canterbury plains. Exposure of the Jurassic beds is not continuous as erosion has preferentially removed these moderately indurated beds to form valleys which have subsequently filled with glacial outwash gravels (e.g. Pudding Valley). The general structural form lines are parallel to the arcuate distribution.

The upper slopes of the Winterslow Range are composed of highly indurated "sub-schistose" rocks thrust over the lower-metamorphic grade Clent Hills beds. The contact is approximately horizontal. The Jurassic beds on the northern and southern flanks of the Winterslow Range are folded near the contact. The folding appears to be a result of drag caused by the thrusting of the overlying block, and if so

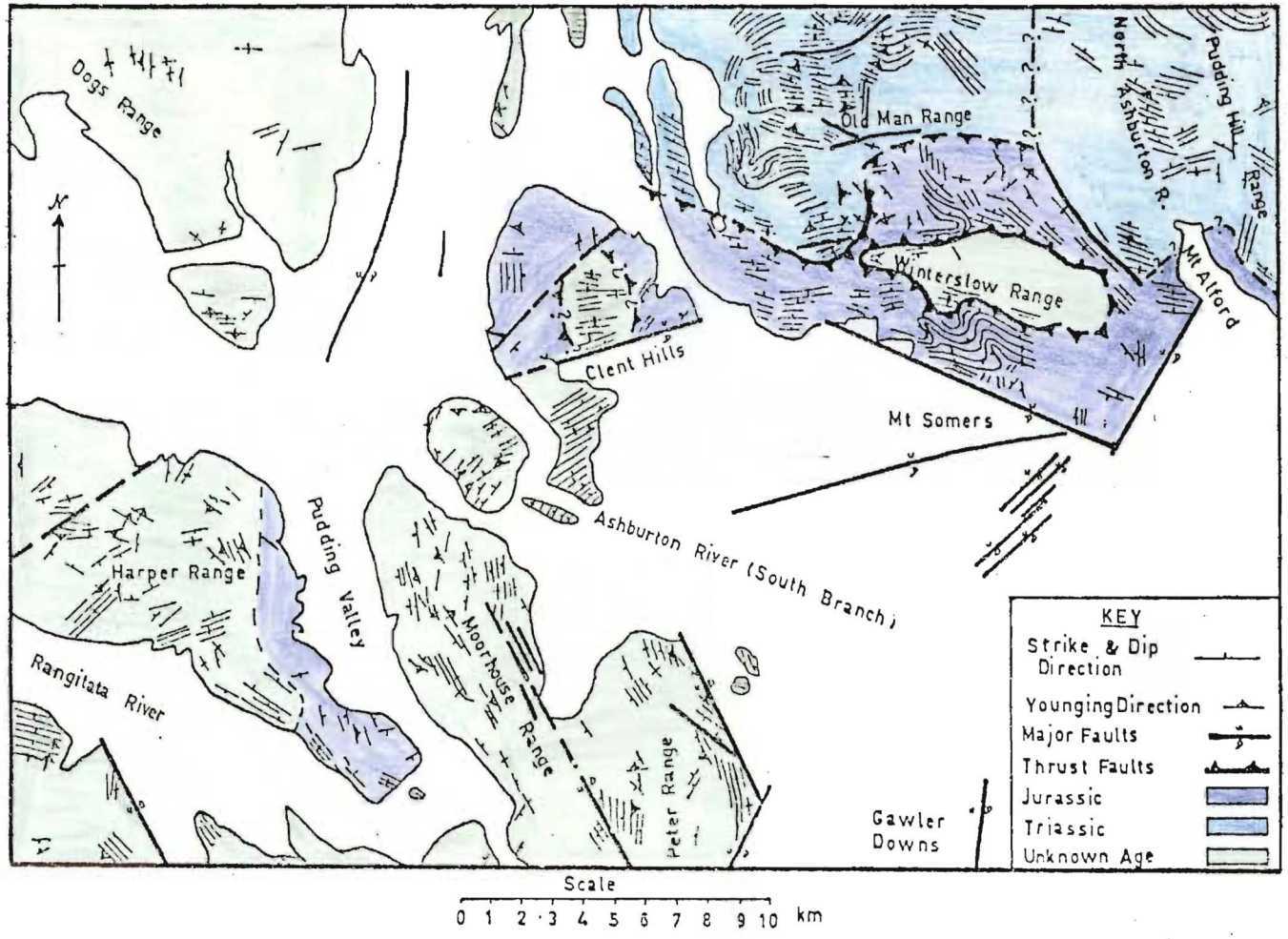

Figure 5. Structural trends in Torlesse rocks from field observations in the Mt Somers area.

implies a thrust direction from east to west. A similar thrust may occur on the Clent Hills although evidence for this is more limited than on the Winterslow Range.

The Torlesse rocks east and west of Pudding Valley are of unknown age and their contact with the Jurassic beds is obscured. The rocks of the Moor house Range, Trinity Hill and Clent Hills, generally have structural form lines that curve parallel to the outline of the Jurassic beds, and thus could be conformable with the Jurassic beds.

Structure in the Dogs Range area is not clear as there is poor exposure. The subschistose rocks are similar to those observed on Mt Winterslow and also in the Ben McLeod - Coal Hill area south of the Rangitata River.

The beds of the Fingers Formation dip to the north and are not overturned. The contact with the Jurassic rocks is a low angle thrust fault. The Triassic beds appear to have been thrust from west to east. The thick sandstone beds of the Fingers Formation are only slightly folded while the interbedded siltstone is intensely deformed and convoluted, particularly near the thrust plane.

The relation between the Fingers Formation and the Pudding Hill Formation is not known and the contact is not exposed. However the structural form lines and younging directions are the same in both Formations, and it is possible that they are conformable.

The contact between the Pudding Hill Formation and the Clent Hills Group is faulted for much of its length. The structural relations in the region of Mt Alford are not known

because of the lack of exposure but the Jurassic beds on both flanks of the Alford Range appear to overlie the Triassic beds.

1.5.2 Fingers Formation

The thick sandstone beds of the Fingers Formation form a regular sequence dipping at 60°-70° in a northerly direction, and younging to the north. These beds are typically unfolded although large scale flexures or undulations are present over distances of several kilometers. The interbedded siltstones are generally convoluted and sheared. Near the contact with the Jurassic beds, in the region of the upper Taylors Stream basin, there is an extensive (several hundred meters thick) siltstone sequence containing only thin (<0.1 m) sandstone beds. This siltstone is complexly folded and sheared and extends along the southern flank of the Old Man Range. The siltstone sequence thins to the west and crops out in Quaker Saddle where it strikes east, has a nearly vertical dip, and is about 500 m thick. In Black Stream the siltstone sequence is complexly folded through 90° to strike north, in which direction it thins rapidly.

The contact of the Fingers Formation with the Clent Hills Group is not well exposed because of extensive scree. Also the thick Triassic siltstone sequence at the contact is adjacent to a similar thick Jurassic siltstone at the head of Taylors Stream valley. Both siltstones are black and very sheared, and distinction between them is sometimes

difficult. The contact runs along the southern flank of the Old Man Range, around the head of the valley, and over Peach Saddle and the saddle between Trig T and Trig TT (Map 1). The contact fault plane forms a low angle surface that can be explained by thrusting of the Triassic beds over the Jurassic.

1.5.3 Pudding Hill Formation

Structures within this Formation are complicated by extensive faulting and by the general lack of exposure because of vegetation cover.

In the area between Centre Spur and Alford Range, slips have exposed many fault crush zones. Another area of intensive faulting is in the upper reaches of Waterfall Creek on the west flanks of Pudding Hill Range. On the slopes of Pudding Hill Range leading down from Mt Bruce a large asymmetric synclinal fold is exposed, with its axis plunging to the north-east.

Much of the bedding of this Formation is regular with the siltstone beds showing the most deformation. In general the beds dip to the north at steep angles. In the area around the Alford Range the beds have vertical dips. Pull-apart structures in these rocks indicate some of the deformation was plastic deformation. Younging directions indicate that the beds are not overturned and young to the north.

1.5.4 Clent Hills Group

The Clent Hills beds, underlying the more indurated beds on the southern side of the Winterslow Range, have been folded into two large scale asymmetric thrust folds with moderate to steep plunges to the north-west. The structure in this area is made clearer by the presence of a thick conglomerate bed and thin red siltstone bed which act as marker beds that can be traced for several kilometers. Figure 6 illustrates part of a recumbent fold exposed on the southern flank of Mt Winterslow.

The Clent Hills beds in Taylors Stream valley are not extensively deformed except for the siltstone sequence near the thrust plane. In general the beds dip to the north-east with moderate to steep dips, but near the northern flanks of the Winterslow Range the strike of the beds swings around to the east and the beds dip in toward the Range. The folding of a thick sandstone bed into a steeply plunging anticline at GR 888525 is consistent with drag from an east to west direction. The thrust folds on the southern slopes of the Range also suggest that the overlying indurated beds have been thrust from east to west.

The contact between the Clent Hills beds and those of the Torlessia-bearing Pudding Hill Formation is also faulted for much of its length. The linear, approximately vertical, fault zone extends from Taylors Stream at GR 916545 to GR 949511. A southern extension beyond this is probable but it is not visible in the field. The lower slopes of Mt Winterslow between Diggers Creek and Hill Creek are marked by a series

Figure 6. Southern flank of the Winterslow Range showing part of a large recumbent fold in Upper Jurassic sediments which are overlain by more indurated Torlesse rocks. The contact is a low angle thrust plane (dashed line).

of parallel ridges that appear to be fault controlled, and are parallel to the major fault zone just referred to above.

The structure in the Clent Hills area is complicated by the lack of exposure and extensive faulting as evidenced from crush zones. The section exposed in Haast Stream reveals a series of approximately north-south trending beds of sandstone and siltstone with four conglomerate beds. At the mouth of Haast Stream gully an outlier of Tertiary sands and silts is preserved which also occur, together with coal measures, at GR 735538 near the site of the old Clent Hills Homestead. The Torlesse beds exposed in Haast Stream show little deformation except for steeply dipping reverse fault formed along the axial plane of a fold which dips steeply to the east. This occurs at GR 728507. The conglomerate beds in the section cannot be traced laterally as they are channel deposits that rapidly lens out either side of Haast Stream. Even the largest of these which is approximately 100 m thick, cannot be traced across adjacent streams. Plant remains were found in the rocks in streams to the north and south of Haast Stream indicating that the Jurassic beds do extend laterally in these directions.

In Potato Stream there is evidence of extensive faulting, in the form of crush zones and pug zones. A major fault zone also occurs on the north side of the Clent Hills where horizontal thrust faults and vertical faults are exposed in slips at an elevation of 1200 m. It has already been stated that the topmost beds on the Clent Hills are of a higher degree of induration than those of Haast Stream. A possible

interpretation is that the older rocks have been thrust over the Jurassic plant beds, as on the Winterslow Range.

The structural relationship between the Torlesse beds of the Harper Range and the Jurassic beds of the Low Hills is difficult to establish without knowing the age of the Harper Range beds. The two most likely possibilities are: 1. the Low Hills beds are younger than those of the Harper Range; and 2. the Low Hills beds are conformable with the Harper Range beds. If the first possibility is considered then the Low Hills beds could lie in a syncline with an approximately north-south axis. The nature of the contact is obscure, but there is also the possibility that the Harper Range beds are thrust over the Low Hills beds. If the second possibility is true, then the structure could still be synclinal with the conglomerate positioned axially. Some evidence for a conformable age is provided by the similarity of rock types, particularly the conglomerates and red/green argillite beds. Excellent examples of parallel beds of conglomerate, sandstone and red siltstone occur on the south western slopes of Mt Tripp in the Moorehouse Range where individual marker beds can be traced for distances of up to 2 km. These also appear to be generally similar to those of the Clent Hills Group.

1.5.5 Undifferentiated Torlesse Rocks

Major faults bound the Moorehouse Range block and the Peter Range block. In the former Range a series of extensive crush zones are exposed in stream beds low on the north-east flank of the Range. A large exposure of the complete Tertiary sequence occurs in the fault-angle depression approximately 1.5 km north-east of Brown Saddle. The fault is well exposed between Mt Pukanui and the South Branch of the Hinds River.

The Peter Range is bounded along its eastern margin by a fault with a vertical displacement of 300 m. The north-east boundary of the Peter Range is also a major fault, downthrown to the north.

Other major faults and structures are discussed in section 2.7.

PART II

MT SOMERS VOLCANICS

2.1 INTRODUCTION

2.1.1 Nomenclature

The subdivision of the volcanic rocks used in this thesis is given in Table 4. The Mt Somers Volcanics are defined as the post-Jurassic pre-Tertiary volcanic rocks of the Canterbury Province that have calc-alkaline affinities. These are predominantly rhyolites and andesites.

The term "Mt Somers Volcanics" has been used previously as a formation name (Gair, 1967) incorporating the andesites and rhyolites of inland Mid-Canterbury together with those on the south bank of the Rangitata Gorge.

Subdivision of these volcanics has been done on the basis of: 1. Field relations, 2. Chemistry, 3. Petrography. The chemistry of a volcanic rock type has been the most significant factor in the classification when the other factors are indistinct. This has been particularly so for the glassy dacites of the Gawler Downs-Hinds River area. Silicified and altered volcanic rock types were classified by petrography. Chemical classification of volcanic rock types used in this study has followed that of Taylor (1969) who proposed the following types for calc-alkaline volcanics:

1. High-Al basalt : <53% SiO_2
2. Low-silica andesite : 53-56% SiO_2; 0.7-2.5% K_2O
3. Low-K andesite : <0.7% K_2O; 53-62% SiO_2
4. Andesite : 56-62% SiO_2; 0.7-2.5% K_2O

5. High-K andesite : >2.5% K_2O; 53-62% SiO_2.
6. Dacite : 62-68% SiO_2
7. Rhyolite : >68% SiO_2

TABLE 4. Classification used for the Mt Somers Volcanics

Group	Formation
Mt Somers Volcanics	Surrey Hills Tuff Alford Rhyolite Graham Dolerite Barrosa Andesite Somers Rhyolite Hinds River Dacite Stew Point Andesite Rata Peaks Rhyolite Malvern Hills Rhyolite Round Top Andesite

2.1.2 Distribution

The known extent of the Mt Somers Volcanics is from the Malvern Hills in North-Canterbury, to the Hewson River in South-Canterbury. These volcanics are exposed in a discontinuous zone that follows the foothills of the Southern Alps in this area. The distribution of individual volcanic formations will be discussed separately below.

Evidence that the volcanics also extend under the gravels of the Canterbury Plains in Mid-Canterbury, has been provided by samples of andesite and rhyolite recovered from

New Zealand Petroleum Exploration Company's 1969 drill hole, J. D. George No. 1, near Ashburton. This exploratory well bottomed in andesite at a depth of 1648 m, after passing through 218 m of volcanics.

2.2 DESCRIPTION OF THE VOLCANICS

2.2.1 Surrey Hills Tuff

This tuff is named after the area east of the Gawler Downs Trig which is known as Surrey Hills. This is the locality (GR 884309) where these tuff beds were first mapped by Haast (1877).

2.2.1.1 Definition

The Surrey Hills Tuff consists of rhyolite tuff beds of white, yellow, green, pink, and red colours. It includes ash-flow tuff; ignimbrite (welded ash-flow tuff); subaqueous bedded tuff and tuffaceous silt; and fused tuff. Induration is variable ranging from friable to flinty silicified tuffs.

The type section is here defined in a gully east of the trig station on the summit of Mt Alford, at GR 984504. In this section 63 m of bedded tuff are discontinuously exposed. The well sorted and well bedded tuffs in the upper part of the type section are similar to those mapped by Haast (1877) at the Surrey Hills, and which he referred to as "palla" in his map of the Mt Somers area. Cox (1877, p3) also referred to these tuffs as "palla", and stated that they were deposited by thermal springs. Later Cox (1884a,p40) described them as siliceous beds formed by subaqueous deposition.

Speight (1938, p19) clarified the use of the word "palla" by obtaining a complicated but indistinct definition from the year-book of the Geological Survey, Vienna, 1863.

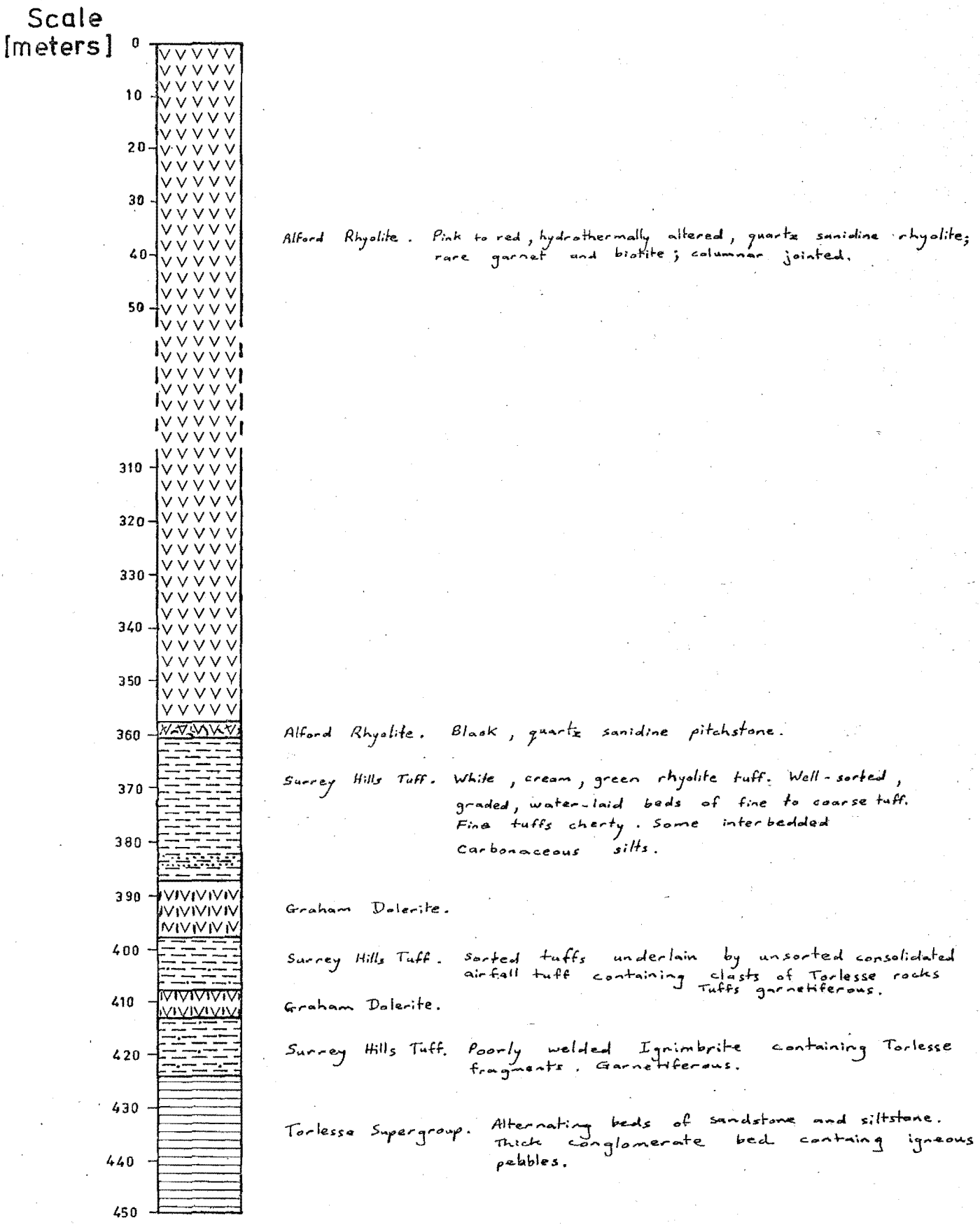

Figure 7. Stratigraphic column at the type section of the Surrey Hills Tuff and the Graham Dolerite.

This broadly defined the term as a white, cream or greenish coloured marl or trachytic tuff, characteristic of a particular district in Austria. Speight (1938, p20) preferred to call these beds "rhyolite tuffs" belonging to his "Rhyolites of the First Period".

The lower part of the type section contains unsorted to poorly sorted tuff with up to 5% of angular Torlesse sandstone and siltstone clasts. These lower tuff beds also contain scattered almandine garnet.

2.2.1.2 Distribution

The Surrey Hills Tuff occurs extensively on both flanks of Mt Alford and the Alford Range where it is commonly overlain by rhyolite and/or dolerite that has protected it from erosion. There is also a large area of the tuff at the "Diamond Field" above Taylors Stream, opposite Diamond Creek (at GR 955507 and 957508).

The tuff to the east of the Gawler Downs trig station is the next largest exposure to those at Mt Alford. Smaller isolated localities of tuff crop out along the east margin of Peter Range at GR 813317 and 815323, and also on top of the hills to the west at GR 801329 and 797333. Small localities of tuff also occur in the gorge of the North Branch of the Hinds River at GR 793383, and nearby at GR 791376 and 798369.

Tuff underlies Barrosa Andesites north of Mt Somers above Morgan Stream (GR 866486), and in a small tributary to the Stour River (GR 836492).

2.2.1.3 Eruptive Form

The Surrey Hills Tuff consists predominantly of ignimbrite, bedded ash-flow tuff, and water-laid tuffs.

(a) Ignimbrite: Unsorted tuff that has been moderately welded occurs on the north-east flanks of Mt Alford (GR 990501, 985505). This tuff contains many angular xenoliths of Torlesse sandstone, and grey-green siltstone, up to 3 cm in diameter. These tuff localities are the only ones found that contain Torlesse clasts of this size other than those described in (b) below, and it is assumed that the tuff originated from Mt Alford.

Although this ignimbrite has been mapped as Surrey Hills Tuff, the trace element chemistry of this rock, particularly its barium content, is totally dissimilar to that of the other tuffs analysed, but instead is comparable with that of the ignimbrite of Mt Somers and also that of the Rakaia Gorge.

The ignimbrite has been fused where it is in contact with the overlying dolerite (GR 990501). The heat from the dolerite also caused a secondary red hematite alteration to the ignimbrite, and to the included xenoliths of Torlesse rocks, for a distance of approximately 20 cm from the contact.

(b) Ash Flow Tuff: Beds of coarse-grained tuff that is relatively unconsolidated, and partially to non-welded, occurs on the east side of Graham Creek spur, at GR 956350. At this locality individual beds of tuff vary in thickness between 2 cm and 30 cm and contain unsorted garnet and large clasts of Torlesse fragments (generally 2 to 5 cm, but occasionally up

to 15 cm long). The beds appear similar to the water-laid tuffs described below, but the presence of unsorted garnet and Torlesse fragments confirms their ash-flow origin. These tuff beds correlate with those described above as ignimbrites.

(c) Water-laid tuff: This forms well bedded and well sorted deposits, stratigraphically overlying the welded ash flow tuff (ignimbrite) described above, and separated from it in places by dolerite. The bedded tuff is widespread, occurring extensively on both flanks of Mt Alford; above Morgan Stream north of Mt Somers; underlying dacite on the Gawler Downs, Hinds River and Peters Range (see Map 1). Evidence that this tuff is subaqueous sediment comes from interbedded carbonaceous silt; the fine sorting and graded bedding, and other sedimentary features such as compaction faults and associated flame structures. This tuff may be a reworked subaerial deposit washed into small lakes.

The water-laid tuff has also been fused by the overlying rhyolite dome at GR 979510. Here it has been converted to a black pitchstone. The well sorted bedding texture can still be seen in fresh samples of the pitchstone, and is accentuated greatly on weathered surfaces.

2.2.1.4 Petrography

The tuff beds vary from sorted to unsorted. The range of grain size, degree of sorting, phenocryst mineral content, and degree of silicification, welding, and compaction of the groundmass, are all extremely variable. It is not proposed

to describe, here, each type in detail. Instead a general description for the major types only will be given.

The fine-grained sorted tuffs are composed of silt-sized particles of angular quartz and sanidine (usually making up less than 15% of the rock) in a matrix of silt-sized glass fragments and shards. The groundmass is frequently silicified making the rock flinty in appearance. No garnet or biotite was found in these fine-grained tuffs.

The coarse-grained sorted tuff beds are also composed of equigranular quartz, sanidine, and glass. The size range is 1 to 1.5 mm in diameter. Quartz and sanidine make up to 30% of the rock and are sometimes contained in a matrix of finer angular fragments of these minerals and glass shards. Garnet is only occasionally present. The coarse-grained beds usually grade up into fine-grained tuff.

Unsorted beds of tuff contain between 5 and 30% quartz and sanidine as angular to subhedral grains in a matrix of glass shards and fragments of ignimbrite (Figure 8). Garnet is present in some samples.

The ignimbrite from Mt Alford contains angular to subhedral quartz and sanidine in the size range 0.5 to 2 mm, which make up 40% of the rock. About 3% is made up of Torlesse sandstone, siltstone, and schistose sandstone xenoliths. These xenoliths range in size from 3 to 6 mm in diameter in the thin sections examined, but larger fragments up to 3 cm in diameter occur. Garnet and biotite both occur in amounts of less than 0.5%. The groundmass of the ignimbrite is composed of partially welded, elongated glass shards.

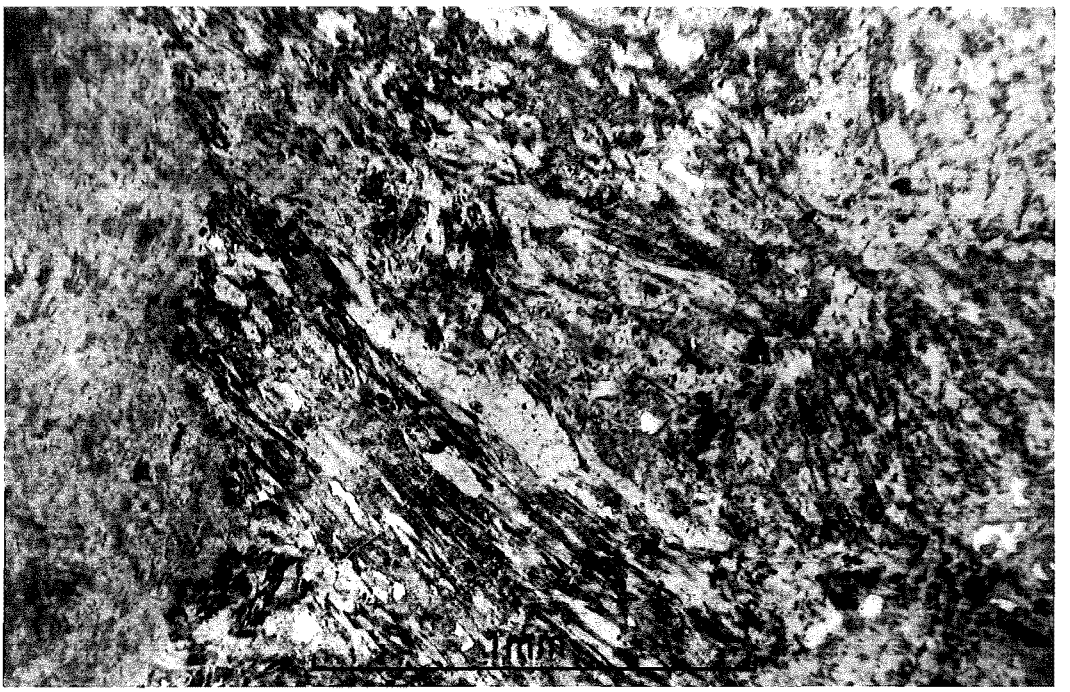

Figure 8. Photomicrograph of Surrey Hills Tuff composed of fragments of welded tuff.

Figure 9. Photomicrograph of pitchstone composed of fused fragments of welded tuff.

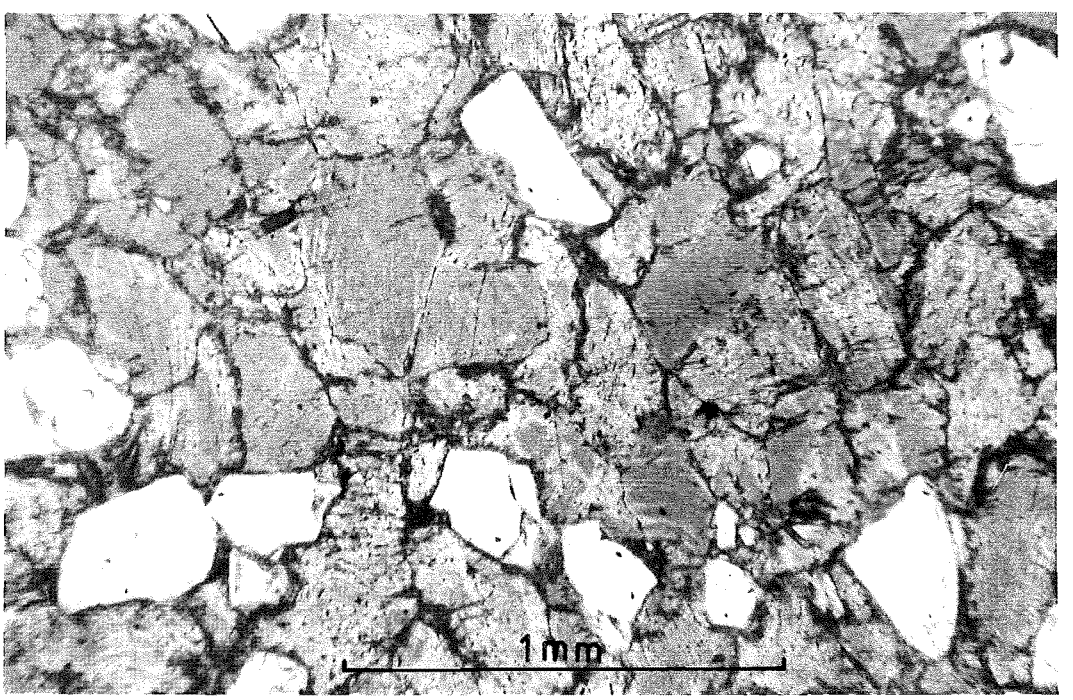

A fused, well-sorted, bedded tuff, that occurs on Mt Alford, is petrographically identical to the sorted tuff described above, i.e. each layer consists of equidimensional fragments of quartz sanidine and glass (Figure 9). This rock has the external appearance of a pitchstone.

2.2.1.5 Relation to Underlying Rocks

The tuff always unconformably overlies Torlesse sediments. It has been preserved in topographic lows that formed either by erosion of the Torlesse rocks, or as crater lakes formed by the initial volcanic explosions. Either case is possible as the tuff is generally preserved where it has been covered by subsequent extrusions of volcanic rocks. The widespread occurrence of the tuff and the fact that it always occurs adjacent to sites of extrusion favours the theory that the present outcrops were deposited in vent or crater depressions.

Near Diamond Creek, at GR 954507, the tuff has slumped into Taylors Stream, where it now forms a truncated anticlinal structure 200 m wide. The north-east plane of contact of the tuff with the Torlesse rocks at this locality has a steep plunge to the south-east, but there is no evidence of faulting along this contact. Carbonised plant remains are common in the tuff along this contact (GR 953507) and have not been observed away from it. The tuff has weathered to a montmorillonite clay which erodes rapidly (and has also been responsible for the slumping at this locality), leaving

exposed the carbonised remains of tree trunks and stems. These range up to 60 cm in diameter. Carbonised plant fragments (possibly roots) were also found extending into the thin alternating sandstone and siltstone beds of the Torlesse rock at the contact. At this locality the tuff overlies a conglomerate which also crops out under tuff at the base of Diamond Creek (GR 957509) and again higher up the creek at GR 961512. The tuff beds near the confluence of Diamond Creek and Taylors Stream have been down-faulted 160 m relative to those at the contact with the base of the Alford Rhyolite (see Map 1).

The Surrey Hills Tuff exposed above Morgan Stream (GR 867486) unconformably overlies the Torlesse rocks. The tuff beds dip at 45° to the south with a strike of 090°, but adjacent to the contact with the overlying Barrosa Andesite they have been tilted to a dip of 75° to the south and a strike of 085°. Immediately above this outcrop the andesite has vertical flow banding and it is probable that extrusion of the andesite took place at this locality. The tuffs are baked to a porcellaneous chert at the contact. A "porcelain jasper" underlying pitchstone agglomerates in Petrifying Gully, described by Haast (1872a,pl43), possibly owes its origin to a similar process.

On the east bank of Grahams Creek the tuff described in section (b) above can be seen to unconformably overlie contorted, sheared, black Torlesse siltstone. Here the dip of the tuff beds is variable but generally about 20° to the east and they strike about 160°.

2.2.2 Alford Rhyolite

This rhyolite is named after the Alford Range which is capped by the rhyolite along its length.

2.2.2.1 Definition

The Alford Rhyolite consists of a characteristic and distinctive red to pink rhyolite, with black glassy basal pitchstone that grades down into a pitchstone agglomerate. This rhyolite has bipyramidal-quartz and sanidine phenocrysts in a devitrified-glass groundmass.

This rhyolite, together with those from Mt Somers, the Rakaia Gorge, and the Malvern Hills, has been referred to by a variety of names in past literature. These include the term "quartz porphyry" used by Haast (1872, 1877, 1879). Cox (1877) also referred to these rocks as "quartz porphyries" of his "Trachytic Series", although Cox (1884a later used the term suggested by Hutton (1874, p40) who called the rhyolites "liparites". Haast (1872b,p14) had dismissed this name on the grounds that real quartzose trachytes had to be Tertiary in age, and therefore he used the name of quartz porphyry for the rhyolite, contrary to his previously stated intention (Haast, 1862) to use the name that Baron von Richthofen had given to these rocks, i.e. "rhyolites". Hector (1884, pxxi) stated that the rhyolites should be referred to as "quartz trachytes". Speight (1938), in accord with modern usage, referred to these rocks as rhyolites, and assigned them to his "Second Period Rhyolites" although he

considered there was little evidence for doing so.

The type locality for the Alford Rhyolite is in Diamond Creek, at GR 961513, where the sequence is from pitchstone agglomerate to pitchstone, to columnar-jointed pink rhyolite. The relations between the rhyolite and the Surrey Hills Tuff, and the Torlesse rocks are also well exposed at this locality.

2.2.2.2 Distribution

The Alford Rhyolite occurs along the ridge of the Alford Range between GR 995490 and 948550 (see Map 1). A small outcrop is exposed, between these two localities, in a saddle on the ridge at GR 953542. No other isolated outcrops of this pink rhyolite have been found in the surrounding district.

2.2.2.3 Eruptive Form

The Alford Rhyolite consists of pitchstone breccia, pitchstone, rhyolite domes, agglomerate, and possibly ignimbrite.

(a) Pitchstone breccia. This is formed at the contact between the Alford Rhyolite and the Surrey Hills Tuff, on the western flank of Mt Alford. The breccia generally passes up into pitchstone and is only developed where there is tuff.

(b) Pitchstone. This rock type probably represents the chilled margin of the overlying rhyolite, and possibly was formed only when the rhyolite came into contact with wet sediments (tuffs). It is usually flow-banded. The thickness

of the pitchstone zone at GR 966491 is greater than 10 m and it has cubic columnar jointing with sides approximately 1 m in width. Cubic columnar joints have been reported for ignimbrites (Ross and Smith, 1961) and for other volcanic rocks (Rittmann, 1962). The possibility that some of the pitchstones on Mt Alford were formed from welded or fused tuff cannot be excluded.

(c) Domes. The main body of Mt Alford was formed by coalescing rhyolite domes. It is not clear from the field evidence how many domes there are, and possibly, as at Mt Somers, Mt Alford was formed by a continuous process of endogenous and exogenous growth along a fissure. This elongated fissure continues to the north of Mt Alford where a smaller rhyolite extrusion took place. Once again tuff underlies this rhyolite, with pitchstone at the contact. It can be deduced from the relation of the bedded tuff to the rhyolite domes that the initial phase of rhyolitic activity was explosive, resulting in ash showers which were subsequently redeposited as sediments, possibly in the craters or depressions left at the vent. This was then followed by a quiet extrusive phase when the rhyolite domes were formed.

(d) Rhyolite agglomerate. This is not common on Mt Alford, but does occur opposite Diamond Creek at GR 957503 and on the south-west corner of Mt Alford at GR 964492. At the first of these localities the agglomerate is flow-banded with an angular blocky fracture and has the appearance of an autoclastic breccia. The second locality is composed of angular blocks of flow-banded rhyolite up to 1 m across but

more typically less than 20 cm in diameter.

(e) Ignimbrite. This is difficult to identify positively, owing to the absence of definite shard texture in the rhyolite. The only localities found at Mt Alford where the rhyolite has a similar texture in thin section to the ignimbrite of Mt Somers are near the "Diamond Fields" (GR 956505) and at the summit of Mt Alford (GR 976506). In both these cases the rhyolite has what superficially appears to be flow banding. In thin section this banding is made up of aggregates of dark and light coloured, discontinuous, glassy shreds, often with ragged ends, and draped over phenocrysts as would be expected in a compacted, welded tuff. Other evidence to support a welded ash-flow origin is the presence of angular fragments of phenocryst minerals (quartz and sanidine). If this rhyolite does represent welded ash-flow deposits (i.e. ignimbrites) then the trace element chemistry restricts it to the same eruptive sequence as the other rhyolites of Mt Alford which is quite distinct from the ignimbrite of Mt Somers and the Rakaia Gorge.

2.2.2.4 Petrography

The Alford Rhyolite consists of phenocrysts of quartz and sanidine which total 15 to 20% of the rock. Generally sanidine is slightly more abundant than quartz. Both phenocryst minerals occur as rounded subhedral grains 1 to 1.5 mm in diameter. The quartz also occurs as rounded bipyramids. In a few places the phenocrysts are fragmented.

The sanidine is typically untwinned and unzoned with no exsolution features visible in thin section. Embayment structures in both the quartz and the sanidine phenocrysts were observed in some specimens. Biotite is rare, and absent from many of the samples. When it does occur, it is strongly pleochroic from red to brown. It is usually partially, or wholly, replaced by an opaque granular mineral (possibly magnetite). The groundmass is of devitrified glass with a microfelsitic texture. Flow banding is subdued and visible in thin section by concentrations of a granular opaque mineral (probably hematite). No garnet is present in this type of Alford Rhyolite.

The rhyolite on Mt Alford that does contain occasional garnet, occurs as a fresh rhyolite without the red hematite alteration so typical of the dominant type of rhyolite described above. In addition to the usual quartz and sanidine phenocrysts, this garnetiferous rhyolite contains small angular fragments of phenocryst minerals in a strongly flow-banded matrix. The appearance is similar to that of the ignimbrite on the top surface of Mt Somers (although it is chemically distinct from that ignimbrite).

The pitchstone of Mt Alford typically has subhedral to anhedral quartz and sanidine phenocrysts 0.5 to 1 mm in diameter. Fractured phenocrysts have been concentrated, during the flow of this rapidly chilled rhyolite, to form zones of small fragments which contribute to the flow-banded texture seen in the pitchstones. As with the other Alford Rhyolites, plagioclase phenocrysts are very rare. Occasional fragments

of garnet are present. The groundmass of the pitchstone is glassy with fine needle-like crystallites oriented in the direction of the flow.

Accessory minerals in the Alford Rhyolite are zircon, ilmenite, and apatite.

2.2.2.5 Relation to Underlying Rocks

The Alford Rhyolite unconformably overlies Torlesse rocks, and conformably overlies the Surrey Hills Tuff. The Torlesse rocks are baked and altered red by hematite for distances of 3 to 7 m from the contact. All the exposed rhyolite/Torlesse contacts along the eastern flank of Mt Alford show this alteration. The rhyolite generally has good columnar jointing perpendicular to the contact surface, and also flow banding which is variable in direction, but commonly sub-parallel to the contact.

At GR 977511 and 973517 a pitchstone, formed from fused bedded tuffs, occurs between the columnar-jointed rhyolite and the Torlesse rocks. This pitchstone shows the well sorted texture characteristic of the water-laid Surrey Hills Tuffs. Confirmation that the pitchstone has originated by the fusing of sedimentary tuffs is shown by the texture seen in thin sections. In these two localities the Torlesse sandstone and siltstone underlying the fused tuff were also baked for a distance of 7 m from the contact.

At other localities where the rhyolites overlie tuffs a pitchstone has formed at the contact (GR 983507, 983505, 983504, 991500, 954545 and 961527).

On the western flank of Mt Alford (at GR 961512, 970498 and 960493) the contact between pitchstone and tuffs is gradational from tuff, through pitchstone blocks imbedded in tuff, to pitchstone. This is a result of the chilled pitchstone being brecciated and intermixed with the underlying tuffs during movement along the contact at the time of emplacement of the rhyolite.

In one locality (GR 963504), 200 m thick columnar-jointed rhyolite overlies 20 m thick bedded tuffs without the formation of pitchstone, or fusing of the tuffs. At this locality Torlesse sandstone and siltstone detritus form a lens, of 5 m maximum thickness, between the rhyolite and the tuff. These sediments have been superficially altered red by hematite.

2.2.3 Graham Dolerite

The dolerite is named after Grahams Creek which is a tributary of Taylors Stream. On the ridge above Grahams Creek there are extensive dolerite outcrops.

2.2.3.1 Definition

The Graham Dolerite occurs as a porphyritic intrusive sill in the bedded deposits of the Surrey Hills Tuff. It is typically hollocrystalline with sub-ophitic plagioclase and hypersthene and interstitial pigeonite. The chemical composition of the dolerite is that of a saturated tholeiitic basalt

although the volatile-free composition lies on the boundary between basalt and andesite.

The type locality for the dolerite is the same as for the Surrey Hills Tuff which it intrudes. This is in the gully, east of Mt Alford trig station at GR 984504.

2.2.3.2 Distribution

The dolerite only crops out in localities along the margin of the Alford Rhyolite where bedded tuffs also occur. This could be explained by the possibility that the dolerite took the weakest line of resistance to the surface, i.e. where the unconsolidated tuffs underlay the rhyolite domes. Alternatively its position could equally well be explained by the tuffs being deposited in primary-phase craters, the conduits of which were used for the passage of all the volcanics (including the dolerites) of this area.

Dolerite was extruded only on the north-east side of the Alford Range, although Speight (1938, p32) considered that a small outcrop west of Taylors Stream (at GR 956506) was dolerite; but in thin section this rock is the same as the adjacent intermediate volcanics which are petrographically and chemically identical to the Hinds River Dacite, and it is therefore not dolerite.

The dolerite occurs at two distinct levels, in the Surrey Hills Tuff at the type locality. On the ridge north of this locality (GR 986507) a very thin veneer of dolerite, overlying tuff and Torlesse rocks, occurs as a series of stepped outcrops down the ridge. These are presumably due

to a series of blocks down-faulted towards the North Branch of the Ashburton River. At this locality, and at some of the other localities where the dolerite crops out (e.g. GR 990501, 962533, 996496), the dolerite is not capped by tuff and rhyolite as these have been removed by erosion. Evidence that this has occurred is found at the northern end of the locality north of Mt Alford (at GR 957537), where a down faulted block of dolerite in the saddle intrudes tuff. The overlying tuff is preserved by a thin covering of rhyolite. Speight (1938, p31) has described this section in more detail.

2.2.3.3 Eruptive Form

The Graham Dolerite occurs on the east flank of Mt Alford, at GR 985504, as concordant sills with subparallel sides. At this locality two dolerite sills occur in the sequence of tuff beds (Figure 7).

In other localities on Mt Alford (e.g. GR 990501, 962533) the dolerite forms small laccoliths.

On the south-east corner of Mt Alford (GR 996496) the dolerite crops out over a large area (see Map 1) and is columnar jointed near the upper contact with the Alford Rhyolite.

2.2.3.4 Petrography

The dolerite is typically holocrystalline with large (1 to 2 mm) phenocrysts of twinned plagioclase (andesine-labradorite) intergrown with hypersthene and pigeonite, forming

a sub-ophitic texture. In thin section both the hypersthene and the pigeonite are colourless. In the coarser-grained dolerite, hypersthene phenocrysts are subordinate to those of pigeonite, but in the finer-grained dolerite the converse is true, the pigeonite occurring as small interstitial crystals. The latter case is seen in the chill margins, and in thin dolerite sills. Olivine is only very rarely present as small ophitically enclosed crystals in plagioclase clusters.

Chlorite and cryptocrystalline quartz fill small vesicles in the dolerite near the upper contacts with the tuff. Some of these vesicles have hemispherical glass structures protruding into them that are similar to those seen in the early stages in the formation of segregation vesicles as described by Smith (1967). Such segregation vesicles have been explained as being formed by an increase in confining pressure, but contraction of the gases in the vesicles, during cooling, could explain the small structures in these vesicles.

The thinner sills of dolerite have dark brown interstitial glass between the plagioclase laths as a result of the more rapid cooling undergone by these sills.

2.2.3.5 Relation to Underlying and Overlying Rocks

The dolerite sills are concordant with the tuff beds. Laccolith-like outcrops of dolerite are exposed only where at present there is no overlying rhyolite and it seems probable that they formed in response to a low confining pressure under

a thin covering of tuff and rhyolite which has since been removed by erosion.

The dolerite at the south-east corner of Mt Alford intrudes the contact between the Torlesse rocks and a rhyolite coulee, although the contact is obscured by debris. Part of this exposure could be an extrusive flow.

Where the dolerite is in contact with the rhyolite tuff, the tuff is baked. The upper contacts of the dolerite have small vesicles filled with agates, as a result of silica-rich water derived from the tuff penetrating the dolerite.

2.2.4 Barrosa Andesite

This andesite is named after Mt Borrosa, the highest point on the Clent Hills, which is capped by andesite flows extruded from dikes near the summit.

2.2.4.1 Definition

The andesite is variable in appearance. The colour is generally black to light grey, but red and green hydrothermally altered andesite also occurs. The texture varies from porphyritic to aphyric but generally the rock has phenocrysts of plagioclase and hypersthene in a hyaloophitic groundmass.

The type section is from the southern corner of the Clent Hills by the Ashburton Gorge Road (GR 760424), to the summit of Mt Barrosa (GR 762458). The exposure in this

section is discontinuous and individual flow boundaries are indistinct. The section represents a thickness of at least 500 m of flows and tuffaceous andesite.

A reference section is defined from the western contact of the andesite with the Somers Rhyolite south of Blue Duck Stream (GR 787447), to GR 763449. This section represents the uppermost flows on the Clent Hills.

Additional reference localities are designated near Morgan Stream at GR 857479 and GR 865486. The reason for having these reference localities is the unresolved relations of these volcanics which renders the interpretation of the stratigraphic order of the sequence of eruptions difficult. It is possible that the andesite in the vicinity of Morgan Stream belongs to two or more periods of volcanic activity, one of which may, or may not, correspond to the period of volcanism on the Clent Hills.

These andesites, together with the dacite of the Hinds River - Gawler Downs region, were referred to as melaphyres by previous workers such as Haast (1872, 1877, 1879) and Cox (1877, 1884a).

2.2.4.2 Distribution

The Barrosa Andesite covers much of the Clent Hills (Map 1). Near the summit of Mt Barrosa there are flows with low angles of inclination, which has resulted in a flat top surface on the Clent Hills. To the east of the summit, near the contact with the Somers Rhyolite, the flows dip up to 50°

to the east and strike at 010°. The flows also crop out on the south side of the Ashburton Gorge at Edendale, and are well exposed at GR 782414.

Andesite flows are exposed in the southern bank of Sandrey Stream from GR 769417 to GR 760410. The most southern occurrence of Barrosa Andesite is in Blondin Creek, (GR 808397) near Inverary Station Homestead.

Barrosa Andesite crops out between the Winterslow Range and Mt Somers in the region of Woolshed Creek and Morgan Stream (Map 1).

2.2.4.3 Eruptive Form

The Barrosa Andesite consists of flows, tuffs, agglomerates and dikes.

(a) Flows make up possibly 80%, or more, of the volume but, as much of the topography is subdued and heavily vegetated, this is only an estimate. The flows vary in thickness from 2 m to greater than 15 m, and many have well formed columnar joints which are generally less than 10 cm in diameter. The columnar jointing is commonly seen as polygonal (dominantly hexagonal) cracks on exposed joint surfaces that are parallel to the flow surface. A well formed curved set of columnar joints in a thick flow can be seen in the Clent Hills at GR 758439.

Other andesite flows on the Clent Hills are non-jointed, blocky, or rubbly. Where the flows are vesicular, secondary deposits of chalcedony varieties, and occasionally calcite, occur. Flow banding is only rarely visible in these andesites.

At the summit of Mt Barrosa, and to the west, the andesite flows are nearly horizontal. Flows exposed in the Ashburton Gorge near the road (GR 860425) have a dip of 20°E and a strike of 340°, while further to the east, near the contact with the Somers Rhyolite, they dip at 50° to the east with a strike of 360°. At the northern margin of the andesites on the Clent Hills, the dip of the flows is to the north-east.

Andesite flows also occur in the region of Morgan Stream (Map 1). Indistinct flows occur on the ridge between Morgan Stream and Woolshed Creek (GR 856492). In other outcrops at this locality distinct flows are not visible. These andesites also have secondary amygdules of silica minerals.

(b) Thin andesite tuff and altered scoriaceous layers alternate with flows. These are generally altered to red and green clay minerals.

(c) Andesite agglomerate crops out at GR 783445, 783441, 780415, 784456. The localities on the Clent Hills and by the "Coal Reserve" on the south bank of the South Branch of the Ashburton River probably belong to the same event. From the limited exposure of the agglomerate it appears that it forms a single flow unit composed of andesite blocks up to 30 cm in diameter, in an andesite matrix.

Andesite agglomerate also occurs in the north-west region of Mt Somers (GR 855480, 839491) where it could be a vent agglomerate as the lateral extent of the outcrops is very limited, and is adjacent to dikes of andesite and rhyolite.

(d) Andesite dikes occur in several localities on the south-west side of the Clent Hills. On the southern point of the Clent Hills (GR 760425, 761424) two distinct dikes crop out. These have horizontal columnar joints and appear to have fed flows or sills above. Dikes are also present south-west of the summit of Mt Barrosa (GR 759457) where they exhibit good columnar jointing (Figure 10). A dike-like outcrop of andesite also occurs 300 m north of the summit of Mt Barrosa, but displays vertical columnar jointing and is therefore more likely to be part of a flow. Dikes with elongated vesicles crop out at GR 749474 and 750477, near the top surface of the Clent Hills.

Andesite with nearly vertical flow banding above Morgan Stream (GR 867485), and a thin tongue of glassy andesite exposed in Woolshed Creek (GR 849492), could also be dikes. A distinctive dike of aphyric andesite also occurs in Woolshed Creek and Morgan Stream. This east-west trending dike has a characteristic platy jointing (Figure 11).

Outcrops of porphyritic andesite occur between two rhyolite domes north of the Blue Duck Stream (GR 796448). Structural contours of the contact between the rhyolite and the andesite indicate that it is unlikely that the andesite outcrop is an inlier. However, the apparent width of the outcrop (approximately 40 m) makes it unlikely that it is an intrusive dike. The problem is unresolved.

Figure 10. Columnar jointing in Barrosa Andesite near the summit of Mt Barrosa.

Figure 11. Platey jointing in a dike of Barrosa Andesite near Morgan Stream.

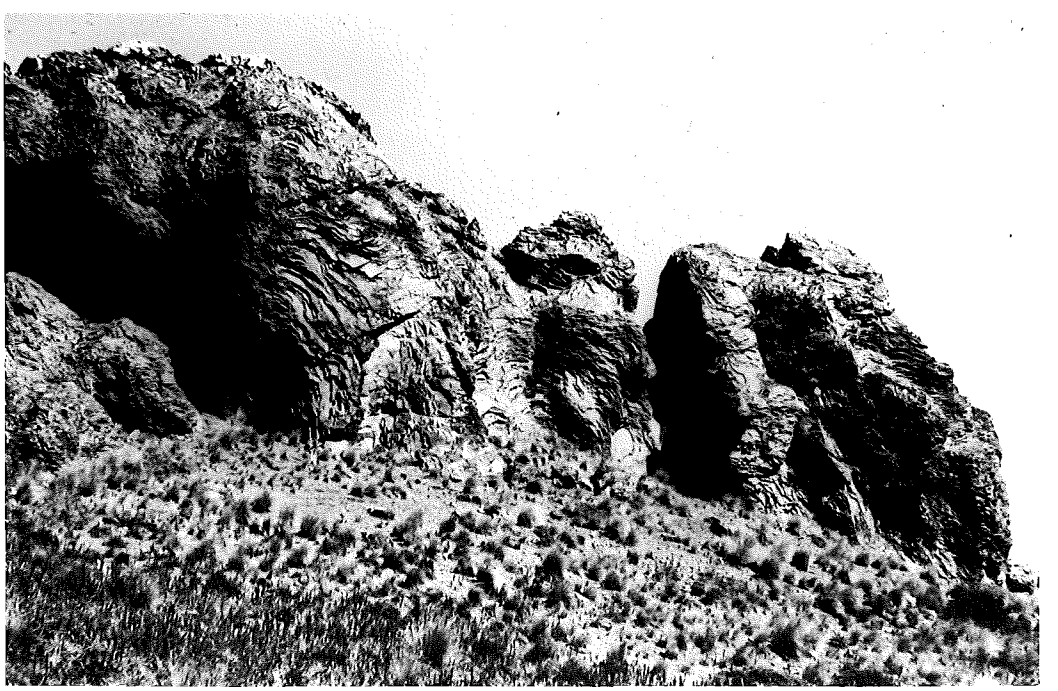

2.2.4.4 Petrography

The Barrosa Andesite is generally porphyritic with subhedral to euhedral plagioclase phenocrysts 0.5 to 1.5 mm in diameter. There are three main types of groundmass texture with gradations between them, hyalopilitic, hyalo-ophitic, and subophitic.

The andesites with hyalopilitic and hyalo-ophitic texture are made up of 5 to 10% andesine and up to 2% hypersthene phenocrysts. The hypersthene occurs as subhedral crystals 0.3 to 0.5 mm in length, usually equant, but also lath-shaped. Clusters of plagioclase and hypersthene with ophitic texture are also present (Figure 12). The hypersthene is colourless and therefore non-pleochroic and lies in the hypersthene-ferrohypersthene composition range. It is occasionally rimmed with pigeonite, which also occurs as small (<0.2 mm) micro-phenocrysts in some samples. Rare grains of olivine with, and without, alteration rims, are occasionally present. Ilmenite and magnetite are present in minor amounts.

Xenoliths of sandstone up to 6 mm in diameter, and similar to those commonly found in the Hinds River Dacites are also present. No garnets were seen in these xenoliths in the thin sections examined. Xenoliths of a coarse grained ophitic textured andesite occur in most samples.

The andesites with subophitic texture are similar in mineralogy to those described above, but in addition they have a high proportion (up to 15%) of lath-shaped labradorite phenocrysts (2 to 4 mm in length). Labradorite laths (An_{50}-An_{62}), with interstitial glass and pigeonite, form a subophitic groundmass.

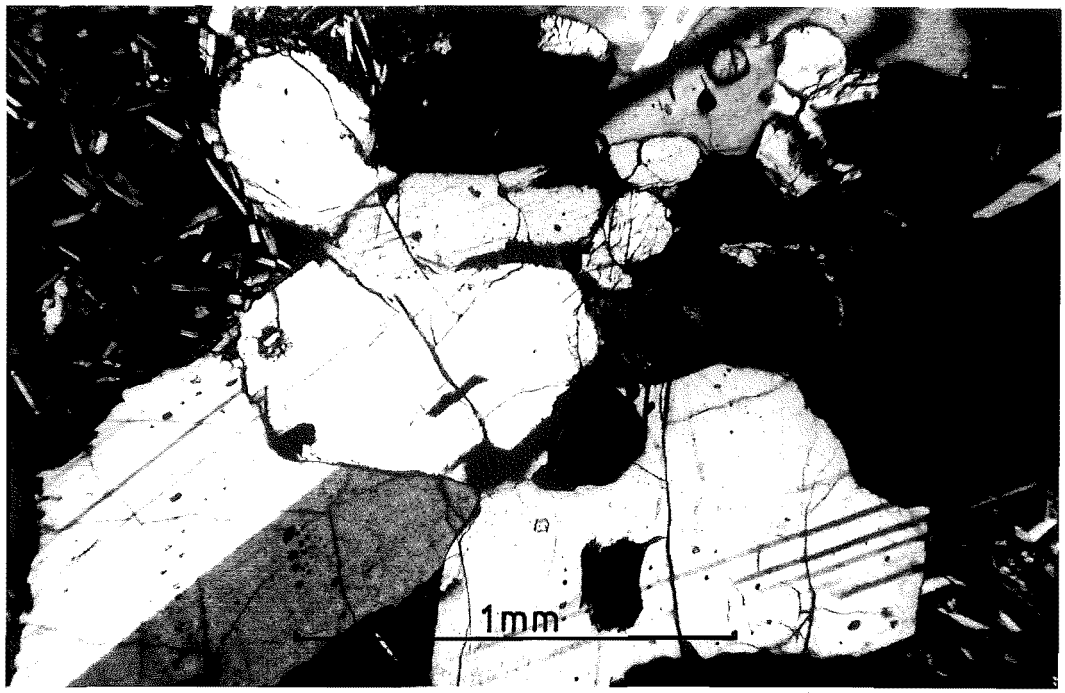

Figure 12. Photomicrograph of subophitic clusters of plagioclase and orthopyroxene in Barrosa Andesite (crossed polarisers).

Figure 13. Photomicrograph of typical hyalopilitic andesite containing plagioclase and orthopyroxene phenocrysts with partial resorption (crossed polarisers).

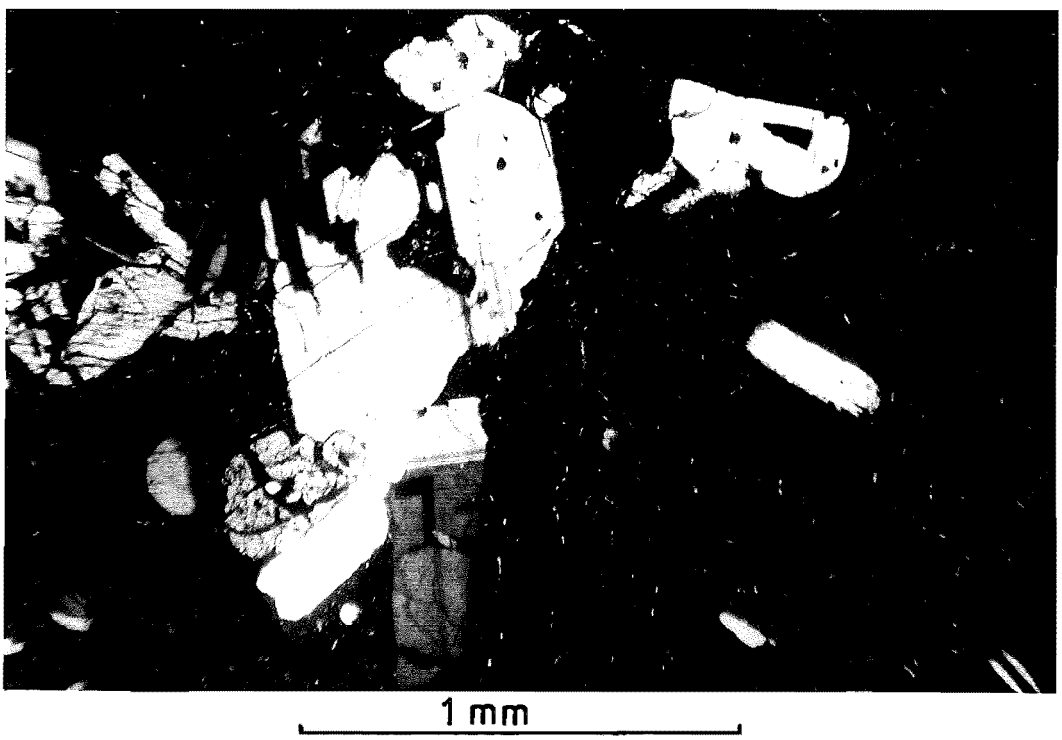

The andesites in the Woolshed Creek/Morgan Stream area, north-west of Mt Somers, have a fine-grained hyalopilitic texture (Figure 13). The plagioclase phenocrysts in these rocks are between 0.3 and 1 mm in diameter and are subhedral. Honeycomb structure is common in the zoned plagioclases. Sedimentary xenoliths have completely recrystallised to form feldspar crystals with an equant, euhedral, granular texture. Hypersthene occurs as rounded grains, generally less than 0.2 mm in diameter. Very rare pigeonite grains (0.1 to 0.2 mm) are also present.

A very characteristic feature of the Barrosa Andesite is the occurrence of amygdules of various forms of silica. Secondary deposits of the silica minerals occur both in veins and as infillings of vesicles in the andesite. The vesicles are typically lined with layers of agate, the centre of which is filled with one or more of the following: further bands of agate; onyx; moss agate; prase; plasma; macro-crystalline quartz (colourless, amethyst, green); white, green, brown, red, and black, opaque to transparent opal. (For definitions of various varieties of cryptocrystalline quartz used, see Appendix I). Other minerals that fill vesicles include calcite, chlorite and alteration products, and rarely zeolites. The size of the infilled vesicles ranges from less than 1 mm to greater than 1 m. Where the vesicles are small (< 1 cm) they are spherical to subspherical in shape. Larger vesicles have been flattened by the pressure of overlying lava flows, and/or have been elongated in the direction of flow, such that they are rounded at one end and drawn out to a point in the direction

of flow (hence the term amygdule - "almond-shaped"). The distortion of the vesicle occurred before any crystallisation of minerals in these cavities. The vesicles have clearly formed by the coalescing of small gas bubbles, which has resulted in a pitted surface texture on the amygdules. Rare flattened disc-shaped agates were found with spiral-shaped elongated casts of bubbles, radially oriented on their surface, indicating that the vesicles formed by the coalescing of small vesicles less than 2 mm in diameter with the larger (about 10 cm diameter) vesicles that were, at the same time, being rotated by the movement of the lava.

Hollow geodes are not common in agates from the Clent Hills area. Agates with their centre filled with calcite occur, which result in hollow geodes when the calcite has later been dissolved.

The agates from this area are predominantly horizontally banded, the bands varying from microscopic thickness to several centimeters thick. The number of bands in a vesicle is unrelated to the size of the amygdule.

Similar agates in andesites have been recorded in many parts of the world. Ingerson (1953) describes large amygdules in andesites from the southern Quitman Mountains, Texas, where he concludes that they have formed along with other secondary minerals from silicious solutions at a temperature of about 100°C. It is not as yet known at what temperature the agates in the Barrosa Andesite were formed but their distribution in the sequence of flows indicates they were formed when the flows were cooling. Only in fragmented blocky flows can the agate amygdules be related to veining.

Very often flows above and below an amygdule-rich flow, will contain no agates.

The agates have a useful structural application. Parallel agate bands were formed perfectly horizontal. They often have a thin white amorphous film on the upper surface of each layer. This has resulted in parting-planes along these surfaces. Thus, in the larger agate amygdules, a surface can be found on which a strike and dip of the agate can be obtained. When only small (less than 1 cm) agates were present, apparent dips were taken on cross sections of several of the small amygdules and the true dip obtained from these apparent dips. The banded agates act as an internal tiltmeter indicating the extent of tilting since the agates crystallised. Multiple phase tilting and rotational tilting obviously cannot be discriminated, but this does not negate the usefulness of the agates.

2.2.4.5 Relation to Underlying Rocks

The Barrosa Andesite unconformably overlies Torlesse sediments along its western margin on the Clent Hills. The contact beneath the summit of Mt Barrosa and around the top of Waterfall Stream, extending to the western extremity of the andesite, is nearly horizontal. The andesite flows here total approximately 100 m in thickness, and are parallel to the contact. The northern contact with the Torlesse rocks is straight (see Map 1), which implies the contact is faulted. However, at GR 758480 the sandstone adjacent to the vertical

contact is intensely baked for a distance of 20 m from the contact. This is also true at GR 746479. It would thus seem that the lava flowed along, and was constrained by, an existing fault scarp in the Torlesse basement rock. Alternatively the faulting could have occurred concurrently with the extrusion.

South of the Summit of Mt Barrosa, the contact of the andesite with the Torlesse rocks, is irregular, with an average apparent dip of 15° to the south-east. Here the flows have a dip of 22° to the north-east and strike at 338°.

At GR 759481 on the northern margin of the andesite in the Clent Hills, coal measures are exposed, in the bank of a small creek, that topographically underlie the andesite. The exposure is small and its stratigraphic position cannot be determined with certainty.

The andesite in the Woolshed Creek/Morgan Stream region unconformably overlies Torlesse rocks, except for a small outcrop west of Morgan Stream (GR 867485) where it overlies rhyolite tuff of the Surrey Hills Tuff. At the contact the tuff has been baked by the andesite.

The relations between the Barrosa Andesite and the Somers Rhyolite are discussed below.

2.2.5 Somers Rhyolite

This formation is named after Mt Somers, which is composed entirely of rhyolite.

2.2.5.1 Definition

The Somers Rhyolite is composed of acid porphyritic rhyolite with phenocrysts of bipyramidal quartz, and sanidine, in a devitrified micro-felsitic groundmass. Garnet and biotite occur as minor minerals but are not ubiquitous. The rhyolite is white to grey in colour. Only rarely is it altered to red by hydrothermal alteration. Black glassy pitchstone occurs where the rhyolite has chilled rapidly. Pitchstone that has been formed by intensive welding of tuff (ignimbrite) is also found.

The term pitchstone is used to describe a porphyritic obsidian-like rhyolite with up to 10% water and a resinous lustre in hand specimen (Williams *et al.*, 1954, 122). This contrasts with obsidian, which has a vitreous lustre. The fracture of pitchstone is hackly and irregular, in contrast to the conchoidal fracture of obsidian. Pitchstone is commonly characterised by crystallites in the groundmass, as for example that of Arran (Hatch *et al.*, 1972, p245). Definitions that distinguish between obsidian and pitchstone on the basis of water content are not suitable, as the pitchstone in the Mt Somers area varies between 0.74 and 4.13% total water content, with an average of 3.92%. In addition there is no distinction in hand specimen, thin section, or chemistry, between pitchstone of high and low water content. The term pitchstone has been used by previous workers in this area (Haast 1877, 1879; S. H. Cox 1877, 1884a, 1884b; P. T. Cox 1926; Speight 1928, 1938).

The rhyolites of Mt Somers were referred to as quartz porphyries by previous workers (see section 2.4.1 for a discussion of this).

Two reference localities have been chosen. One is at GR 828454, in the gorge of Woolshed Creek. Here the basal sequence is of partly welded white, yellow, and green ash-flow tuff (i.e. ignimbrite), passing up into a pitchstone and tuff breccia, and then into a pitchstone. The pitchstone is overlain by a columnar-jointed rhyolite dome. The second reference section, from GR 871478 to 874470 on the north face of Mt Somers, is a sequence of ignimbrite flows (sheets) made up of at least 25 units. The actual number may be many times this, as each discrete unit appears to be made up of several thinner ash-flows welded together. These ignimbrites overlie the domes, and represent the uppermost stratigraphic units in the formation.

2.2.5.2 Distribution

The Somers Rhyolite forms the main mass of Mt Somers and Cox Hills. It extends from Duke Knob in the east, to the Clent Hills in the west. Small outcrops of rhyolite occur as inliers in the valley of the South Branch, Ashburton River (at GR 822416, 822411 and 814428). Rhyolite crops out along the base of Woolmers Hill where it is overlain by glacial outwash gravels with a thickness of up to 130 m. No Somers Rhyolite has been found south of Blondin Creek.

2.2.5.3 Eruptive Form

The Somers Rhyolite can be subdivided into tuffs, domes, plugs, dikes, agglomerates and "flows".

(a) Tuffs are not common in the area due to the post-Cretaceous erosion.

Consolidated, partly welded, green, yellow, and white, unsorted tuffs crop out in Woolshed Creek (GR 827454) opposite the old incline to the "burning coal mine". These tuffs contain cognate xenoliths of dark grey, flinty, aphyric rhyolite, and are overlain by pitchstone, which in turn is overlain by a rhyolite dome. The contact of the tuffs with the pitchstone is indistinct as it has a rubbly transition zone of blocks of pitchstone in a matrix of tuff.

A tuffaceous rhyolite occurs at Duke Knob (GR 924457). This is a yellow-brown weathered tuff that occurs on both sides of Bowyers Stream, and overlies andesite. The tuff occurs both as an aphyric type and as a porphyritic type. The extent of each type is unknown because of the thick bush cover.

Rhyolite tuff also occurs near the end of the Burma Rd (GR 838480) where it is interbedded with unsorted pyroclastic ejecta.

(b) Domes, plugs, and dikes form complex cumulo-dome structures. Individual domes do occur, however, and have volumes of up to 0.2 km^3. Generally the domes are not isolated forms but result from multiple intrusion and extrusion. Such a form is well exposed on the eastern end of the north-east face of Mt Somers (Figure 14).

Individual rhyolite dikes and plugs can be seen (Figure 15) intruding andesite in the area around Morgan Stream (Map 1,3).

The domes are characterised by well formed columnar joints that radiate out from the centre of the dome, perpendicular

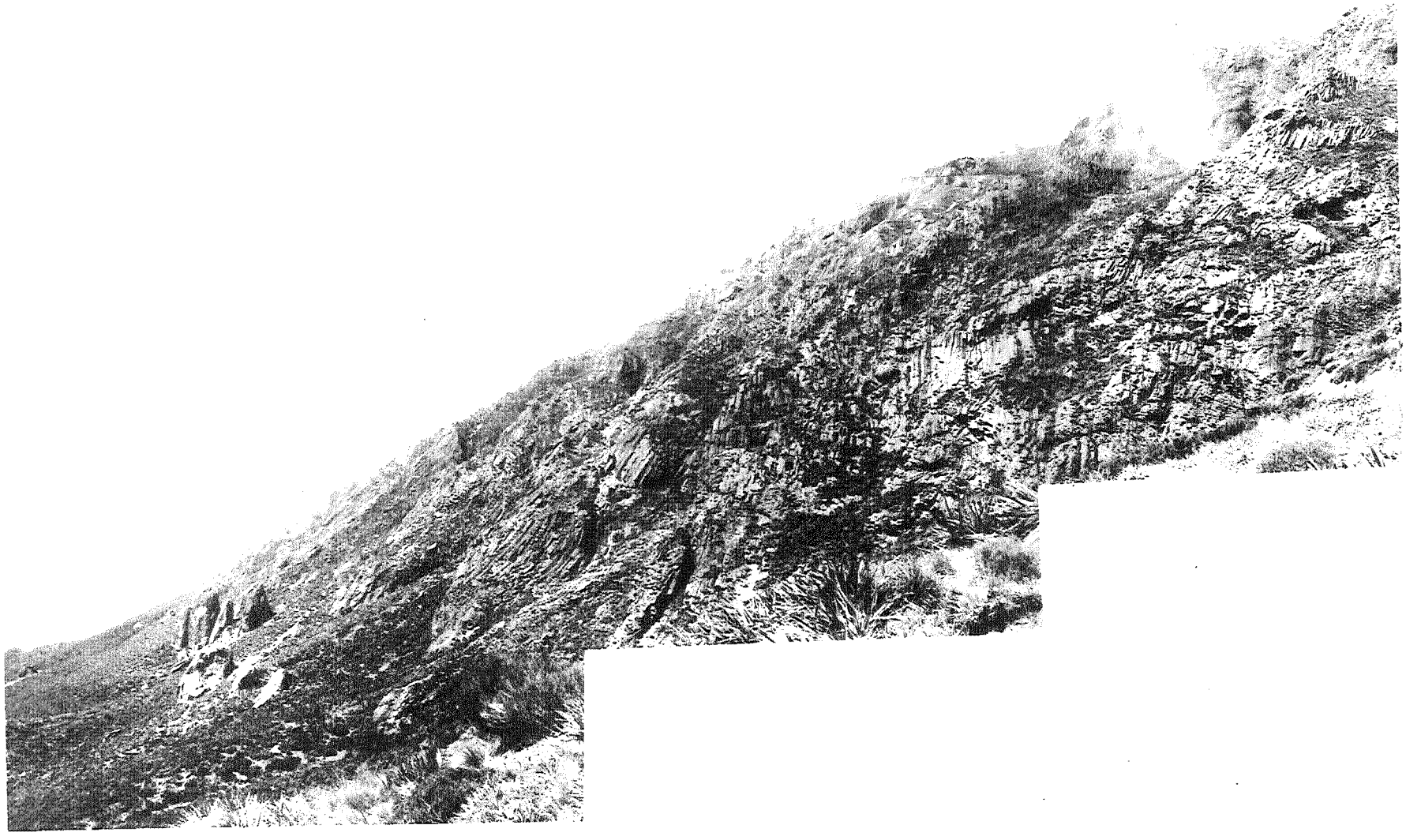

Figure 14. Columnar jointing in cumulodomes exposed in fault scarp on north face of Mt Somers.

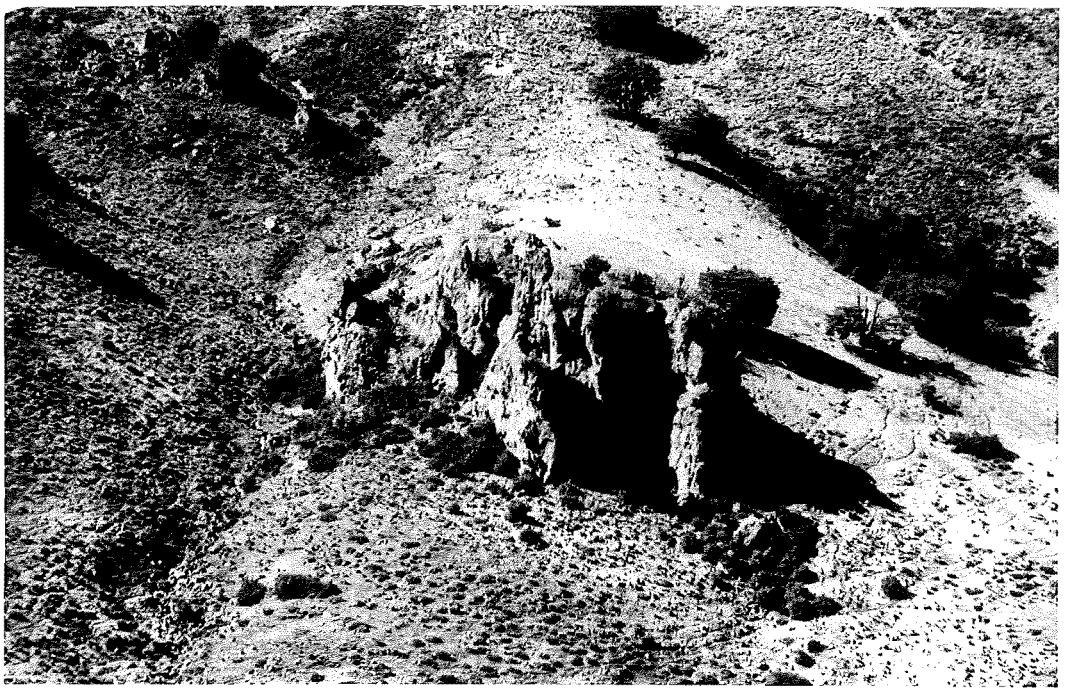

Figure 15. Eroded rhyolite plug on Mt Somers.

Figure 16. Typical columnar jointing in rhyolite cumulodomes of Mt Somers.

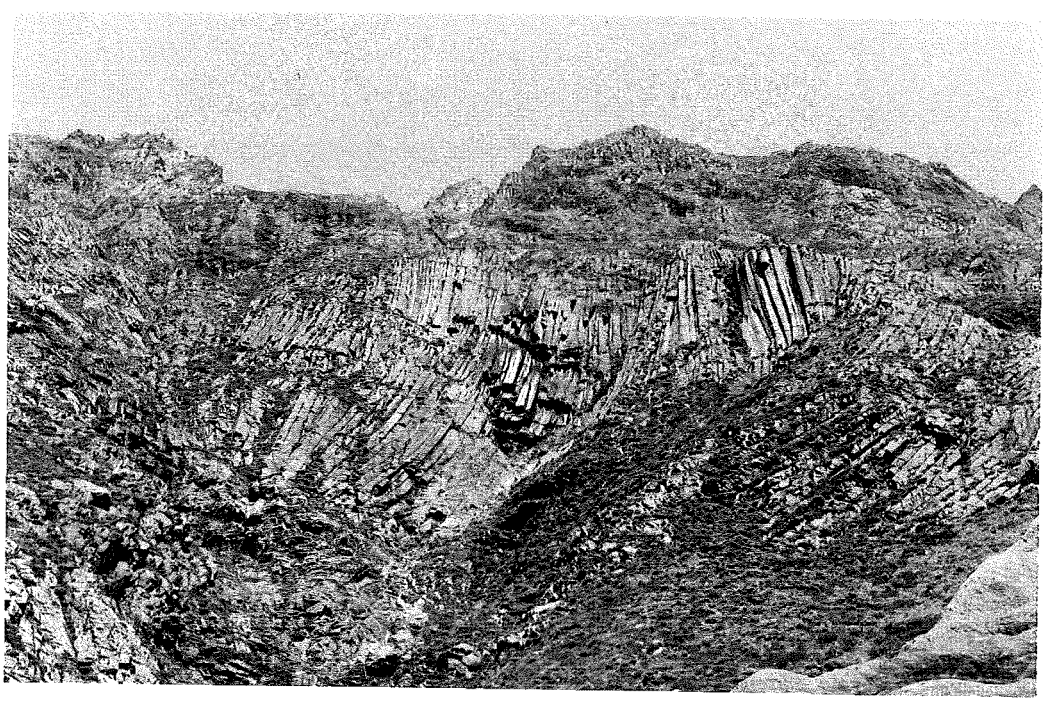

to the cooling surface. The columns range between ½ and 1 m diameter and can have lengths up to 50 m (Figure 16). The outer surface of the domes often display a secondary set of joints parallel to the cooling surface which in exceptional cases gives a layered appearance to the dome (Figure 17).

Rhyolite dikes generally have a flinty appearance. The most notable example being the dike situated on the northern side of the gully that extends from Morgan Stream to the saddle on the north side of Mt Somers (GR 859484 to 867481).

The most basic rock represented in the Somers Rhyolite is a black rhyodacite which is conspicuous in its form as a dike because of the red-brown oxidation that occurs on its exposed surface, which contrasts with the surrounding white-grey rhyolite. This dike is located on the north-east face of Mt Somers east of the saddle (GR 879477 to 877471) and is notably vesicular and glassy. Large blocks of light-coloured rhyolite from the wall rock were found as xenoliths in the dike. Where the dike is exposed on the top erosion surface of Mt Somers it can be seen to have trifurcated (Figure 18). Outcrops of dark green-black, rhyolite occur on the upper erosion surface of Mt Somers, south of where the dike cuts the surface, but lack of exposure prevents determination of the form of emplacement of this rock, and it could be a flow fed from the dike instead of an extension of the dike itself.

An unusual dike-like body of rhyolite occurs along the northern contact of the Somers Rhyolite with Torlesse rocks. The contact is a fault which can be seen as pug zones exposed in stream beds (GR 887473, 922458). The continuation

Figure 17. Section of rhyolite dome showing concentric layering and radial columnar joints. (Centre of dome on extreme left).

Figure 18. Dikes of rhyolite and rhyodacite cutting ignimbrites exposed on the northern face of Mt Somers (note figure for scale).

of this fault can be seen as pug zones to the west (GR 878470; 857487; 851483). The dike-like feature (Figure 19) generally stands as isolated outcrops but near the saddle on the northern side of Mt Somers it merges with the rhyolite domes (Figure 20). It is composed of crushed rhyolite that has been recemented. It does not have any distinctive jointing which has resulted in the relatively slow erosion and rounded form of the body. In contrast to this, the adjacent columnar jointed rhyolite breaks away in large blocks and erosion is relatively rapid (Figure 14).

The two most likely explanations for the origin of this rock are: (a) as a dike, (b) as a fault crush-zone phenomenon. It is conceivable that this linear feature is a vent-brecciated rhyolite dike - a feeder dike for the domes or flows of Mt Somers. It is completely sheared on a microscopic scale, which seems unlikely even for a vent phase rhyolite breccia. Also where this crushed rhyolite is in contact with the main mass of rhyolite there is a gradational, if somewhat rapid, change from finely sheared through coarsely sheared, to unsheared rhyolite respectively with increasing distance south from the known pug-zone. In addition there are two, and in places three, parallel crush zones occurring over a distance of 50 m from the contact, and all in rhyolite. Some horizontal layering is visible in some outcrops (Figure 20). Taken together with the microstructure of the feature, this is conv incing evidence against the feature being a dike. Additional evidence from crush zones in adjacent andesite in line with the known fault supports this point of view. The

Figure 19. Dike-like body of sheared rhyolite along faulted contact on northern flank of Mt Somers.

Figure 20. Sheared rhyolite along northern flank of Mt Somers with sub-horizontal layering (lower right).

andesites in Morgan Stream are extensively crushed in the region of the fault although they do not form a dike-like feature like that of the rhyolite. There is also an intensely crushed zone on the andesite/rhyolite contact, exposed in the bed of Morgan Stream, which is 50 m in width. All the features described are collinear and confirm the existence of a major fault zone along the northern face of Mt Somers.

(c) Agglomerates are not common in the Mt Somers area. A vent-phase agglomerate with vertical flow banding occurs between the Burma Rd and Woolshed Creek (GR 821441). This is composed of large blocks of rhyolite in a matrix of rhyolite. An unusual rhyolite agglomerate outcrops in the bed of Bowyers Stream (GR 921452), at its confluence with Tinstone Creek. The agglomerate is faulted against andesite. The extent of this multicoloured rhyolite agglomerate is not known, owing to the dense bush in the area. Blocks of silicified agglomerate up to 5 m in diameter are found in the stream at this locality, and undoubtedly have been derived from the fault scarp that forms vertical cliffs on either side of Bowyers Stream. This agglomerate would also appear to be a vent breccia, as it contains a variety of rhyolite blocks, including pitchstone.

A large area of agglomerate exists to the north of the confluence of Morgan Stream and Woolshed Creek in the region of the hut (GR 846482). The rhyolite at this locality is extensively weathered to clay, and it is not possible to tell positively whether it represents an agglomerate, or a volcanic conglomerate. No clasts other than of rhyolite

composition were observed, and the boulders of rhyolite were generally rounded, ranging up to 0.5 m in diameter. This agglomerate is overlain by andesite to the north and by rhyolite tuff and beds of unsorted pyroclastic ejecta to the south.

(d) Flows of rhyolite crop out on the erosion surface at the top of Mt Somers and on the western end of its north-east face. Here a continuous series of flows with vertical thickness of 450 m is exposed. The maximum lateral extent of the flows is 4 km, but most are exposed for only half this distance. The thickness of individual flows varies greatly. The thickest flow observed was approximately 30 m and the thinnest flow only 10 cm thick. Generally the flows have a thickness in the range of 2 to 10 m. The thin flows are difficult to account for, because the high viscosity of rhyolite would be expected to produce only thick flows. Also it would seem impossible that rhyolites of the composition of the Somers Rhyolite could form such thin flows over a distance of several kilometers. Viscosities calculated in a following section (2.5.2) give values for the coefficient of viscosity, η, between 10^8 to 10^9 poises at a temperature of 900°C, and 10^9 to 10^{10} poises at 800°C. These are values typical of rhyolite compositions. Walker (1973) gave a median length of 1.3 km, and an average thickness of 100 km for a lava flow of initial viscosity of 10^9 poises, and stated that the viscosity of the lava directly controls the thickness of the lava flow, while only indirectly controlling the length.

Walker (1973) further showed that of the possible factors controlling the lengths of lava flows (i.e. composition, initial viscosity, total volume, slope of ground surface, rate of effusion, and topographic constraints), the most significant factor is the rate of effusion. He showed from measurements taken from a number of observed lava flows of various compositions and flowing over slopes varying from 1° to 30°, that there was a direct correlation between lava length and the rate of effusion, the effect of the other factors being very small.

Measurements of rhyolite flow lengths indicate, however, that rhyolite can, under favourable circumstances, flow for considerable distances. The Star Mountain Rhyolite in Texas extends for at least 35 km from its source (Gibson, 1969). The lengths observed for the Somers Rhyolite flows are small in comparison. However, even with a high effusion rate it would seem improbable that flows of rhyolite as thin as 10 cm could travel the distances, observed at Mt Somers, without cooling rapidly.

The following possibilities could explain the thin flows of rhyolite observed on Mt Somers:

(i) The flows could be the result of large-scale lamellar flow, and the layering caused by stresses within a dome during endogenous growth.

(ii) The flows could be an extreme form of flow banding.

(iii) The flows could be ignimbrites.

Considering each of these possibilities:

(i) The possibility that the flow-appearance of the rhyolites could be formed by lamellar flow and/or shearing in a dome during extrusion is not consistent with the observed facts. It would be impossible to obtain over 30 individual parallel flow units 450 m in total thickness and extending horizontally for more than 2 km in a single dome. The outer surfaces of domes do contain such parallel layering (Figure 17), but these are of limited extent and form only a small part of the dome. They also usually show convex curvature, particularly on the outer margins of the dome.

The fragmented phenocrysts observed in these rhyolites could be explained by lamellar flow and shearing in a semi-solid rhyolite magma, but this was not observed on any significant scale in any of the known rhyolite domes at Mt Somers.

The "less welded" layers between each "welded" layer of rhyolite (Figures 21, 22) are also impossible to explain by lamellar flow within a dome.

(ii) Observations of flow banding in the rhyolite domes, plugs, and dikes, particularly those exposed on the eastern ridge of Mt Somers, indicate that the flow banding is a texture derived during the flow of a vesiculating rhyolite where the vesicles are stretched to an almost infinite extent. This stretching can occur to the point of total collapse of the vesicle. The dark bands of the flow texture represent non-vesicular glass, or totally collapsed bubbles. The lighter coloured bands represent stretched bubbles of submicroscopic thickness which reflect the light to give the pale-coloured

Figure 21. Sharp contact between thin ignimbrite flows on Mt Somers.

Figure 22. Part of the sequence of thin ignimbrite flows on Mt Somers.

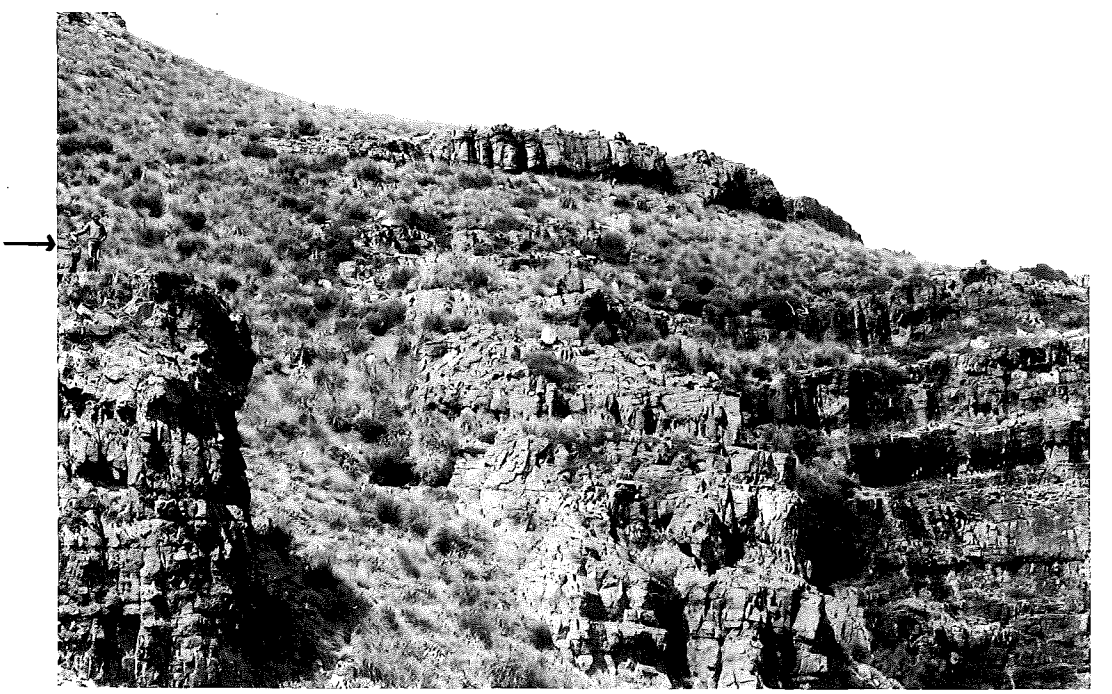

streaks. This process can explain even the thinnest of alternating light and dark bands observed.

If a process of vesiculation occurred in flowing rhyolite magma, the extended vesicles could become glide planes. With the large number of such glide planes present in a flow, the effective viscosity could be lowered considerably. It could therefore be argued that such a mechanism would account for the thin flows or rhyolite observed at Mt Somers. The "partially welded" zones between the flows would then represent zones of greater vesiculation and/or decreased stretching of vesicles.

Many authors, notably those in Russia (e.g. Vlodavetz, 1966; Petrov, 1966; Maleyev, 1966; Shirinian, 1966; and Adamian, 1966), consider that a vesiculating lava flow similar to that described above was responsible for certain volcanic rock types in Armenia. These rocks are referred to by these authors as "tuff lavas". The history of this term has been discussed by Cook (1966). "Tuff lavas" are regarded as distinctly flow rocks although all gradations between vesicular flows and true pyroclastic rock types exist, leading to confusion in terminology.

Locardi & Mittempergher (1967) consider that a post-eruptive vesiculation mechanism can result in ignimbrites, as well as flows and banded flows.

The main argument against the flows at Mt Somers being tuff lavas is the fragmentation of the phenocrysts and the lack of any vesicular forms which would be expected in near-source locations.

(iii) The main objection to the flows being ignimbrite (welded tuffs) is the absence of individual shards in many thin sections of these rocks. However, not all ignimbrite shows shard textures. In particular devitrification can obliterate shard structures, particularly in extremely welded tuffs (Ross and Smith, 1961; Rittmann, 1962; Keller and Villari, 1973). Welding of ignimbrite is usually accompanied by compaction and distortion of the shards, and if welding is intense then the shard texture can be completely eliminated. Rittmann, (1962, p81) described a flowed-ignimbrite (he termed it rheoignimbrite), which is well developed at Monte Amiata, in Tuscany, where it forms broad flat streams in the midst of a large ignimbrite sheet. The rheoignimbrite has no trace of welded glass shards but is completely homogeneous, although flow texture is common.

A further objection that could be raised to the flows on Mt Somers being ignimbrite is the intense welding of even the thinnest layers. However, Macdonald (1972, p162) described the Walcott Tuff, in Idaho, as a densely welded tuff although only 25 ft thick. Even thinner welded tuffs have been described by Walker (1962) from the Súlur Tuff, in Iceland, which is strongly welded where it is 2 ft thick. Gibson and Tazieff (1967) also described an ignimbrite which thins to 1 ft thick near its source, while still being welded.

Macdonald (1972, p161) stated that the minimum temperature of melting of "dry" glass shards is approximately 750°C, but in the presence of gases can be as low as 535°C. Even if the thin layers observed at Mt Somers did not contain

enough heat in themselves to ensure the welding process, the rapid succession of overlying tuffs would have provided enough heat and pressure for the welding to occur.

Thus it can be seen that the two main objections to the flows being ignimbrite can be readily accounted for.

The evidence for the layered rhyolite being ignimbrite is:

(i) The extremely thin layers observed (which are inconsistent with the rhyolites having formed as true flows). (Figures 21, 22).

(ii) The constant thickness of each layer over distances of several kilometers (Figure 23).

(iii) The flat- lying form of the layers and the planar form of the upper surfaces of the flows (Figure 24).

(iv) Angular fragments and shattered phenocrysts together with many very fine angular phenocryst-fragments in the groundmass. (This is inconsistent with a normal flow mechanism as seen in similar rhyolites that form dome structures in the area).

(v) Pitchstone at the base of the flows at GR 856483, Morgan Stream (GR 854484), and in a fault-angle depression in Woolshed Creek (GR 848486), show a distinctive weathering pattern on its surface that confirms that this rock is an ignimbrite. The weathered surface of these pitchstones reveals lenticular fiamme structures of pitchstone that stand out black against the groundmass which weathers white. When a fresh surface of this pitchstone is exposed it is uniformly black with the fiammes no longer visible (Figure 25). This eutaxitic texture is visible only on weathered surfaces. An identical

Figure 23. Ignimbrite flows extending over a distance of 1.5 km.

Figure 24. Flat erosional surface of Mt Somers sub-parallel to ignimbrite flows.

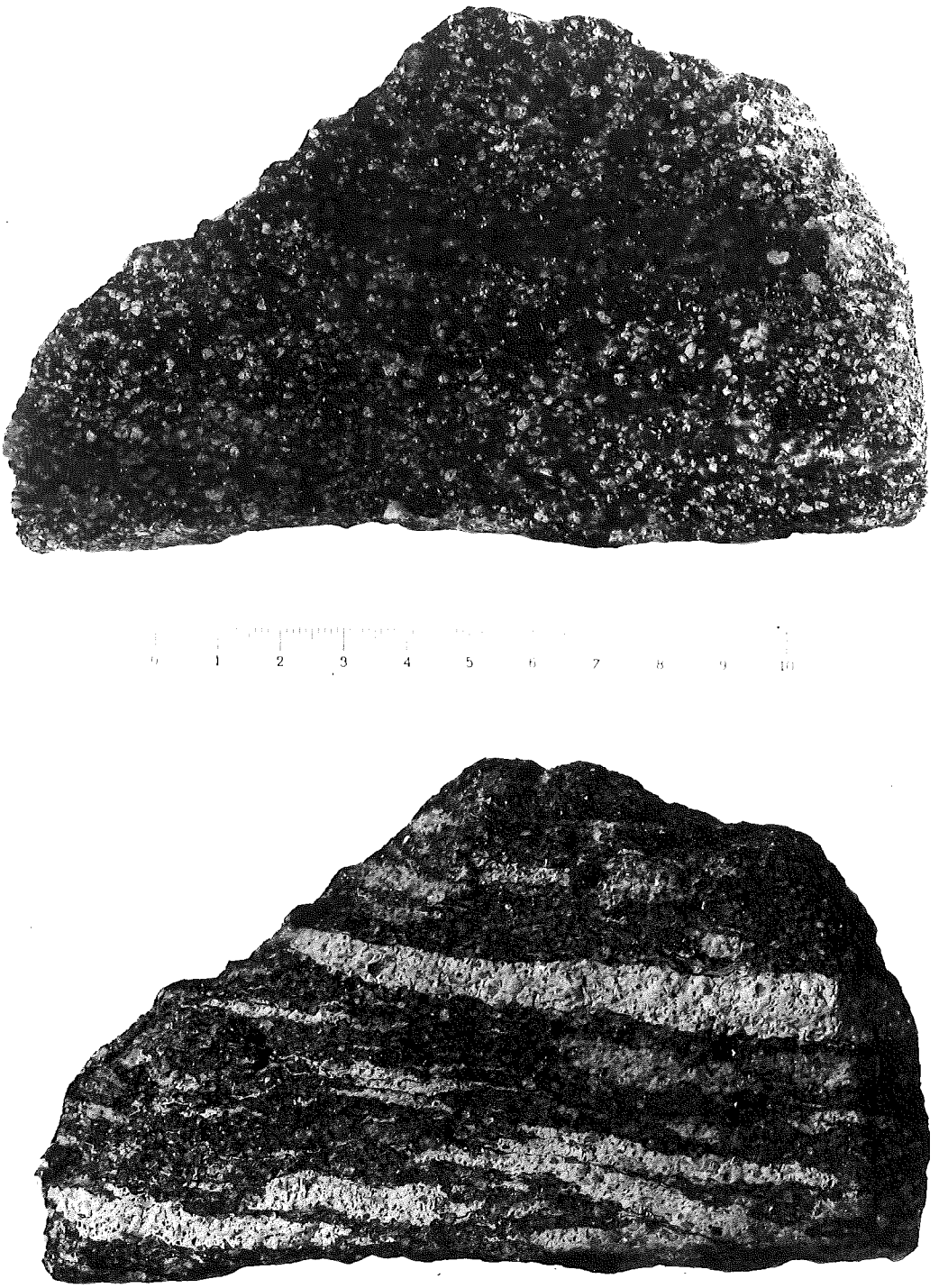

Figure 25. Porphyritic pitchstone formed from a welded tuff (ignimbrite).

Upper: Fresh section through pitchstone.

Lower: Weathered surface of pitchstone, showing eutaxitic structure. (Scale in cm).

"obsidian-like tuff" from near Taxco, Mexico, is described and illustrated by Ross and Smith (1961, p29), and Green and Short (1971, p168B). As with the Mexican rock, the pitchstone at Mt Somers also develops a platy jointing, approximately perpendicular to the plane of the fiamme structures. The dark fiammes represent completely welded collapsed pumice or tuff, while the difference in welding between the groundmass and the fiammes is so slight that only subtle weathering can pick out the difference.

(vi) The layers of rhyolite have poorly indurated margins with the result that vertical scarps have formed, with debris accumulated on benches between the flows (Figure 23). This corresponds to a unit with a partly welded base and/or top, but completely welded middle. Ross and Smith (1961, p20) illustrate an example of this type of ash-flow scarp, from the Valles Mountains in New Mexico, which consists of layers ranging from a few feet in thickness, to 300 ft thick or more. The scarps have columnar jointing in their welded zones. Columnar jointing is also a feature of the scarps formed at Mt Somers. Figure 21 shows the very thin nature of this layering, and the sharp transition that occurs between the welded top of one flow and the base of the overlying flow can be clearly seen.

(vii) The absence of distinct shard texture in most thin sections can be explained by a combination of welding and devitrification. The devitrification of the ignimbrite could have been caused by relatively slow cooling. This would imply that the tuffs accumulated rapidly by a series of rapid

successive eruptive phases, each layer being emplaced before the preceding one had completely cooled. A rapid succession of eruptions would also account for the absence of erosion surfaces, the formation of soils between each layer, and the intense welding of the pile. Figure 26 is a photomicrograph of a welded tuff. Less welded tuffs are uncommon (Figure 27).

Many of the rhyolite layers have flow textures which could be explained by limited flow in the tuff immediately after, or contemporaneously with, welding.

2.2.5.4 Petrography

The rhyolitic ash-flow tuff that occurs at the base of the reference locality in Woolshed Creek consists of subhedral phenocrysts of quartz and sanidine between 1 and 2 mm in diameter. These constitute about 10% of the rock. Many of the quartz phenocrysts have a bipyramid form, rounded slightly by resorption. The sanidine phenocrysts have a round to rectangular or rhombic shape. No garnet was observed in the thin sections. Fresh, pleochroic (red-brown to pale green) biotite is present in minor amount. The groundmass is made up of compacted glass shards with minor small angular fragments of the phenocryst minerals scattered throughout (Figure 28).

The pitchstone that occurs at the base of the Somers Rhyolite is of two types of contrasting origin. The predominant type is chilled rhyolite at the margins of domes or flows; the other is fused ash-flow tuffs or ignimbrite. It is also possible that some of the pitchstones are dikes, as some have vertical flow-banding.

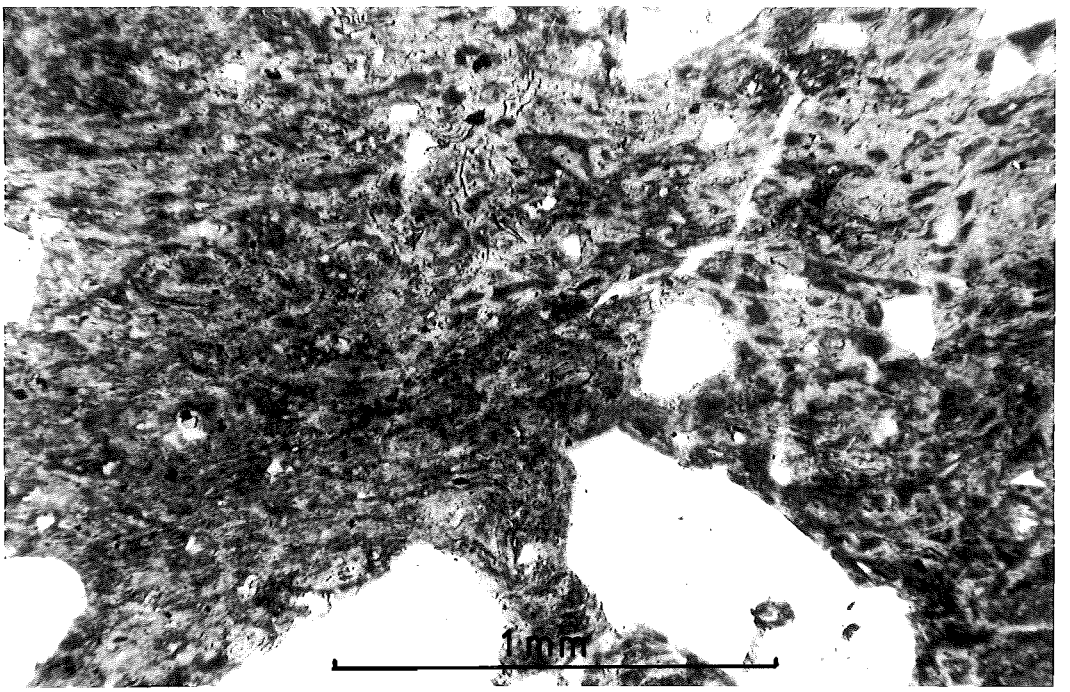

Figure 26. Photomicrograph of flow-banded ignimbrite sheet from Mt Somers. Shards show almost complete welding.

Figure 27. Photomicrograph of partially welded ignimbrite from Mt Somers.

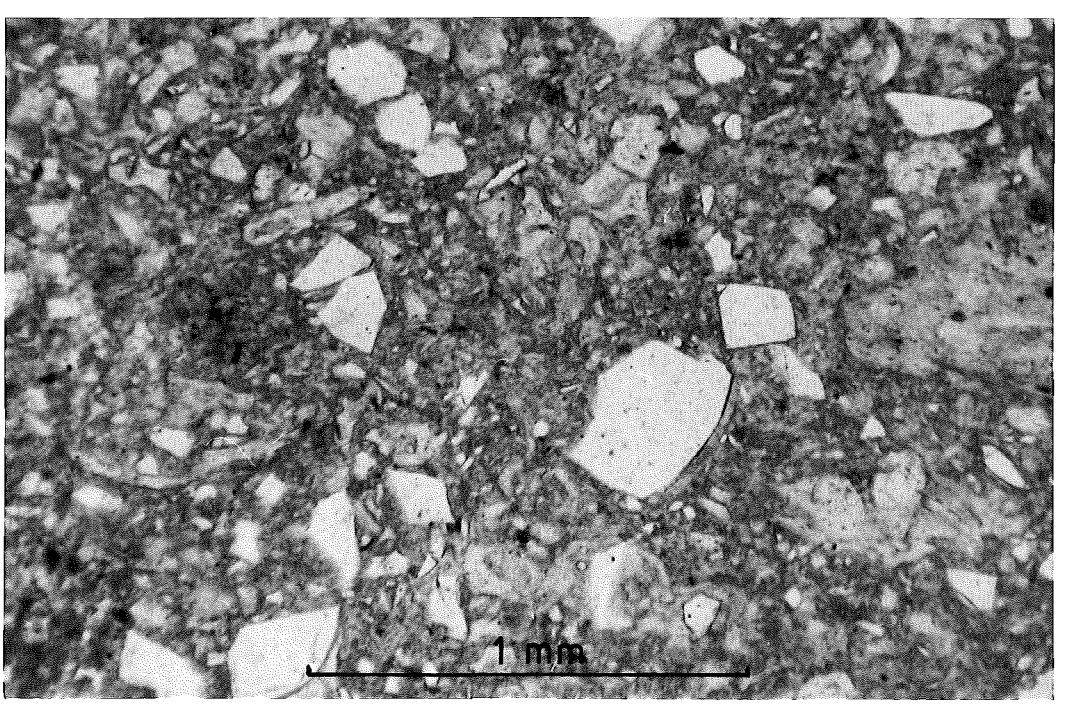

Figure 28. Photomicrograph partially welded rhyolite tuff containing glass shards, quartz and sanidine phenocrysts. Sample from base of Somers Rhyolite.

Figure 29. Typical pitchstone consisting of microlites in a glassy matrix with perlitic cracks. Bipyramidal quartz, and biotite also shown in photomicrograph.

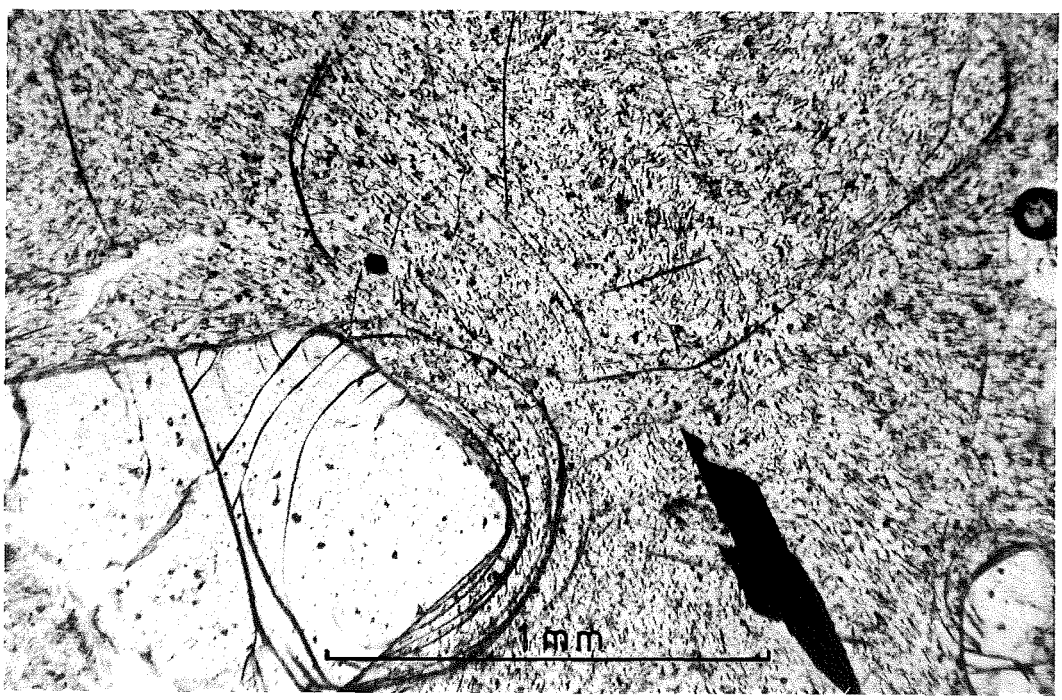

The "chilled rhyolite" pitchstone has quartz and sanidine phenocrysts with occasional plagioclase phenocrysts, all of which range between 1 and 2 mm in diameter. The quartz phenocrysts are commonly rounded or as bipyramids, the sanidine phenocrysts are rounded or rectangular, and the plagioclase occurs as clusters and as single partially resorbed phenocrysts. The phenocryst content varies from 10 to 30% but is generally less than 15% of the rock. Subhedral garnets are seen in some thin sections of these pitchstones. They are between 0.5 and 2 mm in diameter and are associated with, or have inclusions of, ilmenite. One sample (PO409) had small clusters of garnet, ilmenite and hypersthene. Small (up to 0.5 mm) elongated, fresh, pleochroic (light green to red-brown) biotite occurs as a minor phase in some of these pitchstones. The groundmass of the pitchstones is quite characteristic. They never have a microfelistic texture like the rhyolites, but instead are glassy with needle-like crystallites oriented in the direction of flow. Perlitic cracks are present (Figure 29). In addition to the needle or hair-like crystallites in the groundmass, margarites, globulites, and belonites are also present in minor amounts. The pitchstone has a similar texture to that of Squrr of Eigg, in the Hebrides, and that of Glen Shurig, at Arran (Hatch *et al.*, 1972).

The pitchstone that has been formed from the welding, and subsequent relatively rapid chilling, of an ignimbrite, has a texture that confirms this mode of origin. In Morgan Stream (GR 855485) a partly welded tuff with pitchstone lenses can be seen to pass up into a pitchstone exhibiting fiamme

texture on its weathered surface identical to that described and illustrated by Ross and Smith (1961, p28).

This eutaxitic structure is also shown in the same pitchstone that crops out in Woolshed Creek at GR 848487. It is made up of welded glass shards (<0.05 mm) which form the glassy groundmass in which denser pitchstone lenses occur which have the typical needle-like crystallites. The phenocrysts are of bipyrimidal quartz and subhedral sanidine with twinned plagioclase. Phenocrysts make up 20% of the rock. Angular fragments of phenocryst minerals are not common (less than 1%) indicating that these are not an essential part of the ignimbrites. Garnet is more common in this pitchstone than in the type described above, and occurs as crystals up to 1.5 mm in diameter. Biotite is very rare and occurs as elongated crystals up to 0.5 mm in length. The biotite is unaltered, with the usual strong pale green to red-brown pleochroism. A small (0.6 mm) xenolith of andesite was observed in one thin section.

Rhyolite forming domes, plugs, and coulees, consists of phenocrysts of quartz and sanidine in a microfelsitic groundmass (Figure 30). The phenocrysts are 1 to 2 mm in diameter and generally subhedral. They make up between 5 and 15% of the rhyolite, but most commonly about 10%. The quartz forms bipyramids with rounded terminations whereas the sanidine forms rounded rectangular or rhombic sections. As with all the sanidine phenocrysts in the rhyolites of this area, they are unzoned and unaltered. Occasional twinned and zoned plagioclase phenocrysts occur. These are andesine-

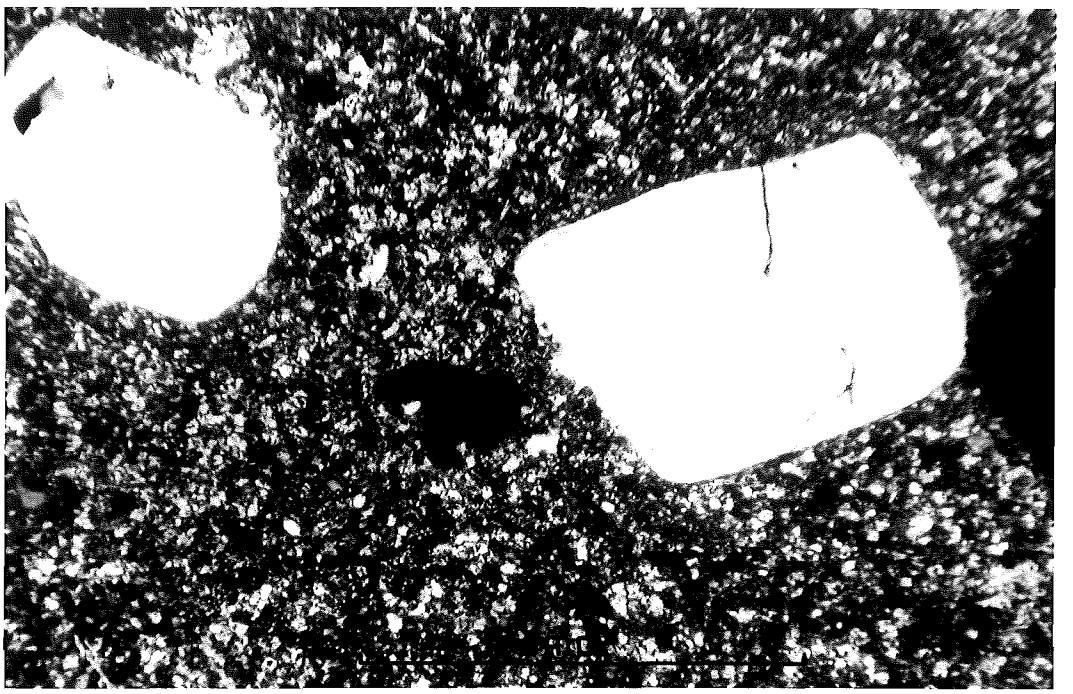

Figure 30. Photomicrograph of typical rhyolite containing bipyramidal quartz (right), and sanidine (left) phenocrysts in a devitrified felsitic matrix. (Crossed polarisers).

Figure 31. Photomicrograph of "flow banded" ignimbrite showing welded shards and phenocryst fragments of quartz and sanidine.

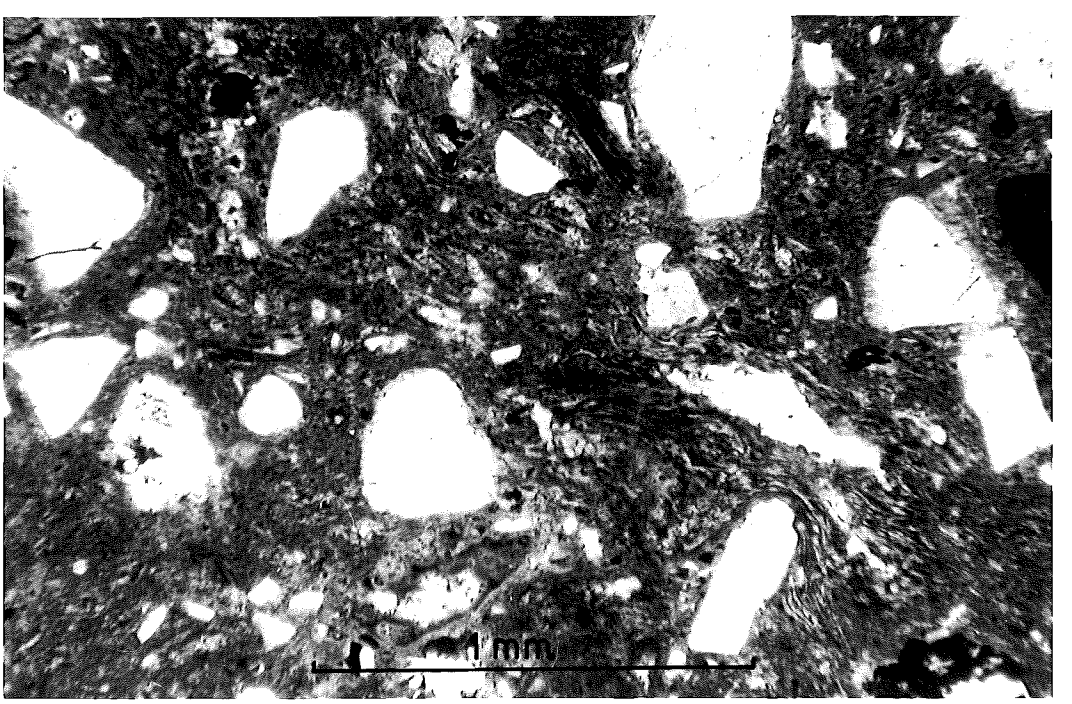

oligoclase in composition. Minor minerals include garnet and biotite. Garnet is very rare, generally occurring only as fragments or rounded crystals up to 1 mm in diameter which often contain inclusions of ilmenite. Biotite is normally absent, or present only in very minor amounts. Rarely biotite occurs in amounts up to 1%. The biotite is predominantly elongated lath-shaped grains up to 1 mm long, but it also occurs as equant or sub-rectangular crystals. When fresh the biotite has a strong pale green to brown-red pleochroism, but it alters to a dark brown colour with granular inclusions of an opaque mineral which completely replaces the biotite in some samples.

The groundmass is a devitrified glass with a micro-felsitic texture. It varies from a fine granular to a patchy appearance, depending on the extent of devitrification. The absence of devitrification texture in rapidly chilled rhyolite (pitchstone) confirms that this texture has resulted from slow cooling of the lava, and is not a phenomenon that occurred after the rhyolite reached ambient temperature.

The ignimbrite "flows" of Mt Somers are composed of quartz and sanidine phenocrysts 1 to 2 mm in diameter. These can be of subhedral form but are more commonly fragmented (Figure 31). Phenocryst content varies greatly from less than 5% to 20%. Most of the ignimbrite contains small (<0.2 mm) angular fragments of the phenocryst minerals. Garnet is rarely present in some samples as fragments or euhedral crystals. Biotite is generally fresh, with strong pleochroism (pale green to red-brown) and occurs as either equidimensional plates or elongated lath-shaped crystals up to 0.5 mm long.

Biotite is not present in all samples of the ignimbrite. Xenoliths are more common in the ignimbrite than in the rhyolite domes. They are generally of a fine-grained silicified rhyolite tuff, or of a schistose sandstone. Rarely small (up to 1 mm) xenolithic fragments of andesite occur in the ignimbrite.

Accessory minerals in the Somers Rhyolites are zircon, ilmenite and apatite. Wood (1974) showed that allanite or monazite are also present as inclusions in the garnets.

2.2.5.5 Relation to Underlying Rocks

The Somers Rhyolite overlies the Barrosa Andesite on the east side of the Clent Hills. Speight (1938, p27) considered the straightness of the contact and "....movement along the junction, indicated by the presence of pug...." suggested either a faulted contact or an intrusive contact. No pug zones were seen at this contact during the present study, although extensive crush zones occur in Blue Duck Stream, and the adjacent stream to the north (GR 789451 and 791455), downstream from the contact. Also the thick soil cover and vegetation growth could have masked outcrops visible 40 years ago. Pitchstone occurs in places along this contact (GR 790455, 789474, 790479 and 794483) and is sometimes weathered. The pitchstone weathers in a quite characteristic manner. Because it usually has perlitic cracks the first stage of weathering makes the pitchstone "crumbly". The pitchstone weathers to whitish green montmorillonite. Partly

weathered pitchstone thus tends to look crushed, and intensely weathered pitchstone tends to look like pug. It seems most probable that the pug zone that Speight referred to was one of these weathered pitchstone zones that occur along this contact. Speight (1938) also considered that the pitchstone was of no use in determining the nature of the contact as its presence also within the main mass of rhyolite made it "...unsafe to draw any conslusions as to the nature of the contact from its presence along the margin." However, the pitchstone clearly represents relatively rapid cooling of a rhyolite. (This is true whether the pitchstone represents the chilled margin of a rhyolite dome, an intensely welded ignimbrite, a fused tuff, or an intrusive dike. Each of these types occurs at Mt Somers. The formation of pitchstone has been discussed fully in a previous section.)

The pitchstone on the Clent Hills could represent isolated dikes along the contact, but this seems unlikely as there is nowhere a distinctive contact between the rhyolite and the pitchstone. Most probably the pitchstone represents localised chilled patches caused by rhyolite coming into contact with a wet surface. The contact between the rhyolite and the andesite forms an almost planar surface striking at 010° and with an average dip of 30° to the east (calculated from structural contours). This contact has the same dip and strike as the flows of the underlying andesite and is clearly therefore formed along the surface of the uppermost andesite flow. The inclination of this contact rules out the possibility of the rhyolite being older than the andesite or intrusive into

it. The rhyolite domes to the west of the Stour River are definitely younger than the andesite flows, and have been extruded over them.

In the vicinity of Woolshed Creek and Morgan Stream the relationships between the Barrosa Andesite and the Somers Rhyolite are complex, and indicate that there were several alternate eruptions of andesite and rhyolite, possibly over a short period of time. The following relations occur in an area 3 km x 1 km:

1. At GR 865483 a rhyolite dike intrudes the andesite.
2. At GR 858483 pitchstone and rhyolite flows overlie the andesite.
3. At GR 863477 and 853479 andesite intrudes rhyolite.
4. At GR 855480 andesite dikes intrude andesite flows.
5. At GR 857487 rhyolite overlies andesite.
6. At GR 847489 rhyolite is faulted against andesite flows.
7. At GR 851483 intrusive andesite (a dike) is faulted against rhyolite.
8. At GR 842488 pitchstone and rhyolite are extrusive against andesite.
9. At GR 836491 rhyolite is overlain by andesite.

Other field relations in this small area are ambiguous and only add to the confusion. It is surprising that Speight (1938, p27) should state that "....the evidence from the area north of Mt Somers is clearly in support of the contention that the rhyolite succeeds the andesite", as he then proceeded with the observations of "....selvages of rhyolite in solid andesite..." (which he claimed could be intrusive veins); and also observations of rhyolite fragments in an andesite breccia.

A close examination of these selvages of rhyolite (at GR 862477), by the writer, showed that the selvages occur within 2 m of the rhyolite/andesite contact (which at this locality is nearly vertical). The number of selvages of rhyolite increases towards the contact. Individual selvages were discontinuous. They were of variable thickness but generally less than 3 mm, and with various lengths up to 30 cm. All selvages were parallel to the contact and did not follow joints in the andesite. Thus it is clear that the selvages represent fragments of rhyolite wall rock that have been remelted and stretched by the upward flow of the andesite, and the andesite at this locality is the younger intrusive (the occurrence of rhyolite nearby in an andesite breccia also confirms this order of events).

In Bowyers Stream andesite is overlain by rhyolite. In the gorge above Goldsmith Rapids, to the west of Duke Knob, the stream has cut through the overlying rhyolite and exposed andesite. It is difficult to tell whether the andesite is intrusive or extrusive, but its aphyric texture and distinctive jointing pattern are identical to the andesite dikes between Morgan Stream and Woolshed Creek. At the confluence of Tinstone Creek and Bowyers Stream a crush zone in an andesite flow is exposed. In the bed of Bowyers Stream, at this locality, is a rhyolite agglomerate which is in contact with the andesite. The nature of the contact with the andesite is not known, as the entire locality is extensively crushed by the major fault that runs along the south face of Mt Somers. In this same locality pitchstone with vertical flow bands is also in contact with the crushed andesite.

Nowhere is the Somers Rhyolite seen in contact with the Torlesse rocks except at the faulted contact along the north face of Mt Somers. Haast (1862, p143) described "splendid sections" at Petrifying Gully that consisted of basal sandstones and siltstones (Torlesse rocks) overlain by green sands and quartzose sands; shales with plant-leaves; coal measures; porcelain jasper; pitchstone agglomerates; pitchstone; and then quartzitic porphyries. Cox (1877, p4) described the same section in greater detail but with essentially the same sequence of rock types. In both cases the descriptions state that the rhyolites overlie the coal measures and silica sands. Mapping for the present study revealed that the rhyolites, pitchstones, and pitchstone agglomerates are separated from the sands and coal measures by one of a series of parallel faults running in a north-east to south-west direction along Fagan Hill, Stephenson Hill, and Cox Hills (see Map 1,3). The basal Torlesse rocks that were referred to by both Haast and Cox are not visible in this section now. The locality is obscured by slumps of weathered pitchstone agglomerate and a covering of gorse.

Haast (1879, p286) gave a further detailed description of the section at Petrifying Gully, and stated that the sands lie on "....palaeozoic sedimentary rocks consisting of a coarse sandstone decomposing to a loose ferruginous gravel.....". Thus it would seem that no actual outcrops of Torlesse rocks were exposed, even in Haast's time. The decomposed ferruginous gravels referred to by Haast are common in this area and belong to outwash from the oldest preserved glacial advance in this area.

2.2.5.6 Relation to Overlying Rocks

The Somers Rhyolite is overlain by Tertiary coal measures. These can be seen to overlie the rhyolite along the upper surface of the west bank of Woolshed Creek (see Map 1).

In Blondin Stream, at GR 807402, the rhyolite overlies Tertiary silica sands. Inspection of this contact revealed the surface to have a dip of 36° to the east and a strike of 165°. The rhyolite contact surface showed extensive slicken-sliding, thus confirming that the rhyolite had been thrust over the Tertiary sediments.

At the Coal Reserve, on the south bank of the South Branch of the Ashburton River opposite Barrosa Homestead, Tertiary clays, coal measures, and silica sands separate Somers Rhyolite and Barrosa Andesite. These deposits could be downfaulted between the volcanics or could have been deposited in a depression. The clays are redeposited, weathered rhyolite blocks, which must have been locally derived. This clay is overlain by coal measures and silica sands which appear to be interbedded with andesite conglomerate beds adjacent to the western boundary (GR 780412). A thick covering (approximately 100 m thick) of glacial outwash gravel obscures the other contact to the south, until Blondin Creek is reached, where extensive deposits of silica sand overlie pitchstone and pitchstone agglomerate at GR 804403.

Near Woolshed Creek (GR 823434) coal measures rest directly on pitchstone which has weathered to a montmorillonite clay.

In the region of Cox Hills, on the South Side of Mt Somers, Tertiary clays, coal measures, silica sands, and

limestones are exposed on shelves that have resulted from a series of down-faulted blocks of rhyolite (see Map 1; Figure 32).

2.2.6 Hinds River Dacite

This dacite is named after the North Branch of the Hinds River, the gorge of which is flanked by dacite flows.

2.2.6.1 Definition

The Hinds River Dacite consists of dark grey to black, glassy, dacite flows. These are generally non-vesicular, although occasional vesicular flows with small amygdules of agate, opaline silica, and more rarely calcite, also occur. Although dominantly aphanitic, the dacite is porphyritic in places. Phenocrysts are of labradorite, and microphenocrysts of hypersthene.

The dacite sometimes looks similar to the andesite of the area, in hand specimen, but it has distinct chemical and petrographic features that distinguish it from the andesite.

The dacite was classified as melaphyre, and grouped with that of the Clent Hills, by Haast (1872b,1877, 1879) and Cox (1877, 1884a). Although Speight (1938) observed one of the characteristic features of this formation (viz. the presence of garnets associated with xenoliths) that distinguish the dacite from the andesite; he never-the-less grouped it with the andesite of the Clent Hills.

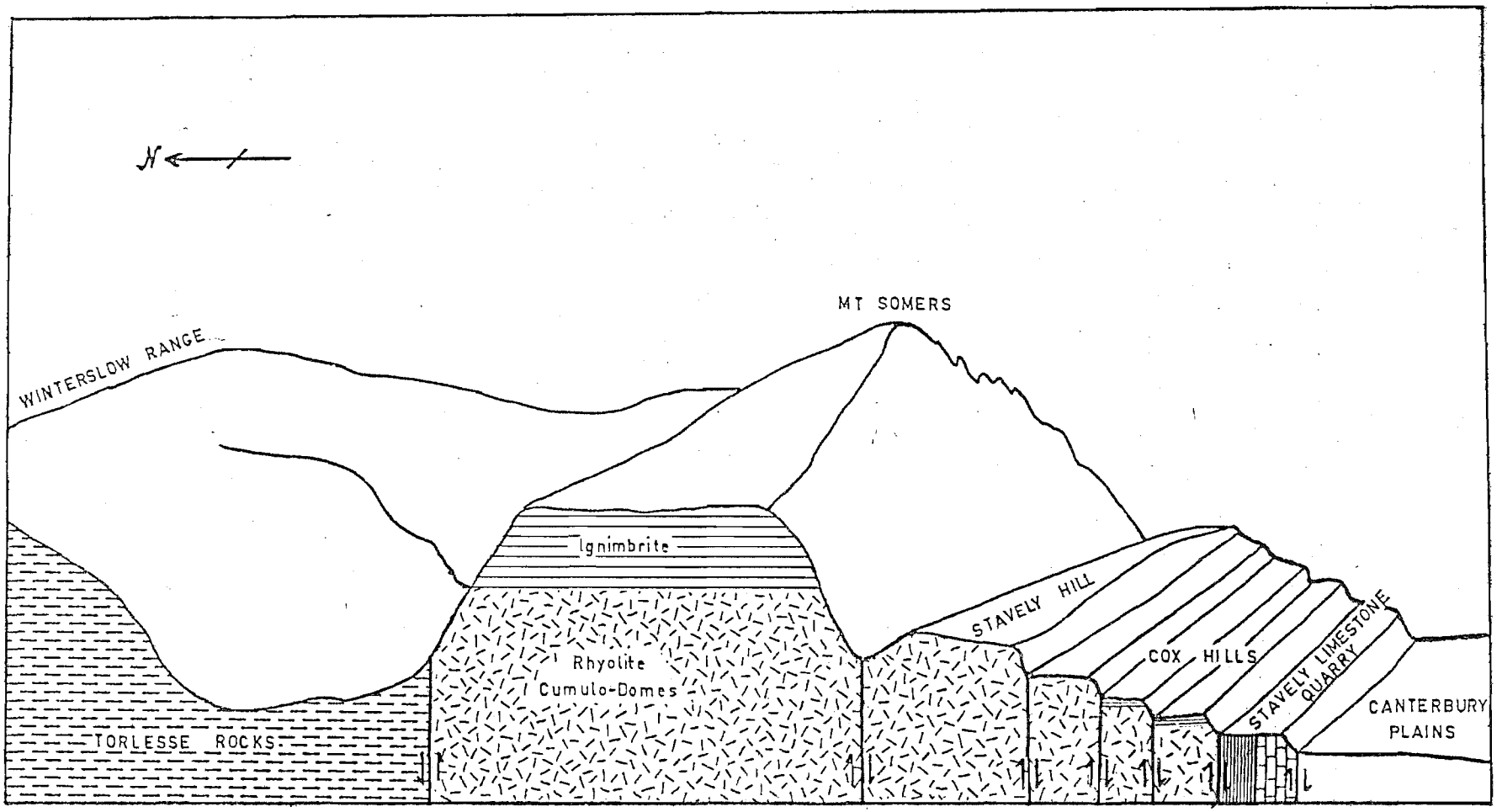

Figure 32. Diagramatic cross-section of the eastern part of Mt Somers, showing block faulting.

The type locality for the Hinds River Dacite is defined as the outcrops exposed in the gorge of the Hinds River at GR 818372. At this locality the dacite is aphanitic and non-vesicular with occasional sets of columnar joints.

2.2.6.2 Distribution

The Hinds River Dacite occurs on both banks of the North Branch of the Hinds River and forms the low hills of the Gawler Downs (Map 1). Isolated outcrops of dacite also occur on the east flank of the Peter Range where they are down-faulted against the Torlesse rocks. A small remnant of dacite occurs on the top surface of the Peter Range in the vicinity of GR 798331. Other isolated outcrops of dacite occur on the south flank of Fagan Hill at GR 890404. In Bowyers Stream, at Goldsmiths Rapids, a deep gorge is cut into the dacite, which also crops out further downstream from GR 924451 to 928450.

Three small outliers of dacite occur between the Winterslow track and Taylors Stream (at GR 956506, 954502 and 954499). At least one of these appears to be a dike and it is possible all three localities are intrusive.

2.2.6.3 Eruptive Form

The Hinds River Dacite is composed of flows, dikes, and agglomerates.

(a) Flows: These are the predominant form. Dark grey to black, aphyric vitric lava flows are exposed in the gorge of the North Branch of the Hinds River. Vesicular flows were also exposed during excavations for the foundations of the T.V. Translator at the summit of the Gawler Downs (GR 877306). The vesicles were infilled with black glass. These lava flows have a thin platey jointing that is vertical to subvertical. On the Gawler Downs the aphyric flows overlie porphyritic dacite flows with visible (up to 1 cm long) xenoliths of sediments that have been extensively metamorphosed. The porphyritic dacite is grey when fresh but has generally been hydrothermally altered to red and green, resulting in conspicuous white feldspar phenocrysts.

Flow banding is either indistinct or absent. A vesicular flow is exposed in Bowyers Stream (GR 925450). From the elongation of the vesicles the apparent direction of flow is 45° to the north with a strike of approximately 060°. This dacite has been block-faulted and tilted, the faults being clearly visible as extensive crush zones in stream.

Dacite also occurs at three isolated outcrops east of the Winterslow track, opposite Diamond Creek, at GR 953502, 554500, and 957506. The first two of these are porphyritic and slightly vesicular and therefore could be flow rocks. The third is fine-grained and dense, and appears to be an intrusive dike, although the mode of eruption of these outcrops cannot be determined definitely from the limited exposure.

(b) Dikes: Dikes are not apparent by their form. Dacite with vertical or near vertical flow banding crops out on the upper erosional surface, and on the eastern side, of the Gawler Downs. It is assumed that these are dikes cutting across the shallow dipping flows.

In the gorge of the North Branch of the Hinds River, at GR 804377, the dacite has elongated vesicles that indicate a vertical flow direction. This also could be an extrusion locality.

(c) Agglomerates: These occur in the same area as the dikes described above. In particular, a north-east to south-west trending line of agglomerate outcrops are exposed near the summit of the Gawler Downs (GR 884316 to 875301). These agglomerates appear to be vent-phases that have undergone hydrothermal alteration and silicification. They are composed of blocks of red altered dacite in a grey dacite matrix.

The agglomerates, together with the dike-like dacite in the same vicinity, provide evidence that a centre of eruption was from fissures located on the Gawler Downs. However, as Quaternary gravels cover much of the surrounding area, the possibility of other centres under the gravels of the Canterbury Plains cannot be ruled out, particularly as evidence for other volcanic centres is provided by gravity anomalies over the Canterbury plains and by the existence of a rhyolite-andesite sequence found as basement rocks by New Zealand Petroleum Exploration Company Ltd's well near Ashburton (J. D. George No.1).

2.2.6.4 Petrography

The Hinds River Dacite has phenocrysts of plagioclase in a fine grained to glassy matrix. The plagioclase composition ranges from oligoclase to andesine, although labradorite (An_{58}) phenocrysts occur in some samples. The phenocrysts occur as euhedral or slightly rounded twinned crystals, which range in size from 0.5 to 1.0 mm and very rarely phenocrysts up to 2 mm in diameter are found. Zoned plagioclases are common, some with honeycomb structure in their inner zones. The plagioclase phenocrysts make up from 5 to 20% of the rock. Amounts of 5 to 7% being the most typical.

Both ortho- and clinopyroxene are sometimes present in the same sample. The orthopyroxene, a colourless hypersthene, is present as phenocrysts with, or without, a rim of clinopyroxene. Hypersthene is also found with plagioclase forming clusters with a subophitic texture (Figure 33). The hypersthene phenocrysts are up to 1.5 mm in diameter but never occupy more than 3% of the rock, and are generally present in amounts of less than 1%. The clinopyroxene is a colourless pigeonite which occurs as rims on the hypersthene, or as small (0.01 to 0.1 mm) crystals in the groundmass, but it is occasionally present in grain sizes up to 0.5 mm. Some of the dacite samples examined contained no pyroxene.

Quartz is very rare in this dacite. When it does occur it is as small (less than 0.5 mm) corroded grains, which could be of xenolith origin.

Very rarely olivine was found with alteration rims. Occasionally biotite occurred as crystals 0.2 to 0.5 mm in

Figure 33. Photomicrograph of plagioclase and orthopyroxene clusters in Hinds River Dacite.

Figure 34. Photomicrograph of plagioclase nucleated on grains of a sedimentary xenolith in Hinds River Dacite. (Crossed polarisers).

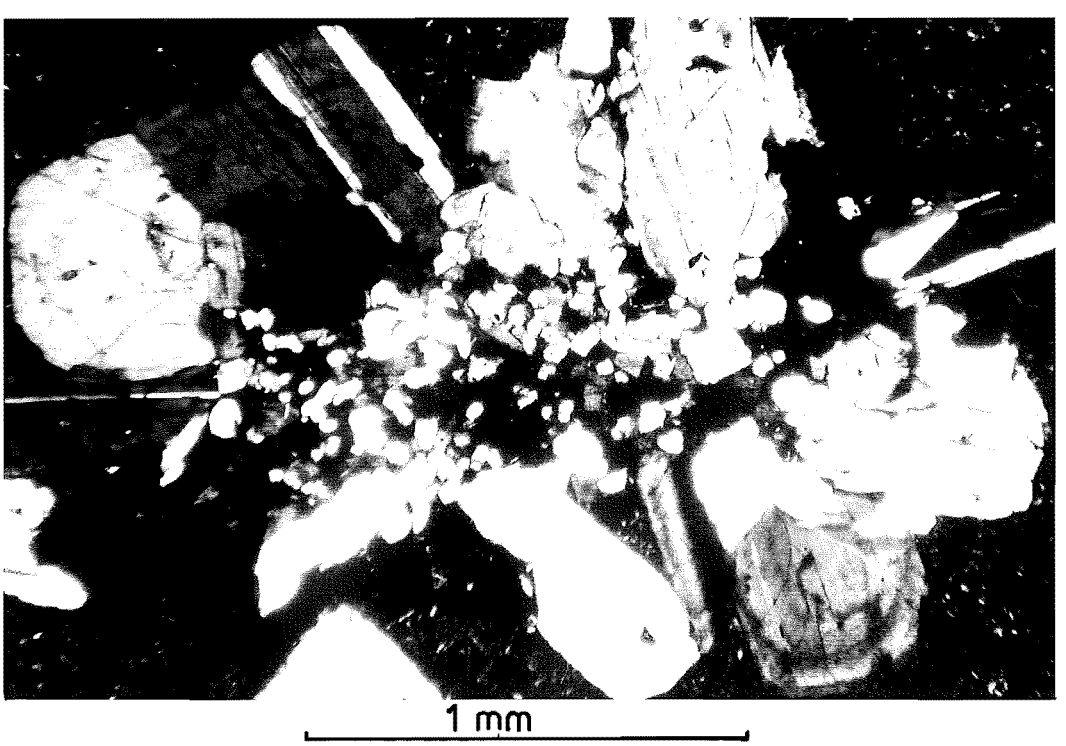

length. It occupies up to 2% of the rock. Some of the biotite has replaced, or has formed a reaction rim on, hypersthene phenocrysts.

The groundmass of these dacites is predominantly of brown glass with specks of an opaque mineral, possibly magnetite. Occasionally the dacites have a hyalopilitic texture with microlites of plagioclase in the glassy groundmass.

Xenoliths were present in all the specimens of this dacite that were examined in thin section and are of three types: 1. Sandstone or siltstone that are relatively unaltered in appearance; 2. Extensively altered sandstone or siltstone; 3. Andesite.

Xenoliths of the first type are very common in some of the dacite flows, and occur in sizes up to 8 mm long and 4 mm in width. They appear to be unaltered and have sharp boundaries with the dacite groundmass, but are composed of quartz and feldspar with an allotriomorphic-granular texture, which indicates that some re-crystallisation of these well-sorted sediments has occurred. In one sample (PO431), a xenolith of a rounded fragment of a quartz vein with hypidiomorphic-granular texture occurred.

The second type of xenolith varies from clusters of feldspar crystals with allotrimorphic texture, to clusters of granular feldspar containing globules of hypersthene and minute crystals of magnetite. These xenoliths generally have a sharp boundary with the groundmass, but examples also were found in which the feldspar granules increase in size towards the outer edge of the xenolith when the outer feldspar crystals

of the xenolith had acted as nuclei for the growth of plagioclase (Figure 34).

The third type of xenolith is the least common. The andesite xenoliths are composed of plagioclase forming a subophitic texture with interstitial pigeonite and ilmenite or magnetite grains.

The most characteristic petrographic feature of the dacite is the presence of almandine garnet which distinguishes (together with the chemistry) the dacite from glassy andesite of the Barrosa Andesite. The garnets were not present in all thin sections of the dacite, but were found in samples from the Gawler Downs; the base of Peter Range; the Hinds River; and near the Winterslow Track opposite Diamond Creek. The garnet ranges in size from 0.5 to 1.5 mm, and is sub- to euhedral. Although garnets are found as isolated xenocrysts in the dacite groundmass, they are predominantly enclosed in both types of the sedimentary xenoliths described above (Figure 35). The altered xenoliths more commonly have garnet crystals in them than the other type. The garnet has inclusions of ilmenite and alters to a semi opaque red-brown mineral (possibly allanite) that sometimes forms a rim around the garnet. Most of the isolated garnets in the dacite have alteration rims which have possibly protected the garnets from reaction with the magma. These garnets are definitely xenocrysts, in contrast to those in the rhyolite which are magmatic phenocrysts. Evidence supporting this difference has been published by Wood (1974). When the dacite does not contain garnet, chemical analysis is the only method of

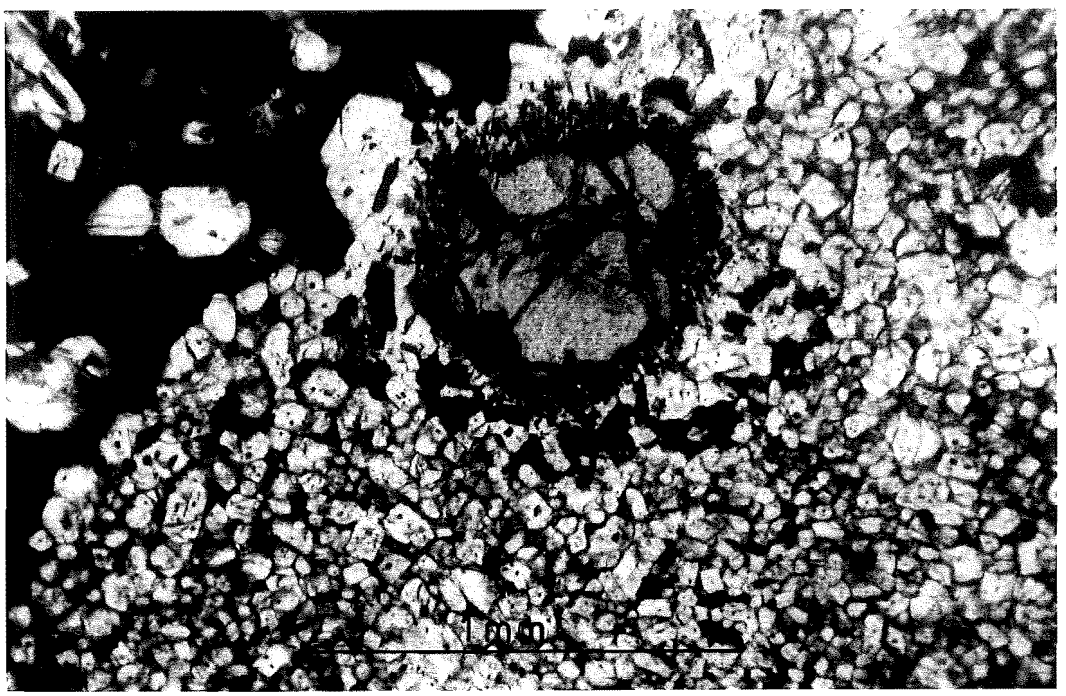

Figure 35. Photomicrograph of garnet in a typical sedimentary xenolith in Hinds River Dacite.

distinguishing it from andesite. Some dacite containing neither garnet nor pyroxene appears to be rhyodacite with a mineralogy between that of the rhyolite and that of true dacite.

In Bowyers Stream samples of dacite had the following mineralogy: plagioclase, sanidine, and minor hypersthene; plagioclase and minor quartz; plagioclase and plagioclase/hypersthene/ilmenite clusters; plagioclase and minor hypersthene, and garnets in xenoliths; plagioclase only (with honey-comb structure).

The rhyolite dike cutting the north face of Mt Somers at GR 878470 contains twinned plagioclase (An_{48} to An_{59}), with some clusters of ophitic hypersthene. Occasional rounded quartz grains are present. Several olivine crystals between 0.5 and 2 mm in size were found in thin section. These usually, but not always, had chlorite alteration rims. Some olivine crystals had intergrown ilmenite crystals, but not plagioclase. The groundmass of this rock is glassy with scattered microlites and ilmenite grains. The petrographic appearance of this rhyolite dyke is similar to those of the Hinds River Dacite.

2.2.6.5 Relation to Underlying Rocks

The Hinds River Dacite unconformably overlies Torlesse rocks in the region of the gorge of the North Branch of the Hinds River and to the east of the Gawler Downs trig station. The dacite outcropping to the south of the Hinds River is

faulted against Torlesse rocks. Small isolated areas of dacite also occur to the west of the Upper Downs Road, where they are faulted against the upthrown block of the Peter Range.

The dacite overlies Surrey Hills Tuff at several places (see Map 1). On the Gawler Downs the basal beds of dacite show considerable hydrothermal alteration as a result of the hot dacite lava having flowed over the wet, bedded tuff. The dacite at this locality is very disturbed, presumably as a result of preatic activity. Opalline veins form a network in this altered dacite, which is well exposed in a road cutting (GR 883308). A small locality of Surrey Hills Tuff that underlies dacite also occurs near the headwaters of Surrey Stream, south-west of the Gawler Downs trig station (GR S91/878299). This locality was mapped as Torlesse rocks by Speight (1938), but actually consists of weathered yellowish-white coarse-grained tuff. Speight (1938, p21) states that green tuff had been found, not in place, in Surrey Stream by a Mr F. Morrow. It now seems probable that it was derived from this locality. White and red tuffs exposed in the bed of the North Branch of the Hinds River (GR 795382) are overlain by dacite, and probably also belong to the Surrey Hills tuff, but are so extensively weathered this cannot be determined for certain from field evidence alone.

The relation of the dacite in Bowyers Stream to the andesite, pitchstone, and rhyolite that crop out adjacent to it, cannot be determined, other than where the contact crosses the stream bed, where it is faulted.

Vegetation also obscures the contacts of the dacite near the Winterslow track. The close proximity of the rhyolite, which lies immediately below and to the east of the dacite at GR 953502, implies that the dacite is the younger of the two. Torlesse sandstone is topographically below, and situated to the north of, this outcrop, and is extensively baked which could indicate either that there was a greater extent of overlying volcanics in the past, or that the dacite outcrops are volcanic plugs with large metamorphosed aureoles.

2.2.7 Stew Point Andesite

This andesite is named after Stew Point, which is an andesite ridge that protrudes into the valley of the Rangitata Gorge.

2.2.7.1 Definition

The Stew Point Andesite is a dark grey to black, porphyritic andesite, with phenocrysts of plagioclase and hypersthene. It is occasionally vesicular which has resulted in the flows containing many amygdules of agate, opaline silica, quartz and amethyst. Zeolites (laumontite, stibite, clinoptilolite) also infill vesicles.

The type locality is adjacent to Rawtor at GR 578347. Here a 150 m thickness of andesite flows is exposed.

Haast (1879, pp15, 282) visited "the porphyritic zone in the McLeod Range" in 1861, where he examined "melaphyres,

tufas, and amygdaloids" between Forest and Coal Creeks on the south banks of the Rangitata River. Haast clearly associated the andesites of the Rangitata Gorge with those of Mt Somers and the Malvern Hills. Gair (1967) classified these andesites as part of the Mt Somers Volcanics.

2.2.7.2 Distribution

The Stew Point Andesite crops out discontinuously from Rawtor Creek to the headwaters of Middle Stream (Map 1).

Haast (1879) recorded a locality of "melaphyre" on Mt Harper, and boulders (not in place) in the lower Waihoa River. No andesite was found on Mt Harper during mapping for this thesis, although basalt dikes do crop out on the slopes to the north of the summit of Mt Harper.

2.2.7.3 Eruptive Form

The Stew Point Andesite forms flows with interbedded tuff. The flows vary in thickness from 5 cm to greater than 10 m. Figure 36 shows the nature of these thin flows, with alternating ash deposits, from a locality east of Rawtor (GR 578347). All of the flows are well jointed and often locally pass into blocky flows. A distinctive porphyritic flow, 1.5 m thick, with a network of quartz veins (Figure 37) can be traced for a distance of 0.8 km, from GR 575346 to 581341, as its silicified nature has resisted erosion. Between Rawtor Creek and Lodge Stream, the flows have a total

Figure 36. Thin flows of Stew Point Andesite with alternate ash layers.

Figure 37. Porphyritic quartz veined andesite flow near Ben McLeod.

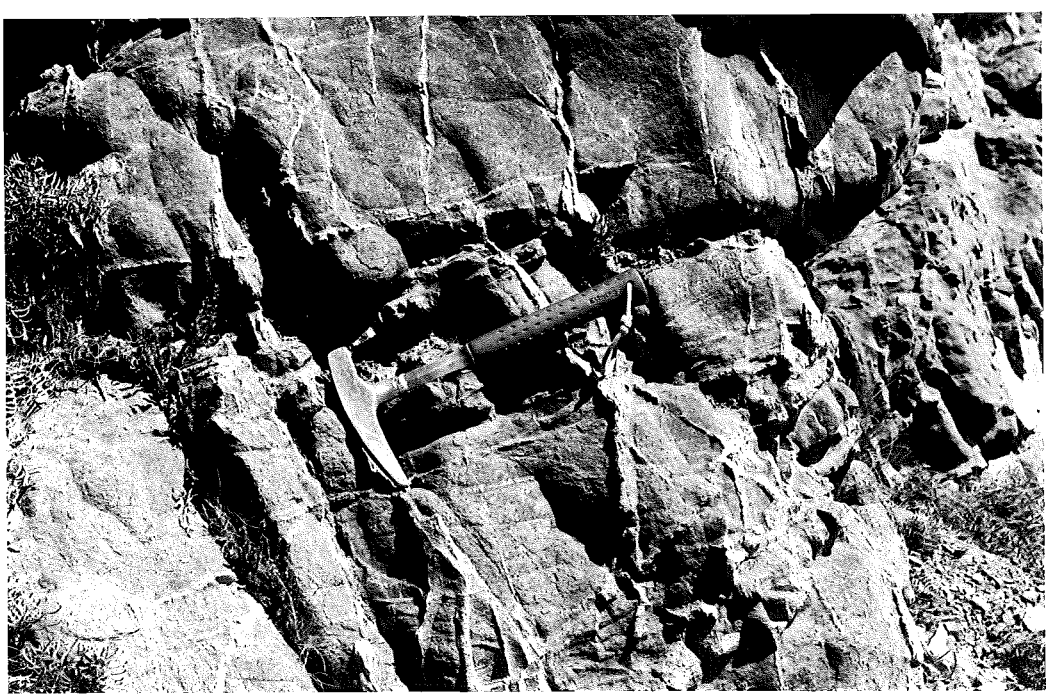

exposed thickness of 150 m. East of Trig G a 300 m thick section of flows is exposed. This is the thickest sequence of andesite exposed in the Rangitata Gorge area. The flows appear to thicken to the north.

No centre, or centres, of eruption of the andesite flows were found, but some indication of the direction of flow can be determined from the elongation of vesicles, the dip of the flows, and the nature of the basement topography. The andesite west of Stew Point generally dips to the north-west at angles of between 12° and 20°. On the eastern margin of this andesite the dip is approximately 12° in a south-west direction. The dip of the flows, together with vesicles tapered in the direction of flow, indicates that the source was at, or adjacent to, the east or north-east extremity of these flows. The thicker flows at this locality are exceedingly vesicular with much secondary infilling of the vesicles by varieties of chalcedony, opaline silica, quartz and amethyst. The thinner flows are less vesiculated and characterised by the centre part of the flows having a thin platey jointing that is nearly perpendicular to the margins.

The flows, between Power House Stream and the track to the Hewson River, dip at 20 to 30° in a north-east direction. The flows east of Rawtor also dip in this direction. Both sequences of flows appear to be derived from the south-west, although no vent was found in the field.

2.2.7.4 Petrography

This andesite is similar petrographically to the Barrosa Andesite. There are two main petrographic types of andesite: those that contain pyroxene, and those that do not.

Most of the andesites contain some pyroxene. Of these, three matrix textures are common: subophitic, hyalo-ophitic, and hyalopilitic, with some gradations between each type.

The andesite with subophitic matrix texture is holocrystalline and contains about 5% subhedral to euhedral plagioclase (labradorite) phenocrysts. These range in size from 2 to 4 mm in diameter and are sometimes extensively zoned (up to 30 zones on a single crystal). Hypersthene phenocrysts (1-2 mm) are present to about 1% of the rock and occur as subhedral clusters or ophiticly enclosed in plagioclase clusters. The hypersthene is colourless in thin section, as in the Barrosa Andesite. The groundmass is composed of interlocking plagioclase laths with 3% interstitial pigeonite and minor ilmenite crystals.

The andesite with a hyalo-ophitic matrix contains about 5% subhedral andesine to labradorite (An_{36}-An_{63}) phenocrysts 0.5 to 2 mm long, but also occasionally lath-shaped phenocrysts up to 4 mm long. Clusters of plagioclase phenocrysts subophitically enclose subhedral hypersthene. The hypersthene occurs in sizes from 1 to 2.5 mm long. The groundmass consists of lath-shaped plagioclase with interstitial glass and fine grains of an opaque mineral. Pigeonite occurs as interstitial anhedral grains in amounts up to 2%.

The andesite with a hyalopilitic matrix contains 5% subhedral plagioclase phenocrysts (0.5 to 1 mm long), and

1 to 3% subhedral hypersthene (0.2 to 0.5 mm in diameter). The plagioclase phenocrysts range from andesine to labradorite (An_{44} to An_{63}). The hypersthene is colourless in thin section, and is rimmed by pigeonite which also occurs as fine grains in the groundmass. The groundmass is dominantly glassy with microlites of plagioclase. A characteristic of these hyalopilitic andesites is the presence of sedimentary xenoliths up to 4 mm in length. These xenoliths are generally allotriomorphic-granular in texture, and are composed of feldspar and quartz with occasional anhedral grains of hypersthene (faintly pleochroic from green to pink), and grains of ilmenite. The grain-size in the xenoliths is from 0.05 to 0.1 mm, although a coarse-grained (0.2 to 0.3 mm diameter) xenolith composed entirely of allotriomorphic-granular quartz was also found in one thin section. Rounded quartz phenocrysts were only rarely present.

The andesite containing no pyroxene is made up of 5% subhedral plagioclase phenocrysts in a coarse-grained (0.2 to 0.5 mm) groundmass of plagioclase laths with a hyalo-ophitic texture. The interstitial glass contains many granular, opaque minerals (magnetite or ilmenite), but no pigeonite.

2.2.7.5 Relation to Underlying Rocks

The Stew Point Andesite unconformably overlies the Torlesse rocks. North-west of Coal Hill, between Quartz Creek and the Rangitata River, it forms a thin veneer between 10 and 200 m thick over a relatively flat erosional surface on

the Torlesse rocks. Near the Southern headwaters of Soup Stream (in the region of GR S91/668298) it appears to be surrounded by Torlesse rocks and it is possible that at this locality it is either intrusive (and if so, then could be the source of the adjacent flows), or it has been down-faulted relative to the adjacent flows.

The western contact between the andesite and the Torlesse rocks, east of Trig G, is faulted for its entire length. This fault has been active in Recent times and displays a clear fault trace along the hillside (Figure 38). The fault cannot be traced, with certainty, north of Power House Stream. The southern contact of the andesite near the Hewson River is obscured by debris, but crush zones in small creeks crossing the contact indicate this is also faulted. Adjacent to Quartz Creek (at GR S91/618298) a small tongue of andesite unconformably overlies Torlesse sandstones and siltstones.

The andesite flows between Lodge Stream and Rawtor Creek unconformably overlie Torlesse rocks. The contact is well exposed along the western margin of the andesite. At the southern extremity these flows are overlain by Torlesse rocks that have been thrust over the flows along a low-angle reverse fault dipping to the South.

2.2.8 Rata Peaks Rhyolite

This rhyolite is named after the Rata Peaks Station, where it crops out along the south bank of the Rangitata River.

Figure 38. Recent fault trace along contact between Stew Point Andesite (lower) and Torlesse rocks (upper) in Powerhouse Stream.

Figure 39. Typical dome of Rata Peaks Rhyolite with glacially eroded upper surface.
Power pole at base for scale.

2.2.8.1 Definition

The Rata Peaks Rhyolite is a white, yellow, grey, or red, porphyritic rhyolite with phenocrysts of sanidine and plagioclase. It is notable for its lack of quartz phenocrysts which are only very rarely present. Hydrothermally altered red rhyolites are common.

A type locality is defined near the boundary with the Stew Point Andesite adjacent to Stew Point (GR 631333), where a compact light-grey porphyritic well jointed rhyolite occurs in a zig-zag track.

A reference locality is also defined at GR 586356 near Harper Lodge where flow-banded rhyolite crops out that has been altered by secondary hematite.

2.2.8.2 Distribution

The rhyolite forms the lower slopes of the south side of the Rangitata Gorge valley between Stew Point and Rawtor Creek. Isolated patches also occur towards the Hewson River at GR 611312, 622308.

Haast (1879, p282) noted the presence of the andesite in this area but failed to observe the rhyolite.

2.2.8.3 Eruptive Form

The eruption of the Rata Peaks Rhyolite was in the form of domes, flows and coulees, with occasional rhyolite agglomerates. In places (e.g. GR 636320, 610312, 596335,

599334 and 621309) the rhyolite overlies Stew Point Andesite and is relatively thin (generally less than 50 m thick), which is consistent with a mode of eruption in the form of a flow or coulee.

A rhyolite plug was found intruding Torlesse rocks (GR 620318). This was approximately 20 m in diameter. Because of a covering of glacial gravels, the form of much of the rhyolite in the Rangitata Gorge is obscured. The rhyolite forms dome-like bodies near the road (Figure 39). Flow-banded rhyolite occurs in places, e.g. at Harper Lodge (GR 586355) where the bands have an almost vertical dip (Figure 41).

South-east of the summit of Stew Point is a large slumped area, the top surface of which is covered with a pinkish-white rhyolite agglomerate and boulders of Torlesse rocks. The agglomerate is composed of angular blocks of whitish-grey rhyolite in a pinkish rhyolite matrix. The size range of the blocks in the rhyolite agglomerate varies up to 10 cm in diameter, but most commonly they are between 2 and 4 cm. As there is an extensive covering of glacial Torlesse boulders, it is difficult to tell whether the agglomerate is in place.

A volcanic conglomerate, or possibly an agglomerate, crops out at several localities along the rhyolite cliffs facing the Rangitata River on Rata Peaks Station. This "conglomerate" is made up of large rounded boulders of rhyolite with minor andesite and Torlesse boulders. The size varies up to 1.5 m but are commonly 15 to 30 cm in diameter. The matrix appears to be of small rhyolite clasts. In Matagouri Stream, at

Figure 40. Rhyolite flow overlain by volcanic conglomerate bed in Matagouri Stream.

Figure 41. Flow banded rhyolite at Harper Lodge.

GR 612336 this bed is 7 m thick and conformably overlies a rhyolite flow tilted at 42° to the north and striking at 100° (Figure 40).

2.2.8.4 Petrography

The rhyolite from the Rangitata Gorge area has characteristic petrographic features that serve to distinguish them from those to the north. The rhyolite is composed of rounded to subangular sanidine phenocrysts, up to 4 mm in diameter, but predominantly 1 to 2 mm in diameter. The sanidine phenocrysts make up between 1 and 10% of the rock, but most typically only 3%. Most of the rhyolite does not have quartz phenocrysts in thin sections, but when quartz does occur it is as rounded corroded grains up to 1.5 mm, and is never more than 0.5% of the rock. Plagioclase phenocrysts (oligoclase-andesine) occur but are almost always extensively altered (Figure 42). In some samples the altered plagioclase phenocrysts are best distinguished from the groundmass under crossed polarisers, and even then the phenocrysts can only be seen as "ghost" structures.

Garnet is not a common accessory mineral but, very rarely, is found as rounded grains less than 0.5 mm in diameter. Biotite is also only very rarely seen. The groundmass is either intensively devitrified with a large patchy microfelisitic texture (Figure 43), or it is flow-banded with many opaque granules scattered throughout. Secondary hematite alteration is particularly common in the flow-banded rhyolite. Occasionally

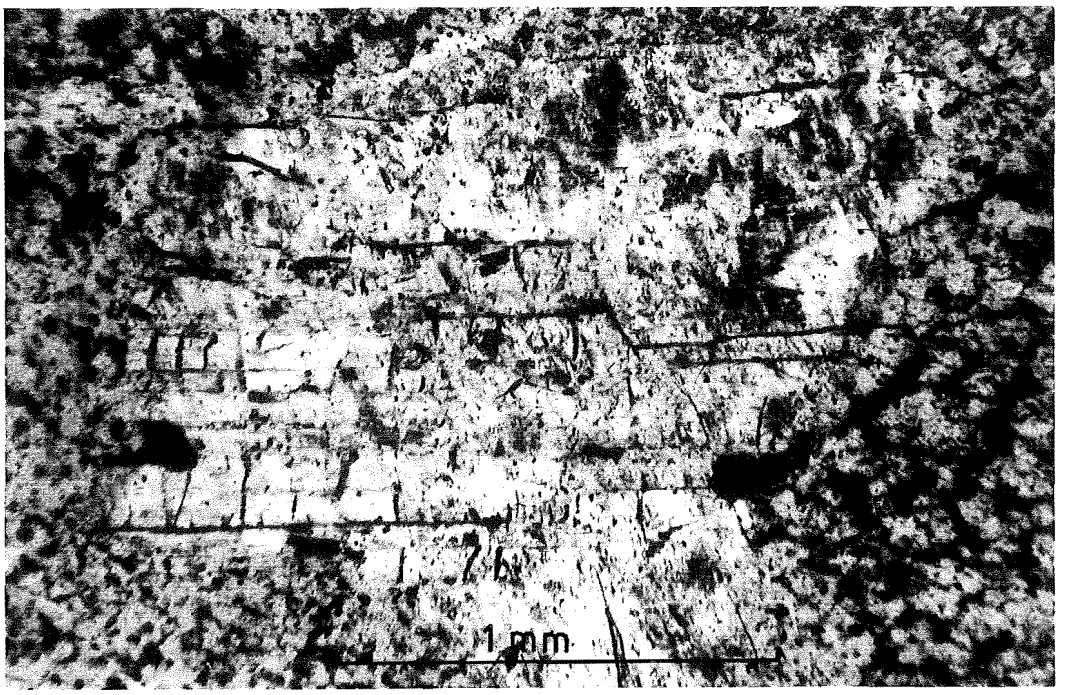

Figure 42. Photomicrograph of partially resorbed and altered plagioclase phenocryst.

Figure 43. Photomicrograph of coarse felsitic texture of Rata Peaks Rhyolite groundmass. (Crossed polarisers).

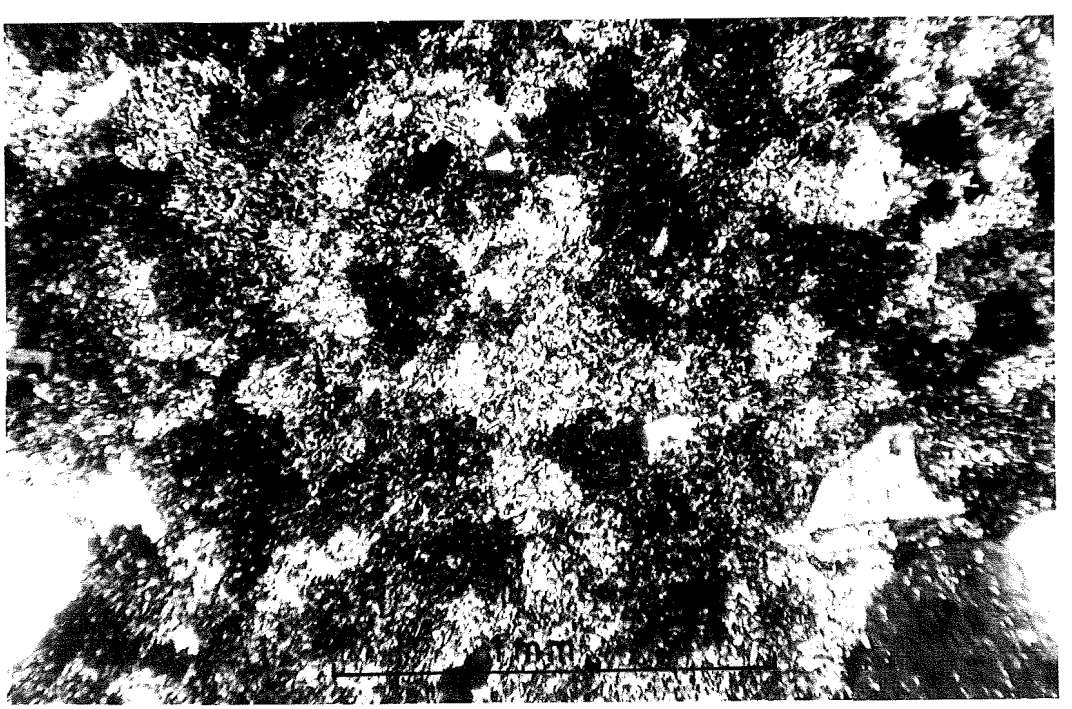

samples of rhyolite have small (less than 0.5 mm) angular fragments of sanidine (up to 2%) scattered through the groundmass, but these rocks do not appear to be ignimbritic in origin.

2.2.8.5 Relation to Underlying Rocks

The rhyolite conformably overlies the Stew Point Andesite at the summit of Stew Point (GR 636321); in Powerhouse Stream (GR 599334, 596335); and at the headwaters of Matagouri Stream (GR 612315). Elsewhere the relation of the rhyolite to the andesite is uncertain.

On the track to the Hewson River (GR 622308) it appears to overlie both the andesite and the Torlesse rocks (see Map 1), but the small extent of this outcrop could equally well support the contention that it is an intrusive plug. The contacts with the underlying rocks are not exposed.

Near the road at Stew Point (GR 633335) the rhyolite appears to be down-faulted against andesite. The contact at this locality is approximately vertical. Higher up the hill the contact is obscured by glacial till.

The relationship of the rhyolite agglomerate, on the surface above Stew Point, to the andesite is uncertain. Its association with glacial gravels leaves open the possibility that it could have been transported from the west. This seems unlikely as no agglomerate of this nature is found in place, or in the glacial till, to the west, and also the large size of the boulders of agglomerate (up to 300 cubic meters) contrasts with that of the small Torlesse boulders in the till.

2.2.9 The Volcanics of the Rakaia Gorge - Malvern Hills Area

Calc-alkaline volcanics of a similar type and age to those in the Mt Somers area are found in the Rakaia Gorge - Malvern Hills area. These have not been mapped or studied in detail for this thesis.

Previous investigations of these volcanics were made by Haast (1872b,1879) and S. H. Cox (1884a). P. T. Cox (1926) published details of the volcanics at the Rakaia Gorge. Speight (1928) published an investigation of the volcanics of the Malvern Hills in his Memoir on that area. Jobberns (1926) made a limited study of the rhyolite at Mt Misery. Recent electron microprobe studies of the garnet in the rhyolite of this area have been made by Wood (1974).

2.2.9.1 Nomenclature

Jobberns (1926) referred to the rhyolite of Mt Misery as the "Mt Misery Rhyolite". Subsequently the term "Mt Misery Volcanics" has been used as a formation name by Oborn and Suggate (1959), Gregg (1964), and Suggate (1973) for the rhyolite of the Rakaia Gorge - Malvern Hills area. The andesite of this area has been called "Round Top Andesite" by Gregg (1964), while Oborn and Suggate (1959), and Suggate (1973) used the formation name "Round Top Volcanics".

For the purposes of this thesis the rhyolite from the entire area is called "Malvern Hills Rhyolite", and the andesite

"Round Top Andesite". Representative samples of these volcanics were collected for chemical analyses, petrographic and paleomagnetic studies, and for K/Ar dating, which have shown the rhyolite and andesite to be the correlatives of those in the Mt Somers area and they have accordingly been incorporated into the Mt Somers Volcanics (Table 4). A brief discussion of the Round Top Andesite and Malvern Hills Rhyolite, based on observations from this present study, follows.

2.2.9.2 Distribution

The rhyolite occurs at Mt Misery, Pullwool Peak - Rocky Ridge - High Peak, on the lower north slope of Snowy Peak, on the lower south slope of Round Top, and on both banks of the Rakaia Gorge.

The andesite forms the top surfaces of Snowy Peak and Round Top, and also occurs in the Rakaia Gorge (see "Geological Map of Malvern Hills", Speight, 1928).

2.2.9.3 Eruptive Form

Haast (1872b,p18) stated that these volcanics were "....without doubt of submarine origin,...", and also believed this was true of those of the Mt Somers area. S. H. Cox (1884a,p36), and all subsequent investigators, refuted this suggestion. S. H. Cox (1884a) considered that the melaphyres (andesites) were flows, the liparites (rhyolites) were formed by "endogenous accretion" accompanied by explosive phases, and

that the pitchstones were dikes belonging to the same eruptive phase (Tertiary) as the dolerite and basalt of the Malvern Hills area. P. T. Cox (1926) considered all the volcanics were of flow origin (except for some andesite breccias and dikes), and Jobberns (1926) thought the Mt Misery rhyolite was "...formed by slow accretion of a viscous lava by endogenous growth."

The evidence obtained in this present study clearly indicates that the rhyolite occurs as ignimbrites, domes, and dikes. (The presence of rhyolite dikes cutting Torlesse rocks was also recorded by Speight (1928, p14)).

South of Round Top, the dike-like body of pitchstone has a low angle of inclination of the flow banding which, although locally variable, would tend to indicate that it is not a dike. A possibility, in the light of knowledge of pitchstone formation in the Mt Somers/Mt Alford areas, is that the pitchstone below Round Top either represents the top surface of an ignimbrite sheet fused by an overlying ignimbrite, or it is the chilled base of the overlying ignimbrite. The second of these possibilities is the more probable. However either possibility would explain the apparently anomalous position of the pitchstone. These explanations would also explain similar relationships between pitchstone and rhyolite (P. T. Cox, 1926) in the Rakaia Gorge.

2.2.9.4 Petrography

(a) Malvern Hills Rhyolite. This rhyolite has subhedral quartz and sanidine as the predominant phenocrysts, with subsidiary plagioclase (oligoclase-andesine). The quartz phenocrysts also occur as rounded bipyramids. Phenocryst content varies from 5 to 35% of the rock. Biotite, often altered to a granular opaque mineral, was present in all samples examined, as was almandine garnet. Two types of rhyolite occur which can be separated on their groundmass texture and composition. One type has a devitrified-glass microfelsitic texture, usually with no obvious flow-banding (e.g. rhyolite from Pullwool Peak and Snowy Peak). It appears to have formed domes or coulees. The second type has a flow-banding and small angular fragments (usually about 5%) of quartz and sanidine in the matrix. This type appears to be an ignimbrite, or possibly a rheoignimbrite, in which devitrification is not extensively developed, but shard textures are only seen as discontinuous, flattened, elongated, glassy shreds. This second type is well exposed at the Rakaia Gorge, and South of Round Top, where the uppermost outcrops are distinctly tuffaceous.

The type of the rhyolite that forms Mt Misery was not determined decisively because of the limited number of samples collected. The rhyolite of the south-west end was exceedingly porphyritic (35% phenocrysts of quartz and sanidine, 1 to 2 mm in diameter). Many small angular fragments of phenocrysts were present in the matrix, but only a poorly developed flow-banding. The petrographic texture favours an origin as an

ignimbrite. At the north-east end of Mt Misery the mountain appeared to be typical rhyolite dome in form. The deep-weathered surface of rhyolite there, was seen to be cut by small (less than 1 m wide) dikes, which is consistent with an origin as a dome. Therefore the evidence from the two ends of the mountain appears to be contradictory.

(b) Round Top Andesite. This andesite is similar petrographically to the Barrosa Andesite and the Stew Point Andesite. It is predominantly porphyritic, although aphyric flows also occur. The porphyritic andesite varies from a hyalo-ophitic to a hyalopilitic texture. The phenocrysts are lath-shaped twinned plagioclases (andesine to labradorite), which are commonly 1 to 2 mm in length. Phenocrysts of hypersthene occur both as isolated phenocrysts and as subophiticly, or sometimes ophiticly, enclosed in plagioclase clusters. Interstitial pigeonite is also present. Very rare olivine crystals occur.

2.2.9.5 Relation Between Andesite and Rhyolite

The stratigraphic relations between the two volcanic types has been in dispute ever since Haast (1872b, p2) stated that the basic volcanics were older than the acidic. S. H. Cox (1884a,p39) explained the fact that the andesite overlies the rhyolite beneath Round Top, by suggesting that the endogenous growth of the rhyolite elevated the "older" andesite flows in the process. Speight (1928, p14) summarised the evidence for the relations, and while personally favouring

an older rhyolite and a younger andesite, could not decide that this was actually the case.

As the rhyolite beneath Round Top has now been shown to be an ignimbrite, it follows that it must be older than the overlying andesite flows. This is in agreement with the bulk of the evidence. The possibility that rhyolite overlies andesite elsewhere in the Malvern Hills (Speight, 1928, p14) does not alter this, it simply means that, if it is true, then there was also a phase of rhyolite eruption after the extrusion of the Round Top Andesite.

2.2.10 Andesite and Rhyolite from J. D. George No.1

The exploratory oil well, drilled in 1969 by New Zealand Petroleum Exploration Company near Ashburton (GR S92/352095) and named J. D. George No.1, bottomed in andesite. The top of this andesite was struck after passing through 1430 m of Recent to Oligocene sedimentary strata (Wood, 1969). After passing through 111 m of dense, hard, green to grey porphyritic andesite, and red to black andesite, a coarsely crystalline rhyolite was logged from 1543 m to 1557 m. This was then followed by further brown and grey andesite and amygdaloidal andesite. The well was abandoned at 1650 m (Wood, 1969).

Samples of the andesite and the rhyolite were examined in thin section. A sample of fresh andesite contained clusters of plagioclase (up to 2 mm in length), ilmenite, and pigeonite, with subophitic texture. The texture was hyalo-

ophitic with plagioclase microlites and interstitial glass containing minute pyroxene and iron grains. A weathered sample of this andesite contained approximately 5% feldspar, altered to sericite, and often almost totally assimilated into the groundmass. These feldspars were up to 2 mm long and in a glassy groundmass with scattered microlites of plagioclase. No ferromagnesian minerals were present but patches of iron oxide and alteration products could have replaced these. The groundmass contained many elongated vesicles up to 4 mm long, and filled with a chlorite alteration product. This weathered sample of andesite was from a core and was the only sample of which there was sufficient quantity to analyse both major and trace elements. The altered nature of this sample (Analysis 129, Appendix II) must be remembered when interpreting the analytical results. The rhyolite sample was a fine grained pink rock that looked like an aplite in hand specimen. In thin section it was composed of rare plagioclase phenocrysts (less than 0.5%) which were altered and generally assimilated into the matrix. It was holocrystalline with a microcrystalline allotriomorphic granular texture, and was composed of feldspars and quartz. The matrix was considerably altered.

2.2.11 Tholeiitic Basalts

Chemical analyses No. 130-135, Appendix II, are of tholeiitic basalts in the Mt Somers/Malvern Hills area. It is not known what the ages of the dikes in the Torlesse rocks

are, but they are probably post-Jurassic and possibly Tertiary. Two basalts from Tertiary limestone near Mt Alford have been included in this group because of their similarity in composition.

A dike (PO419) in Torlesse rocks 3 km north-east of Hakatere, between GR 736476 and 740478, outcrops in the stream bed. Of the many dikes in the Torlesse rocks elsewhere in the area this one is unique in one respect; the nature of the contact. The Torlesse rocks are intensely baked for several meters either side of this intrusion. Most other dikes have only a small zone of altered sediments at the contacts, but the extent of alteration adjacent to this dike indicates that the magma was either exceptionally hot or that the dike fed a prolonged eruption at the surface. The lateral extent of the dike cannot be traced because of overlying screes of andesite. The association of this dike with the andesite is further strengthened by the presence of andesite dikes further to the north-east and in line with the basalt dikes. The petrography of this dike is also distinctly different to the others in the Torlesse rocks, described below. This dike is a holocrystalline rock, with no definite phenocryst minerals although patches of granular iron oxide could be altered remnants of ferromagnesian minerals. The matrix is made up of intergrown plagioclase with a felted texture. The plagioclase crystals are acicular rather than lath-shaped and make up about 70% of the rock. They are up to 0.5 mm in length but less than 0.05 mm in width. Elongated ilmenite crystals make up about 5% of the rock. The remainder is made

up of an interstitial micaceous mineral (pleochroic from yellow to brown). The rock is intensely altered, and calcite has formed interstitially and in the many spherical vesicles (1 to 2 mm in diameter) in this basalt. The chemical composition given in Appendix II must be interpreted in the light of this secondary alteration, particularly with respect to the calcium content which will be higher than the true value.

The basalt dike at Trig TT (GR 839526) is a holocrystalline basalt with subophitic texture. It is composed of approximately 10% olivine phenocrysts which have been altered to a fibrous chlorite mineral. Occasionally there are cores of unaltered olivine. The size of the anhedral olivine phenocrysts is 1 to 2 mm. The matrix is composed of subhedral plagioclase (0.2 to 0.5 mm in diameter), with pigeonite and augite (up to 0.2 mm). The pigeonite and augite together make up about 20% of the rock. Ilmenite occurs as comb-structures and makes up about 5% of the total rock.

A basalt dike (PO511) is one of a number of dikes that have been intruded along the contact between the Mt Misery Volcanics and the Torlesse rocks (Speight, 1928), was included in the analyses (analysis No. 132, Appendix II). This basalt was dated as being Oligocene in age (see section 2.6.3 on dating). It is a holocrystalline rock with elongated phenocrysts of olivine, ranging from 1 to 5 mm in length, and with alteration along cracks across the breadth of the phenocrysts. The matrix is composed of subophitic plagioclase and pigeonite. The plagioclase is labradorite forming laths

0.5 to 1 mm in length. The pigeonite is as equant subhedral crystals, 0.2 to 0.3 mm in diameter and make up about 15% of the rock. Skeletal and elongated (up to 1 mm long) ilmenite crystals make up 2% of the rock.

The basalt from the Landon limestone, was emplaced as pillow lavas. A relatively fresh sample (PO273) was composed of olivine phenocrysts (5%), 1 to 2 mm in diameter, and completely altered to a fibrous chlorite mineral. Occasional fresh cores of olivine remain. Plagioclase occurs in amounts up to 2%, generally as aggregates with pigeonite and augite. The groundmass is hyalophitic with much of the interstitial glass altered to opaque oxides. The groundmass contains fine microlites of plagioclase.

2.3 GEOCHEMISTRY

2.3.1 Previous Geochemical Analyses

The only previous chemical analyses of the Mt Somers Volcanics were by Seelye of the Dominion Laboratory. Twelve of these analyses were published by Speight (1938) which represented rhyolite, tuff, pitchstone, dacite, andesite, and basalt. Samples for these analyses were collected, from Mt Somers, Mt Alford, Gawler Downs, Hinds River, and Clent Hills. In addition, analyses of two rhyolites, a pitchstone, and two andesites, by Seelye, from the volcanic rocks of the Malvern Hills area, were published by Speight (1928). P. T. Cox (1926) published three analyses (a rhyolite, a pitchstone, and an andesite), that outcrop at the Rakaia Gorge. These analyses have been listed by Challis (1971). From this limited number of analyses it appeared that each rock type is similar, in major element composition, in the three areas. The rhyolites of Mt Somers and the Rakaia Gorge tend to be more siliceous than the samples analysed from the Malvern Hills, but are otherwise very similar. The pitchstone analysed from the Rakaia Gorge has a distinctly rhyo-dacitic composition compared to the pitchstones of Mt Somers and the Malvern Hills which have a rhyolitic composition.

2.3.2 Purpose of Geochemical Investigation

A study of the chemistry of the Mt Somers Volcanics provides the best method of classification. Most of these

rocks are glassy or have a large percentage of divitrified groundmass, so their true classification cannot be accurately told from either hand specimens or thin section, alone.

By studying the chemistry of these volcanics, a subdivision of the rock types in the area is possible, and this in turn contributes to a solution of the stratigraphic problems of the area.

Speight (1938) presented several possibilities for the stratigraphic order of deposition of the volcanics. He concluded that there were "three definite series" of volcanism, i.e. "(i) rhyolites of the first period, (ii) andesites, and (iii) rhyolites of the second period". (Speight, 1938, p19). His evidence for this order was however totally inconclusive, and confusing, particularly for the volcanism at Mt Alford where Speight (1938, p34-35) presented not less than five alternatives for the order of volcanism. Based on the evidence available at the time this was not unreasonable, but illustrates the need for further study.

A knowledge of the chemistry is also essential for the purpose of understanding the genetic processes undergone by the Mt Somers Volcanics, and also for a comparison of these volcanics with those of other calc-alkaline provinces.

2.3.3 Analytical Methods

2.3.3.1 Sample Preparation

Rock samples of approximately 1 to 2 kg were collected. Only the freshest samples were used for chemical analyses but

some slight weathering was observed in thin section in most samples. The samples were broken into approximately 1 cm cubes using a steel-jawed hydraulic rock splitter. Any cubes visibly weathered or altered, or those containing xenoliths, were removed by hand sorting. The rock cubes were then ground in a grinding mill for one minute. Approximately 1/4 of the samples were ground in a mild steel grinding mill, and the remainder were ground in a tungsten carbide "Tema" grinding mill. Six samples were prepared by both methods of grinding. These duplicates showed no significant variation in major element chemistry due to contamination from the steel mill. Only rocks ground in the Tungsten Carbide mill were used for trace element analyses.

The first analytical method for major element analysis, that was tried, was Atomic Absorption Spectroscopy. A "Tetron AA5" model spectrophotometer was used. Powdered rock samples were dissolved by fusing 0.1000 grams of sample with 0.7000 grams of flux at 950°C in a platinum crucible. The flux used was composed of a mixture of analytical grade lithium tetraborate, lithium carbonate and rubidium iodide in the ratio of 60:10:1. The fused sample and flux was dissolved in 500.00 ml of 2% HCl and stored in polythene bottles.

Because of instrumental malfunction, acceptable levels of reproducibility, particularly for the elements silicon and aluminium, could not be achieved on the Tetron AA5. For this reason all analyses were repeated using X-ray Fluorescence Spectrometry on a Seimens S.R.S. Sequential X-ray Spectrometer and these are the analyses quoted.

Samples were prepared for XRF analyses by fusing 0.5000 g of flux and 0.035 g of NH_4NO_3. The fused sample was then pressed to form a glass disc. The flux used and method of sample preparation has been described by Norrish and Hutton (1969). Trace element analyses by XRF were made on pressed powder mounts also according to the method of Norrish and Hutton (1969).

Standards used for the analyses were the U.S.G.S. International Rock Standards: G-2 (granite); DTS (dunite); AGV-1 (andesite); BCR-1 (basalt); PCC-1 (peridotite); GSP-1 (granodiorite). The values used were those listed by Flanagan (1973). The Victoria University of Wellington Analytical Facility artificial standard, FSL, was used as the principle standard. FSL was calibrated against the International Standards.

Analyses of ferrous iron, as FeO in samples, were made by the method of Shapiro and Brannock (1956, pA48-A49). Loss on Ignition (L.O.I.) was determined by heating samples for 0.5 hours at 1000°C in an oven. (Samples were cooled in a desiccator prior to weighing).

2.3.3.2 Analytical Data

A total of 128 volcanic rock samples were analysed for major element chemistry. Of these 101 were from the Mt Somers area, 14 were from the Rangitata Gorge area, and 6 were from the Malvern Hills area. The remainder included

samples from basalt dikes intruding Torlesse sediments and 2 were from basalt flows interbedded with Landon limestones from the Tertiary sequence at Mt Somers. A sample of basement andesite from N.Z. Petroleum Exploration Co. Ltd's J. D. George No.1 drill hole, near Ashburton, was also included.

2.3.4 Major Element Geochemistry

Chemical analyses of the Mt Somers Volcanics are given in Appendix II which also lists analyses recalculated to 100% with a standardised $FeO:Fe_2O_3$ ratio; CIPW Norms; Total Iron Values; Modified Larsen Factor; Differentiation Index; Crystallisation Index; coordinates for AFM Diagram, and coordinates for KCN Diagram. The reason for the recalculation of analyses to 100%, was for classification purposes. It is difficult to deduce the water content that these volcanics would have had under magmatic conditions, or to determine the amount of primary magmatic water retained after eruption, but it can be assumed that this would not exceed 2%. As many of the rocks analysed have absorbed water, their water contents were often far in excess of 2%. It was therefore considered that anhydrous compositions would render more correct interpretations when using analytical data for classification and comparative purposes. The standardisation of the $FeO:Fe_2O_3$ was done for the purpose of removing post-eruptive secondary oxidation effects. This is also difficult to determine and varies greatly in individual samples. Inspection of the data indicated that the freshest rhyolites had

$FeO:Fe_2O_3$ ratios of 2:1, which seemed to be an upper limit for the rhyolites from all parts of the area. The dacites and andesites varied greatly in their $FeO:Fe_2O_3$ ratio but a ratio between 2:1 and 3:1 represented the least altered samples analysed. The somewhat arbitrary ratio of 2:1 was adopted for all these volcanics, which had the result of removing hematite from the normative compositions in all but two samples.

It can be seen from Appendix II that all the Mt Somers Volcanics are quartz-hypersthene normative. In addition the rhyolites and dacites have corundum in their normative compositions. From the samples analysed it can be seen that the compositions of the various volcanic rocks in the three main areas of the Malvern Hills, Mt Somers, and Rangitata Gorge, are comparable. As all these would have been erupted from different vents, they may not represent a single differentiated magma, even though they are all chemically similar.

A comparison of the Mt Somers Volcanics with average calc-alkaline volcanics and plutonics is given in Tables 2 and 3. The average Somers Rhyolite is similar to the Average Taupo rhyolite in SiO_2, Al_2O_3 and total iron content, but has significantly less TiO_2, MgO, CaO, and Na_2O than the Taupo rhyolite, while the K_2O content is much greater in the Somers Rhyolite.

A distinctive difference exists between the composition of the Somers Rhyolite that formed domes and that which formed ignimbrite (Table 5). The domes clearly represent a more "fractionated" rock type than the ignimbrite. The average

TABLE 5: Composition of rhyolites of Mt Somers Volcanics compared to average calc-alkaline rocks.

	Somers Rhyolite						Alford Rhyolite		Rata Peaks Rhyolite		Malvern Hills Rhyolite		Average Granite (1)	Average Taupo Rhyolite (2)	Average Grano-diorite (1)
	all rhyolites		ignimbrites		domes										
	$\bar{x}$	s	$\bar{x}$	s	$\bar{x}$	s	$\bar{x}$	s	$\bar{x}$	s	$\bar{x}$	s			
SiO_2	75.51	3.04	72.92	1.77	77.69	1.95	77.49	2.63	73.10	1.04	74.49	1.65	71.2	75.3	66.9
TiO_2	0.18	0.11	0.23	0.06	0.13	0.13	0.11	0.05	0.25	0.01	0.33	0.15	0.40	0.27	0.57
Al_2O_3	13.28	1.28	14.37	0.33	12.36	1.04	12.50	1.63	14.36	0.31	14.06	1.09	14.7	13.5	15.7
Fe_2O_3	0.98	0.63	1.31	0.63	0.66	0.40	0.27	—	0.41	0.77	0.69	0.52	1.60		1.33
FeO	0.66	0.53	0.83	0.67	0.50	0.27	0.45	—	0.04	0.02	0.70	0.26	1.80	∑1.68	2.59
MnO	0.02	0.02	0.03	0.02	0.01	0.01	0.01	0.01	0.04	0.02	0.02	0.01	0.05	0.05	0.08
MgO	0.15	0.10	0.18	0.11	0.14	0.10	0.14	0.19	0.21	0.05	0.27	0.21	0.55	0.25	1.57
CaO	1.02	0.49	1.38	0.41	0.72	0.31	0.74	0.38	0.97	0.40	1.11	0.34	2.00	1.49	3.56
Na_2O	2.75	1.10	3.35	0.53	2.24	1.21	2.65	0.87	3.44	0.25	3.06	0.66	3.54	4.12	3.84
K_2O	5.23	1.08	5.20	0.51	5.26	1.40	5.01	0.63	5.65	0.35	5.12	0.90	4.18	3.39	3.07
P_2O_5	0.05	0.04	0.07	0.03	0.03	0.04	0.03	0.16	0.07	0.00	0.16	0.05	0.16	—	0.21
Rb	250		237		263		247		234		200		145	180	110
Ba	760		1089		431		196		1265		1083		600	870	500
Pb	44		43		46		51		42		38		30	18	15
Sr	82		113		50		20		129		91		285	125	440
Y	65		87		43		11		84		23		40	25	30
Th	28		27		29		37		25		23		17	11	10
Zr	270		236		136		172		356		203		180	160	140
Cu	7		8		5		5		9		7		10	6	25
Ni	4		5		2		6		7		3		4	-	15
V	2		3		1		0		3		2		40	8.5	75
Cr	3		2		1		1		1		3		10	1.7	30
Zn	71		71		70		62		56		35		—	—	—
K/Rb	172		188		157		181		193		229		240	250	230
Ba/Rb	3.19		4.74		1.64		0.79		5.42		5.42		4.1	8.1	4.5
Ba/Sr	11.56		10.19		8.54		9.80		9.89		11.90		2.1	7.0	1.14
Rb/Sr	3.78		2.33		5.22		12.35		11.83		2.20		0.51	0.86	0.25
Th/K x 10^{-4}	6.49		6.01		6.97		8.29		5.55		5.01		4.9	4.02	3.65
Cr/v	0.49		0.86		0.00		0.0		0.38		1.50		0.25	0.20	0.40
V/Ni	0.50		0.60		0.50		0.0		0.43		0.67		10.00	—	5.00
Ca/Sr	95		69		121		2.62		54		58		50	9	6

Note: $\bar{x}$ — arithmetic mean. s — standard deviation. (s not calculated for trace elements, as only a small number of samples were analysed for each Formation). (1) — Average values, from Taylor (1968). (2) — Average values, from Ewart and Stipp (1968). Major element oxide concentrations in percentages; trace element concentrations in ppm.

Alford Rhyolite, Rata Peaks Rhyolite and Malvern Hills Rhyolite also contain significantly higher potassium than the average Taupo rhyolite.

The Hinds River Dacite is closer in composition (Table 6) to an average granodiorite than it is to Taylor's (1969) average calc-alkaline dacite, particularly in respect to the alkali content, and it is notable that the TiO_2 content is approximately double that of the average calc-alkaline dacite.

The Barrosa Andesite, Stew Point Andesite and Round Top Andesite, are all very similar in average composition, and correspond to Taylor's (1969) average andesite, but the Al_2O_3 and CaO values are closer to that in his average high-K andesite. The TiO_2 content is also higher in the Mt Somers andesites than in the average calc-alkaline andesites.

The Graham Dolerite has an anhydrous chemical composition corresponding to Taylor's (1969) average low-Si andesite. Analysis 128, Appendix II, is the most basic of the "andesites" analysed and just corresponds to the upper limit set by Taylor (1969) for a high-Al basalt.

In Appendix II, analyses of basalts from dikes in Torlesse rocks, and from flows from within Tertiary limestone in the Mt Somers area, are also included. There are no definitely Late Cretaceous-Early Tertiary basalts known from the Mt Somers area other than the basaltic andesite already referred to. However the chemical analyses of the tholeiitic basalts from the Torlesse rocks and Tertiary limestone show some affinities to the calc-alkaline volcanics, and have therefore been included in variation diagrams where they, somewhat surprisingly, form continuous variation trends with

TABLE 6: Composition of dacites and andesites of Mt Somers Volcanics compared to average calc-alkaline rocks.

	Hinds River Dacite		Barrosa Andesite		Graham Dolerite		Stew Point Andesite		Roundtop Andesite		Average High-Al Basalt*	Average Low-Si Andesite*	Average Andesite*	Average High-K Andesite*	Average Dacite*	Average Grano-diorite*
	$\bar{x}$	s	$\bar{x}$	s	$\bar{x}$	s	$\bar{x}$	s	$\bar{x}$	s						
SiO_2	67.00	2.41	60.12	2.45	56.46	2.86	60.15	2.54	60.67	7.74	51.7	54.9	59.5	60.8	65.1	66.9
TiO_2	0.97	0.14	1.23	0.10	1.25	0.07	1.20	0.07	1.29	0.55	—	0.82	0.70	0.77	0.51	0.57
Al_2O_3	15.98	0.77	16.05	0.28	16.71	0.15	16.06	0.56	16.06	0.56	16.9	17.5	17.2	16.8	16.5	15.7
Fe_2O_3	1.29	0.81	1.88	0.94	2.13	0.52	2.06	1.51	3.38	1.83	4.70		2.72	2.20	3.20	1.33
FeO	2.89	1.57	5.10	0.70	5.58	1.22	4.89	1.34	3.81	2.37	5.80	8.18	3.65	3.15	0.98	2.59
MnO	0.07	0.03	0.13	0.02	0.15	0.03	0.14	0.01	0.14	0.06	—	0.17	0.15	0.17	0.07	0.08
MgO	1.21	0.56	3.58	1.53	4.70	1.18	3.75	1.70	2.76	2.14	6.5	4.71	3.42	2.15	1.48	1.57
CaO	3.40	0.58	5.80	1.11	7.84	1.54	5.87	1.65	5.44	2.54	11.0	8.47	7.03	5.60	4.75	3.56
Na_2O	3.39	0.56	3.51	0.62	3.16	0.38	3.29	0.43	3.61	0.63	3.1	3.43	3.68	4.10	4.60	3.84
K_2O	3.54	0.52	2.29	0.63	1.62	0.65	2.33	1.16	2.13	0.75	0.4	1.10	1.60	3.25	2.05	3.07
P_2O_5	0.27	0.01	0.25	0.07	0.26	0.01	0.27	0.04	0.32	0.12						
Rb	185		120		78		109		89		9.6	14	31	88	44	110
Ba	695		477		384		559		453		115	200	270	400	520	500
Pb	30		23		15		23		13		1.7	3.3	6.7	7.2	5.2	15
Sr	249		226		228		353		235		328	430	385	620	460	440
Y	58		47		50		51		57		20	22	21	20	20	30
Th	19		13		12		14		12		1.1	1.34	2.2	5.5	1.7	10
Zr	329		268		210		263		254		100	92	110	170	100	140
Cu	21		34		35		34		27		35	60	54	40	22	25
Ni	12		44		30		42		27		25	28	18	3	5	15
V	43		77		89		71		83		255	200	175	160	68	75
Cr	38		108		69		127		56		40	85	56	3	13	30
Zn	86		86		77		81		94		—	—	—	—	—	—
K/Rb	150		167		186		151		203		344	650	430	297	386	230
Ba/Rb	3.82		4.20		4.92		5.35		8.73		12	14	8.7	4.5	11.8	4.5
Ba/Sr	2.77		2.20		1.68		1.62		1.95		0.35	0.47	0.70	0.65	1.13	1.14
Rb/Sr	0.75		0.53		0.34		0.30		0.39		0.29	0.07	0.08	0.14	0.096	0.25
Th/K x 10^{-4}	6.93		6.62		8.27		9.15		11.52		3.33	1.47	1.65	2.11	1.0	0.67
Cr/V	0.71		1.19		0.78		1.14		0.61		0.55	1.43	0.32	0.019	0.19	0.40
V/Ni	3.67		3.51		2.97		2.13		3.29		10.00	7.15	9.73	53.33	13.60	5.00
Ca/Sr	10		19		25		15		21		23	14	13	7	7	6

Note: $\bar{x}$ — arithmetic mean. s — standard deviation. (s not calculated for trace elements as only a small number of samples were analysed for each Formation). * — Average values, from Taylor (1969).

Major element oxide concentrations in percentages; trace element concentrations in ppm.

the Mt Somers Volcanics. It must be emphasised that while some of the basalt dikes may be late Cretaceous in age, and directly related to the Mt Somers Volcanics, this is not thought to be probable.

2.3.4.1 Major Element Variations

The frequency distribution of SiO_2 in the Mt Somers Volcanics is given in Figure 44. From this series of histograms the Somers Rhyolite can be seen to fall into two categories, viz. those with SiO_2 > 75% and those with SiO_2 < 75%. This subdivision coincides with the structural, and petrographic division of the rhyolite domes, and of the ignimbrite (welded ash-flow tuffs) respectively. The Alford Rhyolite appears to be in the form of domes, and this rhyolite also has a SiO_2 composition greater than 75%. The excessively high silica content of some Somers Rhyolite and Alford Rhyolite samples, corresponds to samples of tuff associated with, or pre-dating the extrusion of the domes. The high silica content undoubtedly has resulted from selective sorting in these tuffs. The compositional gap that can be seen, in the histograms, between the ignimbrite and the rhyolite may however be due to sampling bias. The samples analysed from the rhyolite domes, were obtained from the western flank of Mt Somers in the region of the Stour River and Woolshed Creek. East of this the domes are overlain by ignimbrite. A sequence of samples collected from flows on the upper surface of Mt Somers represent only the uppermost ignimbrite flows, and dikes/plugs associated

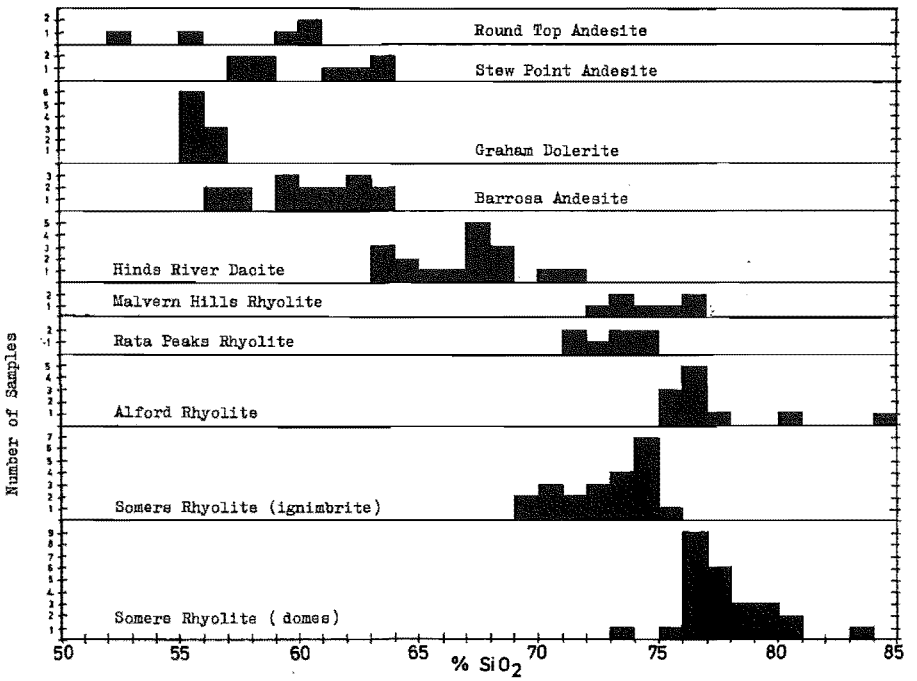

Figure 44 . Histogram showing the frequency distribution of SiO_2 in the Mt.Somers Volcanics.

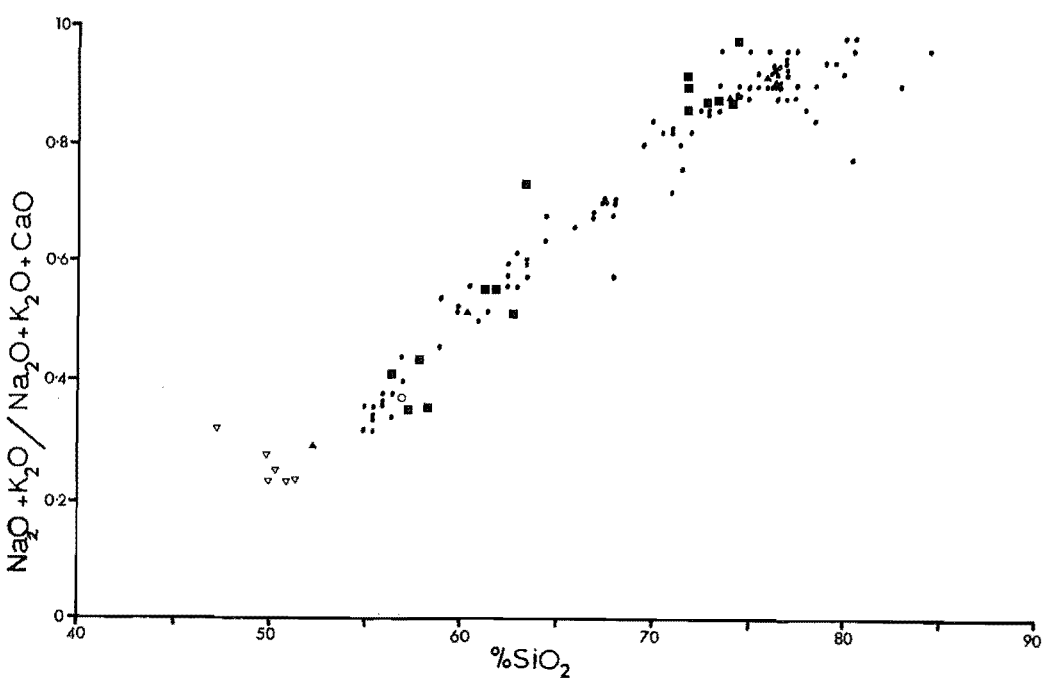

Figure 45 . Plot of the ratio $Na_2O + K_2O/Na_2O+K_2O+CaO$ against SiO_2 in the Mt.Somers Volcanics. Symbols as for Figure 47 .

with these. The rhyolite that should be present in the SiO_2 range 75-76%, is overlain by the ignimbrite sheets and only exposed on the north-east and south-east faces of Mt Somers where it is in the form of a series of vertical columnar-jointed cliffs, hundreds of meters in height, and are therefore relatively inaccessible. Of the samples collected from this area only two were analysed, and these did, as expected, occupy the "gap" in the histogram.

The Rata Peaks Rhyolite appears to be in the form of domes and/or coulees. The silica content of this rhyolite falls on the "ignimbrite-side" of the histogram (Figure 44). As will be shown later (section 2.18), the composition of the rhyolite, and other main factors (e.g. temperature, pressure, volatile content, and rate of eruption) must have controlled the eruption.

In the previous description of the petrography, the most basic Somers Rhyolite samples were petrographically indistinguishable from the most acidic dacite. There is also an overlap in the silica content of these rocks which may be accentuated by the deposition of secondary silica and/or inclusions of sedimentary xenoliths, but as the analysed samples were selected to specifically exclude these factors, it does not seem probable that these could be completely responsible for the overlap of composition between the dacite and the rhyolite in the region of Mt Somers.

The overlaps in the silica frequency distribution histograms (Figure 44) of the rhyolite, dacite, and andesite from all localities in the area, together with their common petrography, indicates that the petrogenetic processes

in all these volcanics could be the same.

To illustrate the relationships between the various volcanic rocks of the area studied, conventional Harker variation diagrams are used. Correlation of the variables with parameters other than SiO_2 (e.g. the Thornton and Tuttle (1960) Differentiation Index (DI); Kuno's (1960) Crystallisation Index (CI); Nockolds and Allen's (1953) modified Larsen Factor; and Simpsons (1954) Felsic Index) have been made and will also be referred to. There are three main "centres" of volcanism which are plotted separately in the variation diagrams (see Figure 47):

1. The Round Top Andesite and Malvern Hills Rhyolite are plotted together as the "Mt Misery volcanics".
2. The Somers Rhyolite, Alford Rhyolite, Surrey Hills Tuff, Barrosa Andesite, and Hinds River Dacite are plotted together as the "Stour volcanics".
3. The Stew Point Andesite and Rata Peaks Rhyolite are plotted together as "Rangitata Gorge volcanics".

Figure 45 is a plot of the ratio $Na_2O + K_2O/Na_2O + K_2O + CaO$ (i.e. Simpson's (1954) Felsic Index), against SiO_2. The excellent correlation between these parameters indicates that the volcanics from the different eruptive centres of the area, form overlapping continuous, differentiation sequences of the same type. In the following discussions of the chemical variation trends, reference to them as "differentiation" trends, or "crystal fractionation" trends, will be made. The validity of this type of petrogenetic mechanism, as applied to the Mt Somers Volcanics, will be discussed in the section on

petrogenesis which examines this, and all the possible alternative mechanisms to crystal fractionation.

The frequency distribution of TiO_2 in the Mt Somers Volcanics is given in Figure 46. This diagram again illustrates the sharp distinction between the ignimbrite "flows" and the domes of the Somers Rhyolite. The distinction between the Hinds River Dacite and the Somers Rhyolite is also quite clearly defined by the TiO_2 Histograms, indicating that a compositional break in the sequence does in fact exist between the acidic dacites and the basic rhyolites. The rhyodacites in Bowyers Stream were not analysed (unfortunately) because of their weathered nature. The absence of hypersthene and quartz in these rocks, together with the presence of sanidine, indicates that the composition of these rocks may lie between the analysed rhyolites and dacites.

The TiO_2 contents of the Stew Point Andesite, Graham Dolerite and Barrosa Andesite are essentially the same, while the Round Top Andesite shows more basic affinities. This basic trend is also true of the Malvern Hills Rhyolite, compared to the other rhyolites of the area. The variation diagram of TiO_2 against SiO_2 (Figure 47) indicates that there is a continuous line of descent between the basic andesite and the acid dacite, with another fractionation trend in the rhyolite, but the break between the dacite and rhyolite is quite distinct. The titanium in the Mt Somers Volcanics would have been removed by the fractional crystallisation of ilmenite, grains of which are occasionally seen enclosed in plagioclase in thin sections.

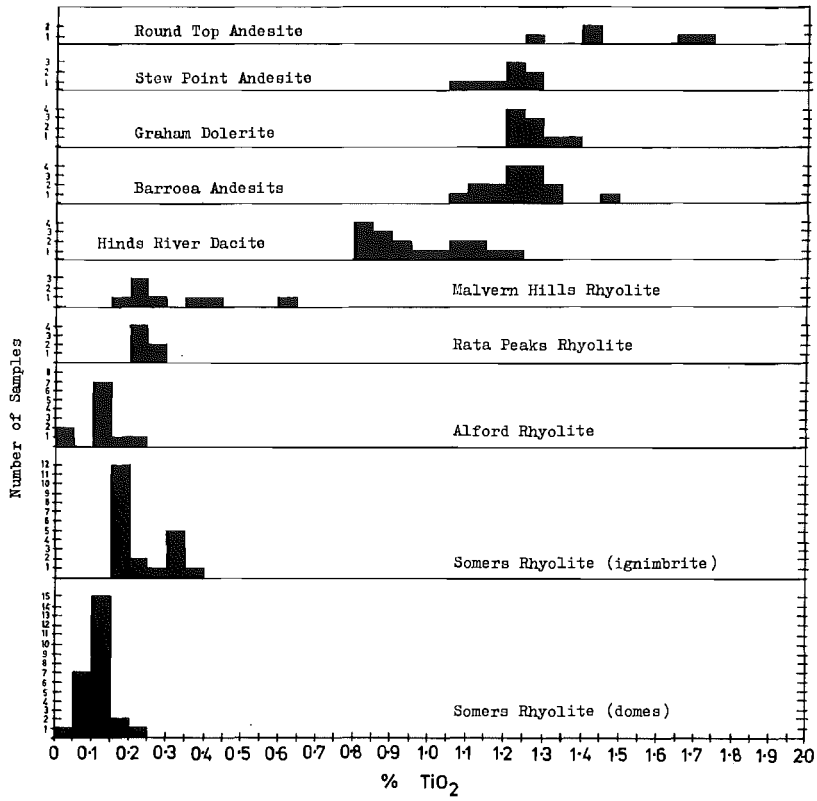

Figure 46. Histogram showing the frequency distribution of TiO_2 in the Mt.Somers Volcanics.

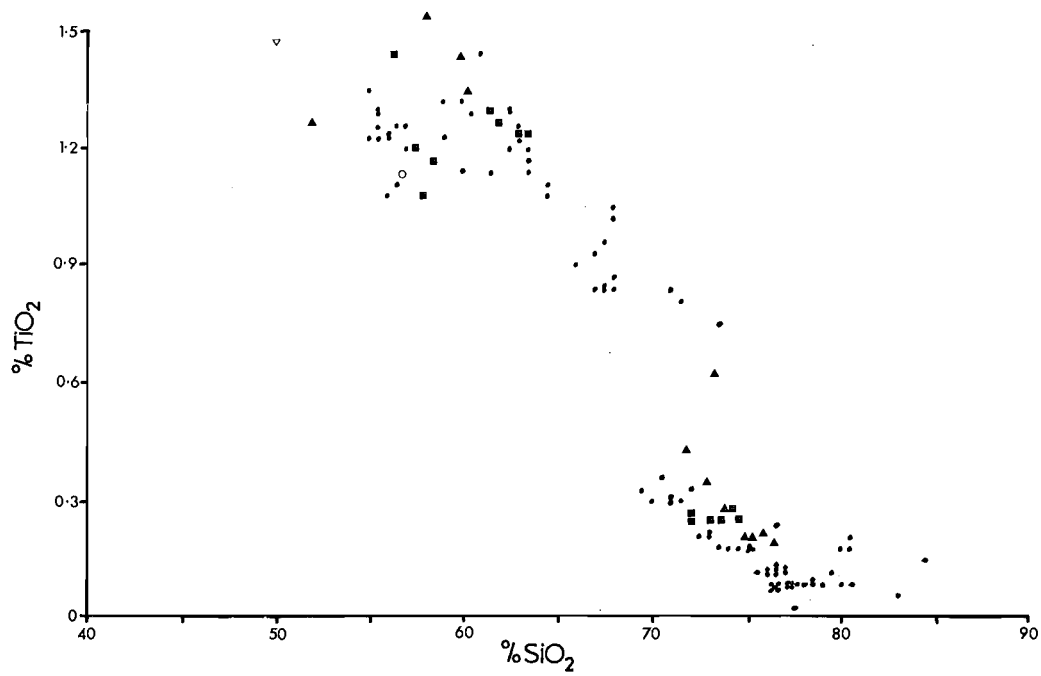

Figure 47. Plot of TiO_2 against SiO_2 in the Mt.Somers Volcanios. Symbols: • Stour volcanics ■ Rangitata Gorge volcanics; ▲ Mt.Misery volcanics; ▽ basalts; ○ J D George No 1 andesite.

The frequency distribution diagram for Al_2O_3 (Figure 48) shows a clear distinction between the ignimbrite and domes of the Somers Rhyolite. The spread towards the low alumina end of the diagram for the Somers Rhyolite (domes), and Alford Rhyolite, is a result of the inclusion of data from rhyolite tuff associated with these rhyolites. Each andesite formation has very little spread in Al_2O_3 values. The variation diagram for Al_2O_3 (Figure 49) shows that there is a continuous variation through all the volcanic types, without the break between the dacite and rhyolite that was also seen in the TiO_2 trend. It is significant that all but one of the basalt samples have very low Al_2O_3 contents compared to the andesite, as if the andesite was derived from compositionally similar tholeiitic basalt, the initial fractionating phase must have been low- or non-alumina phases such as olivine and spinel structure minerals (this will be discussed further in the section on petrogenesis). The decrease in Al_2O_3 in the differentiation sequence (Figure 49) becomes more pronounced towards the rhyolite end of the diagram, which is consistent with an increased removal of Al_2O_3 by fractional crystallisation of feldspar. It is interesting to note that the rhyolite tuff with the lowest Al_2O_3 content does not deviate from the regression trend, and appears to be an extreme differentiate product, rich in silica.

The frequency histograms for total iron, expressed as $FeO + Fe_2O_3$ (Figure 50), show no major differences between any of the rhyolites, or between the andesites. The total iron content of the dacite not only spans the gap between the

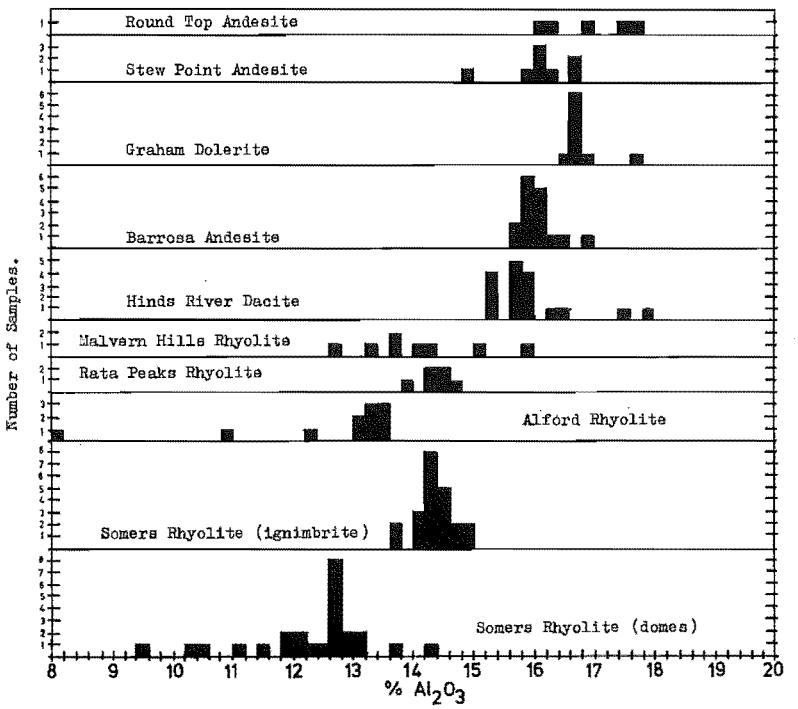

Figure 48. Histogram showing the frequency distribution of Al_2O_3 in the Mt.Somers Volcanics.

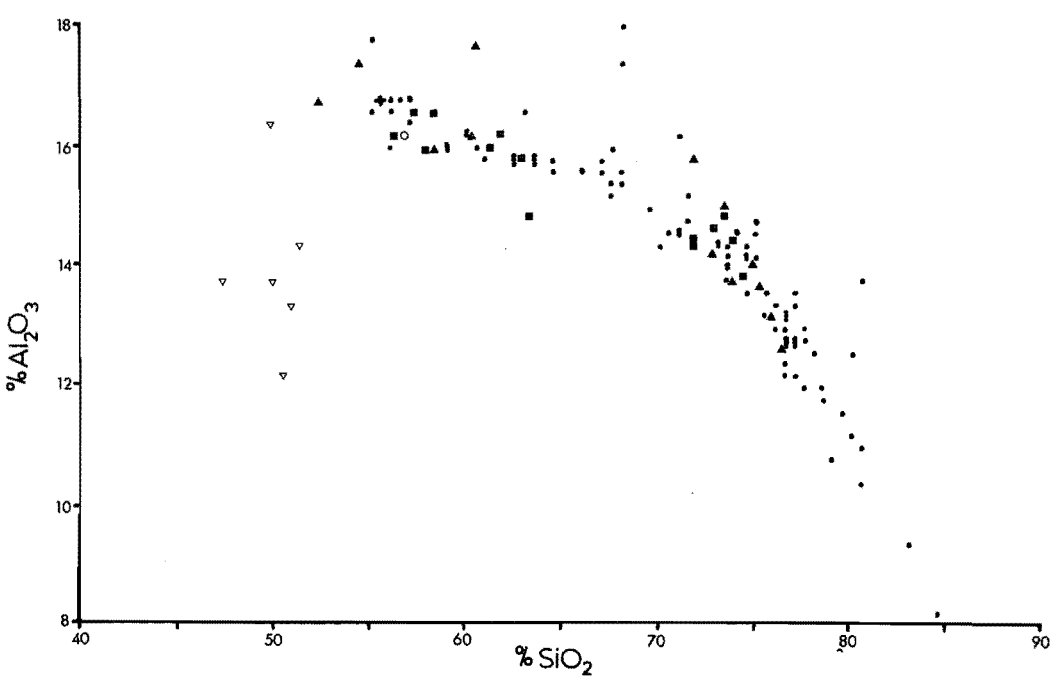

Figure 49. Plot of Al_2O_3 against SiO_2 in the Mt.Somers Volcanics. Symbols as for Figure 47.

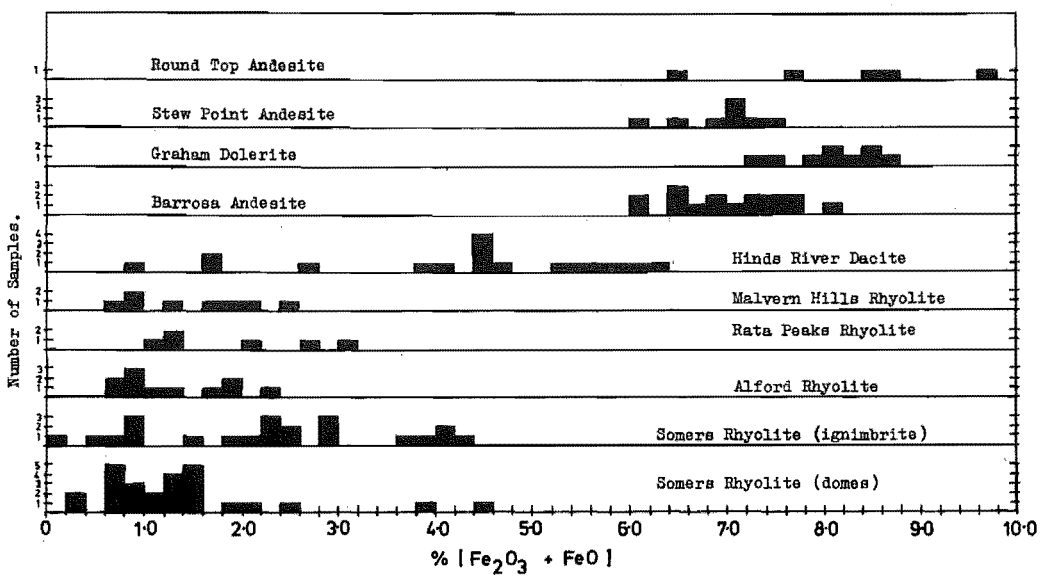

Figure 50. Histogram showing the frequency distribution of Fe_2O_3 + FeO in the Mt.Somers Volcanics.

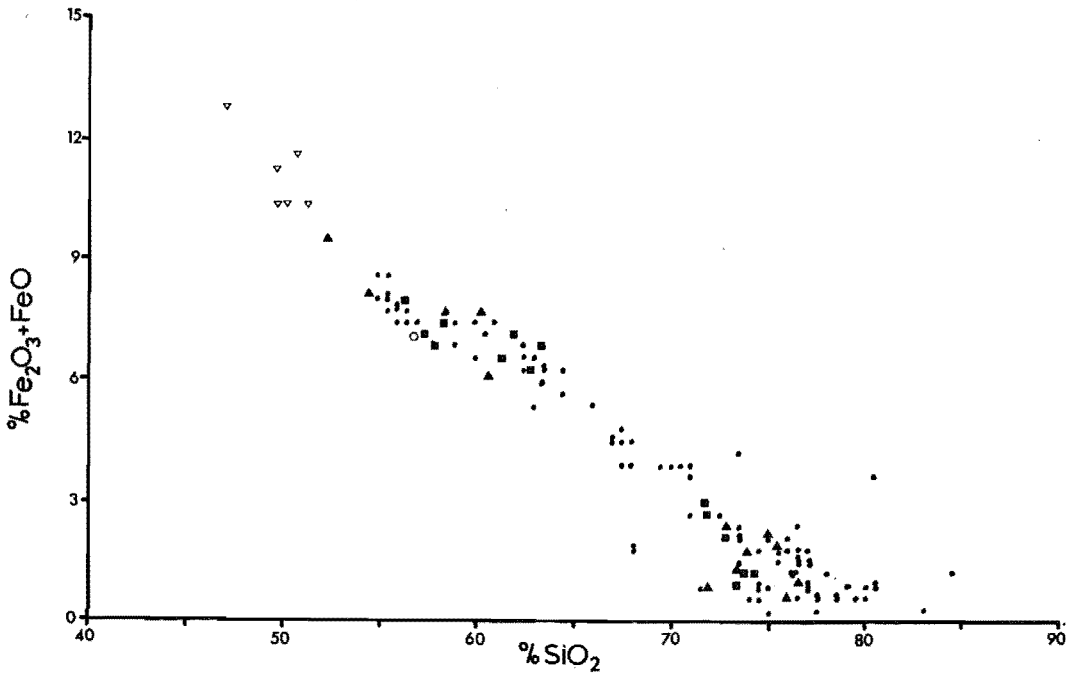

Figure 51. Plot of Fe_2O_3 + FeO against SiO_2 in the Mt.Somers Volcanics. Symbols as for Figure 47.

basic and acidic volcanics, but also overlaps both ranges. This contrasts with the TiO_2 distribution of the dacite. The variation diagram for total iron versus silica (Figure 51), shows the excellent correlation between these elements. There are no distinct breaks in the trend and the basalts also fall on the same regression line. The only important iron bearing phases that crystallised in the andesite and dacite were hypersthene ilmenite and magnetite. It will be shown later that magnetite alone cannot account for the differentiation trend shown by iron, because of the vanadium concentrations of these volcanics. While ilmenite fractionation would also account for some removal of iron, it also could not, by itself, explain the trend shown for iron. A combination of hypersthene and ilmenite with, or without, magnetite would account for the iron fractionation in the andesite and dacite. The trend for iron in the rhyolite is not as well defined. It could have resulted from ilmenite fractionation together with almandine garnet and biotite.

The frequency distribution of MnO (Figure 52) shows the same trend as iron, with no clear distinction among the rhyolites or among the andesites. The dacite overlaps both the basic and acidic MnO ranges. The variation diagram for MnO (Figure 53) also shows the same linear trend as was observed for iron, without any discontinuity between the basic and acid volcanics.

The frequency distribution for MgO (Figure 54) has been split into two scales to accentuate the distribution of MgO in the rhyolite. No significant variations in the

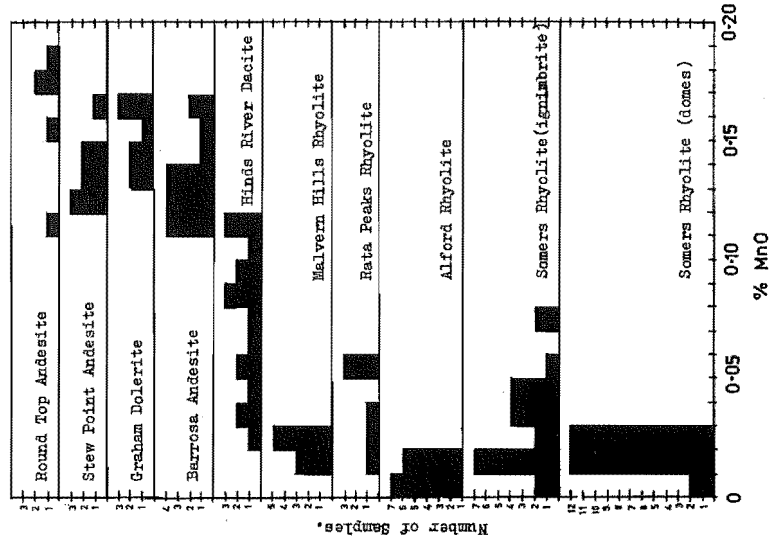

Figure 52. Histogram showing the frequency distribution of MnO in the Mt. Somers Volcanics.

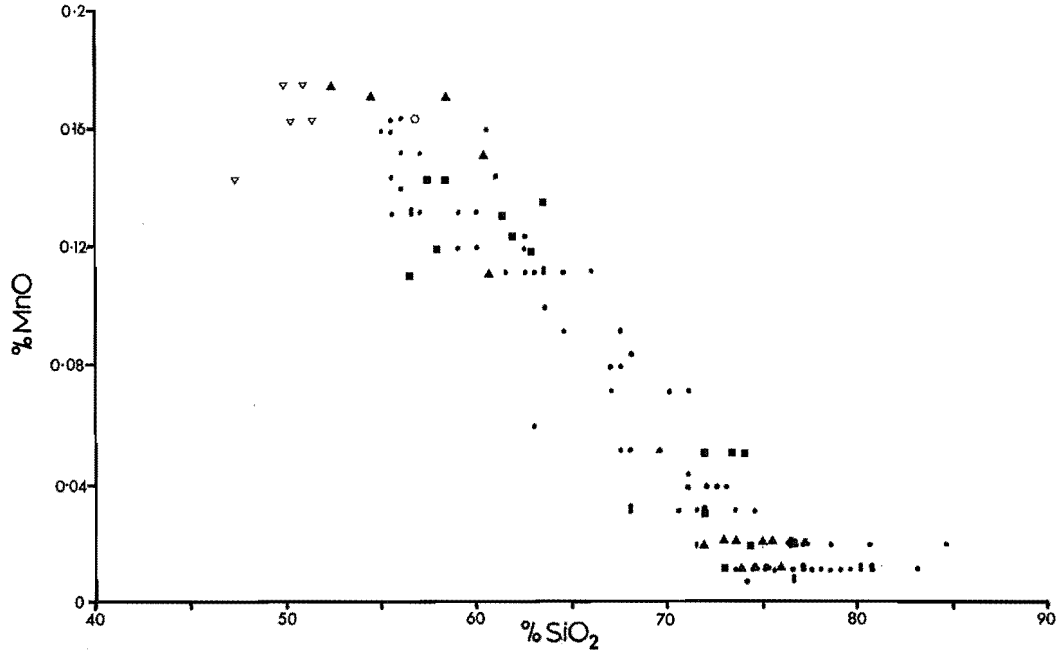

Figure 53. Plot of MnO against SiO_2 in the Mt.Somers Volcanics. Symbols as for Figure 47.

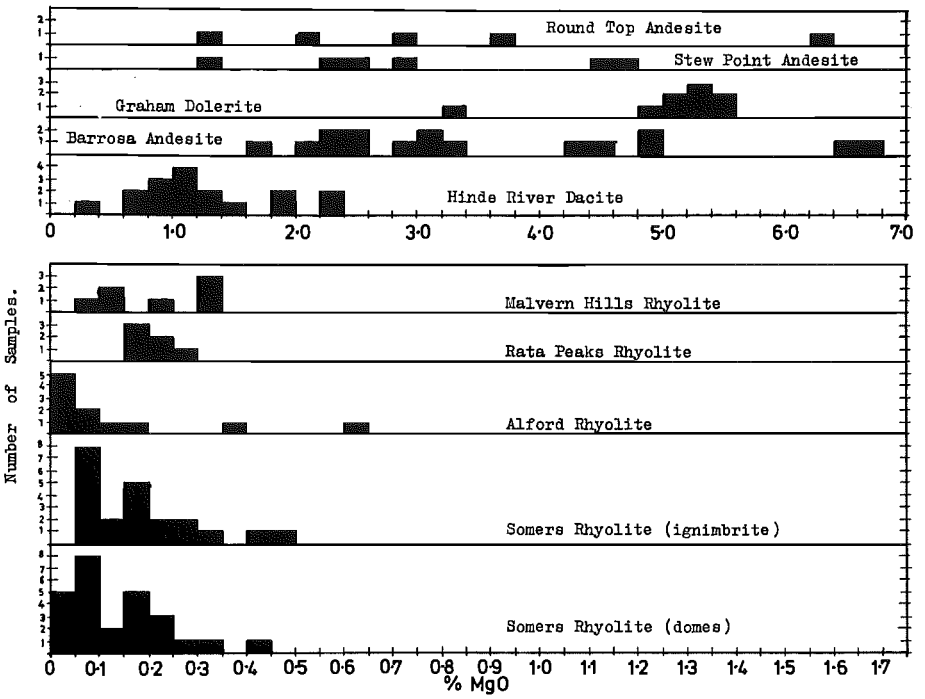

Figure 54. Histogram showing the frequency distribution of MgO in the Mt.Somers Volcanics.

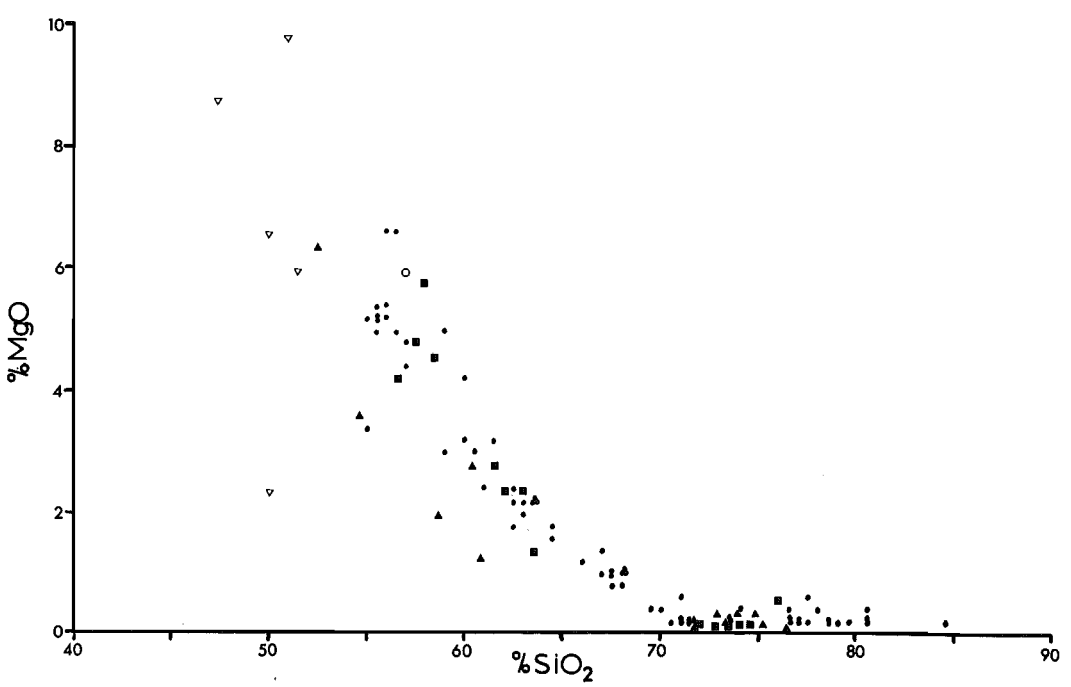

Figure 55. Plot of MgO against SiO_2 in the Mt.Somers Volcanics. Symbols as for Figure 47.

distribution of MgO occurs in the different types of rhyolite, nor in the andesite. The Graham Dolerite shows a more restricted range of values than the andesite. The dacite again spans the pronounced concentration gap between the rhyolite and the andesite. The MgO variation diagram (Figure 55) shows a linear regression, with increasing silica content, until the rhyolite composition is reached, by when the MgO content is less than 0.5%. The trend shown by MgO in the andesite and dacite can be accounted for by fractional crystallisation of hypersthene.

The frequency distribution for CaO (Figure 56) again shows a distinction between the ignimbrite and domes of the Somers Rhyolite and shows that fractionation of plagioclase occurred during the differentiation of the rhyolite. The suggestion of a bimodal distribution of CaO in the ignimbrite is also found in some of the other histograms (e.g. those of TiO_2, K_2O, and P_2O_5), but may indicate sampling bias rather than it being of any genetic significance. The range of values for CaO is similar for all the rhyolites of the area, and for all the andesites. As with MgO, the CaO distribution accentuates the more basic nature of the Graham Dolerite when compared to the andesite. The Hinds River Dacite shows its intermediate character again in its CaO distribution range. The variation diagram for CaO versus SiO_2 is given in Figure 57, which shows the excellent correlation between these elements. The almost linear regression of CaO with increasing differentiation can be accounted for by the fractional crystallisation of calcic-plagioclase and, to a minor extent, hypersthene.

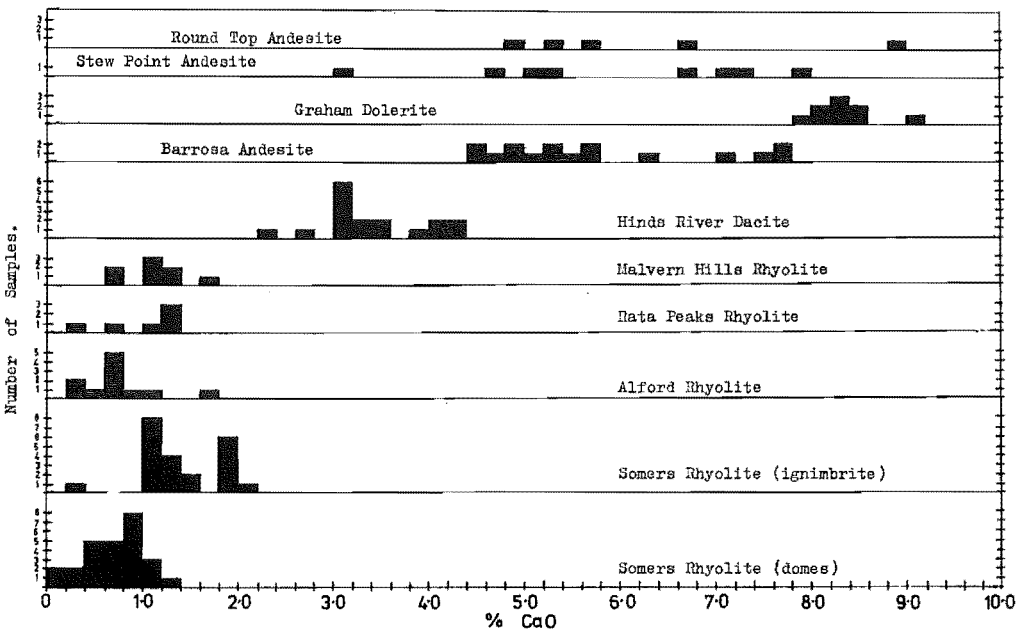

Figure 56. Histogram showing the frequency distribution of CaO in the Mt.Somers Volcanics.

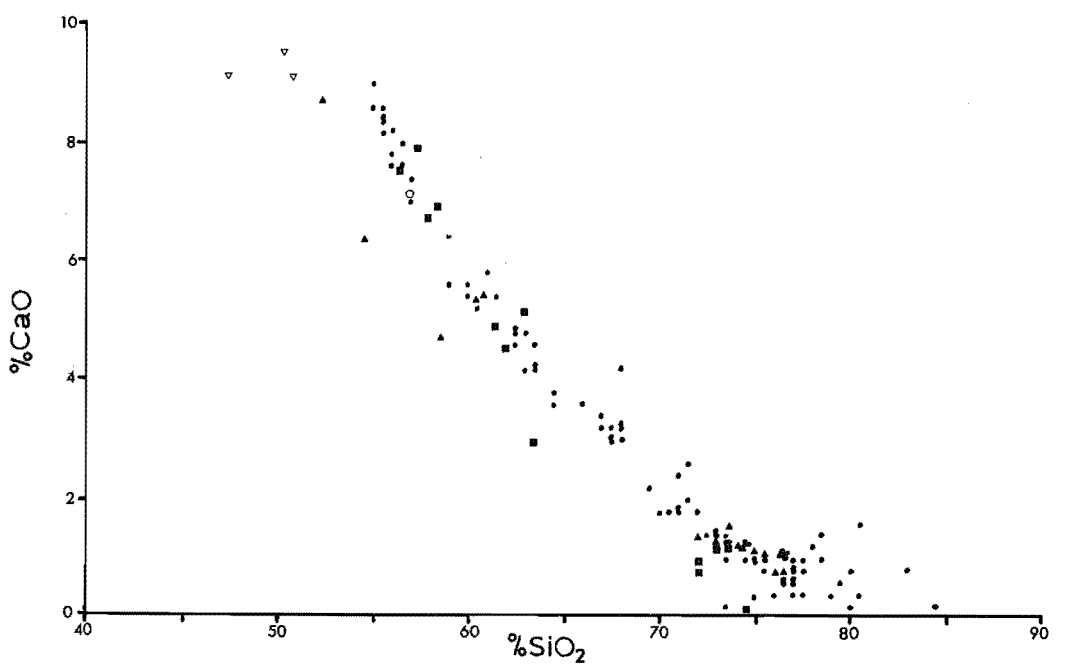

Figure 57. Plot of CaO against SiO_2 in the Mt.Somers Volcanics. Symbols as for Figure 47.

The frequency distribution of Na_2O is given in Figure 58. No distinct break occurs between the histograms of the Somers Rhyolite, although the ignimbrite shows a slightly more sodic tendency than the rhyolite domes. The very low Na_2O samples of rhyolite in the Alford Rhyolite and Somers Rhyolite (domes) are rhyolite tuffs which are either extremely differentiated and/or have been sorted resulting in the removal of some of the sodic-glass matrix fraction. The Na_2O histograms for all the Mt Somers Volcanics cover the same range of values. The Na_2O variation diagram (Figure 59) again shows the limited extent of the change of Na_2O during the differentiation from the andesite to rhyolite. In the andesite-dacite range there is a slight increase in Na_2O content indicating that the sodium content of the fractionating plagioclase, was not quite high enough to result in a depletion of Na_2O in the reduced volume of the residual magma. A decrease in Na_2O content in the rhyolite would have occurred as the result of fractionation of early formed sodic plagioclase, and some sanidine.

The frequency distribution for K_2O is given in Figure 60. The Somers Rhyolite has an apparently bimodal distribution in the ignimbrite, but this may not be significant, as the range of K_2O in these rocks overlaps that of the rhyolite domes. The distribution of K_2O for the dacite and andesite is similar to that of CaO. The K_2O variation diagram (Figure 61) shows a continuously increasing differentiation trend over the range basalt to acid-dacite because of the absence of a fractionating phase that could accommodate potassium. No distinct trend is seen for the rhyolite except for a slight increase in K_2O

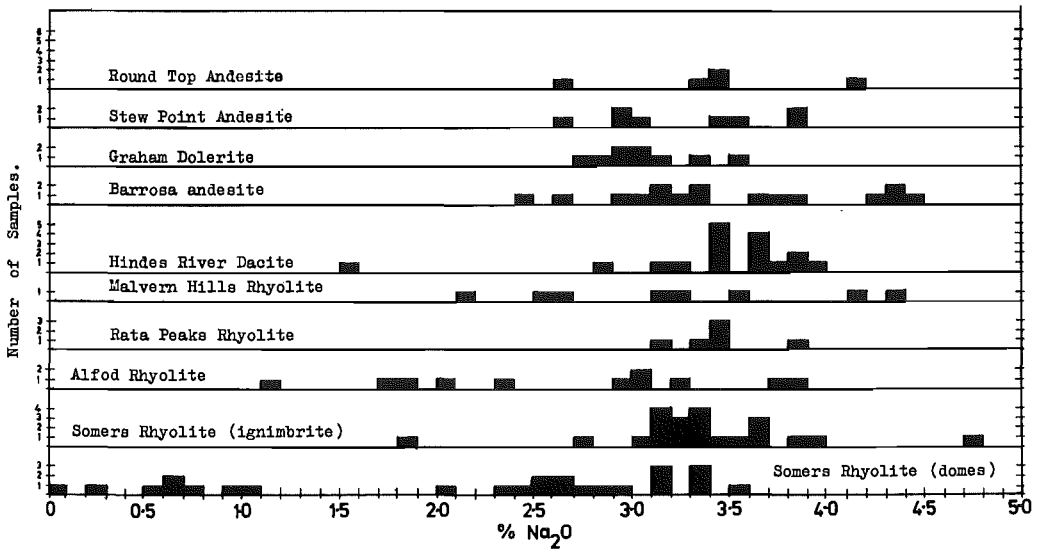

Figure 58. Histogram showing the frequency distribution of Na_2O in the Mt.Somers Volcanics.

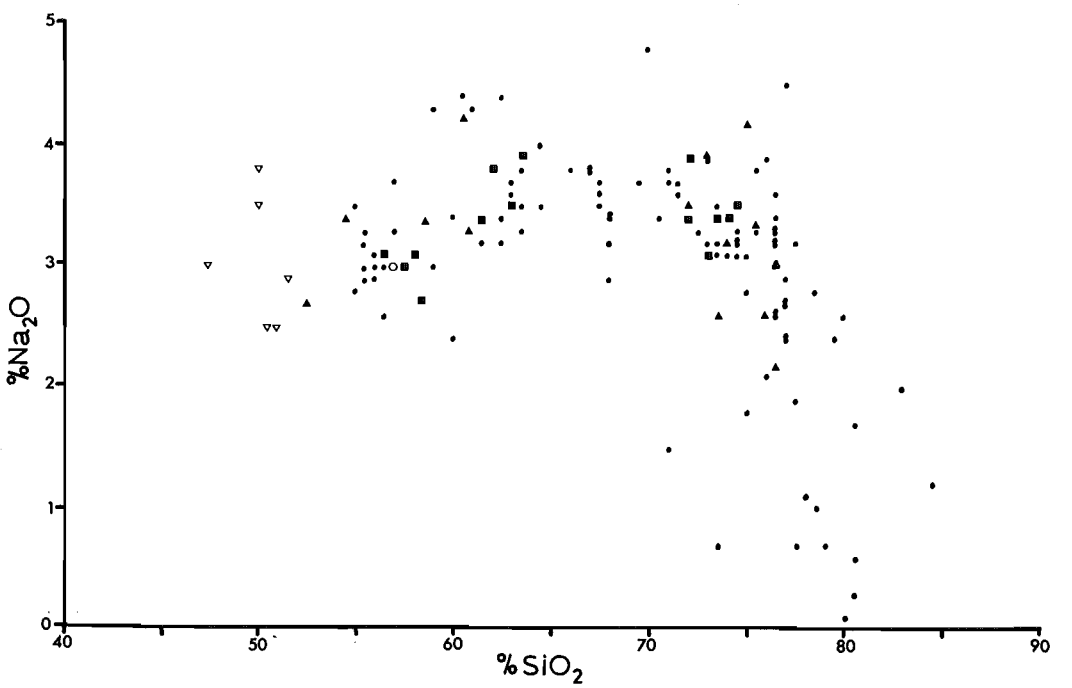

Figure 59. Plot of Na_2O against SiO_2 in the Mt.Somers Volcanics. Symbols as for Figure 47.

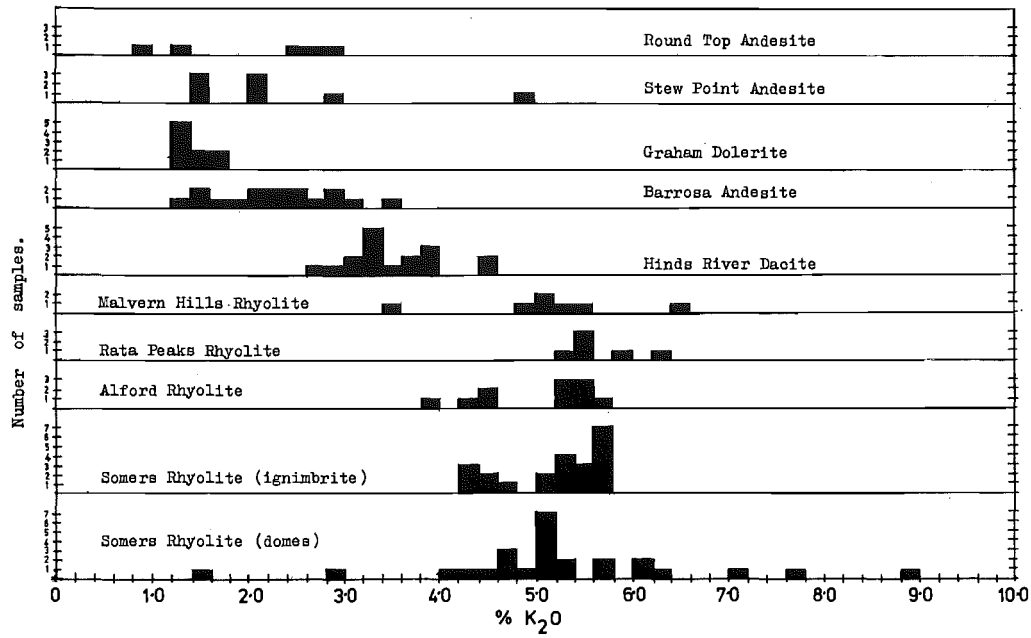

Figure 60. Histogram showing the frequency distribution of K_2O in the Mt.Somers Volcanics.

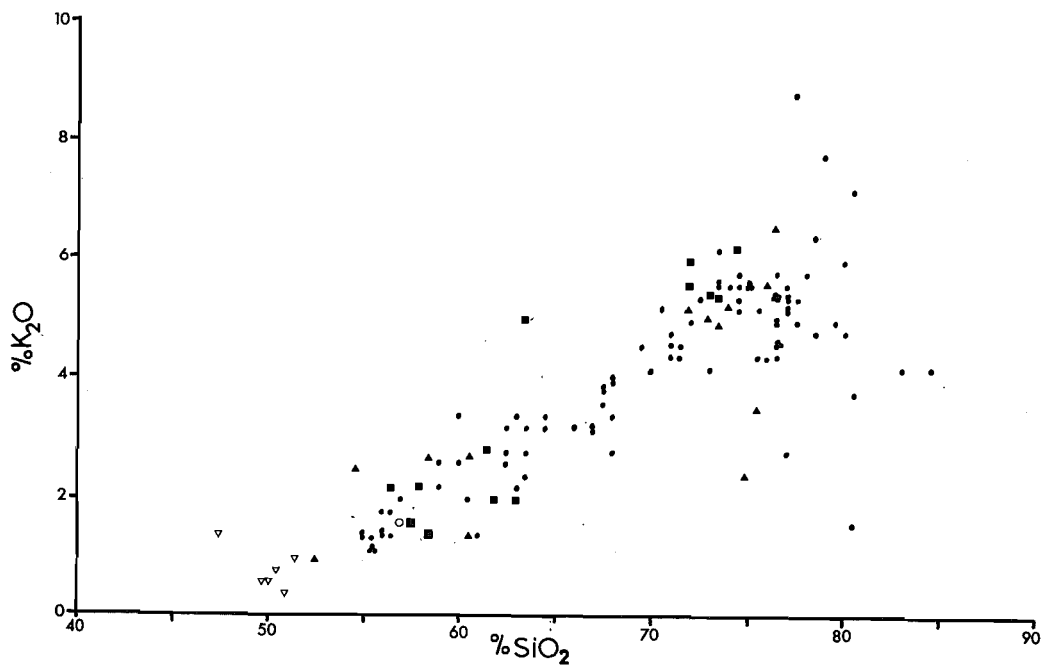

Figure 61 Plot of K_2O against SiO_2 in the Mt.Somers Volcanics. Symbols as for Figure 47.

content in ignimbrite, followed by a decrease in the rhyolite domes. The scatter in the high silica range has probably resulted from sanidine accumulation in some rhyolite accompanied by depletion in others.

The frequency distribution for P_2O_5 is given in Figure 62. The distinction between the Somers Rhyolite ignimbrite and rhyolite domes occurs, together with an apparent bimodal distribution of P_2O_5 in the ignimbrite. The Malvern Hills Rhyolite exhibits a more basic (less differentiated) trend by spanning the gap between the other rhyolites and the basic rocks; a role usually occupied by the dacite for all other major elements. The P_2O_5 distribution of the dacite is similar to the andesite except for Round Top Andesite which includes two samples of high-Al basalt with high P_2O_5 values. The variation diagram for P_2O_5 (Figure 63) indicates that a distinct break between the dacite and the rhyolite occurs that is of a similar trend to that of TiO_2. This gap in P_2O_5 contents is accentuated by the change in slope from the positive andesite regression trend to the negative rhyolite regression trend. The fractional crystallisation of apatite was either non-existent, or very minor, in the andesite with the result that P_2O_5 increased in concentration with increasing differentiation. The dacite shows a decrease in P_2O_5 over the andesite which indicates that apatite was a fractionating phase in that magma. The apparently anomalously low P_2O_5 content of the rhyolite, compared to the dacite, could indicate that crystal fractionation of apatite occurred prior to the fractionation of the plagioclase in the rhyolite melt-fraction.

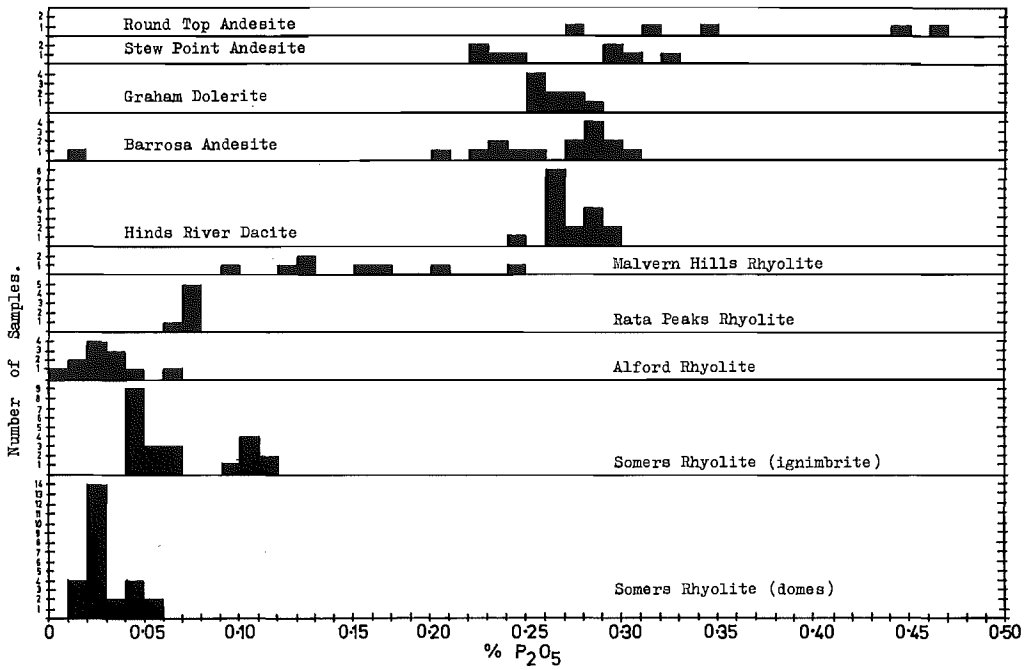

Figure 62. Histogram showing the frequency distribution of P_2O_5 in the Mt.Somers Volcanics.

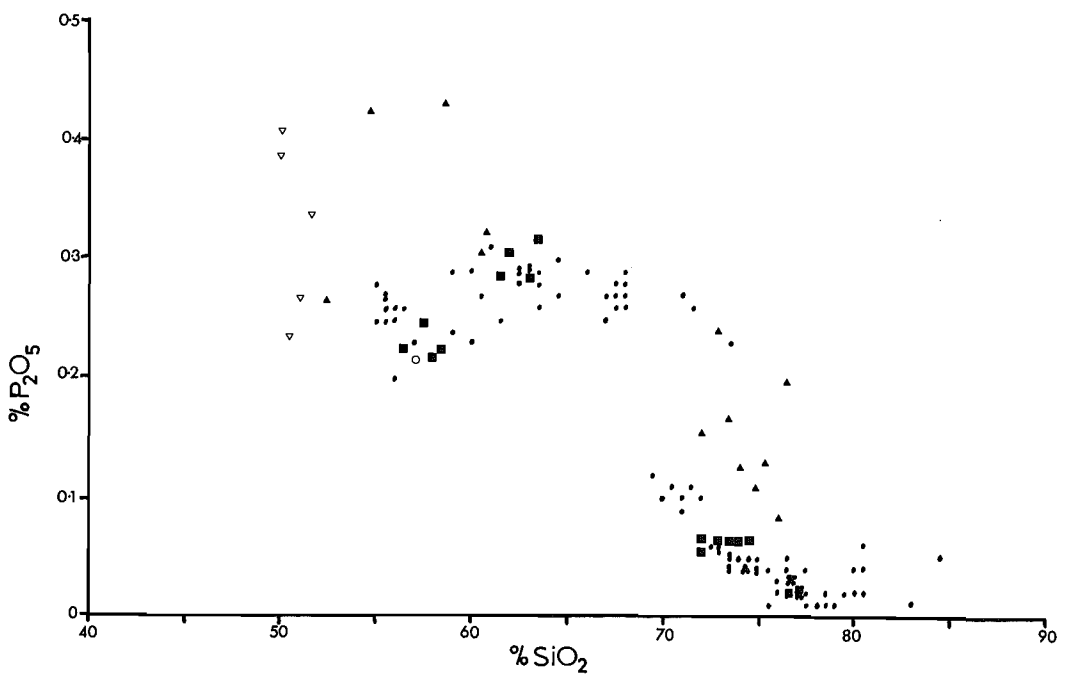

Figure 63. Plot of P_2O_5 against SiO_2 in the Mt.Somers Volcanics. Symbols as for Figure 47.

The presence of the gaps in P_2O_5 and TiO_2 variation trends could also be used as evidence that the rhyolite is derived from a different source to the dacite and andesite, but the absence of analysed samples with SiO_2 content of the critical intermediate composition (68-69% SiO_2) means that it would be unwise to place too much importance on these P_2O_5 and TiO_2 trends alone. This will be discussed in more detail in the section on petrogenesis after the trace element data has been examined.

2.3.5 Trace Element Geochemistry

Trace element chemical analyses of selected samples of the Mt Somers Volcanics are given in Table 7. The Table is arranged after the form suggested by Taylor and White (1966), as this provides all the element values and ratios, used in trace element studies, in readily usuable form.

2.3.5.1 Trace element variations

2.3.5.1.1 Large Cations. The large cations of Rb^+, Ba^{2+}, Pb^{2+} and Sr^{2+} have the ability to enter into 8- or 12-fold coordination (and rarely 6-fold coordination) in the lattice sites of the major silicate minerals, but generally these elements are concentrated by differentiation processes.

(a) Rubidium: The rubidium ion in 12-fold coordination has a radius of 1.81 Å which is only slightly larger than the

Sample Localities for analyses given in Table 7

(Note: All Grid References from S81 unless stated otherwise)

Analysis No.	Sample No.	
1	PO355	Rhyolite. Stour River. GR 809464.
2	PO415	Rhyolite. Staveley Hill, Mt Somers, GR 905444.
3	PO458	Rhyolite. Woolshed Creek. GR 830450.
4	PO279(a)	Rhyolite. Mt Alford. GR 970493.
5	PO514	Ignimbrite. South of Round Top. GR S72/166608.
6	PO457	Pitchstone. Woolshed Creek. GR 827451.
7	PO551	Rhyolite (flow-banded). Summit of Mt Somers. GR 890461.
8	PO553	Rhyolite (flow-banded). Ridge east of the summit of Mt Somers. GR 896460.
9	PO508	Rhyolite. On road near Harper Lodge. GR 586356.
10	PO537	Ignimbrite. Between Woolshed Creek and Morgan Stream. GR 848484.
11	PO496	Rhyolite. Stew Point. on Zig Zag track. GR 631334.
12	PO550	Rhyodacite dike. North face Mt Somers. GR 878473.
13	PO562	Dacite. Gawler Downs (Surrey Hills). GR S91/886298.
14	PO261	Dacite. Winterslow track opposite Diamond Creek. GR 954502.
15	PO341	Dacite. Trig Station on Gawler Downs. GR 880313.
16	PO502	Andesite. East of Raw Tor, near Ben McLeod. GR 572338.
17	PO360	Dacite. Gorge of North Branch Hinds River. GR 802372.
18	PO482	High-K andesite dike. Near summit of Mt Barrosa (Clent Hills). GR 759458.
19	PO477	High-K andesite (aphyric). Mt Somers, near Morgan Stream. GR 853481.
20	PO478	High-K andesite (porphyritic). Mt Somers near Morgan Stream. GR 853481.
21	PO512	Andesite (aphyric). South of Round Top. GR S72/170609.
22	PO142	Andesite. Blondin Creek. GR 806400.
23	PO506	Andesite. Near Hewson River. GR 611303.
24	PO564	Low-Si andesite. J. D. George No.1 well, Ashburton. GR S92/352095.
25	PO356	Dolerite. Mt Alford. GR 996496.

26	PO484	Low-Si andesite. Clent Hills near Ashburton Gorge. GR 776448.
27	PO417	Low-Si andesite. Sandrey Stream. GR 762411.
28	PO513	High-Al basalt. South of Round Top. GR S72/170609.
29	PO237(b)	Basalt dike. Trig TT, Mt Somers Range. GR 839526.
30	PO511	Basalt dike. Road to microwave station, Pullwool Peak. GR S74/277634.
31	PO272	Basalt (pillow lava), Tertiary. Taylors Stream by Winterslow Homestead. GR 959487.
32	PO179	Basalt dike. Clent Hills near Ashburton Gorge. GR 736476.

TABLE 7: Trace element data for Mt Somers Volcanics.

	1	2	3	4	5	6	7	8	9	10	11
SiO_2	77.27	77.14	76.61	76.73	76.15	76.65	74.99	74.47	73.89	74.66	71.86
TiO_2	0.10	0.10	0.10	0.11	0.20	0.10	0.17	0.18	0.26	0.18	0.24
Al_2O_3	12.83	12.87	12.65	13.28	13.28	12.73	14.27	14.25	14.37	14.76	14.32
Fe_2O_3	0.34	0.28	0.49	0.27	0.17	0.68	0.40	0.47	0.88	2.19	2.65
FeO	0.37	0.66	0.84	0.45	0.52	0.82	0.43	0.47	0.34	0.16	0.42
MnO	0.01	0.01	0.02	0.00	0.01	0.02	0.01	0.01	0.05	0.01	0.03
MgO	0.00	0.09	0.17	0.00	0.69	0.00	0.16	0.25	0.19	0.22	0.24
CaO	0.87	0.73	0.85	0.73	0.74	0.95	1.07	1.18	1.26	0.37	0.72
Na_2O	3.18	2.93	3.17	3.02	2.61	3.37	2.77	3.20	3.41	1.82	3.87
K_2O	5.01	5.16	5.07	5.38	5.53	4.65	5.66	5.47	5.28	5.60	5.57
P_2O_5	0.02	0.02	0.02	0.03	0.09	0.03	0.05	0.04	0.07	0.04	0.07
Large Cations											
Rb^+	265	268	269	247	200	251	245	249	230	260	237
Ba^{2+}	421	458	422	196	1083	423	1010	988	1292	1037	1237
$\%K^+$	4.16	4.29	4.21	4.46	4.59	3.86	4.70	4.56	4.38	4.65	4.62
Pb^{2+}	50	46	44	51	38	43	43	42	38	44	46
Sr^{2+}	50	50	49	20	91	53	98	100	139	81	118
$\%Ca^{2+}$	0.62	0.52	0.61	0.52	0.53	0.68	0.77	0.84	0.90	0.26	0.51
$\%Na^+$	2.36	2.17	2.35	2.24	1.93	2.50	2.05	2.38	2.53	1.35	2.87
K/Rb	157	160	157	181	229	154	192	182	191	179	195
Ba/Rb	1.59	1.71	1.57	0.79	5.42	1.68	4.12	3.97	5.62	3.99	5.22
Ba/Sr	8.42	9.16	8.61	9.80	11.90	7.98	10.31	9.88	9.30	12.80	10.48
Rb/Sr	5.30	5.36	5.49	12.35	2.20	4.74	2.50	2.49	1.65	3.21	2.01
Rare Earth Type											
Y^{3+}	33	52	40	11	23	47	109	81	80	68	88
Large Highly Charged Cations											
Th^{4+}	30	29	29	37	23	27	30	26	24	26	26
Zr^{4+}	140	134	135	172	203	135	261	253	364	230	348
$Th/K_{10^{-4}}$	7.22	6.76	6.88	8.29	5.01	7.00	6.39	5.73	5.48	5.59	5.63
Ferromagnesian Elements											
$\%Mn^{2+}$	0.01	0.01	0.02	0.00	0.01	0.02	0.01	0.01	0.04	0.01	0.02
$\%Fe^{2+}$	0.29	0.51	0.65	0.35	0.40	0.62	0.33	0.36	0.26	0.12	0.33
Cu^{2+}	7	4	8	5	7	0	0	11	10	8	8
Zn^{2+}	55	74	98	62	35	55	29	93	65	44	47
Ni^{2+}	1	5	4	6	3	0	1	9	7	6	7
$\%Mg^{2+}$	0.00	0.05	0.10	0.00	0.42	0.00	0.10	0.15	0.12	0.13	0.15
V^{3+}	1	0	0	0	2	1	1	2	4	2	2
$\%Fe^{3+}$	0.24	0.20	0.34	0.19	0.12	0.48	0.28	0.33	0.61	1.53	1.86
$\%Ti^{4+}$	0.06	0.06	0.06	0.07	0.12	0.06	0.10	0.11	0.16	0.11	0.15
Cr^{4+}	16	0	2	1	3	0	3	0	1	0	1
$\%Al^{3+}$	6.79	6.81	6.70	7.03	7.03	6.74	7.55	7.53	7.61	7.81	7.58
Cr/V	16.00	—	—	—	1.50	0	3.00	0	0.25	0	0.50
V/Ni	1.00	0	0	0	0.67	—	1.00	0.67	0.57	0.33	0.29
Small Cations											
$\%Al^{3+}$	6.79	6.81	6.70	7.03	7.03	6.74	7.55	7.54	7.61	7.81	7.58
$\%Si^{4+}$	36.12	36.06	35.81	35.87	35.60	35.83	35.06	34.82	34.54	34.90	33.59
P^{5+}	0.01	0.01	0.01	0.01	0.04	0.01	0.02	0.02	0.03	0.02	0.03
Chalcophile Elements											
Pb^{2+}	50	46	44	51	38	43	43	42	38	44	46
$\%Fe^{2+}$	0.29	0.51	0.65	0.35	0.40	0.62	0.33	0.36	0.26	0.12	0.33
Cu^{2+}	7	4	8	5	7	0	0	11	10	8	8
Zn^{2+}	55	74	98	62	35	55	29	93	65	44	47
Ni^{2+}	1	5	4	6	3	0	1	9	7	6	7

TABLE 7 (continued)

	12	13	14	15	16	17	18	19	20	21	22
SiO_2	71.42	66.90	64.51	64.34	63.01	63.14	62.55	62.54	61.25	60.61	57.11
TiO_2	0.30	0.94	1.07	1.12	1.23	1.24	1.28	1.28	1.13	1.40	1.20
Al_2O_3	14.82	15.71	15.60	15.85	15.91	16.57	15.86	15.80	15.99	16.18	16.44
Fe_2O_3	2.23	0.78	2.77	1.69	1.63	3.50	0.87	2.33	2.33	2.04	3.63
FeO	0.76	3.75	2.96	4.52	5.56	1.99	5.64	4.52	4.20	5.65	3.70
MnO	0.03	0.08	0.09	0.11	0.12	0.06	0.12	0.11	0.11	0.15	0.13
MgO	0.23	1.40	1.82	1.59	2.46	1.94	2.45	1.76	3.29	2.81	4.80
CaO	1.93	3.18	3.56	3.80	5.22	4.28	4.90	4.78	5.38	5.31	7.08
Na_2O	3.62	3.84	3.96	3.46	3.52	3.62	3.18	3.40	3.20	4.16	3.67
K_2O	4.55	3.15	3.39	3.22	2.04	3.36	2.86	3.18	2.86	1.39	2.02
P_2O_5	0.11	0.28	0.27	0.30	0.29	0.29	0.29	0.29	0.25	0.31	0.22
Large Cations											
Rb^+	192	221	155	179	148	145	153	140	140	152	196
Ba^{2+}	1320	753	693	640	700	680	618	637	422	562	445
$\%K^+$	3.78	2.61	2.82	2.67	1.70	2.79	3.38	2.64	2.38	1.15	1.68
Pb^{2+}	42	32	31	27	26	28	27	38	22	20	21
Sr^{2+}	171	242	257	248	467	238	229	233	217	227	245
$\%Ca^{2+}$	1.38	2.27	2.55	2.72	3.73	3.06	3.50	3.42	3.85	3.79	5.06
$\%Na^+$	2.69	2.85	2.93	2.56	2.61	2.68	2.36	2.52	2.37	3.09	2.72
K/Rb	197	118	182	149	115	192	155	189	170	176	175
Ba/Rb	6.88	3.41	4.47	3.58	4.73	4.69	4.04	4.55	3.01	3.69	4.64
Ba/Sr	7.72	3.11	2.70	2.58	1.50	2.86	2.70	2.73	1.94	2.48	1.82
Rb/Sr	1.12	0.91	0.60	0.72	0.32	0.61	0.67	0.60	0.65	0.67	0.39
Rare Earth Type											
Y^{3+}	90	58	59	57	52	42	56	56	52	64	45
Large Highly Charged Cations											
Th^{4+}	24	20	18	18	13	16	18	13	13	14	10
Zr^{4+}	459	351	311	326	301	310	305	386	267	304	227
$Th/K \times 10^{-4}$	6.36	7.65	6.39	6.73	7.66	5.74	7.57	4.92	5.47	12.15	5.95
Ferromagnesian Elements											
$\%Mn^{2+}$	0.02	0.06	0.07	0.09	0.09	0.05	0.09	0.09	0.09	0.12	0.10
$\%Fe^{2+}$	0.56	2.85	2.27	3.42	4.24	1.50	4.28	3.42	3.21	4.29	2.86
Cu^{2+}	12	22	22	19	23	23	22	26	31	25	39
Zn^{2+}	120	79	85	94	85	94	90	103	76	101	85
Ni^{2+}	4	10	14	12	19	13	14	7	18	17	43
$\%Mg^{2+}$	0.14	0.84	1.10	0.96	1.48	1.17	1.48	1.06	1.98	1.69	2.90
V^{3+}	7	41	49	41	56	64	56	54	66	66	104
$\%Fe^{3+}$	1.56	0.55	1.93	1.18	0.44	2.45	0.60	1.63	1.63	1.43	2.54
$\%Ti^{4+}$	0.18	0.56	0.64	0.67	0.74	0.75	0.77	0.77	0.68	0.84	0.72
Cr^{4+}	3	13	71	15	26	30	24	11	43	22	179
$\%Al^{3+}$	7.84	8.31	8.26	8.39	8.42	8.77	8.39	8.36	8.46	8.56	8.70
Cr/V	0.43	0.32	1.45	0.37	0.46	0.47	0.43	0.20	0.65	0.33	1.72
V/Ni	1.75	4.10	3.50	3.42	2.95	4.92	4.00	7.71	3.67	3.88	2.42
Small Cations											
$\%Al^{3+}$	7.84	8.31	8.26	8.39	8.42	8.77	8.39	8.36	8.46	8.56	8.70
$\%Si^{4+}$	33.39	31.27	30.16	30.08	29.46	29.52	29.24	29.24	28.64	28.33	26.70
P^{5+}	0.05	0.12	0.12	0.13	0.13	0.13	0.12	0.13	0.11	0.13	0.10
Chalcophile Cations											
Pb^{2+}	42	32	31	27	26	28	27	38	22	20	21
$\%Fe^{2+}$	0.56	2.85	2.27	3.42	4.24	1.50	4.28	3.42	3.21	4.29	2.86
Cu^{2+}	12	22	22	19	23	23	22	26	31	25	39
Zn^{2+}	120	79	85	94	85	94	90	103	76	101	85
Ni^{2+}	4	10	14	12	19	13	14	7	18	17	43

TABLE 7 (continued)

	23	24	25	26	27	28	29	30	31	32
SiO_2	57.26	56.39	56.12	56.59	56.05	52.73	51.03	50.71	49.83	49.82
TiO_2	1.13	1.42	1.23	1.10	1.08	1.27	1.75	1.47	2.14	3.13
Al_2O_3	16.23	16.08	16.66	16.13	16.07	16.89	13.39	12.30	13.78	16.38
Fe_2O_3	2.24	Σ 8.60	2.24	2.85	2.73	3.39	5.05	2.43	3.72	6.76
FeO	5.06	—	5.64	4.92	4.98	6.34	6.62	7.91	6.89	4.89
MnO	0.16	0.11	0.14	0.13	0.16	0.17	0.17	0.17	0.18	0.21
MgO	5.91	4.19	5.24	6.51	6.62	6.37	9.70	11.89	6.65	2.48
CaO	7.26	7.63	7.82	7.70	7.68	8.88	9.12	9.55	12.31	11.42
Na_2O	2.95	3.13	2.91	2.62	2.98	2.70	2.48	2.54	3.50	3.83
K_2O	1.58	2.22	1.75	1.44	1.44	1.00	0.42	0.80	0.60	0.69
P_2O_5	0.22	0.23	0.25	0.01	0.20	0.27	0.27	0.24	0.41	0.39
Large Cations										
Rb^+	70	181	78	98	71	25	13	26	10	13
Ba^{2+}	418	344	384	361	341	344	78	145	152	145
$\%K^+$	1.31	1.84	1.45	1.20	1.20	0.83	0.35	0.66	0.50	0.57
Pb^{2+}	19	28	15	14	16	6	6	7	0	0
Sr^{2+}	239	145	228	210	209	242	286	280	622	425
$\%Ca^{2+}$	5.18	5.45	5.59	5.50	5.49	6.35	6.52	6.82	8.79	8.17
$\%Na^2$	2.19	2.32	2.16	1.95	2.21	2.00	1.84	1.88	2.59	2.84
K/Rb	188	102	186	122	168	331	269	255	501	440
Ba/Rb	5.97	1.90	4.92	3.68	4.80	13.76	6.00	5.58	15.20	11.15
Ba/Sr	1.75	2.37	1.68	1.72	1.63	1.42	0.27	0.38	0.24	0.34
Rb/Sr	0.29	1.25	0.34	0.47	0.34	0.10	0.05	0.07	0.02	0.03
Rare Earth Type										
Y^{3+}	49	60	50	40	41	49	21	17	22	32
Large Highly Charged Cations										
Th^{4+}	14	17	12	10	10	9	4	6	0	3
Zr^{4+}	225	347	210	191	190	204	94	83	119	188
$Th/K_{10^{-4}}$	10.65	9.23	8.27	8.34	8.37	10.89	11.44	9.07	0.00	5.25
Ferromagnesian Elements										
$\%Mn^{2+}$	0.12	0.09	0.11	0.10	0.12	0.13	0.13	0.12	0.13	0.15
$\%Fe^{2+}$	3.83	—	4.32	3.72	3.78	4.78	4.99	5.92	5.13	3.41
Cu^{2+}	44	21	35	52	42	29	67	69	70	62
Zn^{2+}	76	101	77	75	80	88	101	99	118	118
Ni^{2+}	66	9	30	115	100	37	295	256	272	180
$\%Mg^{2+}$	3.56	2.53	3.16	3.92	3.99	3.84	5.85	7.17	4.01	1.49
V^{3+}	87	50	89	97	97	100	111	116	137	155
$\%Fe^{3+}$	1.57	6.01	1.57	2.00	1.91	2.37	3.53	1.70	2.60	4.73
$\%Ti^{4+}$	0.68	0.85	0.74	0.66	0.65	0.76	1.05	0.88	1.28	1.88
Cr^{4+}	158	9	69	231	240	89	250	360	275	279
$\%Al^{3+}$	8.59	8.51	8.82	8.54	8.50	8.94	7.09	6.51	7.29	8.67
Cr/V	1.82	0.18	0.78	2.38	2.47	0.89	0.25	3.10	2.01	1.80
V/Ni	1.32	5.56	2.97	0.84	0.97	2.70	0.37	0.45	0.50	0.86
Small Cations										
$\%Al^{3+}$	8.59	8.51	8.82	8.54	8.51	8.94	7.09	6.51	7.29	8.67
$\%Si^{4+}$	26.77	26.36	26.23	26.46	26.21	24.45	23.86	23.71	23.29	23.29
P^{5+}	0.10	0.10	0.11	0.00	0.09	0.12	0.12	0.10	0.18	0.17
Chalcophile Elements										
Pb^{2+}	19	28	15	14	15	6	6	7	0	0
$\%Fe^{2+}$	3.83	—	4.32	3.72	3.78	4.78	4.99	5.92	5.13	3.41
Cu^{2+}	44	21	35	52	42	29	67	69	70	62
Zn^{2+}	76	101	77	75	80	88	101	99	118	118
Ni^{2+}	66	9	30	115	100	37	295	256	272	180

Note: Major element oxides given in percentages; all other element ion concentrations given in ppm unless indicated.

potassium ion (1.68 Å) (Whittaker and Muntus 1970). This enables Rb^+ to substitute for K^+ ions in major potassium bearing minerals such as muscovite, biotite and the feldspars.

Because the Rb^+ ion is larger than the K^+ ion, rubidium is preferentially concentrated in 12-fold co-ordination K-sites in micas (relative to enrichment in K-feldspars).

Iiyama (1968) studied the rubidium distribution in K-feldspars and in co-existing plagioclase feldspars, at 600°C and 1000 bars pressure. The results showed that Rb^+ is preferentially fixed in the K-feldspars. Also because of the larger size of the Rb^+ ion (compared to that of K^+) it is preferentially enriched in the lower temperature potassium bearing minerals during magma crystallisation processes. Clinopyroxenes and orthopyroxenes tolerate potassium in preference to rubidium. Generally, however, the overall effect is for Rb^+ to become enriched in residual magmas.

The study of phenocryst/matrix partition co-efficients by Philpotts and Schnetzler (1970) gave the following ranges for partition coefficients for rubidium (partition coefficient, D = concentration of rubidium in mineral/concentration of rubidium in matrix):

Micas (biotite and phlogopite)	D = 0.936 to 3.06
K-feldspar	D = 0.659
Hornblende	D = 0.0448 to 0.427
Clinopyroxene	D = 0.0139 to 0.284
Orthopyroxene	D = 0.0148 to 0.0287
Garnet	D = 0.00851
Olivine	D = 0.0839 to 0.0113

From these partition coefficients it can be seen that the only mineral in a magma likely to result in significant depletion of Rb with progressive differentiation are the micas (biotite and phlogopite). Biotite occurs in the acid rocks of the Mt Somers area, but only as a very minor mineral phase and, as such, is unlikely to have had any noticeable effect on any enrichment of Rb caused by a differentiation process.

In the volcanic rocks analysed, rubidium shows excellent correlation with silica content ($r = 0.95$) and also with the Thornton-Tuttle (1960) Differentiation Index (DI) ($r = 0.95$). There is also an excellent negative correlation with Poldervaart and Parkers (1964) Crystallisation Index (CI) ($r = -0.93$).

The concentration of rubidium in the basalts is similar to that of the high-alumina basalt sample from the Malvern Hills (Figure 64), and is not significantly greater than what would be expected for tholeiitic basalt. The andesites, dacites, and rhyolites all show a considerable enrichment in rubidium compared to the average calc-alkaline volcanics. The rhyolites have a rubidium concentration nearly twice that of an average granite. This enrichment in rubidium is suggestive of a very highly fractionated volcanic series.

The K/Rb ratios (Table 7, Figure 65) are all low and relatively constant for the entire range of volcanic compositions represented, excluding the basalts which have a distinctly higher ratio. In a differentiated series of volcanics it would generally be expected that the K/Rb ratio

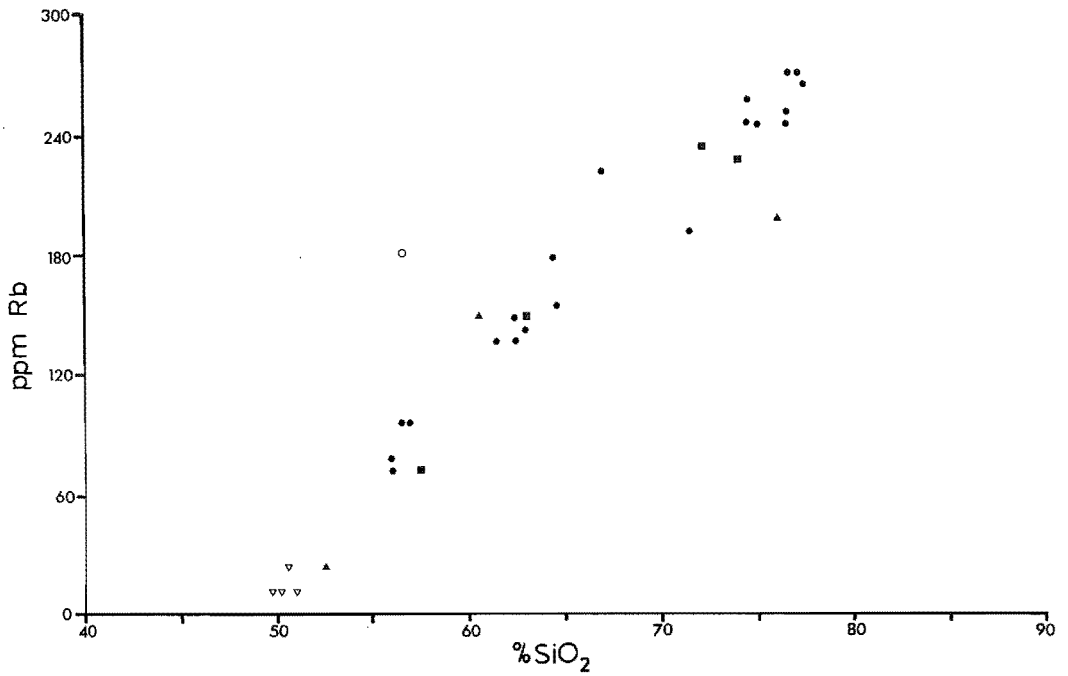

Figure 64. Plot of Rb against SiO_2 in the Mt.Somers Volcanics. Symbols as for Figure 47.

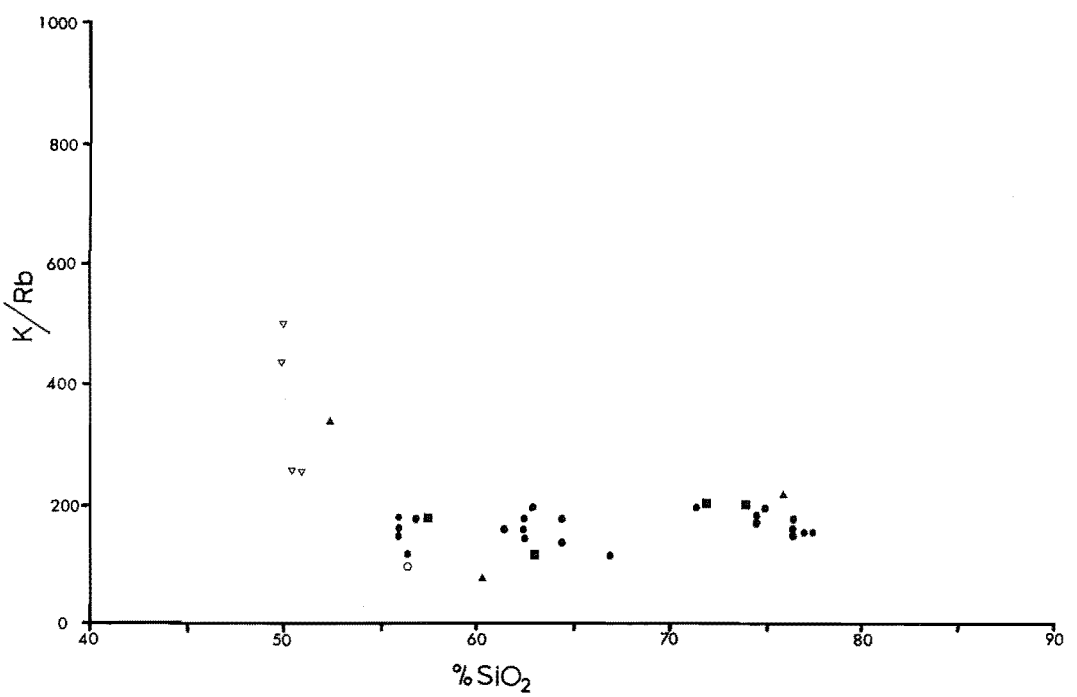

Figure 65. Plot of the ratio K/Rb against SiO_2 in the Mt.Somers Volcanics. Symbols as for Figure 47.

would increase from the basic to the acidic magmas (Philpotts and Schnetzler, 1970; Shaw, 1968). A slightly increasing trend through the range of andesite to rhyolite is seen for the Mt Somers Volcanics but this trend is not significant (correlation coefficient for K/Rb vs. SiO_2 is r = 0.02; and for K/Rb vs. DI, r = 0.01, K/Rb vs. CI, r = -0.001). Although the K/Rb ratio is not a particularly useful ratio to use as an index of magmatic evolution or origin (Carmichael *et al.*, 1974, p74), in the andesites and rhyolites of the Mt Somers Volcanics, it is consistent with a genetically related series of volcanics.

(b) Barium: The Ba^{2+} ion has a radius of 1.55 Å in 9-fold coordination, and substitutes for K^+ in potassium minerals, mainly K-feldspar and micas in igneous rocks. Some substitution by Ba^{2+} for Ca^{2+} also occurs in plagioclase, pyroxene, and amphibole. Of the non-silicates apatite and calcite contain the most barium. The K-feldspars are the most important of all these Ba containing minerals. Studies by Roy (1965, 1967), and Gay and Roy (1968) have shown that there is a continuous solid solution reaction series at high temperatures between the end-members of K-feldspar and celsian. It has been found that in magmas the Ba concentrations of the K-feldspars is highest in those that have crystallised earliest. Residual pegmatite solutions crystallise out K-feldspars that are notably low in Ba content (Shimer, 1943, Bray, 1942). The low content of Ba in these late stages can be attributed to depletion of Ba in the residual fluid by the crystallisation and removal of K-feldspar at an earlier stage in the genetic process.

The plagioclase feldspars can also accommodate Ba. A correlation between the potassium content of a plagioclase and its barium content was found to exist by Duchesne (1968). The intermediate plagioclases contain higher concentrations of Ba than the purer end-members. This can probably be accounted for by the greater number of distorted lattice sites able to accommodate the Ba^{+} ion in the intermediate feldspars.

The experimental hydrothermal studies of Iiyama (1968) which were carried out at 600°C and 1000 bars pressure showed the opposite results to that generally found in nature, namely that the plagioclase feldspar had a higher Ba content than coexisting K-feldspar.

The fact that only the K-feldspars and the micas play any significant role in the depletion of Ba in a magma is given by the partition coefficient, D (where D = Ba concentration in the mineral/Ba concentration in the matrix).

Analyses of phenocryst minerals and their coexisting matrix for volcanic rocks, were made by Philpotts and Schnetzler (1970) who found the following ranges for the partition coefficients:

K-feldspars	D = 6.12
biotite-phlogopite micas	D = 1.09, 6.36, 15.3
hornblende	D = 0.0996, 0.417, 0.731
plagioclase feldspars	D = 0.0537 to 0.589
clinopyroxenes	D = 0.0129 to 0.388
orthopyroxenes	D = 0.121 to 0.141
garnet	D = 0.0172
olivine	D = 0.00864, 0.0112

While values for the partition coefficients will vary greatly depending on pressure/temperature conditions within an individual lava, the trend shown by the data above appears to be consistent with Ba enrichment observed in minerals from a wide range of magmas.

The variations of Ba with silica content for the 32 Mt Somers Volcanics samples, that were analysed for trace elements, showed a distinct grouping for each particular lava type. For this reason Ba analyses were made on all the samples that had been analysed for major elements, and the results have been plotted in Figure 66. From this graph it can be seen that all of the andesites follow the same trend of enrichment in Ba with increasing silica content. The Hinds River Dacite forms a continuation of the andesite trend although the trend bifurcates in the more silica rich samples. The dacite is notably high in lithic xenoliths and partially dissolved xenoliths; there are indications that some of the lava has totally assimilated some xenoliths (only remnant garnets and opaques remaining). This factor could be responsible for the high silica content of the dacite and would result in the reduction of the Ba/SiO_2 ratio observed in the high-silica dacites.

The Ba content of the rhyolites shows a wide range for the different volcanic areas. The Somers Rhyolite can be divided into two distinct groups according to their Ba content. The older rhyolite tuffs and rhyolite domes form a group with low barium concentrations (a range of approximately 300 ppm to 500 ppm Ba) and show a systematic decrease in Ba content with

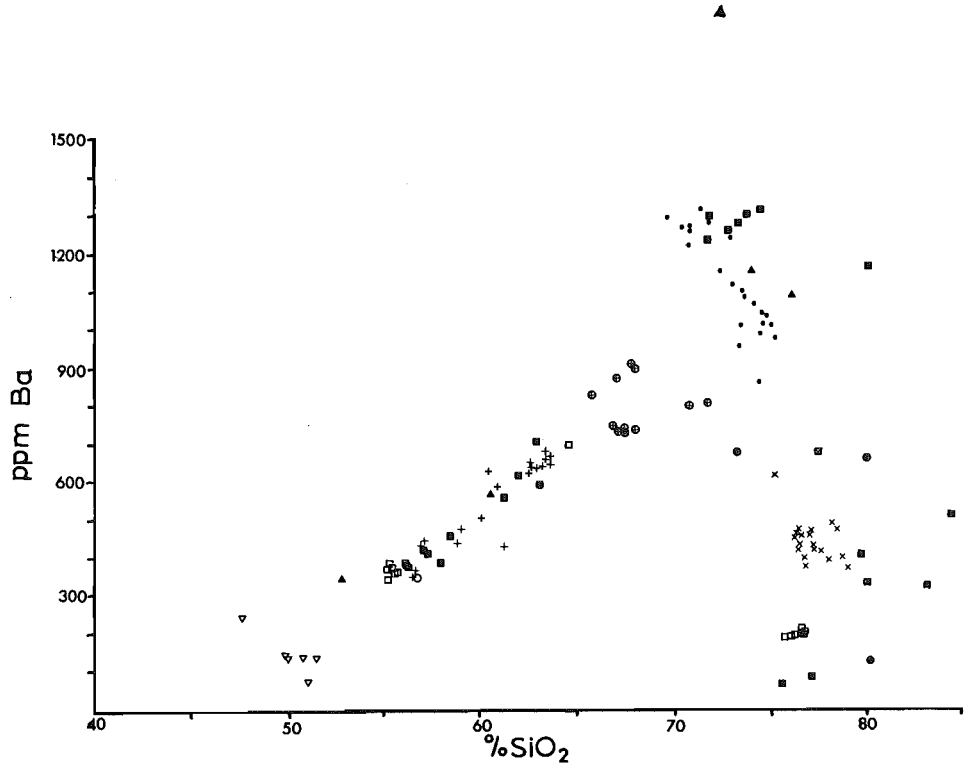

Figure 66. Plot of Ba against SiO_2 in the Mt Somers Volcanics. Symbols: • Somers Rhyolite (ignimbrite); × Somers Rhyolite (domes); ⊛ Somers Rhyolite (undetermined form); ▫ Alford Rhyolite (domes); ⊠ Surry Hills Tuff; ⊕ Hinds River Dacite; + Barrosa Andesite; ■ Rangitata Gorge volcanics; ▲ Mt Misery volcanics; ▽ Basalts.

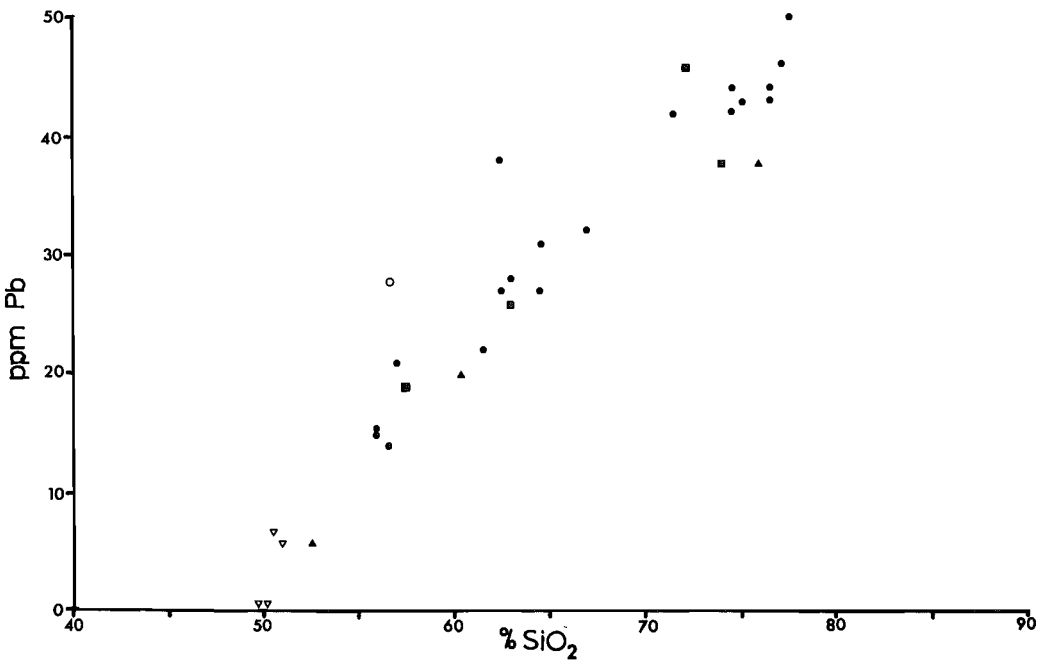

Figure 67. Plot of Pb against SiO_2 in the Mt.Somers Volcanics. Symbols as for Figure 47.

increasing silica. The Somers Rhyolite ignimbrites however have high barium concentrations (range approximately 1000 ppm to 1300 ppm Ba) and also show a systematic decrease in barium concentration with increasing silica content. These two distinct rhyolite types at Mt Somers have also been separated on silica content; those with a silica content higher than 76% (water free) form the domes that are characterised by the lower barium content, and those with a silica content lower than 76% form the flows characterised by the high barium content. From Figure 66 there appears to be only a little gradation between the high and low barium groups of the Somers Rhyolite. This could partly be explained by a lack of analyses of the intermediate rocks. Two samples indicate that rhyolite with intermediate Ba composition does exist and these represent the cumulodome-like structures of the N.E. and S.E. flanks of Mt Somers which underlie the ignimbrite. The decrease in Ba content, in both the ignimbrite and domes, with increasing silica content is consistent with the fractional crystallisation of sanidine within these rhyolites. The trend shown by the andesite and dacite indicates there was an absence of such a crystallising phase capable of removing Ba^{2+} ions from the magma during differentiation of these volcanics.

The Alford Rhyolite has low Ba concentrations. They typically have Ba concentrations of about 200 ppm, which is half that of the domes of Mt Somers. The Alford Rhyolite also forms domes. The rhyolite tuff of Mt Alford (i.e. the Surrey Hills Tuff) like those from other localities in the Mt Somers area, have a wide range in Ba concentration. This

can readily be explained by their form of deposition which has been discussed in a previous section.

The rhyolite from the Rangitata Gorge (i.e. the Rata Peaks Rhyolite) shows a positive correlation of Ba concentration with silica content (which is the opposite to that observed for the Somers Rhyolite), and indicates that sanidine was not the major crystallising feldspar in the rhyolite magma. This is consistent with the petrography.

The overall trend of Ba concentration in the Mt Somers Volcanics (i.e. the trend to increased Ba concentration from basic to acid magma, until the onset of crystallisation of sanidine, whereafter the Ba concentration decreases) has been observed in other volcanic provinces, e.g. Baker (1969) describes a similar trend for the volcanics of Saint Helena.

Heir and Taylor (1959) found that the concentration of Ba in K-feldspars decreases with increasing differentiation, which is consistent with the trend observed in the Mt Somers Volcanics.

(c) Lead: Lead, like the other large cations, tends to become enriched in residual magmas during differentiation processes. The Pb^{2+} ion has a similar radius (1.34 Å) to that of K^{+} (1.59 Å), Sr^{2+} (1.33 Å) and Ba^{2+} (1.50 Å) (all in 8-fold coordination), and can, to some extent, replace these ions in crystal lattices. The most usual substitution, is that of Pb^{2+} for K^{+} in the K-feldspars. However lead can also substitute for Ca^{2+} (radius 1.20 Å) and Na^{+} (radius 1.24 Å) in plagioclase and amphibole if conditions are favourable. The preference for Pb to substitute in K-feldspars is

illustrated by the synthetic solid solution series $PbAl_2SiO_2O_8$-$KAlSiO_3O_8$ (Sorrell, 1962; Scheel, 1971).

Doe and Tilling (1967) studied the distribution factor of Pb between co-existing K-feldspar and plagioclase feldspar for a variety of metamorphic and igneous rocks of widely differing ages. They found that lead is enriched in the K-feldspar by a factor of 2.4 times that in plagioclase feldspar. The distribution factor of D = 1.0 for Pb in co-existing K-feldspar and glass was also determined.

The trend observed in the Mt Somers Volcanics (Figure 67) shows a systematic increase in the Pb concentration from basalt to rhyolite. The correlation between Pb and SiO_2 concentrations is very high (r = 0.95). Lead concentration, has an equally good correlation with DI (r = 0.95) and CI (r = -0.96).

From Table 5 it can be seen that the Mt Somers rhyolites have a much higher concentration of Pb than an average granite (30 ppm) or an average calc-alkaline rhyolite. The andesites and dacite are also proportionally high indicating that the whole sequence of volcanics is highly fractionated.

Wedepohl (1974, p82-E-14) gave average lead concentrations for igneous rocks from all types of provenances. Of 186 rhyolites, obsidians and dacites, the average concentration is 21 ppm. Concentrations of over 50 ppm Pb are represented by only 2% of the samples. A similar trend is shown for 1220 granite samples which have an average Pb concentration of 23 ppm. These figures demonstrate the extent of the concentration of Pb in the magmas of the Mt Somers Volcanics. The

linear regression of Pb vs SiO_2 indicates that the extent of Pb substitution in the K-feldspars (or any other crystallising phase present in the magmas) was not high. The partition coefficients for all the minerals must therefore be $\leqslant 1$. This is in good agreement with the results of Doe and Tilling quoted above. Unlike barium, lead is enriched over the whole range of magmatic fractionation.

Fumarolic sublimates of many recent volcanics (Wedepohl, 1960) indicate that Pb is readily concentrated by magmatic gas transport and deposited around fumaroles as coturite. As $PbCl_2$ is very volatile, it would be expected that some lead is lost by this means, during basaltic, andesitic and rhyolitic eruptions. This means that the high Pb concentrations of the Mt Somers Volcanics could be expected to have been even higher prior to eruption.

(d) Strontium: The ionic size of strontium (1.33 Å , 8-fold co-ordination) is between that of Ca^{2+} and K^{+} and it is therefore able to substitute for potassium in K-feldspars and for calcium in plagioclase feldspars. Although the co-ordination number for Sr^{2+} can vary between 6 and 12, Sr^{2+} does not substitute for Ca^{2+} in pyroxenes or for K^{+} in micas.

The variation of strontium in the Mt Somers Volcanics is shown in Figure 68 from which it can be seen that, in the andesite-dacite range, the Sr concentration increases slightly with increasing silica content. This would indicate that the amount of concentration of Sr in the residual differentiating liquid, was only slightly greater than the amount of removal of Sr in plagioclase feldspars from the melt.

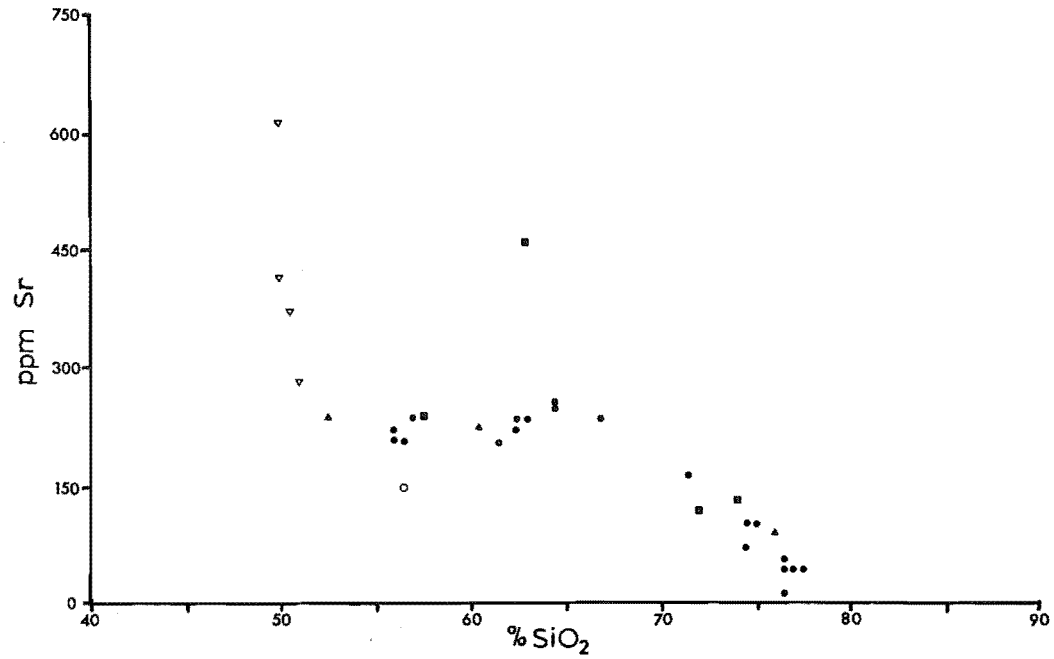

Figure 68. Plot of Sr against SiO_2 in the Mt.Somers Volcanics. Symbols as for Figure 47.

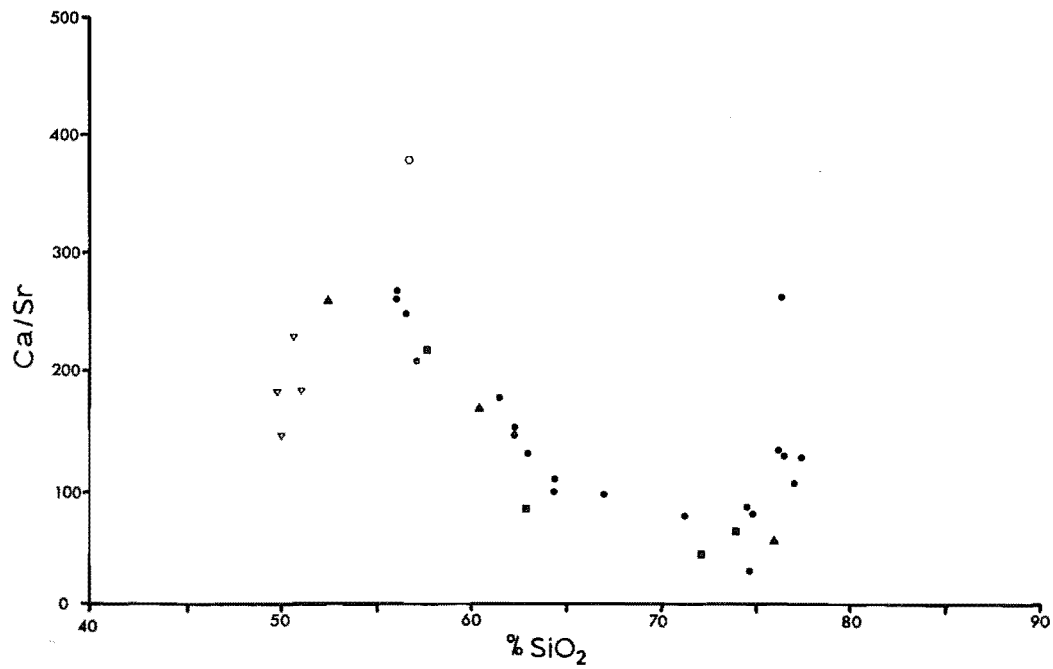

Figure 69. Plot of the ratio Ca/Sr against SiO_2 in the Mt.Somers Volcanics. Symbols as for Figure 47.

The trend for the rhyolite, in Figure 68, can be explained by the substitution of strontium in K-feldspar and/or plagioclase during the fractional crystallisation of these minerals.

The maximum Sr content of plagioclase occurs in labradorite (An_{60}) (Ewart and Taylor, 1969, Taylor, 1969), which can be explained by the greater degree of lattice distortions present in the intermediate plagioclases compared to the pure end members.

Figure 69 is a plot of the ratio Ca/Sr vs SiO_2 and this shows the enrichment of Sr relative to Ca during the fractionation of the andesite and dacite, and the depletion of Sr relative to Ca in the rhyolite. Correlation of Ca/Sr (in the andesite) with SiO_2 is good ($r = -0.85$), but is not so well correlated in the rhyolite ($r = 0.53$). This is a result of the scatter of Ca concentrations observed in the silica-rich rhyolite (shown previously in Figure 57).

A plot of the ratio Ba/Sr against silica content is given in Figure 70, from which it can be seen that all the rhyolite samples possess distinctly higher Ba/Sr ratios than those of the andesite or dacite.

There is a moderate correlation of the Ba/Sr ratio, in the andesite, with the silica content ($r = 0.77$), but the correlation with DI ($r = 0.52$) and CI ($r = -0.54$) is not as good. The rhyolite shows the reverse of this with there being no correlation with silica content ($r = 0.06$) but a moderate correlation with DI ($r = 0.65$), and CI ($r = -0.58$).

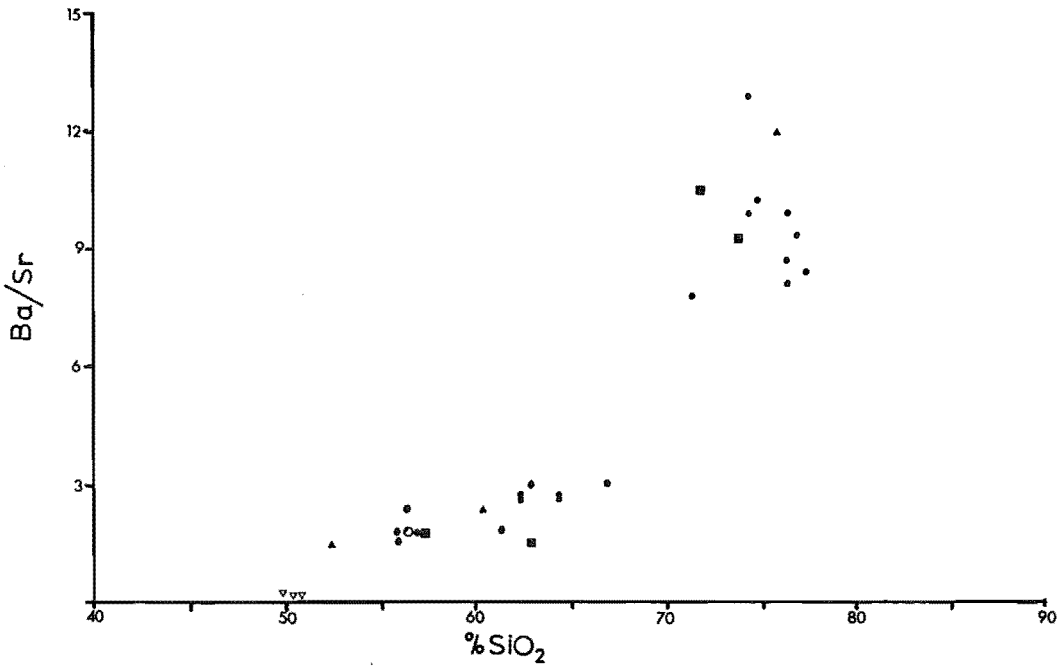

Figure 70. Plot of the ratio Ba/Sr against SiO_2 in the Mt.Somers Volcanics. Symbols as for Figure 47.

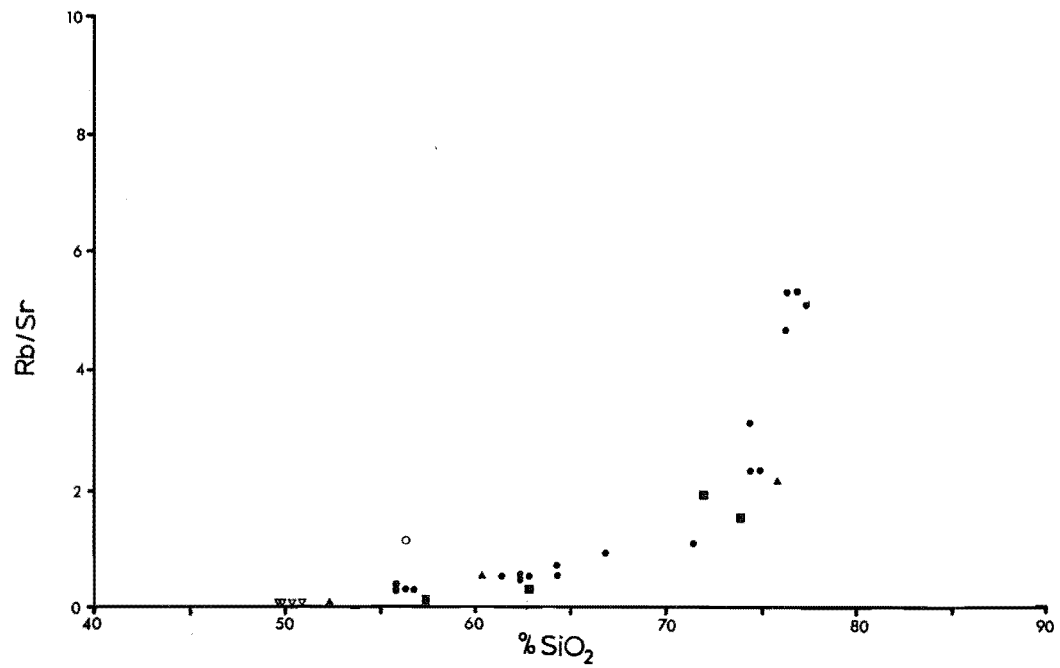

Figure 71 Plot of the ratio Rb/Sr against SiO_2 in the Mt.Somers Volcanics. Symbols as for Figure 47.

From Table 5 it can be seen that the Ba/Sr ratio is only slightly higher for the ignimbrite than it is for the rhyolite domes. This could indicate that both plagioclase and sanidine were crystallising in these magmas, which is consistent with the petrography and the individual trends shown for both Ba and Sr. The ratio Rb/Sr shows a similar variation (Figure 71) to that of Ba/Sr, but without the gap that occurs at the dacite/rhyolite boundary in the Ba/Sr plot (Figure 70). The trend shown by the Rb/Sr vs SiO_2 plot is consistent with the rapid depletion of strontium by the onset of sanidine crystallisation in the rhyolite.

2.3.5.1.2 Rare Earth Type Elements. The only element of this type that was analysed was yttrium (Y), which behaves chemically like the heavier Rare Earth elements of the lanthanide group La-Lu. The heavier RE elements, Gd to Lu, together with Y are usually referred to as the "yttrium group" because of their similar properties.

The yttrium ion, Y^{3+}, in 6-fold co-ordination, has a radius of 0.98 Å which is similar to that of Fe^{2+} (0.86 Å), Ca^{2+} (1.08 Å), and Na^{+} (1.10 Å) (Whittaker and Muntus, 1970).

In general Y^{3+} tends to replace Ca^{2+}, and to a lesser extent Fe^{2+}, in magmatic minerals. Because of the difference in charge the substitutions are usually of the form $Y^{3+}Fe^{2+} \rightleftharpoons Ca^{2+}Fe^{3+}$ (Hasegawa, 1960), or $Y^{3+}Al^{3+} \rightleftharpoons Ca^{2+}Si^{4+}$ (Lambert and Holland, 1974). Zircon and monazite are exceptions in which yttrium substitution takes place in the

absence of calcium. The mineral xenotime (YPO_4) is isostructural with zircon ($ZrSiO_4$) so the isomorphous tendency of Y in zircon is not surprising. Monazite is essentially a Rare Earth mineral (Ce, La, Th)PO_4 and the isomorphous substitutions of all RE elements including Y and also Ca, Fe^{3+}, Al, and U can take place.

Of the Ca-bearing and Ca-Fe-bearing minerals, not all act as Y-acceptors. Calcite, plagioclase, augite-clinopyroxenes, and kaersutite all have notably low concentrations of yttrium (Lambert and Holland, 1974).

Determinations of partition coefficients for yttrium in magmatic minerals are few, however the behaviour of yttrium could be expected to be similar to the RE elements dysprosium (Dy) and holmium (Ho), as these are similar to yttrium in ionic size, ionic charge, properties, and abundance in minerals and magmas (Cotton and Wilkinson 1966; Semenov and Barinski, 1958; Lambert and Holland, 1974; Hermann, 1970).

From the partition coefficients of Schnetzler and Philpotts (1970), for the yttrium group elements, garnet would have a partition coefficient greater than unity, while clino- and ortho-pyroxenes, olivine, amphiboles, and micas would all have partition coefficients less than unity. That is to say that of these minerals, only garnet fractionation would be expected to result in a depletion of yttrium in the residual magma.

In general the magmatic minerals that will accept significant amounts of yttrium are: zircon, allanite, spessartine, sphene, apatite, hornblende, almandine-pyrope,

riebeckite, grossular-almandine, pyrope, orthopyroxene, K-feldspar, muscovite and biotite. Of these only orthopyroxene is present in the andesite of the Mt Somers Volcanics; orthopyroxene and very minor garnet and allanite in the dacite; and minor zircon, allanite, apatite, almandine garnet, biotite, and phenocrystic sanidine, are present in the rhyolites.

The K-feldspars generally have very low Y contents (<40 ppm) (Gavrilova and Turanskaya,1958; Hermann, 1970; Lambert and Holland, 1974), and generally have partition coefficients ≤ 1. The crystallisation of sanidine in the Mt Somers rhyolites would not deplete residual magma in yttrium.

Orthopyroxenes have a Y content of between 10 and 30 ppm (Green, 1964; Ewart and Taylor, 1969) and, like K-feldspar would have partition coefficients ≤ 1. The crystallisation of hypersthene in the andesites and dacites of the Mt Somers Volcanics would therefore have enriched the residual magma in yttrium.

The garnet present in the Somers Rhyolite is almandine, with a minor grossular component while that from the Malvern Hills Rhyolite is almandine with minor pyrope and grossular components (Wood, 1974).

Spessartine garnet ($Mn_3Al_2Si_3O_{12}$) is known which contains over 2% Y_2O_3 (Deer *et al.*, 1966). In these garnets Y.Al substitutes for Mn.Si (Jaffe, 1951). There is complete solid solution between the synthetic end members of the system $Mn_3Al_2(Si_3O_{12})$ - $Y_3Al_2(Al_3O_{12})$ (Yoder and Keith, 1951).

Thus the ability of the Y^{3+} ion to substitute in the garnet structure is quite evident. The fractional crystallisation of garnet from Mt Somers Volcanics would be expected to result in depletion of Y in the residual magma. The significance of this is discussed below.

Apatite, zircon, and allanite, all have the ability to accommodate high concentrations of yttrium (>1000 ppm Y), (Gavriolova and Turanskaya, 1958; Khomyakov, 1967; Pavlenko *et al.*, 1959; Tauson *et al.*, 1968; Herrmann, 1970; Lambert and Holland, 1974), and these minerals are present as accessory minerals in the rhyolites of the Mt Somers area.

The trend shown by yttrium in the Mt Somers Volcanics is shown in Figure 72. The andesites and dacites show a slightly increasing enrichment of Y with increasing silica content. There is a moderately good correlation between Y and SiO_2 content ($r = 0.77$), but poor correlation with DI ($r = 0.51$) and CI ($r = 0.43$). The rhyolites show a very steep decrease in Y concentration with increasing silica content. The correlation of Y with SiO_2 ($r = -0.74$), DI ($r = -0.60$) and CI ($r = 0.43$), are similar to that of the andesites.

The trend shown by Y in the Mt Somers Volcanics (Figure 72) is similar to that shown by Ba (Figure 66). One difference between the two graphs is that there is not such a distinct break, in Y concentration, between the ignimbrite ($SiO_2 < 76\%$), and the rhyolite domes ($SiO_2 > 76\%$). The Y values would indicate that these rhyolites represent a continuous series.

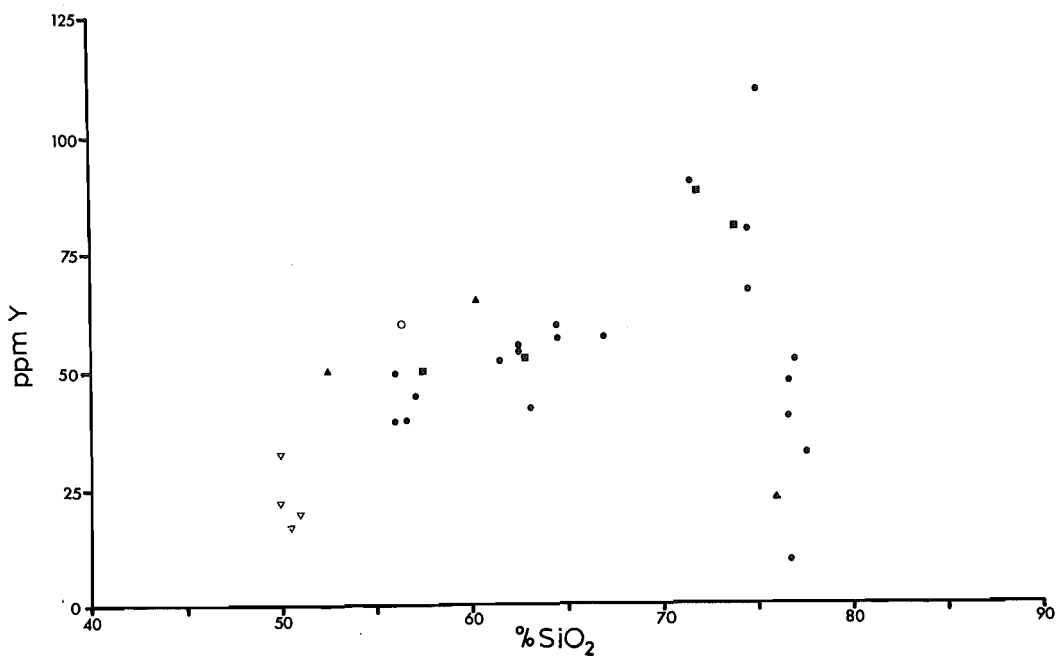

Figure 72. Plot of Y against SiO_2 in the Mt.Somers Volcanics. Symbols as for Figure 47.

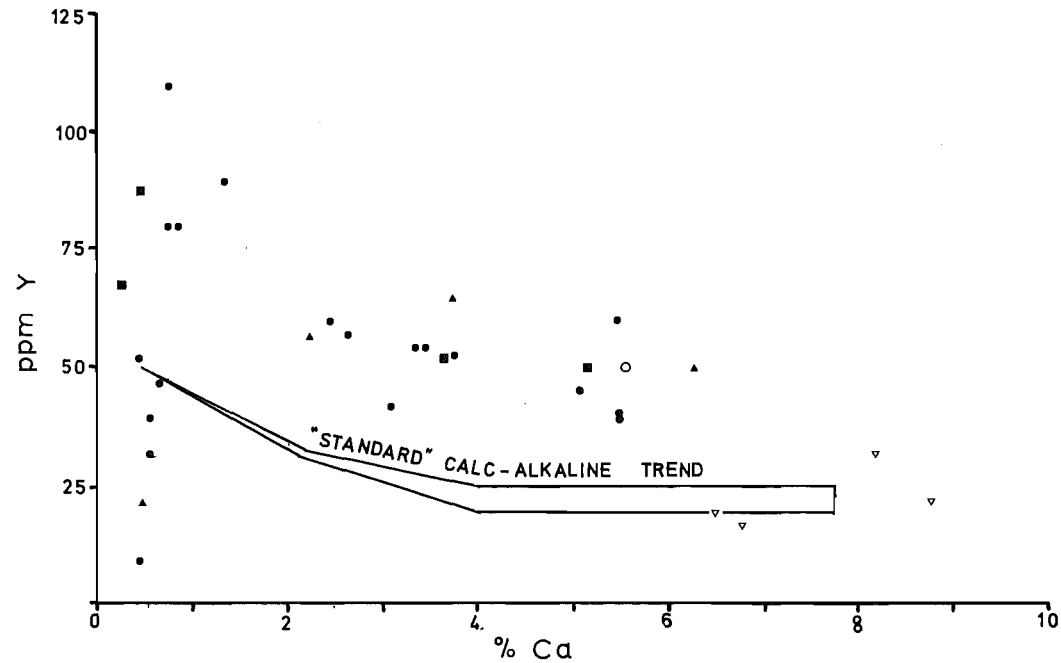

Figure 73. Plot of Y against Ca in the Mt.Somers Volcanics. Symbols as for Figure 47.

The abundances of Y in the Mt Somers Volcanics is higher than average for the calc-alkaline volcanics (Table 5,6). Values for yttrium concentration of 1,300 rocks were summarised by Fleischer (1969), from which it was found that the average values for 244 basalts was 38 ppm Y; for 159 andesites, 37 ppm Y; for 114 dacites, 31 ppm Y; and for 179 rhyolites, 60 ppm Y. Overall the averages for all volcanics was 35 ppm Y; for plutonics, 36 ppm Y; and for intermediate rocks, 35 ppm Y.

The relatively high concentration of Y in the Mt Somers Volcanics (particularly in the ignimbrites of the Somers Rhyolite), implies that these rocks are strongly fractionated.

The systematic variation of yttrium with calcium concentration in magmas, has been studied for a wide range of magma types by Lambert and Holland (1974). According to these authors the trends shown by yttrium can be directly related to the genetic processes of differentiation, and a classification on the basis of these trends can be made for igneous rocks. As a standard, the average values for calc-alkaline rock series taken from Taylor (1969); Gulson (1972); Wilkinson (1971); Bryan *et al.* (1972); and 996 unpublished analyses by G. M. Brown and J. G. Holland, were plotted and found to fall within a very restricted area (Lambert and Holland, 1974). This is shown in a modified form in Figure 73 as the "Standard" calc-alkaline trend. It is immediately apparent from Figure 73 that the Mt Somers Volcanics behave in a distinctly different way to those of the "Standard" calc-alkaline type. Relative to the Standard trend the andesites, dacites and rhyolite flows are enriched

in Y by a factor of approximately two. The rhyolites, however, show a rapid decrease in Y concentration with decreasing Ca concentration. The most likely cause of this is the removal of Y in accessory minerals and garnet during differentiation of the rhyolite.

2.3.5.1.3 Large Highly Charged Cations

(a) Thorium: Thorium has a preference for substitution in 8- and 6-fold co-ordination lattice sites, where the Th^{4+} ion has a radius of 1.12 Å and 1.08 Å, respectively (Whittaker and Muntus, 1970).

Thorium has a similar ionic size and electron configuration to cerium, uranium, and zirconium, with the result that crystal lattices, and bond characteristics of compounds of these elements are often isostructural (Bayer, 1969).

The most usual minerals for thorium to substitute into, are allanite, huttonite, and monazite although Th^{4+} can probably substitute for Zr^{4+} in zircon. Thorium forms the mineral thorite ($ThSiO_4$) which is isostructural with zircon ($ZrSiO_4$), and also a monoclinic variety huttonite which is isostructural with monazite (Bayer, 1969). It is not known if Th^{4+} forms an isomorphous series with Zr^{4+} in zircon. The Th/Zr ratio has been found to be relatively constant for a wide range of igneous rocks (Adams *et al.*, 1959), which would suggest there is some equilibrium between the two elements. Thorium does not occur in high concentrations in major magmatic phenocryst minerals (Rogers and Adams, 1969) and would be

expected to be concentrated during magmatic differentiation processes, unless there was crystallisation of significant amounts of accessory minerals.

Thorium is not as mobile in magmas as is the element uranium which is readily oxidised to the hexavalent state which then tends to enter volatile phases and thus escape from magmas (Whitfield *et al.*, 1959). For this reason, thorium is a better indicator of differentiation in a volcanic magma than is its associated element uranium.

The variation of thorium with silica concentration for the Mt Somers Volcanics is shown in Figure 74, in which it can be seen that there is a systematic increase from the basic to the acidic volcanics. The correlation of Th with SiO_2 ($r = 0.95$), DI ($r = 0.92$) and CI ($r = -0.92$) are all very high, and are consistent with a highly fractionated sequence of volcanics. The Mt Somers Volcanics have higher average thorium contents than average calc-alkaline plutonics, or volcanics (Tables 5,6).

The Th/K ratio for the Mt Somers Volcanics are higher than would be predicted. Heier and Rogers (1963) found that the arithmetic mean of all Th/K x 10^4 ratios in granites is 4.9, and that in basalts it is 2.8. The values for the rhyolites (Table 5) of the Malvern Hills and Rangitata Gorge are near to the granite average, but those of Mt Somers and Mt Alford are distinctly higher. The high Th content of these volcanics is reflected by the exceptionally high Th/K x 10^4 values for the andesites (6.6 to 11.5), (Table 6).

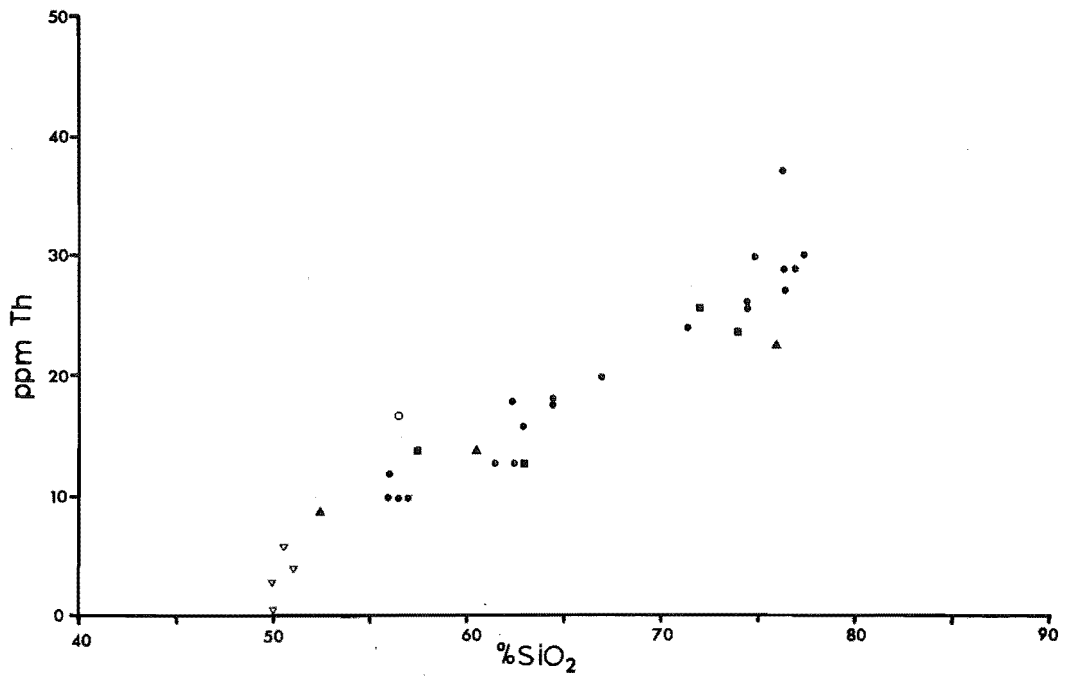

Figure 74. Plot of Th against SiO_2 in the Mt.Somers Volcanics. Symbols as for Figure 47.

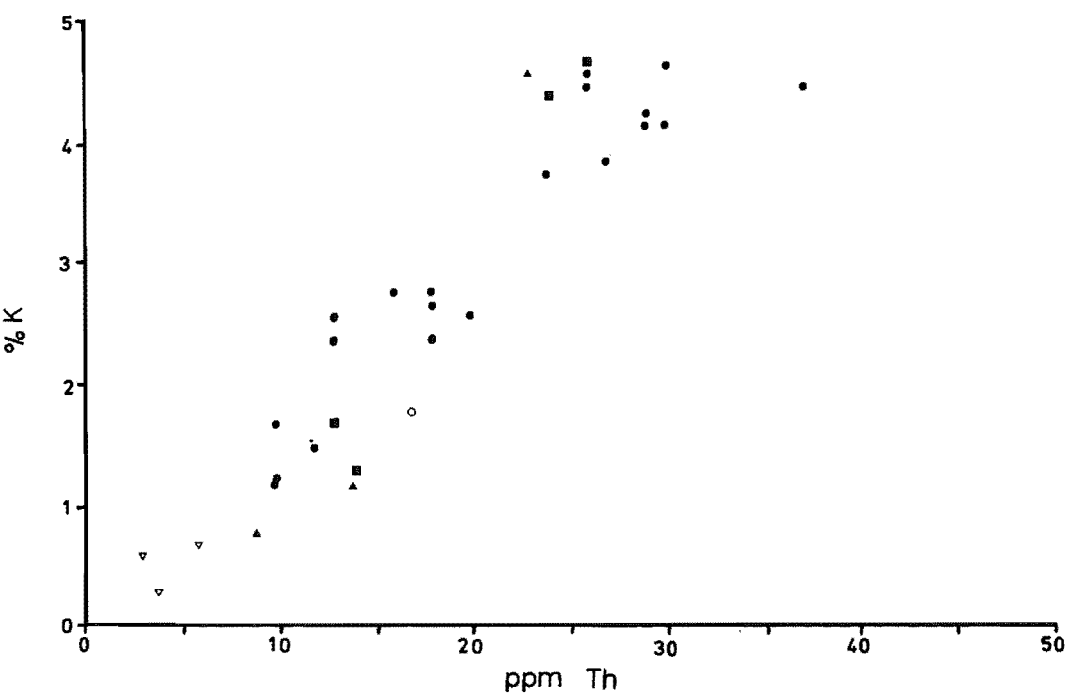

Figure 75. Plot of K against Th in the Mt.Somers Volcanics. Symbols as for Figure 47.

The relation between Th and K concentration is shown in Figure 75. The correlation coefficient between Th and K is excellent (r = 0.93), indicating that both Th and K were concentrated in the residual melt of the fractionating magma.

(b) Zirconium: Zirconium commonly crystallises with the Zr^{4+} ion in 6- or 8-fold co-ordination, where it has a radius of 0.80 Å and 0.92 Å respectively (Whittaker and Muntus, 1970). The most common zirconium mineral in magmas is zircon ($ZrSiO_4$), in which Zr^{4+} is in 8-fold co-ordination. This mineral can crystallise throughout the range of magmatic processes and thus occurs as inclusions in many volcanic phenocrysts. The ability of zircon to accommodate Rare Earths (particularly hafnium), and also yttrium and thorium, has already been discussed above.

In the Mt Somers Volcanics, zirconium is progressively enriched in the sequence andesite - dacite with increasing SiO_2 content (Figure 76). Correlation of Zr with SiO_2 is good (r = 0.75), and is very good with DI (r = 0.87) and CI (r = -0.85). The rhyolite also shows excellent correlations of Zr with SiO_2 content (r = -0.95); DI (r = -0.87), and CI (r = 0.66). From Figure 76 it can be seen that the decrease in Zr with increasing SiO_2 in the rhyolite, is very rapid and could represent the rapid removal of Zr in the form of zircon during differentiation of the rhyolite. From the trend shown in Figure 76 for the andesite and dacite there could have been no significant removal of zirconium from the melt during the differentiation of these rocks.

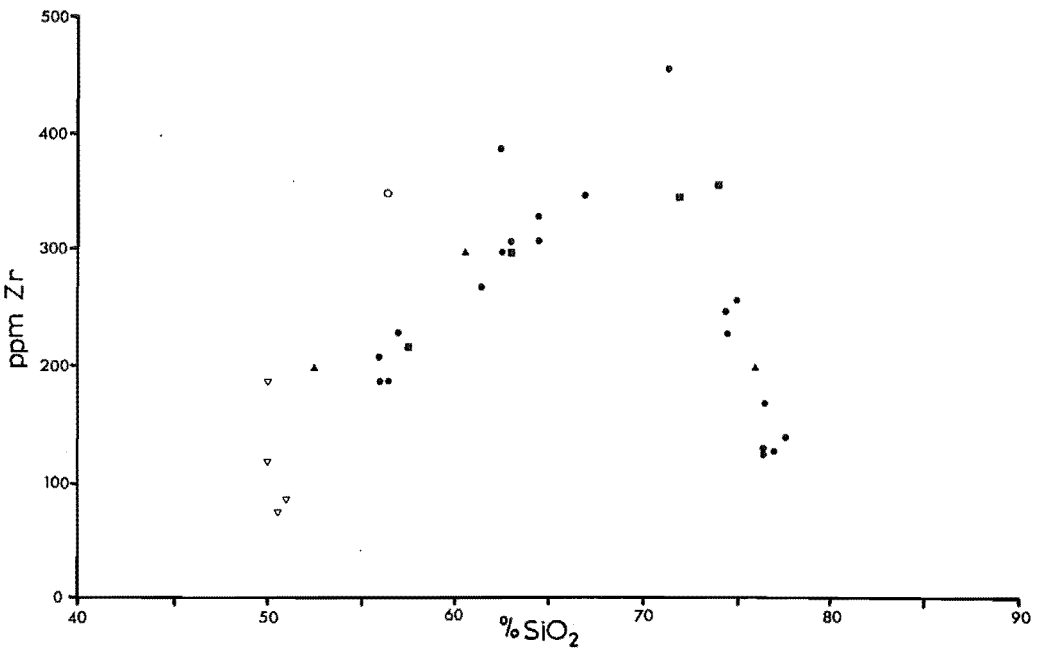

Figure 76. Plot of Zr against SiO_2 in the Mt.Somers Volcanics. Symbols as for Figure 47.

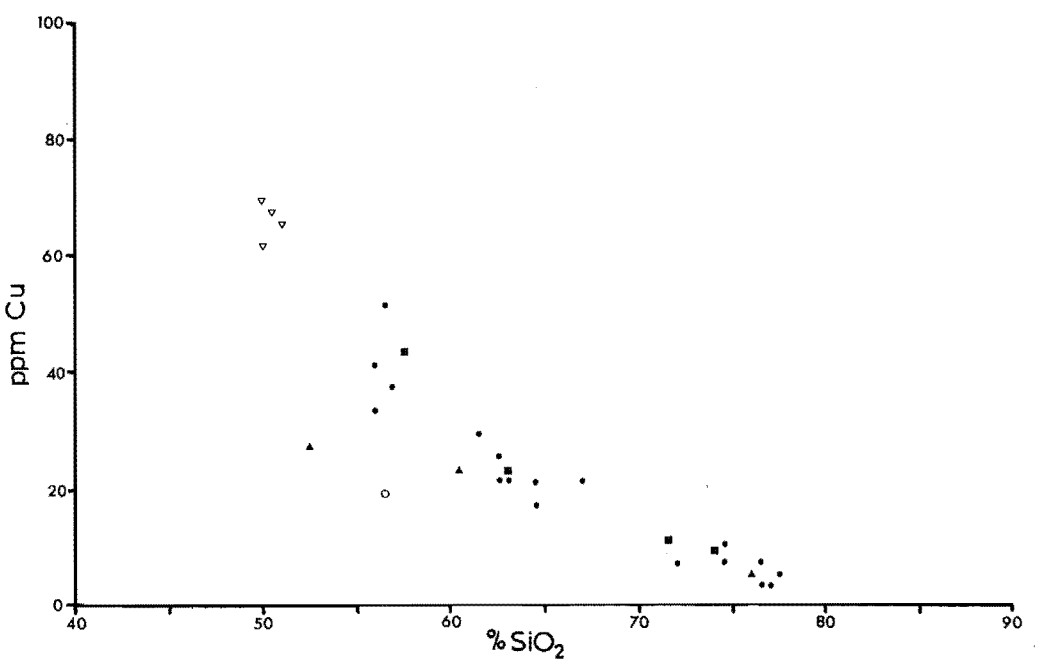

Figure 77. Plot of Cu against SiO_2 in the Mt.Somers Volcanics. Symbols as for Figure 47.

2.3.5.1.4 Ferromagnesian Elements. The ferromagnesian elements are all transition metals, and these have a tendency to be incorporated into the early forming crystal phases in magmas. The behaviour of these elements is not determined by ionic size and electronegativity alone, although these are the important factors. In the magma the transition metals are mainly in tetrahedral coordination in the silicate liquid, but in crystals these elements have a preference for octahedral sites (Burns and Fyfe, 1964). Octahedral and tetrahedral stabilization energies for transition metals were determined by Dunitz and Orgel (1957), and McClure (1957). The uptake of transition metals by magmas was examined by Williams (1959) who showed that the increases in coordination number with a decrease in inter-ionic distance, that takes place when a transition metal enters a crystal lattice from a magma, results in increased bond energy and a lowering of heat content.

Predictions on the order of uptake of transition metals from a magma based on octahedral and tetrahedral stabilization energies, were made by Burns and Fyfe (1964), and Curtis (1964). The orders predicted by Burns and Fyfe (1964) for octahedral site preference, are: Ni > Cu > Co > Fe > Mn $\geqslant$ Ca, Zn for univalent ions, and Cr > Mn > V > Ti > Fe $\geqslant$ Sc for trivalent ions.

The only significant difference in orders predicted by Curtis (1964) were those of Mn^{3+} and V^{3+} which were reversed in order to that given above.

The preference for octahedral co-ordination generally explains the removal of the transition elements from a basic

magma. In acidic magmas the number of tetrahedral sites in the magma is increased (Burns and Fyfe, 1964) and so the tendency for these transition elements to enter crystal phases is even greater. A further complication is introduced by the effect of octahedral distortion on the stabilization order (the Jahn-Teller effect). Curtis (1964) showed that Cu^{2+} and Mn^{3+} will be destabilised in an octahedral field, and Cr^{3+} will be destabilised in a tetrahedral field, because of Jahn-Teller distortion effects, and proposed the resulting modified stability order:

Ni > Co > Fe > Mn > Cu for divalent ions in octahedral co-ordination;

Cr > V > Ti > Fe > Mn for trivalent ions in octahedral co-ordination; and

$V^{3+} > Fe^{3+}$ for trivalent ions in tetrahedral co-ordination.

This revised order of stabilities accounts for anomalous behaviour of Cu^{2+} and Mn^{3+} in magmas.

(a) Copper: Copper has the exceptionally strong chalcophilic tendency to form primary sulphide minerals, under magmatic conditions, often in preference to entering the lattice structure of early forming silicate minerals.

In the Mt Somers Volcanics, copper shows a systematic decrease from basalt to rhyolite (Figure 77). The important point to arise from this graph is the continuation of the same trend from the basic andesite through to the rhyolite domes. This is similar to the variation shown by iron and manganese (Figures 51, 53), but is different to that of the other ferromagnesian elements discussed below which show rapid depletion with increasing acidity.

The only mineral present in the andesites that would accommodate significant amounts of Cu is orthopyroxene. The distortions of Cu^{2+}, due to the Jahn-Teller effect, can be accommodated by the distorted octahedral sites in this mineral (Burns, 1970, 1973).

Copper has a high correlation with SiO_2 ($r = -0.80$); DI ($r = -0.69$); and CI ($r = 0.90$).

(b) Nickel: Nickel with a divalent radius of 0.77 Å is very similar to that of Mg^{2+} (0.80 Å) in octahedral co-ordination. The substitution of Ni for Mg in such early forming minerals as olivine has long been recognised. Burns and Fyfe (1966) demonstrated that the solid-liquid distribution coefficients for Ni/Mg concentration in olivine in the binary system Mg_2SiO_2-Ni_2SiO_4 are reversed to that in a basaltic system. This is because of the larger number of tetrahedral sites present in the basaltic magma. Divalent nickel ions have a strong preference for octahedral coordination. From the relative orders given above it can be seen that Ni^{2+} has the highest known preference energy of the divalent transition metal ions. For this reason it would be expected that Ni would tend to be preferentially enriched in octahedral sites in early forming mineral phases, and in a differentiating magma this would tend to rapidly deplete the magma in this element.

The trend shown by nickel in the Mt Somers Volcanics (Figure 78), indicates that there was a rapid depletion of Ni in the basic andesites. The concentration of Ni in the more acidic andesites and dacite is very small, and not much different to that in the rhyolites.

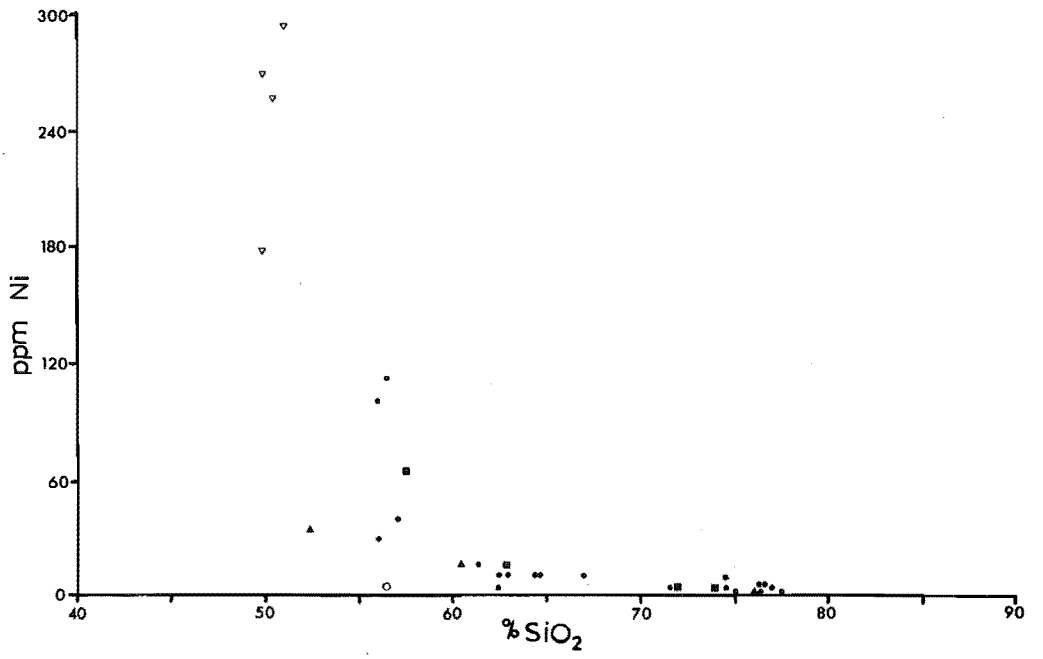

Figure 78. Plot of Ni against SiO_2 in the Mt.Somers Volcanics. Symbols as for Figure 47.

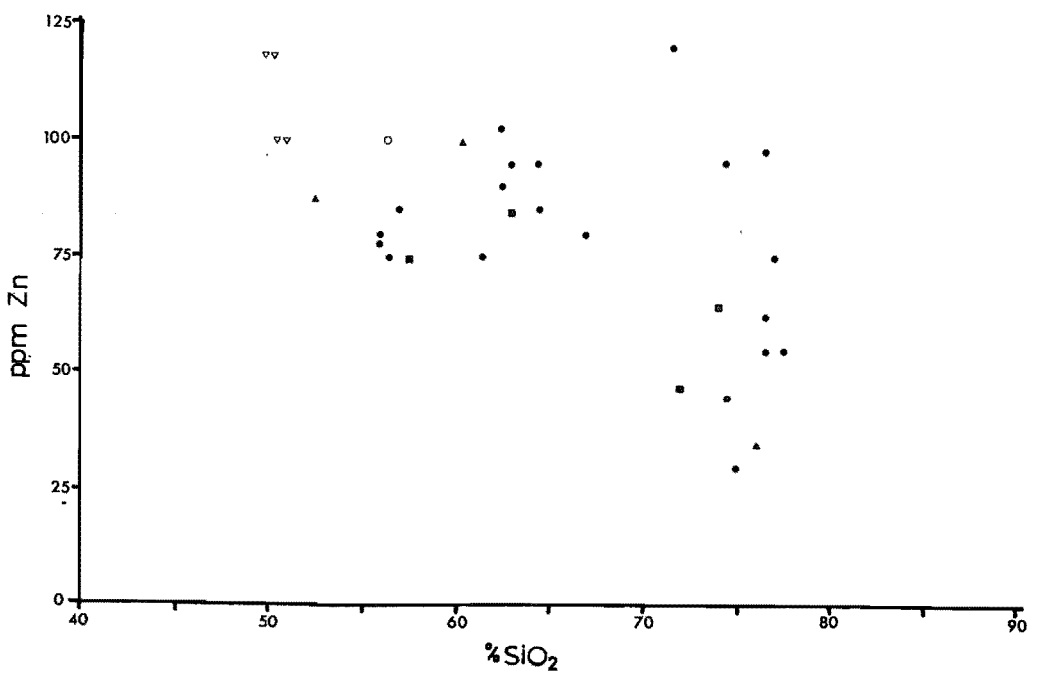

Figure 79. Plot of Zn against SiO_2 in the Mt.Somers Volcanics. Symbols as for Figure 47.

(c) Zinc: Zinc has a divalent radius of 0.83 Å for octahedral co-ordination. This is similar to that of Fe^{2+} (in high-spin state) with a radius of 0.86 Å, and Mg^{2+} (0.80 Å), (Whittaker and Muntus, 1970). From the order of octahedral site preference energies given above it can be seen that zinc is the least stable of the transition elements in octahedral co-ordination. The only magmatic minerals that can accept significant amounts of Zn are: magnetite, biotite, garnet, and to a lesser extent pyroxenes and amphiboles (Wedepohl, 1972).

The plot of Zn vs. SiO_2 (Figure 79) for the Mt Somers Volcanics shows a considerable scatter, although the rhyolites show a rapid decrease in Zn concentration with increasing silica content. This could be caused by removal of garnet and/or magnetite, by fractional crystallisation of these, although this is by no means certain, particularly as magnetite has not been identified as a mineral present in the rhyolites (C. P. Wood, pers. comm.). Lambert *et al.* (1974) found a correlation between the fractionation trend shown by Zn and the presence of magnetite-ilmenite in the calc-alkaline lavas from Mt Ararat, Turkey.

The lack of any differentiation trend in the Mt Somers andesite and dacite would therefore suggest that magnetite was not fractionating from these magmas.

(d) Vanadium: Vanadium in the trivalent state has an ionic radius of 0.72 Å (octahedral co-ordination) which is similar to that of Fe^{3+} in the high-spin state (octahedral co-ordination), which has a radius of 0.73 Å. Vanadium tends to substitute into

those minerals that also contain Fe^{3+} ions. From crystal field stabilization energies, V^{3+} has both a greater octahedral preference and also a greater tetrahedral preference, than the Fe^{3+} ion. Magmatic minerals that show enrichment in vanadium are: magnetite; ilmenite; micas; and to a lesser extent pyroxenes and amphiboles (Landergren, 1974).

In the Mt Somers Volcanics there is a systematic decrease in vanadium concentration with increasing silica content (Figure 80). There is excellent correlation of V concentration with SiO_2 ($r = -0.97$); DI ($r = -0.97$); and CI ($r = 0.97$).

The abundance of V in the Mt Somers Volcanics is low compared to average calc-alkaline concentrations (Tables 5, 6). The decrease in iron oxide concentration of >3% (shown by variation diagram, Figure 51), between a basaltic Barrosa Andesite (Sample PO484) and an acidic Hinds River Dacite (Sample PO562), cannot be accounted for by magnetite ($Fe^{2+}Fe^{3+}{}_2O_4$) crystallisation. The crystallisation and removal of the quantity of magnetite necessary would have resulted in greater vanadium depletion than is observed to have occurred. The relevant values are given in Table 8.

Duncan and Taylor (1968), and Taylor *et al.* (1969a) have shown that magnetite from andesite and dacite from Mt Edgecombe, New Zealand, contain concentrations of vanadium from 0.45 to 0.80%. The average value was 0.60% vanadium. On this basis it can be predicted that only about 1% total iron oxide can be removed in the form of magnetite to account for the vanadium depletion observed between the Barrosa Andesites and the Hinds River Dacite in Table 8.

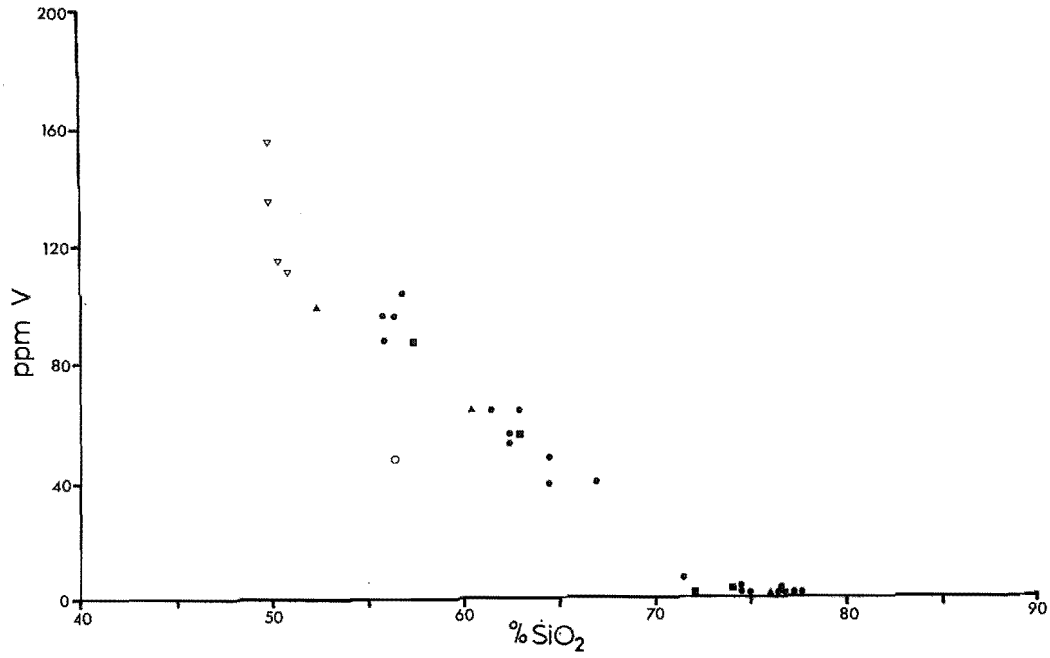

Figure 80. Plot of V against SiO_2 in the Mt.Somers Volcanics. Symbols as for Figure 47.

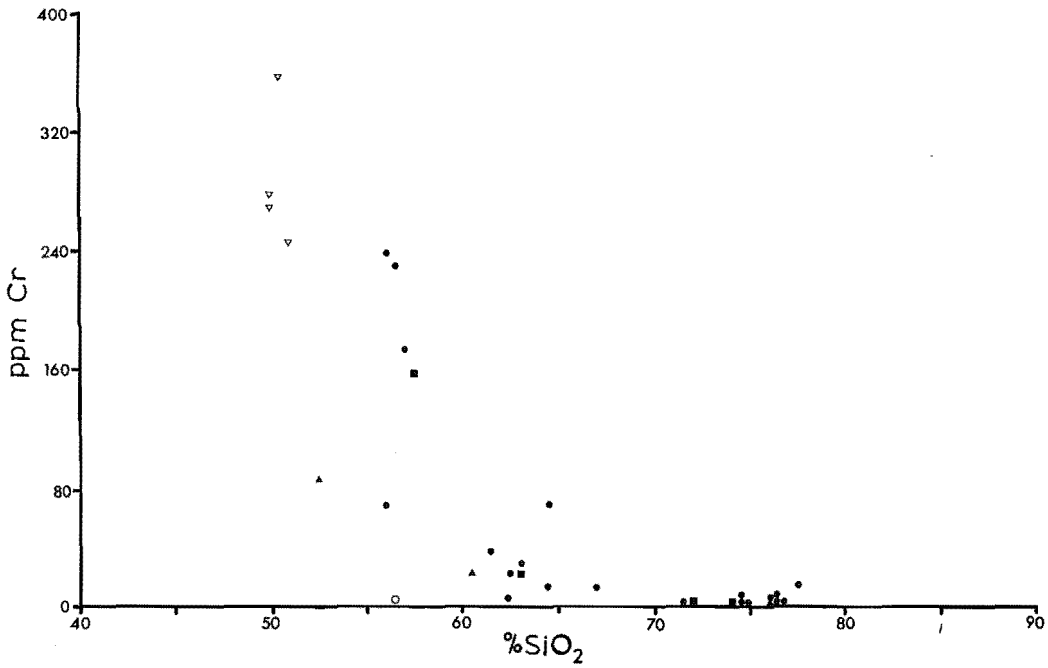

Figure 81. Plot of Cr against SiO_2 in the Mt Somers Volcanics. Symbols as for Figure 47.

Table 8. Fe, V, Cr, and Ni depletion in dacite, compared to andesite

	Barrosa Andesite (PO484)	Hinds River Dacite (PO562)	Δ concentration
% Fe_2O_3	2.85	0.78	2.07
% FeO	4.92	3.75	1.17
ppm V	97	41	56
ppm Cr	231	13	118
ppm Ni	115	10	105

As vanadium has a lower stabilization energy than Cr or Ni, these latter two elements are preferentially concentrated in the octahedral sites in spinel structures (e.g. magnetite, chromite, trevorite), and in ortho- and clino-pyroxenes.

(e) Chromium: Chromium has a trivalent radius of 0.70 Å. With an octahedral stabilization energy greater than any other trivalent transition metal, Cr^{3+} readily enters the smaller octahedral positions in minerals, particularly pyroxenes, amphiboles and spinel structures.

In the Mt Somers Volcanics there is a rapid decrease in chromium concentration with increasing silica content of the andesite, with a subsequent decreased rate of depletion in the dacite (Figure 81). The abundance of phenocrysts of hypersthene and opaques in the andesite is consistent with the trend observed.

The Cr and Ni contents of the high-alumina basalt from the Malvern Hills (PO513: Analysis 28, Table 7) are very close to that of a sample of the Graham Dolerite

(PO356; Analysis 25, Table 7), which could indicate that chromite and olivine have crystallised, and settled out, from these magmas. The amount of Cr in the rhyolites is exceptionally low (Table 7), which is consistent with an origin from either anatexis of sediments of granitic composition, or by fractional crystallisation and differentiation of a more basic magma.

2.3.5.2 Additional Trace Element Variation Trends

In addition to the continuous variation trends shown by all the major and trace elements when plotted against silica content, a plot of trace (and some major) elements against a modified Larsen Factor (1/3Si+K-Ca-Mg) also shows continuous trends (Figure 82). Data used for this diagram are given in Table 7 and Appendix II. In this diagram values for the tholeiitic basalts of the area have also been included.

The highest element concentration for each element plotted in Figure 82 coincides with the onset of crystallisation of a phase containing that element, such that the distribution for the element in the mineral relative to the magma, is greater than unity (Carmichael *et al.*, 1974). From Figure 82 it can be seen that fractional crystallisation rapidly removed Cr and Ni earliest in the differentiation sequence. These elements were followed by depletion of Cu, Fe, V, and Mn throughout the range basalt to rhyolite. Titanium shows a dramatic drop in concentration between the basalts and the andesites such that if a similar tholeiitic basalt

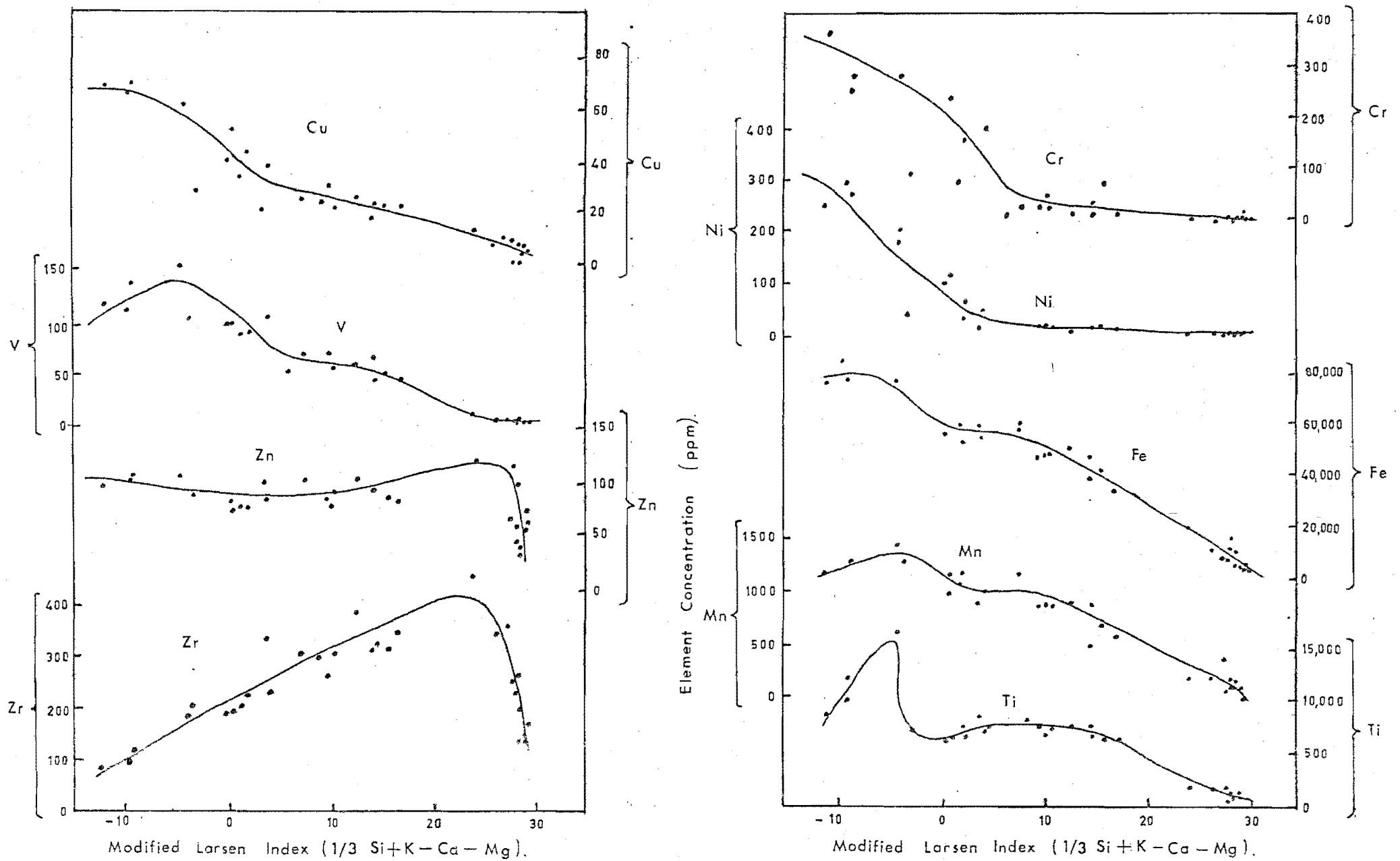

Figure 82 . Plots of element concentrations against a modified Larsen Factor.

was the parent magma of the andesites then rapid fractionation of ilmenite would be necessary in the more basic andesites to account for the observed trend. The levelling out of the Ti trend in the range andesite to dacite indicates that ilmenite was not the most important Fe-removing phase. From the previous discussion, magnetite can also be ruled out as the major Fe-removing phase from the andesite to dacite sequence, because of the variation trend of vanadium (which also shows a slight levelling in this composition range in Figure 82). The only other Fe-rich fractionating phase, that could account for the Fe-trend, is hypersthene. This is consistent with the major element trends observed.

The trend shown in Figure 82 by Zn and Zr, indicates that these were both removed in late-phase fractions during rhyolite differentiation. Zr accumulated throughout the sequence and was removed by the fractional crystallisation of zircon in the earliest formed rhyolite. The trend shown by Zn can be explained by the removal of Zn in magnetite, ilmenite, and/or hypersthene in the andesite, and to a lesser extent in the dacite. The distribution coefficient for Zn in these minerals is low enough for no rapid depletion to have occurred. With the onset of garnet crystallisation in the rhyolite, rapid removal of Zn would have occurred which would account for the trend seen in Figure 82.

2.4 PETROGENESIS

2.4.1 Theories of Petrogenesis

There are five general theories for the origin of calc-alkaline volcanics. These are:

1. Melting (partial or complete) of sialic crust.
2. Fractional crystallisation of a basaltic magma.
3. Mixing of a basaltic magma with an acid magma.
4. Assimilation of crustal material by basaltic magma.
5. Partial melting of the upper mantle.

Combinations of these processes are also possible, and fractionation of magmas formed by any of the above processes can subsequently occur. Objections have been raised to all the theories when applied to calc-alkaline rocks as a whole, and it is possible that different mechanisms apply in individual cases.

The Mt Somers Volcanics represent a typical calc-alkaline suite of volcanics. From the variation trends discussed in the previous chapter it is apparent that the andesites and dacite follow the same differentiation trend, and that the rhyolites are also part of a differentiation trend. The origin and relations between these volcanics will now be discussed.

2.4.1.1 Melting of sialic crust

The main difficulty when applying this theory to the volcanic rocks of the Mt Somers area is the determination of the composition of the crust in this region. It would be reasonable to expect the crust to have a composition similar to that of the Torlesse Supergroup "greywacke" sandstones and siltstones which make up much of the Southern Alps. Alternatively the composition could be similar to the "Alpine" schist which, because of the remobilization of elements that accompanied region metamorphism, could have a significantly different composition to that of the Torlesse sediments. Because of this remobilisation, the depth at which melting took place is important. A further complication arises if only a partial melt was extracted from the sialic material to form the magma. The resulting composition would depend on the mineralogy of the crustal material, and the extent of the melting would depend on such unknowns as temperature, pressure and volatile content (which are also dependent on the depth).

Although it is impossible to test this hypothesis, it is possible to predict on the basis of existing experimental work (Wyllie and Tuttle, 1961; Winkler and von Platten, 1961; Rogers, 1966; Wyllie, 1971), that a granitic to granodioritic melt would result from the melting of "greywacke" type sediments. Temperatures of 600° to 800°C (at P_{H_2O} = 2 kbars) would yield over 70% and up to 96% melt according to Winkler and von Platten (1961). The proportion of the crust melted would be inversely proportional to the quantity of quartz and anorthite-rich plagioclase in the sediments (Winkler and von

Platten, 1961; Rogers, 1966). Wyllie and Tuttle (1961) consider that more than 50% melting of shales is unlikely due to the amount of superheating required for a greater degree of melting, and that a 50% melt of shales occurs at 150°C above the initial melting point (with temperatures in the range 700°C to 800°C) and results in compositions not more acidic than a granodiorite.

An anatectic melt of lower sialic material (e.g. norites, charnockites, hypersthene granulites and kuzigites) has been proposed by Rittmann (1971) as the origin of high-alumina basalt and associated calc-alkaline andesite, by a process of "degranitisation" of the lower crust followed by melting. This theory involves the upward migration of K_2O, in the melt, from the lower parts of the crust, which then results in granitisation of the upper parts of the crust to provide the acid calc-alkaline volcanics.

It is not possible to tell, at this stage, what the nature of the lower crust is in the Mid-Canterbury area. There are no large xenolithic blocks in the magmas that could indicate the composition of the lower crust, although small xenoliths of altered sediments do occur in the dacite. These could have been picked up anywhere in the magma's ascent. Also the extent of metamorphism in these xenoliths that is original, and that which has resulted from contact with the magma, cannot be distinguished, thus making it difficult to evaluate this theory.

A primary melt, or partial melt, of granulite facies rocks has been proposed for the origin of the Mt Somers

rhyolites by Wood (1974) who suggested that progressive anatexis of the crust occurred at pressures equivalent to depths of 33 to 55 km, and at temperatures ranging from 900°C to 1050°C, with variations between the rhyolites of the Mt Somers and Malvern Hills area being attributed to phenocryst crystallisation under differing conditions of temperature and P_{H_2O}. Wood (1974) determined the following sets of conditions:

(a) Garnet rhyolite; 1000-1050°C, with P_{H_2O} about 500 bars and water content up to 4%.

(b) Garnet-biotite rhyolite; 900-950°C with P_{H_2O} about 1000 bars and water content up to 4%.

(c) Garnet-orthopyroxene (± biotite) rhyolite; 900-1000°C, with P_{H_2O} approximately 1.5-2.5 kbars and water content about or over 5%.

Wood (1974) thus reasoned that the garnets would have crystallised in the rhyolite magma at total pressures of 10-15 kbars, equivalent to depths of 33-55 km, and that the heat source for the melting process of crustal anatexis was provided by the normal geothermal gradient while the water pressure was provided by water contained in the sedimentary rocks.

From the available analyses of "greywackes", argillites, and schists (Reed, 1957, 1958; Vitaliano, 1968), the H_2O^+ water content of these rocks only rarely exceeds 3% and it is probable that the water content is even lower at pressures of 10-15 kbars and temperatures approaching 1000°C. It is therefore doubtful if water contents of up to 5% could be available directly from the sedimentary rocks.

Experimental work by T. Green (1976) on high pressure melting experiments on a pelitic composition resulted in the formation of a granitic melt containing garnet at pressures greater than 7 kbars. At 5% H_2O, garnet was obtained at 7 kbars with temperatures down to 820°C.

Thus a partial melt of sialic crust could theoretically produce the major element chemistry and mineralogy observed in the Mt Somers rhyolites providing sufficient water was available. Depending on the composition of the original sediments and the degree of partial melting, it would be possible to account for most observed major element variations within the rhyolite, but not the trace element variations. The very low contents of ferromagnesian elements observed in these rhyolites are lower than would be expected even from a partial melt, while the concentrations of Ba, Y, Th, Tb and Zn are generally too high to be derived directly from crustal anatexis without subsequent enrichment. Some form of differentiation of the rhyolites is clearly indicated by the variation trends for both major and trace elements, in particular: Al_2O_3, ΣFeO, MnO, CaO, Na_2O, TiO_2, P_2O_5, Ba, Sr, Rb, Pb, Th, Y, Zr, and Cu. The least acidic rhyolite samples have the highest concentrations of Ba, Y, Zn and Zr. As the differentiation within the rhyolite would have proceeded from the low- to the high-silica rhyolite, this differentiation cannot account for the initial high concentrations of these elements in the low-silica rhyolite. In addition the low-silica rhyolite also has an anomalously high Th, Pb, and Rb for a magma composition that would have been near to that of the initial melt (Tables 7 and 9).

TABLE 9: Composition of typical rocks forming sialic crust.

	1.	2.	3.	4.	5.	6.	7.
SiO_2	69.7	64.2	71.2	71.2	66.9	64.7	66.6
TiO_2	0.6	0.6	0.55	0.40	0.57	0.78	0.65
Al_2O_3	14.3	16.3	14.3	14.7	15.7	15.5	16.2
Fe_2O_3	1.0	0.73	4.07	1.60	1.33	0.87	0.46
FeO	2.5	4.1		1.80	2.59	4.80	3.00
MnO	0.1	0.06	0.07	0.05	0.08	0.11	0.05
MgO	1.2	1.9	1.56	0.55	1.57	1.97	1.10
CaO	1.9	1.4	1.88	2.00	3.56	2.35	1.50
Na_2O	3.5	2.2	2.94	3.54	3.84	3.95	3.20
K_2O	2.4	3.7	2.87	4.18	3.07	2.05	4.50
P_2O_5	0.2	0.14	0.16	0.16	0.21	0.17	0.14
H_2O, CO_2	2.40	3.95				2.54	2.34
Rb			—	145	110	61.5	139
Ba			480	600	500	450	930
Pb			nd	30	15	nd	nd
Sr			300	285	440	382	227
Y			nd	40	30	20*	28
Th			—	17	10	nd	nd
Zr			170	180	140	210*	205
Cu			17	10	25	34	32
Ni			nd	4	15	14	14
V			68	40	75	96	75
Cr			20	10	30	27	26

1. Average NZ Lower Mezozoic "Alpine" greywacke (sandstone), average 14 analyses. Reed, 1957, p 22, Table 2.
2. Composite argillite (17 samples), Wellington. Reed, 1957, p 28, Table 3.
3. Quartz-albite-biotite schist (Arahura Series), sample T-5. S.R.Taylor (1955).
4. Average granite. Taylor (1968).
5. Average granodiorite. Taylor (1968).
6. Marginal facies greywacke, Tauwhare Quarry (P 26192), Ewart Taylor & Capp (1968).
7. Marginal/shelf. Argillite Huntly (P 26186). Ewart, Taylor & Capp (1968).

nd — not determined.

* — values taken from A.R.Duncan (1970).

Note: Major element oxide concentrations in percentages; trace element concentrations in ppm.

It is not therefore possible to derive the rhyolites directly from a partial melt of sialic crust of "greywacke/ argillite" or schist composition.

The Hinds River Dacite has an average major element composition very similar to that of a granodiorite (Table 6). The trace element composition is also similar to that of granodiorite and it is therefore a possibility that this rock type could have been derived by partial melting of sediments of granitic to granodioritic composition. However, major element chemistry of the dacite when compared to sediments of Table 9 show that the values for TiO_2 and CaO cannot be the result of partial, or complete, anatexis of the sediments with the composition given. Calcium in particular presents a problem as this is present in anorthite-rich plagioclase, which is the most refractory of the feldspars, and would therefore have a tendency to deplete the melt in Ca (Winkler and von Platten, 1961).

The concentration of the elements Rb, Ba, Cu, Ni, and Cr in the dacite is similar to that of an average granodiorite; while Pb, Y, Th and Zr show relative enrichment; and Sr and V show relative depletion. The element variation trends for the dacite are more consistent with their being derived by crystal fractionation of an andesite of the composition of those observed in the Mt Somers area than from a partial melt of sialic crust.

The composition of the andesite precludes it from being derived as a partial melt from sediments of a granitic to granodioritic composition, because of the TiO_2, ΣFeO, MgO,

CaO, Y, Zr, Ni, and Cr concentrations (compare Tables 6 and 9). Also Wyllie and Tuttle (1961), and Wyllie (1971) showed that the temperatures required to form andesite by crustal anatexis are too high even under favourable conditions.

It can therefore be concluded that none of the volcanic types of the Mt Somers Volcanics were derived directly from anatexis of the upper-crust.

2.4.1.2 Fractional Crystallisation of a Basaltic Magma

The theory of the origin of the calc-alkaline suite of volcanic rocks by the fractional crystallisation of olivine, plagioclase and pyroxene was used by Bowen (1928) to explain the observed trends of this type of volcanism. This mechanism would however favour iron enrichment, which is not a characteristic of calc-alkaline magmas.

Osborn (1969, a & b) concluded, on the basis of experimental work (Osborn, 1959, 1962; Osborn and Roeder, 1960; Roeder and Osborn, 1966) that fractional crystallisation of an olivine-basalt crystallising out plagioclase, pyroxene, olivine, magnetite, with oxygen being supplied to the system by the inflow of water and the release of hydrogen, would result in an andesite liquid residual, with a peridotite cumulate. Some plagioclase formed by this mechanism would stay suspended in the magma which would contribute to the high-alumina nature of calc-alkaline magmas. Kuno (1968a) has also supported the concept of the formation of andesite by crystal fractionation from a basalt.

Serious objections to this model have been summarised by T. Green and Ringwood (1968a) and Taylor *et al.* (1969a & b). These are mainly the lack of oxidation of calc-alkaline rocks, and the absence of Ti and V depletion which would result from titanomagnetite fractional crystallisation. The volume relations observed i.e. the small amount, or absence, of basalt eruptive rocks in calc-alkaline areas (e.g. Pichler & Zeil, 1972) is not a convincing argument against Osborn's theory. The non-constant oxygen fugacity in sequences of calc-alkaline acid volcanics (Carmichael, 1967), and the presence of titanomagnetite in andesite of low oxygen fugacity (Wilkinson, 1966) were also considered by Green and Ringwood (1968a) to be evidence against Osborn's model. However, as the titanomagnetite essentially post-dated the formation of the andesite, they do not necessarily reflect conditions present during the andesite genesis. Miyashiro and Shido (1975) consider that calc-alkaline volcanics may be generated by two or more different processes.

The Cretaceous Mt Somers Volcanics appear to have no directly associated tholeiitic basalt flows or dikes. The most basic flow analysed was sample PO513 (Analysis 28, Table 7) - a high-alumina basalt which is chemically and mineralogically associated with the andesite. For all major elements, and most trace elements, this high-alumina basalt forms part of the continuous sequence of differentiated andesite. The exceptions are the distinctly higher Ba/Rb ratio than the andesite, and the relatively low Cr, Cu and Ni concentrations (Table 7). It is significant that the ferromagnesian and

V content of this high-alumina basalt are compatible with that of the andesite. The low content of Ni could be accounted for by fractional crystallisation and removal of olivine from the parental magma from which the high-alumina basalt was derived. The relatively high content of vanadium and low content of chromium indicates that chromite, not magnetite, was the predominant spinel-phase to be crystallised during the formation of the high-alumina basalt. (Vanadium is enriched in magnetite, thus precluding this mineral).

From the trace element chemistry, it can be seen that the high-alumina basalt must have been derived from the same source as the Mt Somers andesites, and must have followed essentially a similar fractionation trend. A difference being that the andesites represent a more advanced differentiate.

When considering the possibility that the Mt Somers andesites could have been derived from an olivine basalt, it is of interest to compare the compositional trends of these volcanics with that of the saturated basalts in the area. These include dikes of unknown age in the Torlesse Supergroup, and Tertiary basalt flows and pillow lavas. On field evidence it seems possible that the dikes are younger than the volcanics of the Malvern Hills area. This is confirmed by the one K/Ar date on a dike intruded at the contact of the Cretaceous volcanics and the basement Torlesse rocks. Dikes in the Torlesse rocks of the Harper Range, Mt Somers Range, and the area around the North Branch of the Ashburton River, are of unknown age but are similar in composition (Table 7) to the Tertiary volcanics that are interbedded with the Landon limestones of the Mt Somers area.

Although these younger basalts belong to an entirely different volcanic episode within the Mt Somers area, this fact could not be determined from their composition alone, which form continuous trends with those of the Mr Somers andesite and rhyolite. The extent of differentiation of a basalt magma would be determined by the time taken to reach the surface, or the time that the magma was stationary in a magma chamber, thus providing variations in type of volcanism at the different centres of eruption.

Taylor *et al.* (1969a) provided evidence to show that calc-alkaline andesite and associated high-alumina basalt could have been derived by a two stage process, of partial melting of an alkali or tholeiitic basalt; this basalt would have already been depleted in Ni and Cr by being derived by an initial process of partial melting of the mantle. However, a process of differentiation of a tholeiitic basalt which was crystallising out olivine and chromite would also give a residual magma depleted in Ni and Cr from which andesite could be subsequently derived by pyroxene and plagioclase fractionation. The arguments against this last differentiation process that were put forward by Taylor *et al.* (1969a and b), (i.e. the lack of enrichment observed, in typical andesite, of Ba, Rb, REE's, Th, Zr and Pb, compared to average basalt; and the lack of vanadium depletion in the andesite), do not apply to the Mt Somers Volcanics where the converse is true.

From the variation trends shown by the Mt Somers Volcanics it is clear that, while all the volcanics have a common "parental" magma, individual centres of volcanism have

erupted lavas that have undergone different degrees of fractionation. In this respect the high-alumina basalt appears to have undergone differentiation involving olivine and chromite - crystal phases which did not fractionate to any extent from the andesite magmas.

Evidence in favour of a differentiation process for the formation of the Mt Somers Volcanics is:

- the continuous major and trace element composition trends.
- low K/Rb and Ba/Rb ratios.
- constant K/Rb and Ba/Rb ratios.
- high Rb/Sr and Ba/Sr ratios.
- high abundances of Th, Zr, Ba, Pb, Rb, and K.
- low abundance of V and Sr.
- continuous variation trends shown by Ca/Sr and Rb/Sr ratios.

Evidence against an origin by differentiation is:

- the apparent absence of a primitive (basalt) parental magma as an eruptive phase.
- the absence of any significant volume of volcanics with a mineralogical composition transitional between the rhyolite and the dacite (corresponding to the volcanics with a chemical composition between 68-70% silica).

2.4.1.3 Mixing of Basaltic Magma with an Acidic Magma (Hybridisation)

The role of hybridisation of acid and basic magmas is an obvious method to obtain an intermediate magma. While major element chemistry can often be accounted for by this

method, trace element chemistry and strontium isotope data are often not compatible (Taylor, 1969).

In the Mt Somers area there are no tholeiitic basalts of late Cretaceous age that can be definitely associated with the calc-alkaline volcanism. The basalt dikes that occur in the Torlesse rocks, and pillow lavas and flows of the Tertiary limestone, have been described above, and could be compositionally similar to the type of basalt that could have been involved in a hybridisation process. A mix of basalt with Mt Somers rhyolite can be used to investigate the possibility of hybridisation.

Table 10 gives mean compositions (volatile free) for Mt Somers andesite calculated from the values given in Table 10 for Barrosa Andesite, Rata Peaks Andesite, and Round Top Andesite. Also given in Table 10 are average values for the Somers Rhyolite; representative basalt dikes from in the Torlesse rocks; the high-alumina "basalt" from Round Top Andesite; and a mean value for the low-silica "andesites" of Graham Dolerite. Using the values calculated for the average andesite and rhyolite, theoretical compositions for basalt were calculated that would be required for a 1:1, 2:3; 1:2; and 1:3 mix of rhyolite:basalt that would result in an "average andesite" composition. These are also given in Table 10.

By extrapolation and interpolation of the calculated values, it can be seen by inspection, that dilution of a basalt by 50%, or more, of the rhyolite is not possible, as this would involve negative concentrations of K_2O, Rb, Pb,

TABLE 10: Calculated basalt compositions required for mixing with Somers Rhyolite to give resultant magma of andesitic composition.

	Andesite 1.	Rhyolite 2.	Basalt 3.	Basalt 4.	High-Al Basalt 5.	Dolerite 6.	Calculated Basalt Compostions 1:1mix 7.	2:3mix 8.	1:2mix 9.	1:3mix 10.
SiO_2	60.31	75.51	51.03	49.82	52.73	56.46	45.11	50.18	52.71	55.24
TiO_2	1.24	0.18	1.75	3.13	1.27	1.25	2.30	1.95	1.77	1.59
Al_2O_3	16.19	13.28	13.39	16.38	16.89	16.71	19.10	18.13	17.64	17.16
FeO_3	2.44	0.98	5.05	6.76	3.39	2.13	3.90	3.41	3.17	2.93
FeO	4.60	0.66	6.62	4.89	6.34	5.58	8.54	7.23	6.57	5.91
MnO	0.14	0.02	0.17	0.21	0.17	0.15	0.26	0.22	0.20	0.18
MgO	3.36	0.15	9.70	2.48	6.37	4.70	6.57	5.50	4.97	4.43
CaO	5.70	1.02	9.12	11.43	8.88	7.84	10.38	8.82	8.49	7.26
Na_2O	3.47	2.75	2.48	3.83	2.70	3.16	4.19	3.95	3.83	3.71
K_2O	2.25	5.23	0.42	0.69	1.00	1.62	-0.73	0.26	0.76	1.26
P_2O_5	0.28	0.05	0.27	0.39	0.27	0.26	0.51	0.43	0.39	0.36
Rb	106	250	13	13	25	78	-38	10	34	55
Ba	496	760	78	145	344	384	232	320	364	408
Pb	19	44	6	0	6	15	-6	2	6	11
Sr	271	82	286	425	242	228	460	397	365	334
Y	52	65	21	32	49	50	39	43	45	48
Th	13	28	4	3	9	12	-2	3	4	8
Zr	262	270	94	188	204	210	254	257	258	259
Cu	32	7	67	62	29	35	57	49	45	40
Ni	38	4	295	180	37	30	72	61	55	49
V	77	2	111	155	100	89	152	127	115	102
Cr	97	3	250	279	89	69	191	159	144	128
Zn	84	71	101	118	88	77	97	93	91	88

1. Mean andesite composition of Barrosa Andesites, Rata Peaks Andesites, and Round Top Andesites.
2. Mean composition of Somers Rhyolite.
3. Basalt dyke from Trig. TT. Sample P0273.
4. Basalt dyke from Clent Hills. Sample P0179.
5. High-alumina basalt from Round Top. Sample P0513.
6. Mean composition of Alford Dolerite.

7 to 10. Calculated composition required for a basalt to give an andesite resulting from a Rhyolite: Basalt mix of 1:1; 2:3; 1:2; 1:3 respectively.

Note: Major element oxide concentrations in percentages; trace element concentrations in ppm.

and Th, and excessively high concentrations of Al_2O_3, in order to compensate for the concentrations of these elements present in the rhyolite used in the mix. However, dilution of less than 40% of a basalt by the rhyolite would be possible.

When the composition of the basalts (Tables 7,10) found in the Mt Somers area (i.e. those occurring as dikes in the Torlesse rocks, and those conformable with the Tertiary limestones) are compared to the calculated values, it is found that the compositions are similar (Table 10). However Al_2O_3, CaO, Ba, Y, Zr, Ni, and Cr provide deviations from the calculated values that make the mixing of basalt and rhyolite an unlikely mechanism for the formation of the andesite. This is shown by Figure 83 where a direct comparison between the average andesite and the rhyolite: basalt mixture can be made. Deviations from the 45° line (on which are plotted the values for the average andesite) indicate differences in composition between the average andesite and the calculated mixtures. From this figure it can be seen that the fit for Ni is very poor and that the fit for Cr, Zr, and Ba are also poor.

The composition of the high-alumina basalt of the Round Top Andesite (sample PO513: Analysis 28, Table 7) is close to the calculated basalt required for a 1:2 mix, but concentrations of TiO_2, Al_2O_3, MgO, Na_2O, P_2O_5, and Sr deviate significantly from the required values.

The Graham Dolerite is similar to the calculated composition required for a 1:3 mix of rhyolite/"basaltic magma". The deviations that exist (notably TiO_2, Al_2O_3, P_2O_5, Sr, and Cr) are not sufficient to rule this out as a

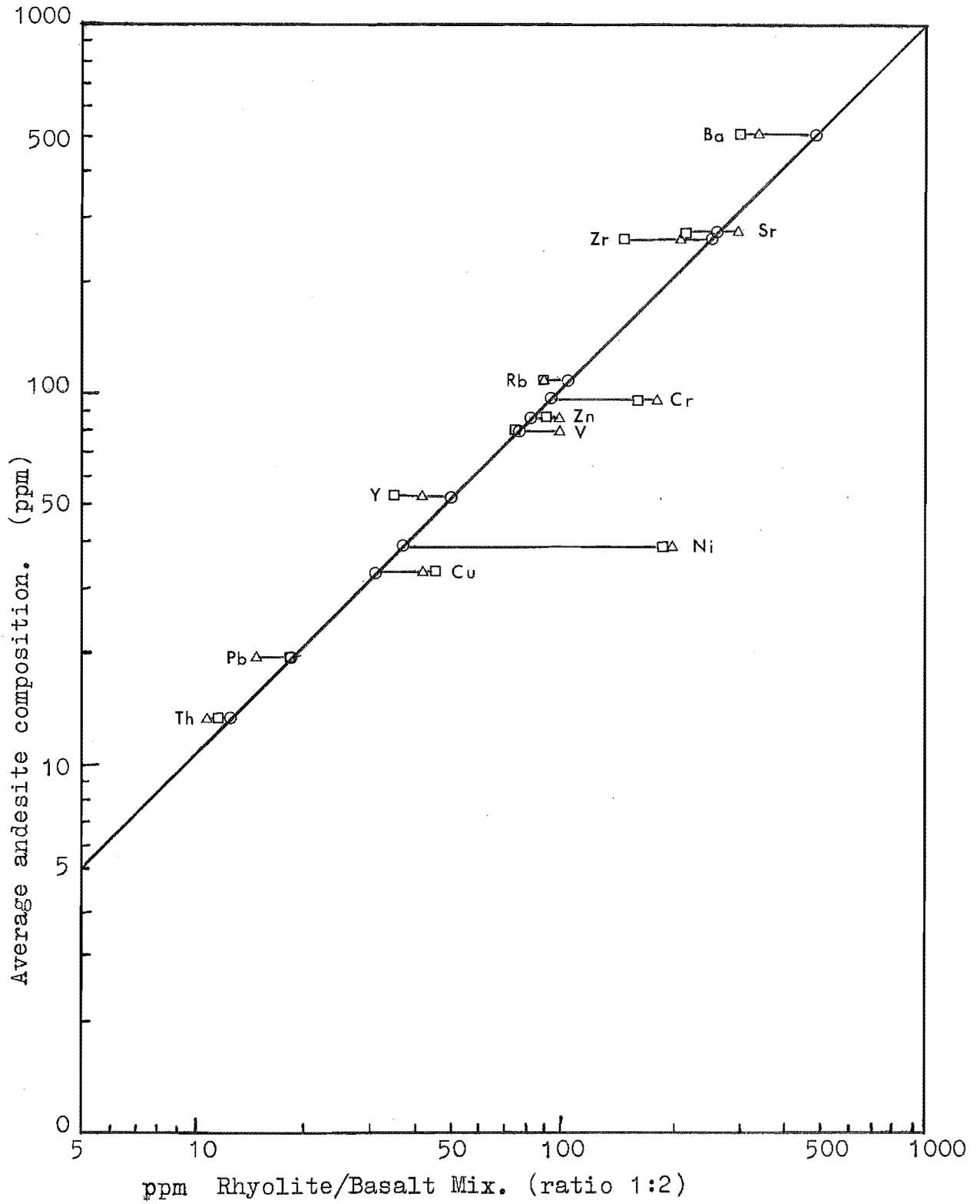

Figure 83. Comparison of trace element composition of an average Barrosa Andesite with mixtures of Rhyolite and Basalt, calculated for best fit of major elements. △ mixture of rhyolite (column 2) and basalt, (column 3, Table 10); □ mixture of rhyolite (column 2, Table 10) and basalt (column 3, Table 10); ○ average andesite (column 1, Table 10).

possible mixing process. However, as the "basaltic magma" is progressively diluted with less rhyolite the deviations from the andesite composition become larger. Therefore progressive addition of rhyolite to the basaltic magma would not produce the observed variation trends in the Mt Somers Volcanics.

Another difficulty associated with this theory is the lack of a suitable explanation of the physical process of mixing of two magmas of differing temperature, density and viscosity.

Eichelberger (1974) considered that basalt contamination of rhyolite produces dacite, and that rhyolite contamination of basalt produces andesite. Lavas erupted from Glass Mountain, Medicine Lake, graded through dacite, banded rhyodacite to rhyolite, with abundant basalt inclusions in the early formed lavas, and phenocrysts of plagioclase, olivine, and clinopyroxene derived from the basalt (Eichelberger, 1974). The mixing process suggested by Eichelberger was the disintegration of basaltic xenoliths, which subsequently became "strewed" through the rhyolite magma. In the Mt Somers Volcanics the dacite contain no basaltic xenoliths, and the phenocryst content of the dacite has little resemblance to that of the rhyolites. Therefore, it is not possible that the mixing process described by Eichelberger (1974) could be applied to the Mt Somers Volcanics.

2.4.1.4 Contamination of Basaltic Magma with Sialic Crust

Contamination of a tholeiitic or alkaline basalt by a partial or complete melt, or assimilation, of sialic crust is another possible origin for the andesite. The intrusion of a large volume of basalt into the crust could cause contact anatexis, particularly if the basalt is stationary in a magma chamber for any length of time. The high temperatures (usually >1100°C) of basalt are sufficient to melt sialic crustal material to form a granitic to granodioritic melt (Wyllie and Tuttle, 1961; Winkler and von Platten, 1961; Rogers, 1965; Wyllie, 1971).

The average calc-alkaline granite plots very close to the "Alpine greywacke" sandstones of the Torlesse Supergroup, on a modified von Wolff Q-L-M diagram (Reed, 1957). The main difference being that the "greywacke" has a higher normative quartz content. An anatectic melt would therefore be expected to have a major element composition very similar to an average granite. The "Marginal" facies "greywacke" sandstone and siltstone have an andesitic provenance, in contrast to the granitic provenance of the "Alpine" (Torlesse) sandstones and siltstones. No reliable trace element data is available for the "Alpine greywacke" but trace element data for an "Alpine schist" is given in Table 9, from which it can be seen that there is a close similarity between the schist and the average granite composition. For contamination of a basalt by Torlesse-type sediments, of granitic composition, to produce the Mt Somers andesites, a mixture of approximately equal parts basalt to sediment are required for the best fit

of the major elements. A comparison of average Mt Somers andesite (column 1, Table 10) with a granite/basalt mixture (column 7, Table 5; and column 4, Table 10 respectively) of equal parts, is shown in Figure 84. The elements Ni, Cr, Y, and Zr show significant deviation from the average andesite values and it is therefore unlikely that contamination of basalt by a sediment of this granitic composition could produce the andesite.

The observed high xenolith content of the Hinds River Dacite suggests that the composition of this lava has been modified by contamination by sialic crust. To test whether a mixture of sialic crust with andesite could produce the dacite, a mixture of equal parts of a rock of granitic composition with andesite is required to obtain the correct major element composition. Figure 85 is a comparison of this mixture, with the Hinds River Dacite, from which it can be seen that the deviations from the expected value are not great enough to totally reject this as a possible mechanism for the formation of the dacite. However the large amount of sialic material required (50% by weight) limit the extent of mixing possible. Ewart and Stipp (1968) use the presence of a large proportion of plagioclase phenocrysts in andesite of the Central North Island of New Zealand as an argument in favour of crustal assimilation by a basaltic magma. The dacite of the Mt Somers area is characteristically aphyric, which is contrary to what would be predicted for magmas assimilating a large quantity of sediment.

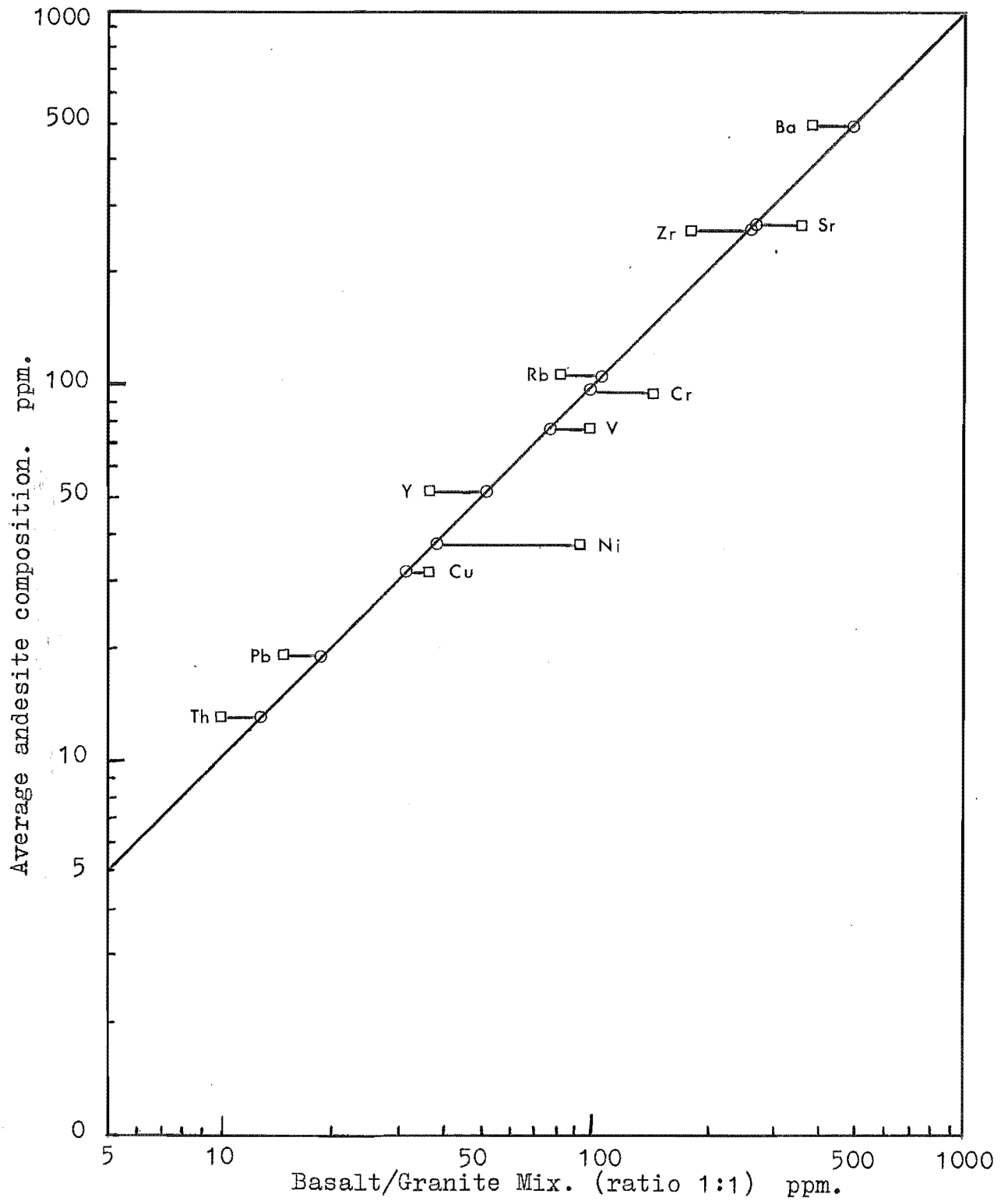

Figure 84. Comparison of trace element composition of an average Barrosa Andesite with a mixture of basalt and granite, calculated for best fit of major elements. □ mixture of basalt (column 4, Table 10) and granite (column 7, Table 5); o average andesite (column 1, Table 10).

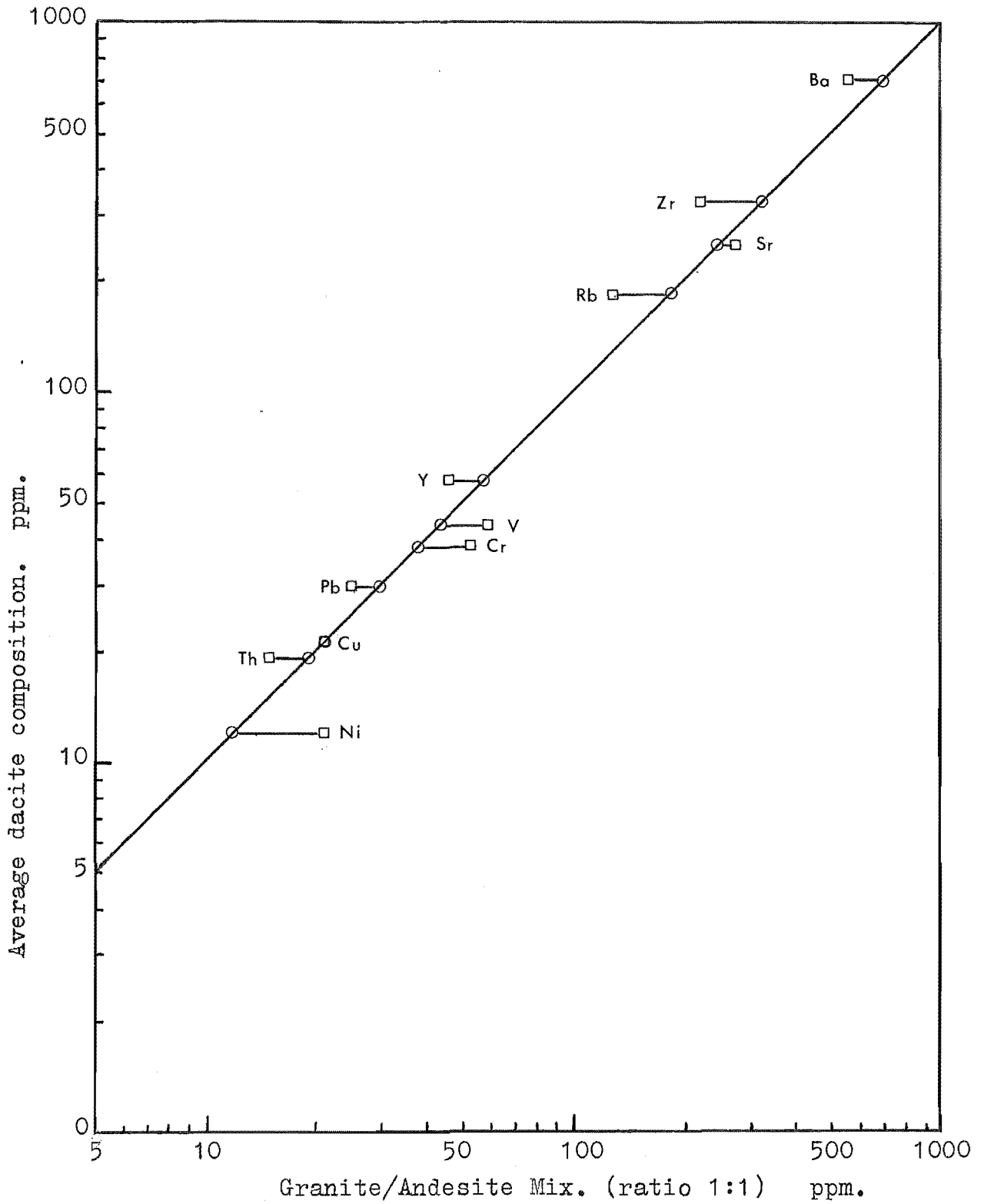

Figure 85. Comparison of trace element composition of an average Hinds River Dacite with a mixture of granite and andesite, calculated for best fit of major elements. □ mixture of granite (column 7, Table 5) and andesite (column 1, Table 10); o average dacite (column 1 , Table 6).

2.4.1.5 Single- and Multiple-Stage Processes Involving Partial Melting of the Upper Mantle

In recent years High Pressure/High Temperature experimental phase studies, aided by analysis of minerals using the electron microprobe, have resulted in an explanation for petrogenesis of the calc-alkaline suites by partial melting processes of upper mantle material. These theories have had a general application and thus have been useful in explaining calc-alkaline genesis, particularly in areas where there is no continental crust to act as a contaminant or to act as a source rock for anatectic models.

There have been many theories for the generation of magmas from the mantle. These have been reviewed by Wyllie (1971, p190-210), and by Carmichael *et al.* (1974). In general these theories involve the formation of a basalt from a partial melt of mantle material.

T. Green and Ringwood (1968a) and Ringwood (1974), have suggested basaltic magma generation from a partial melt of "pyrolite" of a composition equivalent to three parts harzburgite to one part Hawaiian olivine tholeiite. Ito and Kennedy (1968) chose a "picritic" mixture of equal parts of olivine tholeiite and peridotite. O'Hara and Yoder (1967), and Kushiro *et al.* (1968) considered a "picritic" magma could be formed from garnet lherzolite (olivine + orthopyroxene + clinopyroxene + garnet) of the type found as xenoliths in kimberlites.

T. Green and Ringwood (1968a), O'Hara (1968), Kushiro and Yoder (1969), Kushiro *et al.* (1972), and Ringwood (1974) all claimed that an andesite magma, and possibly a dacite magma, could be derived directly from the mantle by a process

of partial melting. On the basis of extensive experimental work T. Green and Ringwood (1968a) proposed three alternative mechanisms for the origin of calc-alkaline rocks by melting processes involving mantle materials:

1. The extrusion of a large pile of basalt lava which was subsequently buried and transformed into quartz eclogite and sank into the mantle. At depths of 100 to 500 km this eclogite partially melted to form calc-alkaline magmas.
2. The extrusion of a large pile of basalt lava which became hydrated and transformed into an amphibolite. With increased burial the amphibolite then either partially melted to produce calc-alkaline magmas, or if water was driven off in the process, it transformed into eclogite.
3. The contamination of a basaltic magma by water, followed by fractional crystallisation under hydrous conditions at 30-40 km depth. Crystallisation was predominantly amphibole, with smaller amounts of pyroxene, calcic plagioclase, and garnet. The residual liquids provided the calc-alkaline magmas. The original basalt magma was itself derived by a partial melting of the mantle.

Ringwood (1974) revised these processes for the formation of calc-alkaline magmas, and suggested the following mechanisms:

(a) Fractional crystallisation of amphibole from a basaltic magma, or, partial melting of an amphibolite.
(b) Fractional crystallisation of eclogite from a basaltic magma, or, partial melting of quartz eclogite.
(c) Partial melting of primary pyrolite under conditions of high load pressure and high water pressure.

(a) Amphibole fractionation: In the Mt Somers Volcanics there are no amphibole phases represented in any of the rock types. This suggests that either amphibole was not a crystallising phase during the evolution of the volcanics, or that amphibole phenocryst became unstable and were replaced by other phases.

Stewart (1975) concluded that crystal "clots" (in andesite from Crater Lake, Oregon), that consisted of plagioclase, hypersthene, augite and magnetite, were the result of breakdown of cognate xenoliths of high-alumina amphibole.

Crystal aggregates of this nature also occur in the Mt Somers andesite, and could conceivably be cumulate relicts of a fractionation process in the parental magma that have been swept up with the rise of residual liquid. However, while the criteria used by Stewart (1975) for distinguishing between "crystal clots" and "random accumulation aggregates" of phenocryst minerals apply to the Mt Somers andesite, it does not follow that the "crystal clots" are a breakdown product of previously crystallised amphibole. In particular the oscillatory zoning in the feldspars (often more than 20 zones to a crystal) in the "clots" cannot readily be explained if the feldspars were formed by a replacement process after amphibole, as the conditions required for the diffusion gradients, that normally result in oscillatory zoning (Smith, 1974; Sibley *et al.*, 1976) do not as readily apply in a solid such as an amphibole crystal. The fact that some of the crystal aggregates are dominantly plagioclase is also not consistent with an origin as a breakdown product of amphibole.

It is probable that the "crystal clots" are cognate xenoliths composed of the cumulate that has been swept up with the movement of the magma and as such they probably represent the actual minerals fractionating from the melt during the differentiation process that formed the andesite magma.

Amphibole is unstable at pressures greater than about 25 kb, and breaks down to form garnet + pyroxene + water (D. Green and Ringwood, 1967; Lambert and Wyllie, 1968). The stability of amphibole at low pressures was studied by Boyd (1959) who found that amphibole became unstable at very low pressures. Yoder (1969) observed that relic hornblende grains are common in andesite which also supports the theory that amphibole fractionation plays a part in the formation of andesite magmas, but the amphibole subsequently becomes an unstable phase at reduced pressure.

Holloway and Burnham (1972) consider that andesite can be generated from a tholeiitic magma by the crystallisation and removal of amphibole, olivine and clinopyroxene, while Cawthorn and O'Hara (1976) think that the partition coefficients for iron in amphibole are high enough for this mineral alone to account for the lack of iron enrichment observed in calc-alkaline rocks, and that the crystallisation of hornblende containing 38% to 42% SiO_2 would result in rapid enrichment of SiO_2 in the residual melt to give the calc-alkaline trend without unacceptably large amounts of cumulus material. Thus it is conceivable that amphibole-controlled fractionation could have been responsible for the genesis of the Mt Somers

andesite even though there is now no evidence of this. The most probable "parent" magma consistent with this would have been a tholeiitic basalt which would have fractionally crystallised amphibole, olivine, clinopyroxene, and minor spinel phases (to account for the composition of the most primitive andesites erupted).

The differentiation trends and petrography observed in the Mt Somers Volcanics indicate that whatever the origin of the most basic andesite - as a residual magma from basalt differentiation, or as a primary magma from partial melting of the mantle - amphibole fractionation played no part in the subsequent differentiation of the andesite magma to form the dacite and rhyolite observed in the eruptive sequence.

(b) Eclogite fractionation: The experimental work by T. Green and Ringwood (1968a) showed that garnet and clinopyroxene can fractionate from a basalt at 20-40 kb pressure (anhydrous). The most acidic residual liquid formed by this method was an andesite.

T. Green (1972), and T. Green and Ringwood (1972) demonstrated that, under hydrous conditions (P_{H_2O} = 3 to 5 kb), iron-rich garnet crystallised at temperatures as low as 900° to 1100°C. The result of eclogite fractionation under hydrous conditions produced a residual magma of dacitic to rhyolitic composition. Two effects that result from fractionation of eclogite are: an increase in K relative to Na, because Na is preferentially incorporated into pyroxene, and secondly

rapid depletion of the heavy Rare Earth Elements, and yttrium, as a result of garnet fractionation. The high yttrium content and variation trend of the Mt Somers Volcanics precludes this process as an explanation for the formation of this volcanic sequence.

It should be noted that Ringwood (1974) considers fractional crystallisation to be the opposite equivalent of partial melting. The results of much experimental work (e.g. that of T. Green and Ringwood (1968a), were derived from fractional crystallisation studies of a melt, but interpreted in terms of partial melting. The two processes are comparable only if solid-solution phases are minor. As these systems involve olivine, pyroxene, amphibole, garnet and plagioclase, all of which exhibit marked solid solution in nature, deviations from the predicted trends seem likely.

(c) Direct Partial Melting of the Mantle Under High Water Pressure: Kushiro and Yoder (1969) suggested that andesite and dacite could be derived by partial melting of pyrolite at 20-30 kb under high water pressure. Kushiro *et al.* (1972) conducted melting experiments on natural garnet and spinel lherzolites at high pressure. Under anhydrous conditions a 10 to 15% partial melt of garnet lherzolite with 2% phlogopite, produced an alkali picritic liquid at 30 kb. Under hydrous conditions a 20% partial melt of spinel lherzolite produced andesite to dacite liquids at pressures about 25 kb. They suggested that calc-alkaline andesite and dacite could be derived from more complete partial melting of lherzolite. D. Green (1973), and Nicholls

and Ringwood (1973) studied similar partial melts, and found the results of Kushiro *et al.* (1972) were the result of metastable crystallisation during quenching of the melt, and equilibrium crystallisation.

Nicholls (1974), and Nicholls and Ringwood (1973), concluded from their experimental work that direct partial melting of a pyrolite mantle could not produce calc-alkaline andesite and dacite at depths greater than about 40 km. Partial melting of pyrolite under high water pressure would, however, produce basalts with compositions ranging from olivine tholeiitic to saturated tholeiite at depths between 70 to 100 km. This magma, on rising, would crystallise olivine and spinel, and thus could produce a basaltic andesite (Nicholls and Ringwood, 1973).

Beeso and Jackson (1970) described xenoliths of clinopyroxenite, websterite, garnet websterite, and garnet clinopyroxenite from the lavas of Hawaii. They concluded that the xenoliths are related to their enclosing magmas and that they represent the parent residue of a partial melting of mantle material. They also noted that garnet pyroxenites were interbanded with lherzolite and could have resulted from partial melting of the lherzolite.

Melting studies on garnet websterite nodules from Hawaii, by Mysen and Boettcher (1976), showed that amphibole was not a liquidus phase in the quartz normative basaltic melt formed by partial melting of garnet websterite under hydrous conditions. Therefore it would not be permissible to produce an andesite liquid by the fractionation of amphibole from this melt. An andesite liquid could however

be formed from the melt by the fractional crystallisation of 10-20% An-rich plagioclase at low-pressure, which would then restrict the depth of origin to 75-80 km (Mysen and Boetcher, 1976).

In the Mt Somers Volcanics, the concentrations of the incompatible elements K, Th, Rb, Pb, Y and Zr are too high to have originated as a result of direct partial melting of a pyrolite or lherzolite, while the concentrations of Ni, Cr and V are too low. The trace element data are consistent with derivation by differentiation from a basaltic magma which in turn may itself have been derived by partial melting of the mantle and subsequently modified by fractional crystallisation of olivine and spinel phases.

2.4.2 The Role of Magmatic Gaseous Transfer

If a basaltic magma rises rapidly in the crust then the pressure of the volatiles in the magma can become greater than the hydrostatic pressure, with the result that gas exsolves from the magma and can permeate the surrounding country rock, or anatectic melt if this exists. With this gaseous release many elements will be transported. The most abundant are Na, K, Ca, Mg, Al, Fe, Si, S and Cl; with minor F, Br, B, P, As, Zr, Cu, Pb, Mn and Su; and very small amounts of Li, Be, Ag, Ni, Co, V, Mo, Ga, Ge, Ti, Zr, Cr, Cd, Sb, Bi, Sr, Ba, Se and Te (Krauskopf, 1967, p466).

From this it can be seen that the incompatible elements observed to be enriched in the Mt Somers Volcanics are capable

of being transported by gaseous transfer. The high concentration of incompatible elements in the rhyolite could conceivably have resulted from the enrichment of an anatectic melt by gaseous transfer of elements concentrated (by differentiation) in an andesite in contact with the anatectic melt. The main difficulty with this theory is that the sum of the element concentration of the anatectic melt plus the concentration added by gaseous transfer, would have to be equal to the value required for the continuation of the andesite element concentration trends, for each element. The probability of this occurring is very low. The same argument goes against the origin of the rhyolite by any other process independent of the andesite genesis. That is to say the probability of two totally independent differentiation trends (of rhyolite, and of andesite) together forming continuous trends for all major and trace elements, is very remote.

2.4.3 Relation of Plate Tectonic Theories to Petrogenesis

The position of calc-alkaline volcanic rocks in areas of orogenesis and the location of present day active calc-alkaline volcanics, adjacent to, or above, Benioff Seismic Zones which are associated with the subduction of oceanic crust along continental margins and island arcs, has led to refinements of many of the current theories of magma genesis.

Kuno (1960) described three zones of "primary" magma (tholeiitic, high-alumina, and alkali olivine basalt) which he related to the inclined Benioff Zones beneath Japan. The tholeiitic and high-alumina basalt have associated dacite and rhyolite which Kuno (1966) considered to be differentiates of the "primary" magma.

A correlation between depth to known Benioff Zones and the potassium content of calc-alkaline volcanics has also been shown to exist (Sugimura, 1961; Dickinson and Hatherton, 1967; Hatherton and Dickinson, 1969; Dickinson, 1970, 1973), although this correlation is not always strong. Nielson and Stoiber (1973) have shown in general that K_2O and SiO_2 are mutually weakly proportional to the depth of the Benioff Zone. Dickinson (1975) refined his model by showing that a better general correlation of K and h (depth) could be achieved by grouping rocks into those of continental margin arcs, and those of intra-oceanic arcs, with these two groups then subdivided to obtain good K-h correlations.

The Mt Somers andesites, with a silica content of 57.5% (volatile free) and an average K_2O content of 1.8% (based on a best fit regression line for data from Appendix II), would have originated at a depth of approximately 190 km, using Dickinson's (1975) model for "Continental margin arc volcanism".

There have been several explanations for this increase in K content with depth to a subduction zone. Dickinson (1968) suggested a pressure-controlled variation of the partition coefficient of potassium in olivine and pyroxene which

were undergoing partial melting in the mantle. Another pressure dependent process was described by Marsh and Carmichael (1974) who consider that sanidine acts as a buffer in eclogite undergoing partial melting along a narrow strip (restricted pressure range) to produce andesite magma. The eclogite being oceanic crust transformed by subduction at a plate boundary (Marsh and Carmichael, 1974).

The breakdown of amphibole, which is complete at pressures of 25-30 kb at 1200°C (Holloway and Burnham, 1972; Holloway and Ford, 1973; Lambert and Wyllie, 1968, 1972, 1974; Stern, 1974), has been suggested as a possible process for the release of K from amphibole, thus yielding potassic magmas (Boettcher, 1973). However without a buffering process as suggested by Marsh and Carmichael (1974), the trend observed for potassium would be similar to that for sodium, which is present in amphibole and which would also be released by the same process.

Other theories for the origin of calc-alkaline magmas along Benioff Zones include that of McBirney (1973) who suggested that dehydration of subducted oceanic crust released water into overlying peridotite mantle which resulted in partial melting of the peridotite. Kushiro (1973) and Mysen (1973) consider that this partial melting occurs at depths of 80 km (25 kb) above the Benioff Zone. The derivation of andesite directly from partial melting of peridotite is theoretically possible only at depths down to 60 km according to Boettcher (1973). However recent experimental studies (Nicholls, 1974; Stern and Wyllie,

1973; Stern, 1974) have shown that it is not possible to derive a calc-alkaline magma directly from a partial melt of a peridotite at depths of about 100 km, and that the partial melt compositions of hydrous peridotite diverge to a greater extent than anhydrous partial melts, from that of calc-alkaline rocks. A completely anhydrous melt, while giving compositions closer to those required, would however require temperatures greater than would be expected at that depth in a subduction zone (Stern, 1974).

The subduction zone of an oceanic plate is often associated with a deep trench when the plate is moving in a direction perpendicular to the edge of the continental plate. The trench forms a geosyncline which is supplied with sediment from the continental landmass or from volcanic island arcs. It seems possible that some sediments could get carried down the subduction zone with the descending lithosphere. It is difficult to test whether sediments are in fact subducted and have subsequently taken part in partial melting processes. Taylor *et al.* (1969a) consider that the trace element composition (particularly Ni) of deep sea clays precludes any significant involvement of these with the formation of magmas derived by partial melts of the ocean crust. From the lead isotope composition of the Tonga-Kermadec volcanics Oversby and Ewart (1972) conclude that the upper limit of assimilation is less than 1%. Gill and Compston (1973) present Sr^{87}/Sr^{86} ratio data for island arc volcanics of the South West Pacific from which they deduced that sialic crust or its derived sediments played an insignificant role in the formation of island arc

volcanics. Church (1973) concluded from Pb and Sr isotope abundances and Th/U ratios, that less than 2% of oceanic sediment, or less than 10% of continental sediment could have been involved in the genesis of the Cascade Mountains. However Ewart and Stipp (1968) consider that the Sr^{87}/Sr^{86} ratios of the calc-alkaline rhyolite of the Central North Island of New Zealand are consistent with its derivation from miogeosynclinal sediments while the andesite of this region could have been derived from contamination of a basalt, or a primary andesite magma, with Mesozoic eugeosynclinal "greywacke" type sediments. Ewart and Bryan (1973) also consider that the strontium isotope composition of andesite of the Western Pacific could be accounted for by alteration of the ocean basalt by sea water (prior to being subducted and melted), or by admixture of oceanic sediment to the downthrust lithosphere and their subsequent melting.

Thus it is not definite that sediments do not play a part in the formation of magmas along the Benioff Zones. However their absence from such areas as the central Kuril Islands, Izu Islands, Tonga arc, Mariana arc, and Aleutian arc (Gorshkov, 1969) indicates that their presence is not a prerequisite for calc-alkaline magma genesis.

The suggestion that partial melting of the ocean crust descending down a Benioff Zone produces calc-alkaline parent magmas has been shown to be unlikely by Gill (1974), because of the problem of reconciling observed trace element and isotope compositions in volcanics of the Fijian arc with

those of the ocean floor basalt. Nicholls and Ringwood (1973), and Ringwood (1974) describe a multistage process of derivation of an acidic partial melt from subducted ocean crust (altered to eclogite) to produce a hydrous acidic magma which reacts with overlying pyroxenite to yield a garnet pyroxenite; this then undergoes diapiric uprise and partial melting to produce magmas which subsequently fractionate by eclogite and amphibole crystallisation to produce the calc-alkaline rocks. Best (1975) considers that the trend shown by potassium and also other incompatible elements e.g. Rb, Ba, Zr, Th, Pb (Jakes and White, 1972), can be explained by either hydrous fluids rising from the descending slab of ocean crust, and scavenging and zone melting these elements from the overlying peridotite. The concentrations of these elements would be proportional to the path-depth of the fluids.

Ewart and Bryan (1973) consider that the relation of K with depth, as observed in the Tongan Islands, is coincidental and not a first order genetic correlation. Sugimura (1973) has shown that multiple correlation of combinations of normative minerals in calc-alkaline volcanics, with depth to the Benioff Seismic Zone is very high, and supports the origin of andesite by differentiation and contamination from a basaltic parent magma. Jakeš and White (1972) showed that the range of the incompatible elements was continuous over the range of magma types from tholeiitic through calc-alkaline rocks to shoshonites. Jakeš and White (1972) consider this gradation typical of island arcs (but not of continental

margin calc-alkaline volcanism), and that it is time dependent.

From the data obtained from the Mt Somers Volcanics, these rocks could not have been derived directly from subducted ocean crust, nor its transformed equivalent (eclogite). The data are inconsistent with a direct (single stage) derivation of the volcanics from a pyrolite mantle. The presence or absence of a Mesozoic Benioff Zone underlying the South Island of New Zealand and dipping to the west, cannot be directly demonstrated. But the existence of the New Zealand Geosyncline in Permian-Triassic-Jurassic times could be interpreted as the infilling of such a trench formed by subduction of the lithosphere. Waterhouse and Norris (1972) related Permian and Mesozoic volcanism and plutonism to a westward dipping Benioff Zone. A late Paleozoic subduction zone for the South Island has also been suggested by Griffiths (1975) to account for the presence of the New Zealand Geosyncline. An increase in K_2O content, of Permian volcanics, from east to west has been described by Challis (1968), which is consistent with magmatism and volcanism associated with a Benioff Zone dipping to the west. Griffiths (1975) considers that during a short period of about 50 Ma duration, in the Cretaceous, subduction once again was active, and this was responsible for the Upper Cretaceous calc-alkaline volcanism in New Zealand. Assuming that such a subduction zone did exist along the eastern margin of New Zealand during the Cretaceous, the most likely mechanism for the generation of the Mt Somers

Volcanics, consistent with their chemistry, is a process involving the release of a hydrous, perhaps highly siliceous, fluid phase from the dehydration of the descending oceanic crust. This descending crust would be converted to amphibole which would then convert to eclogite at depths corresponding to pressures greater than 25 kb, and would release water in the process (Ringwood, 1974). The presence of even a small amount of serpentine in the descending slab would also release water by progressively becoming dehydrated at pressures above 40 kb (Ringwood, 1974). These hydrous fluids would rise through the overlying mantle pyrolite and would result in partial melting of the mantle to form a basaltic magma. The rise of the basaltic magma would be accompanied by differentiation involving the fractional crystallisation of olivine, pyroxene and amphibole, ± spinel phases, to produce saturated hydrous basalt which, on rising further through the crust, would fractionate orthopyroxene, plagioclase, ± minor spinel phases to form the calc-alkaline andesite - dacite - rhyolite sequence erupted at the surface. Phenocryst crystallisation in the rhyolite occurred at depths of 33 to 55 km (10-15 kb) according to Wood (1974). The high water content required for the rhyolite crystallisation (2-5%) could be achieved by the concentration, in the last stages of the differentiation process, of the volatiles initially present in the hydrous parent magma. Assimilation of crustal material melted during the ascent of the andesite magma could not have played more than a minor role in the evolution of these volcanic rocks.

The Upper Cretaceous Mt Somers Volcanics could have been the result of magma genesis that was initiated during the Rangitata Orogeny in the Lower to Middle Cretaceous. The process of magma generation, and the time for this to migrate to the surface would have been sufficient for considerable differentiation of the parent magma to have taken place, and this could explain the absence of any significant quantity of contemporaneous basaltic parental magma at the surface. Sugisaki (1976) has shown that there is a direct correlation between andesite genesis and the presence of water in the mantle. Thus, if water is supplied by dehydration of the ascending ocean floor slab, then a rapid rate of subduction would be accompanied by large volumes of calc-alkaline andesite volcanism. This has been found to be generally true for andesites around the Pacific by Sugisaki (1976), who also showed that slow rates of subduction resulted in alkaline volcanism along the plate boundaries. This is consistent with the results of D. Green and Ringwood (1967) who showed that alkaline magmas could be formed by fractionation from a tholeiitic basalt under anhydrous conditions. When applied to the Mt Somers Volcanics, this theory would imply that the Cretaceous calc-alkaline volcanism was the result of a rapid rate of subduction over a relatively short period of time, which would coincide with the rapid uplift that accompanied the Rangitata Orogeny.

2.5 PHYSICAL CONSTRAINTS CONTROLLING THE VOLCANIC EVENTS

2.5.1 Temperature and Pressure

Extrusion temperatures for a range of lava types have been listed by Carmichael *et al.* (1974, p7), from which it can be estimated that Mt Somers andesite is likely to have extruded at temperatures of between 950°C and 1100°C; the dacite at about 925°C; and the rhyolite at about 800° to 900°C. Wood (1974) used the Kudo Weill igneous plagioclase thermometer method to obtain equilibrium temperatures of phenocryst crystallisation in the rhyolite. The pressure and temperature values determined by Wood have been quoted in section 2.4.1.1. In general these ranged from 900°C to 1050°C with total pressures of 10 to 15 kb.

Eruptive temperatures of some of the rhyolite tuffs were high enough for these to result in the formation of welded ash flow tuffs (ignimbrites) which occur at the Rakaia Gorge, Mt Alford, and Mt Somers.

2.5.2 Viscosity

Viscosities for the rhyolite and andesite are given in Appendix III. These were calculated on a volatile free basis, using the method of Bottinga and Weill (1972). Calculated viscosities for nine representative samples have

been plotted in Figure 86, from which viscosities at lower temperatures can be obtained by extrapolation. A comparison of calculated and observed viscosities has shown that this method of extrapolation for determining viscosities is generally valid (Bottinga and Weill, 1972; Shaw, 1972). From Appendix III and Figure 86 it can be seen that the viscosity increases from basalt through to dacite with an apparent gap in the calculated viscosities between the dacite and the rhyolite. An exception is the dacite (PO562) which has a viscosity near to that of the rhyolite. Calculated viscosities for the rhyolite, at a temperature of 900°C, range between $\eta = 10^9$ to 10^8 poise, while at 800°C, $\eta = 10^{10}$ to 10^9 poise. The dacite and andesite (at 1,000°C) have calculated $\eta = 10^4$ to 10^5 poise.

The petrographic evidence for the occurrence of ignimbrite in the rhyolitic volcanics has been discussed in section 2.2.5.4. Glass shards - the definitive characteristic of ignimbrite - were not always observed in thin section because of welding and/or flow within the ignimbrite. Where no other evidence of an ignimbrite was found and a rhyolite "sheet" did not appear to grade into an ignimbrite, there remains the possibility that it could be a coulee or flow. The absence of ignimbrite features has therefore resulted in some of the Mt Somers rhyolites being classified as flows, e.g. those of the Rangitata Gorge area.

The physical properties of lava (mainly viscosity and temperature) can be used to explain why flows could have formed rather than domes or ignimbrite. Ignimbrite only

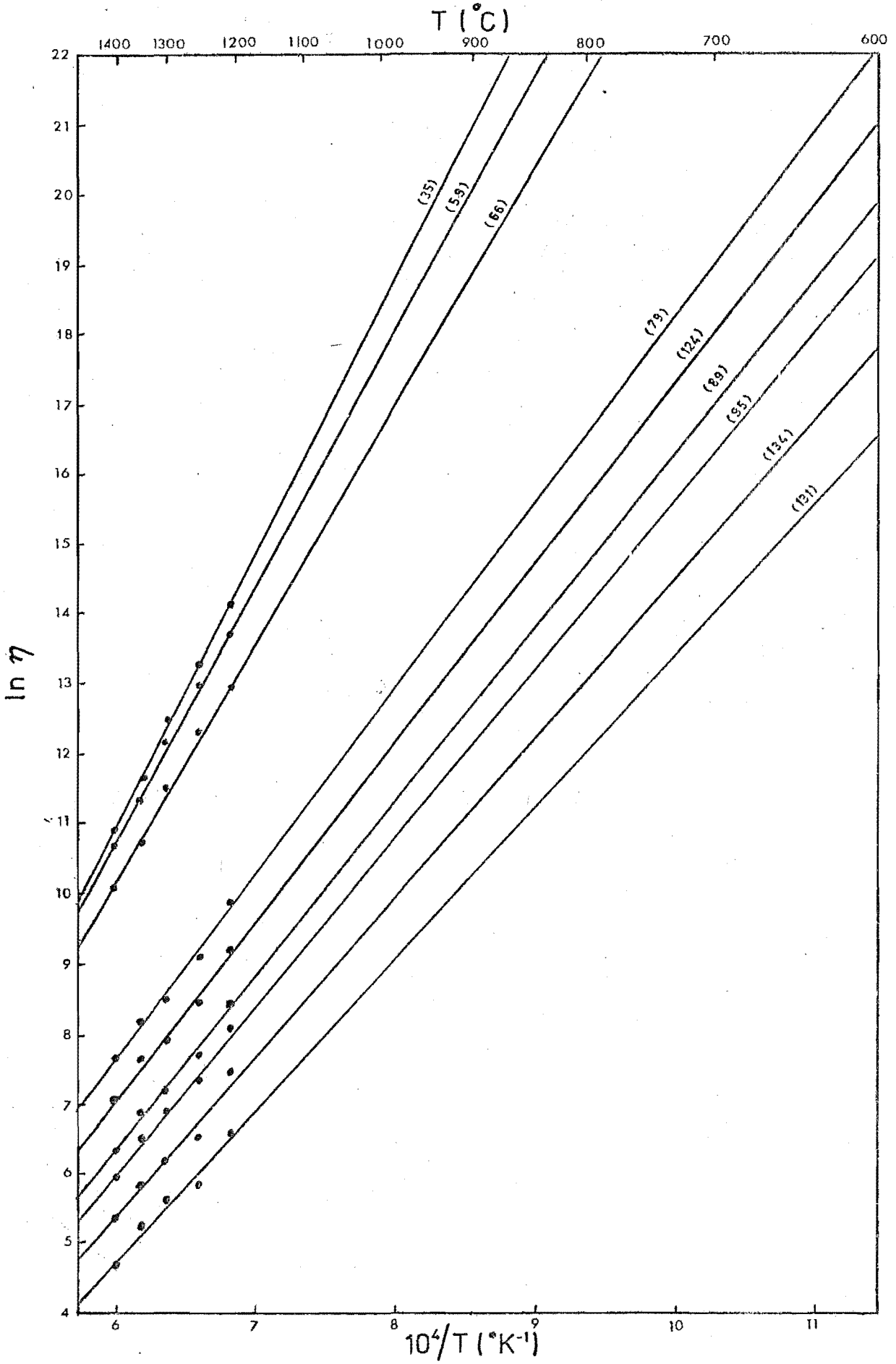

Figure 86. Calculated viscosities for selected volcanic samples using anhydrous compositions. Numbers in parentheses refer to analyses in Appendix II.

forms if the volatile content and confining gas pressure are great enough to form an explosive phase at the vent. Where this is not the case the high viscosity of rhyolite generally results in the formation of a dome. From Figure 86 and Appendix III it can be seen that there is no significant variation in viscosity over the range of the rhyolite chemical compositions. Possible explanations for the formation of flows of rhyolite with the same calculated viscosity as that forming domes are:

1. The flows could represent a volatile-rich lava while the domes represent a volatile-impoverished lava. Field evidence indicates that the cumulo-dome extrusions were preceded by an explosive phase resulting in an ash eruption. This would be consistent with the accumulation of volatiles in the upper part of a magma chamber. The rhyolite flows could be a pulse of rhyolite magma in which segregation of volatiles did not occur thus leaving the magma with a high homogeneous volatile composition. The presence of volatiles could facilitate rhyolite flow even if vesiculation occurred. The presence of gas bubbles in liquids of low viscosity has the effect of increasing the overall viscosity, but when the energy required for deformation of a bubble is less than the energy required for viscous flow of the enclosing liquid, then the effective viscosity is lowered (Bottinga and Weill, 1972)

2. The temperature of extrusion of the domes could have been significantly lower than the flows. From Figure 86 it can be seen that a decrease in temperature from 900°C to

800°C would lower the viscosity considerably more than a 100°C decrease at higher temperatures, i.e. temperature changes have a more significant effect on viscosity in magma with a low initial temperature (such as the rhyolite), than in magma with a high initial temperature (such as andesite).

3. A third possibility to account for the difference in apparent viscosities of the rhyolite domes and flows is that of silica polymerisation. Shaw (1972) has shown that the onset of rapidly increasing linkage between Si-O tetrahedra occurs at mole fractions of SiO_2 above 0.8. From Appendix III it can be seen that the rhyolites all have mole fractions of SiO_2 equal to, or greater, than 0.8. This could mean that the calculated viscosities are in error for the more silica rich rhyolite samples, and if so, this could account for the observed differences in their mode of eruption.

2.6 AGE OF THE VOLCANICS

The volcanic rocks of the Mt Somers and Malvern Hills areas were considered to be of a similar age by previous workers. Haast (1877, p13) thought the "melaphyres" (andesite), and "quartziferous porphyries" (rhyolite) were of Cretaceous age. A wider age range, from Cretaceous to Tertiary, was given by S. G. Cox (1884a,p24). Speight (1928, 1938) gave a time range for the Mt Somers Volcanics of late Jurassic to late Cretaceous. This was based on the following evidence:

1. The volcanics rest on a subaerially eroded "fairly level" surface of Triassic and Jurassic beds.
2. Early Tertiary re-peneplanation of the volcanics was followed by deposition of "Bortonian coal measures".
3. The Mt Misery Volcanics overlie "Jurassic conglomerates and plant beds" and were overlain by "Senonian coal measures".
4. The volcanics in the Mt Somers area are similar to those in the Malvern Hills area and therefore could be of a similar age.

Speight then suggested that the most likely age of the volcanic rocks from the Mt Somers district was from early to late Cretaceous. The oldest volcanics are tuffs (the Surrey Hills Tuff) which were considered by Speight to probably be Lower Cretaceous. The "andesite" (Barrosa Andesite and Hinds River Dacite) and rhyolite (Somers Rhyolite and Alford Rhyolite) were considered to be lower to upper Cretaceous in age, although a post-Awamoan age was

also contemplated for the rhyolite (Speight, 1938, pp19,35). Speight (1938, p32) was uncertain of the age of the dolerite on Mt Alford (Graham Dolerite) but a relationship with the andesite was implied to exist.

Gair (1967) stated that the andesite and rhyolite from Mt Somers were of late Jurassic or early Cretaceous age. The andesite and rhyolite of the Malvern Hills and the Rakaia Gorge were thought to be of ?early to middle Cretaceous age by Gregg (1964), and of Cretaceous age by Suggate (1973).

Indirect evidence of the age of the Mt Somers Volcanics was provided by the 81 Ma age of the andesite from J. D. George No.1 (Hulston and McCabe, 1972), which was correlated with the Mt Somers Volcanics (C. P. Wood, pers. comm.; Suggate, 1973).

2.6.1 Fission Track Dating

2.6.1.1 Principles

This method relies on the fission of radioactive nuclides, in particular the isotope of uranium ^{238}U. The spontaneous fission of ^{238}U results in trails of damage in the crystal lattice, or in the glass, containing the uranium. By using suitable etching reagents on a polished surface of the specimen, the fission tracks can be enlarged to such an extent that they become visible under a high-power optical microscope. The number of fission tracks observed is

proportional to the amount of ^{238}U present in the sample, and the time since formation of the sample. The amount of uranium in the sample can be determined by irradiating the sample with a known amount of slow (thermal) neutrons. These cause fission of uranium-235, a less abundant isotope of uranium, which generates a new set of fission tracks in the sample. By counting the number of induced tracks, and knowing the dose of thermal neutrons, the amount of uranium-238 in the sample can be calculated.

This process, while intrinsically simple, does rely on several assumptions. It is assumed that the naturally induced fission tracks are formed from the spontaneous fission of uranium-238 only. This is a reasonable assumption as no other naturally occurring elements are known to cause fission tracks at a significant rate (Price and Walker, 1963; Fleischer and Price, 1964; Fleischer *et al.*, 1969). It is also assumed that the ratio $^{238}U/^{235}U$ is constant, and once again no variation of this ratio has been reported (Fleischer and Hart, 1970). No annealing of tracks by heat or natural processes, is assumed to have occurred in the sample. However, where it is known to have occurred (e.g. metamorphosed rocks), the natural tracks record the age of the thermal event. The other major assumption is that all tracks can be distinguished from naturally occurring inclusions and dislocations in the sample.

The neutron flux applied to the sample, to induce tracks from the uranium-235, is measured by including a standard uranium-glass dosimeter (Carpenter, 1972a & b) with the sample. The United States National Bureau of Standards

supply standard glass wafers, with precisely known concentrations of uranium in them, that are suitable for this purpose.

The calculations required for the age determinations have been given by Fleischer and Price (1964), and Fleischer and Hart (1970), and can be summarised by the equation:

$$A = (p_s/p_i)(C^{235}/C^{238})\sigma\Phi/\lambda_f$$

where: A = age

p_s = the number of spontaneously produced etch tracks per unit area.

p_i = the number of induced etch tracks per unit area.

C^{235} = concentration of uranium-235 atoms.

C^{238} = concentration of uranium-238 atoms.

σ = cross section for inducing fission of uranium-235 with thermal neutrons.

Φ = thermal neutron flux (thermal neutrons per unit area).

λ = decay rate of spontaneous uranium-238 fission.

The choice of samples is determined by the uranium content and the annealing properties of the sample. Soda glass, calcite, feldspar glass, aragonite, and autunite have track fading temperatures of less than 400°C (Fleischer *et al.*, 1965), and therefore such samples will give unreliable fission track ages.

2.6.1.2 Dating of the Mt Somers Volcanics

The samples used from the Mt Somers Volcanics were dacite glass; quartz, sanidine, and garnet crystals from rhyolite; and pitchstone glass.

The smooth fracture surfaces of grains of sample and also the highly polished surface of specimens mounted in epoxy resin, were etched. For the samples of volcanic glass etching was tried by using a range of HF concentrations from 5% to 40% and durations varying from 5 seconds to 5 minutes. In both the dacite glass and the pitchstone glass, no conditions were found that enabled the etched fission tracks to be unmistakably distinguished from the many crystallites and microscopic elongated bubbles present. For this reason phenocryst minerals were then etched. Quartz was etched using 40% HF at room temperature for durations of between 1 and 2 days. No fission tracks were observed. Similar conditions were used by Fleischer and Price (1964) on natural and irradiated quartz crystals, where they found fission tracks only on the irradiated specimens. This lack of tracks in quartz crystals is because of the low uranium content of this mineral.

Garnet crystals in the Sommers Rhyolite were separated and tested for the presence of spontaneous fission tracks. Haack and Potts (1972) have shown that fission tracks in garnet are completely stable with no measurable annealing at temperatures below 200°C. Etching conditions tried included boiling 40% HF solution for 5 to 30 minutes, and boiling 50N KOH solution for durations of up to 1 minute.

Only occasional fission tracks were found. Dislocations and inclusions were also etched under these conditions. A study of different types of garnet by Haack and Gramse (1972) showed that, in the 22 pyrope and almandine garnets investigated, all contained <3 ppm uranium and produced tracks of $<10^3$ per cm^2, and were therefore not suitable for fission track dating.

Sanidine phenocrysts were also separated from the rhyolite. Recommended etching conditions for plagioclase feldspars (Lal *et al.*, 1968) were 50N NaOH at 150°C. These etching conditions were tried on the sanidine using the apparatus of Lal *et al.* (1968), but the epoxy resins, used to mount the feldspar grains in, were all found to decompose under these conditions.

These time consuming investigations to find suitable fission track dating samples and etching conditions, were terminated in favour of K/Ar dating techniques which gave positive results.

2.6.2 Potassium-Argon Dating

2.6.2.1 Principles

The K/Ar dating method uses the decay of the naturally occurring radioactive isotope of potassium ^{40}K which forms ^{40}Ar gas as a breakdown product. If the ^{40}Ar gas has been retained in the sample and the concentration of this isotope, together with the ^{40}K concentration of the sample are known, then the age of the sample can be determined.

The principles and method used in this dating technique have been described in detail by Dalrymple and Lanphere (1969) and are briefly summarised below.

The decay of ^{40}K results in two stable products. One of these is ^{40}Ar, which is mainly produced by electron capture to form ^{40}Ar, in an excited state, which then decays to form ^{40}Ar, in, the ground state, by the emission of γ-rays. (Direct decay of ^{40}K to ^{40}Ar (ground state) also occurs by electron capture without γ-ray emission, and also by positron emission, but these are mirror decay reactions). The decay constant for this is $\lambda_\varepsilon = 0.58 \times 10^{-10}$ yr^{-1}. The other product formed by the decay is ^{40}Ca, which is formed by β-decay of the ^{40}K. The decay constant for this is $\lambda_\beta = 4.72 \times 10^{-10}$ yr^{-1}.

The total decay constant is $\lambda = \lambda_\varepsilon + \lambda_\beta = 5.305 \times 10^{-10}$ yr^{-1}.

The ratio of ^{40}Ar to ^{40}Ca produced by this decay is called the branching ratio, R.

$$R = \frac{\lambda_\varepsilon}{\lambda_\beta} = 0.124$$

$$\text{The half-life of } ^{40}K = \frac{\log_e 2}{\lambda} = \frac{0.693}{\lambda_\varepsilon + \lambda_\beta} = 1.31 \times 10^9 \text{ yr.}$$

This half life enables a measurable quantity of argon to accumulate in potassium bearing minerals, over geologically useful times.

By measuring the potassium-40 (K_t) and radiogenic argon-40 (Ar_t) concentrations in a mineral the age (t) can be determined by the equation:

$$t = \frac{1}{\lambda_\varepsilon + \lambda_\beta} \cdot \log_e \left[\frac{Ar_t}{K_t} \cdot \frac{\lambda_\varepsilon + \lambda_\beta}{\lambda_\varepsilon} + 1 \right]$$

$$\therefore \quad t = 1.885 \times 10^9 \log_e [9.068 \frac{Ar_t}{K_t} + 1]$$

(Dalrymple and Lanphere, 1969).

For the determination of the age of a volcanic sample it is assumed that there was no argon present in the sample at the time of eruption, and that no loss (or gain) of the radiogenic ^{40}Ar has occurred since that time.

2.6.2.2 Dating of the Mt Somers Volcanics

Twenty-four samples of Mt Somers Volcanics were dated by the K/Ar method. Sample collection followed the requirements of Adams (1970). Generally 1 to 2 kg was collected. Altered, jointed, glassy, or vesicular rocks, were avoided where possible.

The samples were prepared by breaking into cubes approximately 1 cm^3 in size, using a hydraulic rock splitter. These were then hand sorted to remove any small amygdaloids, veins, xenoliths, and altered or weathered zones. The samples were then broken down by hand in a steel mortar to minimise the heat generation caused by normal mechanical grinding processes. During this grinding process the samples were constantly sieved using mesh sizes 120, 80 and 45.

Samples of whole rock (20 g) were retained of each mesh size; the remainder was magnetically separated to obtain the non-magnetic fractions. The non-magnetic fractions

were then separated, using heavy liquids, to obtain feldspar separates (sanidine in the case of the rhyolites, and plagioclase in the case of the andesites). Between 5 and 10 g of each mineral was obtained for each sample.

The mineral separates together with the whole-rock specimens were then analysed at the Institute of Nuclear Sciences, D.S.I.R., Wellington, by C.J.D. Adams, J. Park and W. Mason, for ^{40}K and ^{40}Ar. The method used has been described by Adams (1975). Results obtained from these K/Ar analyses are given in Table 11, and sample localities on Figure 87.

2.6.3 Interpretation of Radiometric Ages

The Barrosa Andesite has an age range of 43 to 93 Ma (Samples PO142, PO417, PO471, PO484, PO581 in Table 11). Sample PO581 which consistently gave an age of 44 Ma is clearly in error as this andesite flow stratigraphically underlies PO484 which gave ages of up to 91 Ma. One alternative is that this flow is a younger sill. Although dikes also occur at this locality these appear to have been contemporaneous with, and fed, overlying flows. Palaeomagnetic samples from PO484 had steep inclinations in agreement with the overlying flows, which also indicates that the flows are not of Mid-Tertiary age.

There is no consistency between the ages obtained from whole rock (TR) samples and those of plagioclase separates in the Barrosa Andesite. Sample PO417 clearly gives an older age for the TR sample; while samples PO484 gives an older

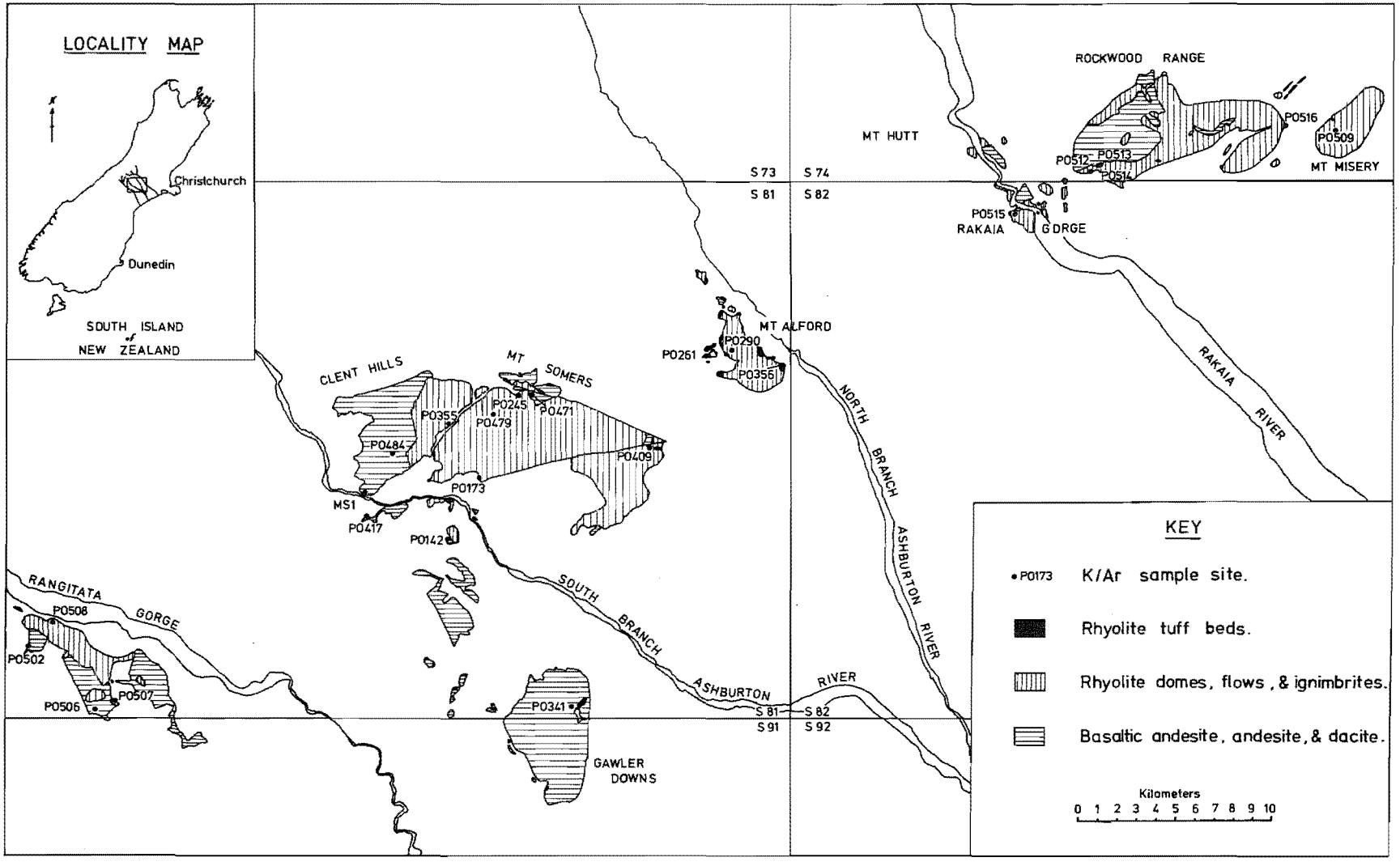

Figure 87. Locality map for K/Ar sample sites.

TABLE 11: Sample details and K/Ar ages of Mt Somers Volcanics.

Sample No.	Sample Type.	Mesh size	Rock Type.	Locality.	Grid References.	K (%).	^{40}Ar (nl/g)	^{40}Ar (% total)	Age. (Ma)
P0142	TR	-45 +80	Andesite	Blondin Stream	S81/807398	1.667	5.42	74.14	79.9 ±0.6
P0417	TR	-44 +80	Andesite	Sandrey Stream	S81/762411	1.233	4.70	72.41	93.3 ±0.7
	Pl	-44 +80				0.280	1.01	55.82	88.4 ±0.6
							1.01	71.73	88.3 ±0.6
							0.94	56.71	82.2 ±0.6
P0471	TR	-44 +80	Andesite	Morgan Stream	S81/853481	2.275	8.16	94.19	88.0 ±0.6
	Pl	-44 +80				0.422	1.49	75.47	86.7 ±0.6
P0484	TR	-44 +80	Andesite	Mt. Barrosa	S81/776447	1.176	3.38	80.48	70.9 ±0.5
							3.42	77.51	71.7 ±0.6
	Pl	-44 +80				0.266	0.87	35.57	80.9 ±0.6
							0.99	61.00	91.0 ±0.7
P0581	TR	-422 +211	Andesite	Ashburton Gorge Road	S81/760424	2.151	3.84	56.13	44.3 ±0.3
							3.79	60.67	43.8 ±0.3
							3.88	59.11	44.8 ±0.3
	TR	-422 +211				2.087	3.69	50.07	43.9 ±0.3
P0245	Sa	-45 +80	Rhyolite	Morgan Stream	S81/848479	7.759	29.49	97.57	93.1 ±0.7
							29.77	95.57	94.0 ±0.7
P0355	Sa	-45 +80	Rhyolite	Stour River	S81/808465	7.890	29.61	97.52	91.9 ±0.7
P0173	Sa	-44 +80	Pitchstone	Woolshed Creek	S81/824434	7.109	27.85	86.56	95.9 ±0.7
P0409	TR	-44 +80	Pitchstone	Bowyers Stream	S81/922451	3.478	13.47	94.50	94.8 ±0.7
							13.94	95.80	98.1 ±0.7
	Sa	-44 +80				7.899	29.51	96.04	91.6 ±0.7
P0479	Sa	-44 +80	Rhyolite	Burma Road	S81/834470	5.226	19.06	95.81	89.4 ±0.6
							19.23	87.50	90.2 ±0.6
P0261	TR	-45 +80	Dacite	Winterslow track	S81/954502	2.981	10.46	95.19	86.1 ±0.6
	Pl	-80 +120				0.801	2.92	81.46	89.5 ±0.6
P0341	TR	-45 +80	Dacite	Gawler Downs Trig	S81/880313	2.568	9.08	82.31	86.8 ±0.6
						0.757	2.79	76.07	90.4 ±0.7
							2.76	73.30	89.4 ±0.7
P0290	Sa	-80 +120	Rhyolite	Mt. Alford	S81/967507	5.775	20.25	96.04	86.0 ±0.6
							21.75	94.82	92.3 ±0.7
P0358	TR	-45 +80	Dolerite	Mt. Alford	S81/994495	1.463	5.21	93.87	87.4 ±0.6
P0502	TR	-44 +80	Andesite	Lodge Stream	S81/572338	1.667	4.18	63.87	61.9 ±0.5
							4.19	64.13	62.0 ±0.5
	Pl	-44 +80				0.673	2.36	68.24	86.0 ±0.6
							1.99	44.37	72.7 ±0.5
P0506	TR	-44 +80	Andesite	Quartz Creek	S81/611303	1.270	3.92	76.59	75.9 ±0.6
							4.32	65.02	83.5 ±0.6
	Pl	-44 +80				0.3115	1.08	80.97	85.3 ±0.6
							1.08	60.06	85.2 ±0.6
							1.10	48.84	86.3 ±0.6
P0507	Sa	-44 +80	Rhyolite	Hewson River Track	S81/621309	3.555	13.50	91.29	93.0 ±0.7
							13.66	87.35	94.1 ±0.7
							13.58	94.19	93.6 ±0.7
P0508	Sa	-44 +80	Rhyolite	Harper Lodge	S81/586356	4.463	15.45	90.59	85.0 ±0.6
							15.87	90.72	87.2 ±0.6
							15.03	88.68	82.7 ±0.6
P0512	TR	-44 +80	Andesite	Roundtop	S81/170609	1.129	3.89	59.35	84.5 ±0.6
							3.91	51.90	85.0 ±0.6
P0513	TR	-44 +80	Andesite	The Point Roundtop	S74/170609	0.832	3.08	60.36	90.8 ±0.7
							2.97	82.97	87.4 ±0.6
	Pl	-44 +80				0.347	1.22	68.96	86.2 ±0.6
							1.20	71.35	84.8 ±0.6
P0511	TR	-44 +80	Basalt	Pullwool Peak Road	S74/277634	0.536	0.73	19.14	34.0 ±0.4
							0.82	15.84	38.2 ±0.4
P0509	Sa	-44 +80	Rhyolite	Yorkies Saddle	S74/304629	4.949	18.01	92.83	89.6 ±0.6
P0514	Sa	-44 +80	Rhyolite	The Point, Roundtop	S74/166608	5.916	21.03	97.70	87.2 ±0.6
							21.56	91.99	89.3 ±0.6
P0515	Sa	-44 +80	Rhyolite	Rakaia Gorge	S82/129585	6.310	23.88	94.40	92.7 ±0.7

TR = total rock ; Pl = plagioclase ; Sa = Sanidine.
Age errors are one standard deviation.

age for the plagioclase separate. These two samples are petrographically and chemically indistinguishable, and they could even be products of the same eruptive phase.

The Somers Rhyolite (samples PO245, PO355, PO173, PO409, PO479, Table 11) has an age range of 89 to 98 Ma. The ages given by sanidine from pitchstone appear to be older than those given by sanidine from rhyolite. This difference may be due to the rate of cooling of these different forms of rhyolite. In the pitchstone the sanidine phenocrysts would remain in their high-form, as these were chilled rapidly, whereas the sanidine phenocrysts in the rhyolite domes would have cooled slowly. The slow cooling of the rhyolite domes possibly allowed some unmixing of the sanidine to occur. Unmixing was not observed in thin sections of the rhyolite, but even if this had occurred the unmixing would not be expected to be visible under the microscope (Deer *et al.*, 1966). Unmixing in sanidine has been shown to result in radiogenic argon loss in pre-Tertiary samples (Dalrymple and Lanphere, 1969, p170), which has resulted in anomalously young ages being recorded. The albite member of the unmixing process is triclinic while the pure sanidine member is monoclinic. Presumably lattice distortions resulting from any unmixing process results in more radiogenic argon loss than do either pure end-members of the high-albite/high-sanidine solid solution series. A study of leakage of radiogenic argon from sanidine by Baadsgaard *et al.* (1961) showed that argon is retained in high-sanidine, except when the grain size is less than 325 mesh, or when the sanidine has lattice irregularities.

The Hinds River Dacite (Samples PO261 and PO290; Table 11) gave an older age for the plagioclase separate than the total rock. The groundmass of the dacite contains glass and which could have lost some radiogenic argon. The ages are comparable with those of the Barrosa Andesite.

The Graham Dolerite appears to be younger than the Alford Rhyolite (Table 11), but although the Graham Dolerite should be younger on stratigraphic grounds, the actual difference indicated by the dates (4.9 Ma) is not significant because only one sample of each rock type was dated.

The Stew Point Andesite (samples PO506 and PO507; Table 11) gave older ages from the plagioclase separates, than from whole rock, but even the oldest plagioclase date is 7.8 Ma younger than the oldest Rata Peaks Rhyolite (samples PO507 and PO508; Table 11), and as the rhyolite definitely overlies the andesite in the Rangitata Gorge area, the ages obtained for the andesite must be in error. Studies by Evernden and James (1964) established that high temperature plagioclase feldspar, with potassium contents of less than 0.9% by weight, quantitatively retain radiogenic argon for hundreds of millions of years. Thus, all the plagioclase separates from the andesite of the Mt Somers Volcanics should give reliable ages. No consistent variation in ages with potassium content was observed in the analysed samples (Table 11), and therefore this factor cannot be used to explain the discrepancies.

The difference in K/Ar dates between, the rhyolite samples PO507 and PO508 (Table 11) could be due to the more fractured and fragmented nature of the sanidine

phenocrysts in sample PO508, and to slight alteration of the sample.

The basalt dike from the Malvern Hills (PO511; Table 11) gave a date of 34 Ma. Even allowing for some argon leakage from this sample, the age is still considerably younger than the calc-alkaline volcanics. The basalt dike could be associated with the Harper Hills Volcanics which have been placed in the Miocene by Suggate (1973), and Gregg (1965), on the basis of interbedded bentonite containing Upper Miocene pollens. It is more likely, however, that the basalt dikes are associated with the pillow lavas and tuffs of the Landon limestones (Gair, 1967) of the area.

The rhyolite and andesite from the Rakaia Gorge-Malvern Hills area (samples PO512, PO513, PO509, PO514, PO515; Table 11) gave similar K/Ar ages to the other volcanics of the Mt Somers Volcanics.

2.6.4 Adopted Ages

Although the K/Ar dates cover a wide span of time, stratigraphic limitations restrict the age range. The oldest date obtained was 98 Ma. This was for a pitchstone in Bowyers Stream (PO409). Although this date was obtained on a whole rock sample of glassy pitchstone, it is unlikely that any significant amount of enrichment of radiogenic argon in the glass occurred, as a sanidine separate from another pitchstone (PO173) gave a similar result. This age of 98 Ma is the best age for the Somers Rhyolite and the Barrosa Andesite.

The oldest date for the other volcanics can be taken as a reliable minimum. Exceptions include the Barrosa Andesite already mentioned, and the Stew Point Andesite which stratigraphically underlies the Rata Peaks Rhyolite. As with the Barrosa Andesite, the Stew Point Andesite gave a maximum K/Ar date of less than the overlying rhyolite. The minimum age for the Stew Point Andesite is therefore the same as for the Rata Peaks Rhyolite, i.e. 94 Ma.

The measured age range for the volcanics of the Rakaia Gorge-Malvern Hills area is 91 to 93 Ma, but there is a high probability that the volcanics are of the same age as the Somers Rhyolite (i.e. 98 Ma).

Hinds River Dacite (90 Ma) and the Graham Dolerite (87 Ma), only give a reliable minimum age, and probably were erupted soon after the Somers Rhyolite. If a time gap existed between the eruption of the rhyolite and the dacite, then the tuff beds over which the dacite was erupted (the Surrey Hills Tuff) would be expected to grade up into sediments derived from erosion of the rhyolite, andesite, and Torlesse rocks. The similarity between the tuff beds overlain by rhyolite at Mt Alford, and andesite near Morgan Creek, with those overlain by dacite, indicates that there is no erosional or depositional difference between these beds. Therefore the dacite must have been deposited contemporaneously with, or soon after, the andesite-rhyolite eruptions.

2.7 STRUCTURE AND TECTONIC DEFORMATION

Mt Somers is a triangular shaped mountain with the north-eastern and south-eastern sides bounded by faults which have formed steep scarps. The upper surface of the mountain is remarkably flat and dips at angles of 10° to 20° to the west. The dip of this surface is largely controlled by ignimbrite flows which are generally subparallel to the surface. While the ignimbrite is predominantly flat lying, there are local variations in dip. These can be explained by post-depositional deformation although some undulations in the ignimbrite may follow sub-surface features. The western half of Mt Somers is downfaulted along a line approximately north-south from GR 879476 to 876455. This down faulting was a collapse, consequent on the extrusion of the rhyolite. It can be recognised in the field by a break in slope of the upper surface of Mt Somers, by the presence of intrusive rhyodacite dikes, and by the local dip of the ignimbrite in towards the fault. This last feature is most clearly seen on the northern face of Mt Somers where the complete sequence of ignimbrite flows is exposed. A complication is the deformation caused by the extrusion of andesite, on the north-east corner of Mt Somers, through the ignimbrite. This has resulted in an upwarping of the ignimbrite at the contact.

The main evidence that the northern face of Mt Somers is an eroded fault scarp comes from the pug zones and crush zones found along the contact between the rhyolite and the Torlesse rocks in the gullies of the streams that descend from the north face of Mt Somers. The direction of movement

along the fault is not easy to determine. If the tuff in Woolshed Creek (GR 827454), by the incline to the "Burning Coal Mine", represent the basal section of the main mass of Mt Somers, then the basal contact is over 300 m below the elevation of the contact of the andesite and the Torlesse rocks to the north of Mt Somers. The Mt Somers block is therefore probably downthrown a minimum of 300 m to the south. In Bowyers Stream above Goldsmiths Rapids, the Torlesse beds strike perpendicular to the line of the fault, but within a 20 m zone of the contact the Torlesse beds are bent through an angle of 90° until they lie parallel with the contact. A sinistral movement of 250 m along this fault is indicated by the off-set of rhyolite/andesite boundaries in the Woolshed Creek and Morgan Stream area. The fault zone exposed in Bowyers Stream above Goldsmiths Rapids is a series of pug zones indicating the faulting was not along a single plane.

The south-east face of Mt Somers is also bounded by a fault which again is not a single fault plane, but a series of close parallel faults. The main evidence for these faults is the large crush zones at the confluence of Tinstone Creek and Bowyers Stream. Tinstone Creek runs along the valley caused by erosion of the crush zone. No definite lateral displacement can be determined along this fault, but vertical movement is indicated. The block to the south of the fault is downthrown relative to that to the north. The vertical displacement is as much as 700 m if Stavely Hill was

originally at the same height as the upper surface of Mt Somers. South of Stavely Hill the Cox Hills are block faulted by at least five sub-parallel faults. The blocks are successively downfaulted to the south. The evidence for this block faulting is the presence of colinear pug zones and waterfalls in the streams that descend from Cox Hills. These line up with linear scarps that are clearly visible on aerial photos and in the field. Other evidence for the faulted blocks comes from remnants of Tertiary coal measures and silica sands that can be found perched on the surface of the lower blocks. The lowest block has the thickest sequence of Tertiary deposits. North of Reid Stream the beds of limestone strike north-south with a vertical dip. In places they are overturned by a few degrees. The vertical nature of these limestone beds is a direct result of the block faulting. These beds have either slumped over the fault scarp or have been dragged into their vertical position by the block faulting, which indicates that this tectonic event occurred in the late Tertiary Kaikoura Orogeny. The block faulting is illustrated in Figure 32.

Other evidence of late Tertiary tectonic activity can be found west of Woolshed Creek where coal measures rest on Somers Rhyolite. At the "Burning Coal Mine" (GR 826460) the coal measures lie at an elevation of 730 m above sea level. Near the Ashburton Gorge Rd (GR 812433) coal measures are at an elevation of 550 m. The difference of 180 m indicates that some block faulting has also occurred between these localities. The coal measures are also tilted. At the "Burning

Coal Mine" the surface of the rhyolite dips at 12° to the south and strikes at 036°. However the dip of the coal measures is difficult to determine as the coal mine has been open cast mined and all signs of the original bedding has been destroyed. Speight (1938, p76) described the variation in dip in coal measures exposed in drives of this mine. Generally the beds dip at shallow angles (about 5°) to the south-east. Approximately 700 m south-west of this mine (GR 820455) are some old drives at the same height as the open cast "Burning Coal Mine". The coal measures extend around the hill for about 400 m. Dips obtained from these coal measures were also variable but generally dip to the east at shallow angles. The old coal mines near the Ashburton Gorge Rd (at GR 812433) have been opencast mined since 1975. This has enabled a good average dip of the beds to be established at 13° to the east and with a strike of 200°. All the evidence from the Tertiary coal measures on the ridge west of Woolshed Creek indicates that the tectonic tilting was to the east or south-east. This is in the opposite direction to the flat surface eroded on this ridge and on Mt Somers. This supports the argument that the flat erosional surface on Mt Somers was controlled by the ignimbrite flows.

North of the main fault separating the Mt Somers and Mt Winterslow blocks, a complicated relationship occurs between the andesite and the rhyolite which was described in section 2.2.5.5. The relationships are further complicated by tectonic deformation and faulting. The contact between the

andesite and the Torlesse rocks can be seen on either side of Morgan Stream and in places in Woolshed Creek. From these exposures the average dip of contact was determined to be 27° to the south with a strike of 120°. The tilt measured on banded agates in the andesite indicated that the tectonic tilt of the block was 35° to the south with a strike of 105°. Further evidence for the tectonic tilt is provided by the dip of the ignimbrite overlying the andesite, at GR 858483, which is approximately 30° to the south with a strike of 145°. The reasonably good agreement between these measurements of tilt confirms that the values obtained by measuring the dip of the agate bands is reliable as an indication of tectonic tilt.

In Woolshed Creek above the hut, at GR 847487, a reverse fault dips at 85° to the south and strikes at 125°. On the upthrown side of the fault the sequence exposed in the section is: andesite flows, overlain by a pitchstone-ignimbrite, overlain by ignimbrite. The pitchstone-ignimbrite (a tuff that has been rapidly chilled after being welded) has been described in section 2.2.5.3. This pitchstone is characterised by fiamme texture. The dip measured on the fiamme was variable but approximately 24° to the south-east with a strike of 036°. This dip is similar to that obtained for the dip of nearby banded agates in andesite.

The main fault on the north side of Mt Somers appears to branch, west of Morgan Stream, into the one described above and one further to the south (see Maps 1 and 3). The ridge between these two faults (extending from GR 847485 to

838491) is of andesite which is "overlain", on its southern margin by pitchstone agglomerate, pitchstone, and rhyolite (all of which are of ignimbritic origin). The contact between the andesite and the rhyolite appears to be steeply dipping to the south, and may be vertical, but this is difficult to tell for certain as the contacts are not clearly exposed. This ridge appears to have been tilted to the south by the upward movement of the Winterslow block relative to the Mt Somers block, the ridge being a small block rotated between these two.

The Clent Hills has not been tilted as a single block. Banded agates in vesicular andesite dikes near the western margin of the Barrosa Andesite (GR 749475 and 751477) have an average tilt of 20° to the north with a strike of 070°. At the southern extremity of the Clent Hills near the Ashburton Gorge Rd (GR 761425), the andesite flows are tilted to the east. The dip on agate bands at this locality is 10° to the east with a strike of 360°. In Blue Duck Stream, west of the andesite/rhyolite contact, the flows of andesite can be observed to increase in dip from 15° near the upper reaches of the stream, to over 50° near the contact. The dip of banded agates also increases indicating that the andesite along the contact has been down-warped. This is most likely to have occurred contemporaneously with, or immediately subsequent to, the extrusion of the overlying rhyolite. Similar phenomena were observed in the Rangitata Gorge near the andesite/rhyolite contacts.

At the Coal Reserve between Woolmer Hill and the Ashburton River an outlier of Tertiary clays, coal measures,

and silica sands crops out between rhyolite on the east and andesite on the west. Wellman *et al.* (1945), and Speight (1938) considered that the coal measures overlay the volcanics. The coal measures show small scale slumping, folding and faulting, and form a shallow syncline with an approximately north-south axis. These Tertiary sediments appear to have been deposited in their present location, and the upper beds grade from coal measures into sands and sandy conglomerates of andesite along the western contact with the andesite. The clays are kaolinised rhyolite boulders and pebbles which were presumably locally derived, and were deposited in the depression in the early Tertiary. There is no evidence in the field to support the possibility that these Tertiary deposits are fault bounded (Wellman *et al.*, 1945).

In Blondin Stream there is evidence to support late Tertiary tectonism, as a fault extends from GR 809397 to 806403. At GR 807402 on this fault, rhyolite is thrust over the Tertiary silica sands at a shallow angle (dip 36° to the east and strike 165°).

The Hinds River Dacite is faulted along its south-western boundary at the northern end of the Peter Range. Banded agates in the dacite cropping out in the banks of a small tributary to the Hinds River at GR 805377, are approximately horizontal, which suggests that tectonic tilting at this locality is zero. The dacite also occurs as isolated outcrops along the east flank of the Peter Range where it is faulted against Torlesse rocks. On the summit of the hill west of Wakare Station, at GR 798331, dacite overlies tuff beds. The vertical movement of this block is 300 m. The

tilted Tertiary beds along the eastern flank of the Peter Range indicates that, as before, this tectonic movement occurred in the late Tertiary.

The Gawler Downs block is bounded by faults along its north, east and southern sides. A north-south trending fault parallel to the eastern fault extends the length of Surrey Stream. Although the Gawler Downs has a flat erosional surface dipping gently to the west there is no indication that this represents the overall tilting of this block. Beds of Surrey Hills Tuff dip at angles of 10° to 20° to the east in the gully east of the Gawler Downs Trig Station (GR 885309) which suggests tilting of this block has occurred in the same direction as the Mt Somers and Clent Hills blocks. The difference in elevation between the base of the dacite in this gully and that near Wakare Station is less than 50 m, which is consistent with a shallow dip to the east.

Tectonic movements of Mt Alford are not easy to distinguish from those that accompanied the extrusion of the rhyolite. The tuff beds underlying the rhyolite on both the eastern and western flanks of the Alford Range dip in towards the centre of the range at inclinations of up to 35°. Tectonic movements along the flanks of Mt Alford take the form of a series of sub-parallel block faults downthrown to the east of the range, and also to the west. On the east side of the range, a series of downthrown blocks each with vertical displacements of less than 3 m can be observed by remnants of dolerite and tuff beds that outcrop down the ridge from GR 984506. The faulting on the western side of the range is of greater extent. In Diamond Creek tuff beds underlie the

rhyolite. These beds also occur near the confluence of Diamond Creek and Taylors Stream, where they have been vertically displaced by 170 m.

The southern end of Mt Alford is bounded by a fault or faults that also extend along the south flanks of Mt Hutt, Pudding Hill, Mt Winterslow and Mt Somers. The presence of a major fault along these foothills was confirmed by seismic profiling near Pudding Hill (G. Mansergh, pers. comm.).

Tectonic movements of the Rangitata Gorge volcanics indicates that they have not acted as a single block. The andesite between Rawtor Creek and Lodge Stream has been tilted 21° to the east with a strike of 209°; this was determined by small banded agates near the base of the series of flows. At GR 572337 the upper contact of this andesite is overthrust from the south by Torlesse rocks, along a low angle fault.

The andesite at the headwaters of Matagouri Stream is bounded on its south-west margin by an active fault (Figure 38) that separates the andesite from the Torlesse rocks. The andesite at this locality has not been tilted to any great extent as banded agates have dips of less than 10° and strike at 160°.

At Stew Point banded agates in a blocky lava flow (GR 635337) indicate that the andesite at this locality has been tilted 38° to the east with a strike of 017°. This would give the andesite flows at this locality (which at present dip at 30° to the west) a tectonically corrected dip of approximately 70° degrees to the west. The andesite

to the east of this ridge (GR 644323) have flows dipping at 12 to 15° to the west and striking at 025°. Separating these two andesites is a faulted zone marked by large scale slumping. It would appear that the steeply dipping andesite immediately in contact with the rhyolite had undergone deformation contemporaneously with the extrusion of the rhyolite. Andesite flows at the headwaters of Soup Stream have large banded agates with approximately horizontal bands. No tectonic correction appears necessary for these flows which are continuous with those of the locality at GR 644323, just described.

There is no way of telling what tectonic movements, if any, have occurred to the rhyolite in the Rangitata Gorge. As the only deformation of the andesite appears to be in the form of localised collapse at the margins of the rhyolite, but otherwise very little deformation away from the contacts, it may be assumed that there is no net post-eruptive regional tilting of the volcanics in this area. Whether this assumption is valid is difficult to prove, but at this stage it can only be stated that there is no evidence to suggest that the rhyolite has been tilted to any great extent.

2.8 PALEOMAGNETISM

2.8.1 Objectives

The main objective for a paleomagnetic study of the Mt Somers Volcanics was to find the position of the geomagnetic pole (relative to New Zealand) during late Cretaceous times, and hence by comparison with paleomagnetic poles for other Gondwana countries, to find the relative position of New Zealand at that time. It should also be possible to tell if there has been any relative movement between the east side of the South Island of New Zealand, and the Chatham Islands since the Cretaceous. Other correlations with Cretaceous volcanics throughout New Zealand would also provide useful information of relative tectonic movements (particularly rotational movements).

2.8.2 Principles

Many books have covered the principles of paleomagnetism in detail (e.g. Irving, 1964; Collinson *et al.*, 1967; Tarling, 1971; McElhinny, 1973); and therefore only a brief description will be given here.

Most rocks contain magnetic minerals which impart an overall magnetic field to the rock (called the natural remanent magnetism, NRM). In both igneous and sedimentary rocks the net magnetic field of each magnetic mineral is aligned with the earth's magnetic field. As an igneous rock cools below the Curie temperature for each mineral, generally

between 400 and 600°C, the magnetic field of each mineral is preserved. In sedimentary rocks the ferromagnetic and ferrimagnetic minerals align themselves with the earth's field as they are deposited, and thus the direction of the earth's field is also preserved in these rocks. This preservation of the earth's magnetic field in rocks is generally referred to as paleomagnetism.

The earth's magnetic field is assumed to have always approximated a geocentric axial dipole field, with the dipole parallel to the rotational spin-axis of the earth. Deviations from the axial dipole models, in the form of secular variation, are known to exist at the present time and to have existed in the past. Studies of secular variation from precisely dated archaeological data have shown that secular variation has a periodicity of about 10^3 years and an amplitude of approximately 20°, which correlates well with the studies of varve deposits and lava sequences (Tarling, 1971, p100). In addition to secular variation there are fluctuations in intensity of the earth's field, and also reversals of pole directions which have occurred throughout geological time. Studies of the boundaries between normal and reversed polarity events show that these changes are associated with a decrease in remanent intensity, which may be due to a decay of the geomagnetic field strength, or to the presence of opposing magnetic directions within the rocks (Løvlie, 1976). The pole reversal transitions usually occupy a relatively short period of time, often as little as 10^3 years (Creer and Ispir, 1970).

Secondary magnetism can occur in both igneous and sedimentary rocks as the result of magnetic alteration products (e.g. secondary hematite). Alteration of the primary and secondary magnetic fields in rocks can also occur by reheating of the rock, metamorphism, exsolution, diagenesis and (in the case of sedimentary rocks) compactional rotation of elongated magnetic minerals, all of which can result in NRM inclination errors.

The primary remanent magnetism of rocks can be altered by superimposed subsequent magnetic fields. This is more likely to occur if the magnetic minerals are large, as large crystals tend to have complex magnetic polarity domains in them. Each domain has a particular polarity, with the overall effect being to reduce the magnetic field of the mineral. This is effected by adjacent domains adopting opposite polarities in a grain. An external field applied to such a crystal will tend to enlarge the size of the domain that is parallel to the external field and reduce the size of the other domains. If the enlarged domain has surmounted an energy barrier (a "Bloch wall") during this enlargement, then the superimposed magnetism will remain after relaxation of the applied external field, and is called isothermal remanent magnetism (IRM). This effect, which is controlled by the shape and size of the grains and the presence of impurities and dislocations in the crystal lattice, means that to obtain the true primary magnetism of a sample a demagnetising process to remove all secondary magnetic effects must be carried out on the sample.

2.8.3 Sample Collection

Samples of the Mt Somers Volcanics used were as fresh as possible, to avoid secondary remanent magnetism from alteration or weathering products. It was relatively easy to collect fresh andesite and dacite but the rhyolite is invariably well jointed with iron oxides contained in the joints.

Samples were collected where the original altitude of the volcanics could be deduced. Where possible, andesite samples were taken at, or adjacent to, flows containing banded agate amygdules, as these act as an internal tiltmeter for post-depositional tectonic tilt. Sites for which radiometric ages were known, were sampled, and also those where the stratigraphy placed limitations on the age. Where possible, samples were collected from a sequence of lava flows in an attempt to determine secular variations. Baked tuff at the lower contact of dolerite and andesite were sampled in order to compare the results with tuff away from the contact.

Two methods of sampling were employed. One was to collect oriented blocks of the volcanic rocks. These were then reoriented, set in plaster, and cored using a diamond drill corer in the laboratory. Cores with a diameter of 25 mm were cut into lengths of 25 mm. This usually provided two or three suitable specimens from each sample. Generally only one sample was collected from each site (i.e. each flow, dome, or bed). The second method of obtaining samples, was to core the rocks in the field using a portable coring machine which consisted of a converted chain-saw motor fitted with a

chuck to take diamond core bits, and a water cooling system that fed water into the coring bit. Prior to the removal of the core from the outcrop, an orienting device was used to mark the declination and inclination of the core. The equipment and method used has been described in detail by Doell and Cox (1965, 1967) and McElhinny (1973). Details of the paleomagnetic collecting sites are given in Table 12, and Figure 88.

2.8.4 Measurement of Paleomagnetism

Samples were measured on one of three types of spinner magnetometer. The most sensitive magnetometer, used for samples with the lowest intensities, was a fluxgate spinner-magnetometer connected to a PAR, model 129, two phase/vector lock-in amplifier. Samples with higher intensity were measured on a 5 Hz fluxgate spinner-magnetometer similar to that described by Foster (1966). The strongest samples were measured on a 24 Hz fast-spinner magnetometer described in detail by Lumb and Roberts (1969).

Magnetic vector component intensities and directions were measured for the three dimensions. Corrections for the orientation of the core and for tectonic tilt were then applied, to obtain NRM directions. Final calculations of virtual geomagnetic poles (VGP) and paleomagnetic pole positions were obtained by using the computer programmes described by Lumb (1967).

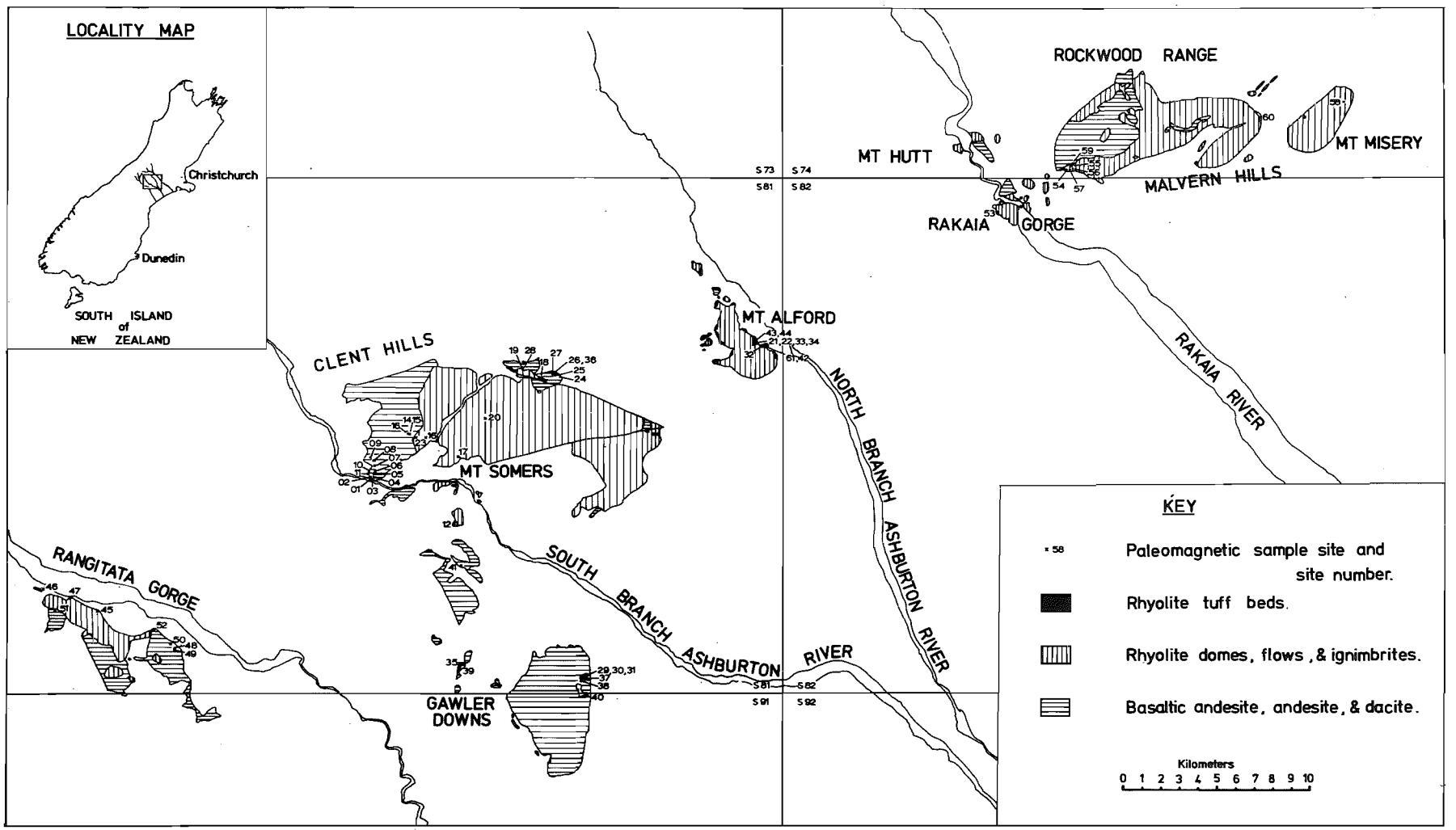

Figure 88. Locality map for paleomagnetic sample sites.

TABLE 12: Paleomagnetic sample sites.

Field No.	Site No.	Geophysics Cat. No.*	Locality	Rock type	Grid Reference.**
MS1	1	7673	Ashburton Gorge	Andesite	760424
MS1A	1	7745	" "	"	764424
MS1B	1	7746	" "	"	764424
MS2	2	7674	" "	"	760425
MS3	3	7674	" "	"	760423
MS20	4	7796	" "	"	762425
MS21	5	7797	" "	"	762427
MS22	6	7798	" "	"	763429
MS23	7	7799	" "	"	762432
MS24	8	7800	" "	"	762435
MS25	9	7801	" "	"	760437
MS26	10	7802	" "	"	759429
MS27	11	7803	" "	"	759427
MS39	12	7817	Blondin Stream	"	808398
MS48	13	7827	Blue Duck Stream	"	783450
MS49A	14	7828	" "	"	782450
MS49B	15	7829	" "	"	782450
MS2A	16	7747	" "	Rhyolite	792448
MS2C	16	7748	" "	"	792448
MS2D	16	7749	" "	"	792448
MS3A	17	7750	Burma Road	"	811437
MS44	18	7823	Morgan Stream	"	859483
MS46	19	7825	Woolshed Creek	"	848487
MS47	20	7826	" "	"	827460
MS30A	21	7807	Mt. Alford	"	784504
MS30B	22	7808	"	"	784504
MS50	23	7830	Blue Duck Stream	"	786448
MS40	24	7818	Morgan Stream	Andesite	870483
MS41	25	7819	" "	"	867485
MS42A	26	7820	" "	Rhyolite Tuff	867486
MS43	27	7822	" "	Andesite	866486
MS45	28	7824	Woolshed Creek	"	848488
MS5A	29	7753	Gawler Downs	Rhyolite Tuff	884309
MS5B	29	7754	" "	" "	884309
MS5C	29	7755	" "	" "	884309
MS6A	30	7756	" "	" "	884309
MS6B	30	7757	" "	" "	884309
MS7A	31	7758	" "	" "	885309
MS7B	31	7759	Gawler Downs	Rhyolite Tuff	885309
MS29A	32	7805	Mt. Alford	" "	989501
MS31	33	7809	" "	" "	984504
MS32	34	7810	" "	" "	985504
MS35	35	7813	Waikare	" "	811316
MS42B	36	7821	Morgan Stream	" "	867456
MS4B	37	7752	Gawler Downs	Dacite	883308
MS8A	38	7760	" "	"	882306
MS8B	38	7761	" "	"	882306
MS36	39	7814	Waikare	"	812314
MS37	40	7815	Gawler Downs	"	886298
MS38	41	7816	Hinds River	"	812374
MS28	61	7804	Mt. Alford	Dolerite	988501
MS29B	42	7806	" "	Rhyolite Tuff	989501
MS33	43	7811	" "	Dolerite	985504
MS34	44	7812	" "	"	985504
RG3A	45	7667	Rangitata Gorge	Rhyolite	602348
RG3B	45	7668	" "	"	602348
RG4	46	7669	" "	"	571361
RG5A	47	7670	" "	"	587357
RG5B	47	7671	" "	"	587357
RG1A	48	7664	" "	Andesite	647327
RG1B	48	7665	" "	"	647327
RG2	49	7666	" "	"	647326
RG6	50	7672	" "	"	645329
MS9A	51	7662	" "	"	577349
MS9B	51	7763	" "	"	577349
MS9C	51	7764	" "	"	577349
MS10	52	7765	" "	"	635337
MH1A	53	7676	Rakaia Gorge	Rhyolite	S82/125581
MH1B	53	7677	" "	"	S82/125581
MH2A	54	7831/1	Round Top	"	S74/166605
MH2B	54	7831/2	" "	"	S74/166605
MH3	55	7832	" "	"	S74/169608
MH5	56	7834	" "	"	S74/169606
MH6	57	7835	" "	"	S74/168605
MH8	58	7837	Mt. Misery	"	S74/327645
MH4	59	7833	Round Top	Andesite	S74/170609
MH7	60	7836	Pullwool Peak Road	Basalt	S74/278636

* = Geophysics Division, Wellington, Rock Catalogue No.

** = Grid References for S81, unless otherwise indicated.

Samples from each site were selected for a pilot study, and stepwise demagnetised in an alternating magnetic field. The samples were tumbled in all directions during this demagnetisation. The initial demagnetising field was $4x10^3$ A/m and was increased by steps of $4x10^3$ A/m to $40x10^3$ A/m. The demagnetisation was occasionally carried on beyond $40x10^3$ A/m when no change in intensity of the sample was recorded; or was terminated prior to reaching $40x10^3$ A/m if the sample became too unstable to measure. Immediately after each demagnetisation run, the samples were measured on the spinner-magnetometer, to avoid ambient magnetic fields affecting them. When the optimum demagnetising field was found for each sample, the other specimens from the same site were then demagnetised at that level.

2.8.5 Results

2.8.5.1 Magnetic Properties of the Samples

The magnetic properties for all samples measured are given in Table 13. In this table NRM values are uncorrected for tectonic tilt. The 95% circle of confidence (α_{95}) for these NRM values is only given where three or more core specimens were measured from a sample. The magnetic susceptibilities of samples were measured by T. Mumme, Geophysics Division, Wellington. The Koenigsberger ratio (Qn) gives some indication of the stability of the remanent magnetism. In general values of $Qn > 1$ indicate stable single domain magnetism, and values of $Qn < 0.5$ indicate

multiple domain magnetism in the magnetic grains of the rock (Irving, 1964, p92; McElhinny, 1973, p104). From Table 13 it can be seen that the majority of samples have high to very high Koenigsberger ratios. Exceptions are the Surrey Hills Tuff (sites 29-36), the Hinds River Dacite (sites 38, 40), and one sample of Barrosa Andesite (sample MS23).

2.8.5.2 Application of Tectonic Tilt Corrections

A major difficulty in obtaining valid paleomagnetic results from Mesozoic rocks in New Zealand is the difficulty in predicting reliable tectonic tilt corrections. Local variations in tilt make it unwise to use a regional trend as a correction.

The andesite of the area conveniently contain banded agates which can be used as internal tiltmeters, as the bands were originally horizontal. The main assumption that must be made using agate inclinations, is that the agates were deposited at the time of, or soon after, the extrusion of the andesite. Arguments in favour of this assumption have already been discussed in a previous section (section 2.2.4.4).

Unless there was evidence to the contrary, it was assumed that no rotational movement has taken place.

Another indicator of tectonic tilt was the bedding attitudes in subaqueous tuff. These beds are of a uniform thickness, well sorted, and can be assumed to have been deposited with an approximately horizontal attitude. Banding due to compaction and/or post depositional flow of ignimbrite

TABLE 13: Paleomagnetic properties of Mt Somers Volcanics

Sample No.	Site No.	n	J	D	I	α_{95}	χ	Qn
MS1	1	5	3.76	49	-82	1.6	0.65	122
MS2	2	3	0.249	171	-81	1.1	0.52	10.1
MS3	3	4	2.63	93	-80	1.0	1.3	42.7
MS1A	1	1	3.88	63	-88		0.69	119
MS1B	1	1	3.41	39	-84		0.62	116
MS20	4	3	0.328	176	-83	2.2	2.3	3.01
MS21	5	1	7.66	125	-71		2.3	70.4
MS22	6	3	1.64	122	-76	10.7	8.3	4.17
MS23	7	2	0.000659	212	-60		1.1	0.0126
MS24	8	3	0.123	17	-81	2.8	1.9	1.37
MS25	9	2	0.123	64	-75		1.5	1.73
MS26	10	2	1.28	103	-78		0.77	3.51
MS27	11	3	9.20	156	-79	0.8	1.8	108
MS39	12	2	3.03	19	-71		16	4.00
MS48	13	2	2.13	50	-64		3.7	12.2
MS49A	14	2	4.12	54	-67		8.9	9.78
MS49B	15	2	0.0534	68	-62		0.1	630
MS2A	16	1	0.0561	354	-71		1.4	0.847
MS2C	16	1	0.132	43	-79		3.6	0.775
MS2D	16	1	0.171	356	-84		4.4	0.821
MS3A	17	1	0.145	23	-74		2.6	1.18
MS3B	17	1	0.131	21	-76		2.7	1.03
MS44	18	2	0.0565	198	-81		0.54	2.21
MS46	19	3	5.68	147	-71	3.4	3.5	34.3
MS47	20	3	0.135	39	-80	14.2	2.9	0.983
MS30A	21	3	0.387	232	-66	2.5	3.9	2.10
MS30B	22	3	2.66	219	-35	5.5	4.8	11.7
MS50	23	2	0.0534	91	-70		0.14	0.806
MS40	24	3	7.32	247	-71	1.3	1.3	119
MS41	25	3	0.701	205	-76	3.0	12	1.23
MS42A	26	2	0.00390	205	-72		0.1	0.830
MS43	27	2	3.68	215	-50		1.9	40.9
MS45	28	2	4.56	104	-84		0.0084	11.5
MS5A	29	1	—	—	—		0.35	
MS5B	29	1	0.00256	322	-86		0.36	0.151
MS5C	29	1	—	—	—		0.41	
MS6A	30	1	0.00302	0	-77		0.55	0.116
MS6B	30	1	0.00277	2	-85		0.55	0.107
MS7A	31	1	0.00364	237	-80		0.65	0.119

Sample No.	Site No.	n	J	D	I	α_{95}	χ	Qn
MS7B	31	1	0.00285	244	-78		0.56	0.108
MS29A	32	2	0.142	185	-76		0.77	3.90
MS31	33	2	0.00184	246	-71		0.15	0.259
MS32	34	2	0.00156	257	-69		0.1	0.332
MS35	35	2	0.00104	36	-82		0.23	0.0954
MS42B	36	2	—	—	—			
MS4B	37	1	1.71	306	-76		2.6	13.9
MS8A	38	1	0.0184	283	-66		0.96	0.405
MS8B	38	1	0.0160	15	-49		1.0	0.338
MS36	39	2	8.87	78	-62		8.3	22.6
MS37	40	2	0.00121	121	-56		0.64	0.0400
MS38	41	2	0.213	21	-79		1.6	2.81
MS28	61	3	3.45	152	-72	8.0	4.8	15.2
MS29B	42	3	0.0931	248	-74	3.6	0.19	10.4
MS33	43	3	3.11	190	-73		13	5.05
MS34	44	1	3.09	271	-74		19	3.44
RG3A	45	2	0.388	346	-80		10	0.820
RG3B	45	2	0.478	6	-65		12	0.842
RG4	46	3	0.879	18	-63	7.9	22	0.844
RG5A	47	2	0.339	23	-66		17	0.422
RG5B	47	2	0.501	14	-66		13	0.814
RG1A	48	3	6.68	340	-71	4.7	20	70.06
RG1B	48	2	14.0	25	-80		17	17.4
RG2	49	2	6.27	6	-64		9.5	6.27
RG6	50	3	5.18	354	-77	4.4	28	3.91
MS9A	51	1	0.346	56	-77		6.2	1.18
MS9B	51	1	0.333	58	-75		7.9	0.891
MS9C	51	3	0.112	54	-73	15.5	2.7	0.877
MS10	52	3	6.52	326	-28	0.7	5.3	26.0
MH1A	53	3	1.92	325	-44	1.1	26.3	15.4
MH1B	53	3	1.30	321	-43	0.9	39.3	7.0
MH2A	54	2	0.662	324	-81		10.2	13.8
MH2B	54	3	0.403	18	-81	4.6	1.0	132
MH3	55	2	—	—	—		1.0	
MH5	56	2	3.30	110	+22		15.6	44.6
MH6	57	2	0.703	163	-83		19.8	7.48
MH8	58	2	0.00440	18	-67		1.0	0.880
MH4	59	2	1.46	32	-76		39.9	7.73
MH7	60	3	0.0292	335	-66	9.6	19.2	0.321

n = Number of specimens from each sample. J = Intensity of remanent magnetisation (A/m). D = Declination of remanent magnetisation (degrees). I = Inclination of remanent magnetisation (degrees). α_{95} = Radius (degrees) of 95% confidence cone about mean direction. χ = Volume magnetic susceptibility (SI units x10^{3}). Qn = Koenigsberger Ratio (J/ H), where H is intensity of the geomagnetic field. — = not determined.

was also used to indicate the horizontal direction in thick ignimbrite with uniform flow-band inclinations.

Inferred tectonic corrections were applied where conformable beds or flows of known tectonic correction also occurred. Where there were overlying coal measures of lower to middle Tertiary age, these were also used as an indication of tectonic tilt in the absence of other evidence. Any tilting prior to the deposition of the coal measures was therefore not taken into account in these cases.

Table 14 gives NRM directions before and after tectonic corrections were applied. Grouping was improved by the application of the tectonic tilts.

Barrosa Andesite: Samples were collected from near the Ashburton Gorge Road (sites 1-15), and the area near Morgan Stream and Woolshed Creek (sites 24-28). The intensity of remanent magnetism in sample MS23 is exceptionally low for an andesite (Table 13). The Koenigsberger ratio of 0.0126 indicates that the sample has unstable multiple domain magnetic minerals or that there has been viscous decay of NRM. When tilt corrections were made to sample MS23 the inclination of the NRM decreased to -54°. As this sample was one flow in a sequence of andesite flows, its anomalous behaviour indicates it is unsuitable for paleomagnetic determinations.

Sample MS42A (Table 14) is a baked porcellaneous tuff at the contact with the overlying andesite, and has been included with the andesite for the paleomagnetic determinations. This tuff bed had an inclination of 75° and strike of 265°

TABLE 14: Paleomagnetic NRM directions corrected for tectonic tilt.

Sample No.	Site No.	Uncorrected NRM D	Uncorrected NRM I	Tectonic tilt correction Strike	Dip		Corrected NRM D	Corrected NRM I
MS1	1	49	-82	24°	6°E	(a)	5	-82
MS2	2	171	-81	24°	6°E	(a)	215	-82
MS53	3	93	-80	24°	6°E	(b)	70	-86
MS1A	1	63	-88	24°	6°E	(b)	320	-85
MS1B	1	39	-84	24°	6°E	(b)	438	-82
MS20	4	176	-83	360°	10°E	(a)	233	-78
MS21	5	125	-71	360°	10°E	(a)	150	-78
MS22	6	122	-76	360°	10°E	(b)	177	-82
MS23	7	212	-60	360°	10°E	(b)	223	-54
MS24	8	17	-81	360°	10°E	(b)	320	-79
MS25	9	64	-75	340°	15°E	(a)	340	-89
MS26	10	103	-78	340°	10°E	(b)	155	-83
MS27	11	156	-79	24°	6°E	(b)	195	-83
MS39	12	19	-71	80°	15°E	(a)	71	-81
MS48	13	50	-64	330°	35°E	(b)	264	-80
MS49A	14	54	-67	340°	30°E	(b)	288	-80
MS49B	15	68	-62	340°	30°E	(b)	265	-88
MS2A	16	354	-71		0°	(e)	354	-71
MS2C	16	43	-79		0°	(e)	43	-79
MS2D	16	356	-84		0°	(e)	356	-84
MS3A	17	23	-74	221°	13°SE	(e)	347	-68
MS3B	17	21	-76	221°	13°SE	(e)	344	-69
MS44	18	198	-81	105°	35°S	(b)	14	-64
MS46	19	147	-71	80°	25°S	(f)	37	-80
MS47	20	39	-80	225°	10°SE	(e)	358	-75
MS30A	21	232	-66	310°	25°SW	(e)	341	-85
MS30B	22	219	-35	310°	25°SW	(b)	218	-60
MS50	23	352	-70		0°	(e)	352	-70
MS40	24	247	-71	105°	20°S	(a)	315	-73
MS41	25	205	-76	105°	35°S	(b)	2	-67
MS42A	26	205	-72	105°	35°S	(d)	6	-73
MS43	27	215	-50	105°	35°S	(a)	254	-76
MS45	28	104	-84	100°	35°S	(a)	21	-65
MS5B	29	322	-86	182°	16°E	(d)	280	-71
MS6A	30	0	-77	138°	9°NE	(d)	317	-80
MS6B	30	2	-85	138°	9°NE	(d)	265	-84
MS7A	31	237	-80	269°	11°S	(d)	300	-80
MS7B	31	244	-78	269°	11°S	(d)	295	-78
MS29A	32	185	-76	90°	10°S	(d)	203	-86
MS31	33	246	-71		0°	(d)	246	-71
MS32	34	257	-69	310°	24°SW	(d)	340	-76
MS35	35	36	-82	295°	19°S	(d)	28	-63
MS4B	37	306	-76	182°	16°E	(b)	289	-62
MS8A	38	283	-66	182°	16°E	(b)	280	-50
MS8B	38	15	-49	182°	16°E	(b)	357	-50
MS36	39	78	-62		—		78	-62
MS37	40	121	-56	161	16°E	(e)	146	-63
MS38	41	21	-79		0°	(b)	21	-79
MS28	61	152	-72	90°	10°S	(a)	122	-80
MS29B	42	248	-74	110°	15°S	(b)	302	-78
MS33	43	190	-73	320°	15°SW	(b)	130	-79
MS34	44	271	-74	320°	15°SW	(b)	336	-79
RG3A	45	346	-80		0°	(b)	346	-80
RG3B	45	6	-65		0°	(b)	6	-65
RG4	46	18	-63		0°	(b)	18	-63
RG5A	47	23	-66		0°	(b)	23	-66
RG5B	47	14	-66		0°	(b)	14	-66
RG1A	48	340	-71		0°	(b)	340	-71
RG1B	48	25	-80		0°	(b)	25	-80
RG2	49	6	-64		0°	(b)	6	-64
RG6	50	354	-77		0°	(b)	354	-77
MS9A	51	56	-77	209°	21°E	(a)	344	-72
MS9B	51	58	-75	209°	21°E	(a)	346	-72
MS9C	51	54	-73	209°	21°E	(a)	354	-66
MS10	52	326	-28	17°	38°E	(a)	354	-53
MH1A	53	325	-44	40	45°W	(f)	41	-78
MH1B	53	321	-43	40	48°W	(f)	52	-81
MH2B	54	324	-81		—		324	-81
MH2B	54	18	-81		—		18	-81
MH5	56	110	+22		—		110	+22
MH6	57	163	-83		—		163	-83
MH8	58	18	-67		—		18	-67
MH4	59	32	-76		—		32	-76
MH7	60	335	-66		—		335	-66

NRMS and tilt corrections given in degrees. Tectonic tilt determinations: (a) Inclination of banded agates. (b) Same as adjacent flows or tuff beds. (c) Surface perpendicular to columnar jointing. (d) Bedding in tuffs. (e) Inferred from overlying or adjacent coal measures. (f) Banding in ignimbrites. — no tilt correction applied, see text for explanation. D = Declination of remanent magnetisation (sample mean). I = Inclination of remanent magnetisation (sample mean).

which, if applied as a tectonic correction, gave NRM directions D = 345° and I =-30°. When, however, the tilt correction applied to the overlying andesite was applied to the baked tuff, the NRM was found to be similar to that of the overlying andesite (MS43), as can be seen from Table 14. (A sample of tuff taken away from the contact (MS42B) gave totally inconsistent and weak NRM measurements, with α_{95} = 180°).

Somers Rhyolite: Samples were collected from Blue Duck Stream (sites 16, 23), on the Burma Rd near the Ashburton Gorge Rd (site 17), and near Morgan Stream (site 18). A pitchstone-ignimbrite from Woolshed Creek (site 19), and a rhyolite above the gorge of Woolshed Creek (site 20), were also collected. Of these only the ignimbrite (site 19) has a very high Koenigsberger ratio (Table 13), and this is also the rhyolite sample with the most reliable tectonic tilt (due to its mode of origin). The tilt correction for site 16 and 23 was estimated to be approximately zero, on the basis of adjacent coal measures with locally variable shallow dips. A tilt correction of 10° to the east was also tried for these samples as this was the tilt applied for the andesite of the Clent Hills block, of which the rhyolite of sites 16 and 23 are part. This did not result in any significant improvement in grouping and the change in NRM inclination was less than 4°. The tectonic tilts applied to sites 17 and 20 were based on overlying coal measures. Problems in determining the tilt on site 20 resulted from the absence of suitable strata to obtain correction (a result of recent opencast mining).

Speight (1938) described the attitude of these coal measures in some detail, when they were being mined by underground methods, which showed that the dip was always shallow but extremely variable. Mapping for this thesis established that the attitude of the coal measures in adjacent outcrops was approximately 10° to the SE with a strike of 225°. This is similar to the dip of the coal measures cropping out at site 17 which have a dip of 13° SE and a strike of 221°. The dip on the coal measures is in the opposite direction to that of the general trend of the nearby ignimbrite on the upper surface of Mt Somers and at the northern end of the Burma Rd, which dip to the north-west at angles of 15° to 20°. When this latter dip was used as a tectonic correction for the sites 17 and 20, the NRM inclinations increased by 2° and the declinations changed by about 90°. It is difficult to establish which of these is the correct tectonic tilt correction for sites 17 and 20, as local block faulting has complicated the overall trends. The coal measures have been preserved by local down-faulting and therefore these were chosen as the best indicators of tectonic tilt of the underlying rhyolites at the sites sampled.

The rhyolite at site 18 is a dike cutting andesite flows. The tilt given to the dike was that determined by agate bands in the andesite. It is assumed that the dike was originally vertical and that it intruded the andesite prior to the tectonic movement.

Alford Rhyolite: Two samples of this rhyolite were collected from the gully east of the summit of Mt Alford (sites 21 and 22). The tectonic correction applied was the direction perpendicular to the columnar joints of the rhyolite, based on the assumption that the columnar joints at the base of rhyolite would have been perpendicular to the cooling surface which, in this case, was bedded tuff. The tilt thus obtained was identical to the dip of the underlying tuff at site 34. The rhyolite from site 21 gave a similar NRM direction to that of the underlying tuff bed of site 34. However, the pitchstone at the contact (site 22) gave an anomalously low value for NRM inclination (Table 14). A possible explanation is that the rapidly chilled pitchstone was disturbed by the extrusion of the rhyolite. The fact that the pitchstone at Mt Alford generally formed an agglomerate near the contact indicates that rotated blocks are almost certainly present, and the sample is therefore unreliable for paleomagnetic determinations.

Surrey Hills Tuff: Samples of tuff were collected from the Gawler Downs (sites 29-31), near Morgan Creek (site 36), Waikare Station (site 35), and from Mt Alford (site 32-34). Tectonic tilts were taken from the attitude of the beds.

The intensity of remanent magnetism in the tuff samples is very low and they have very low Koenigsberger ratio. The one exception is the ignimbrite (MS29A) which has a higher intensity and Qn ratio (Table 13).

Hinds River Dacite: Samples of dacite were collected from the Gawler Downs (sites 37,38,40), Waikare Station (site 39)

and the Hinds River (site 41). None of these sites have good tectonic control. The dacite from the Gorge of the Hinds River (site 41) has been given a tectonic tilt inferred from banded agates in nearby flows, which is a reasonable inference for that locality. There is no reliable tilt correction for site 39 as, although there are adjacent rhyolite tuff beds overlain by dacite, the tuff beds are at a higher topographic level indicating local down-faulting. This together with the position of the dacite along a major block fault, make it unwise to infer tectonic tilt corrections from the adjacent tuff beds. Tectonic tilts applied to sites 37, 38 and 40 were inferred from underlying or adjacent tuff beds, but this resulted in anomalously low NRM inclinations, again indicating that these corrections are unreliable.

Graham Dolerite: Samples were collected from sites 61, 43 and 44, east of Mt Alford summit. A sample of ignimbrite (MS29B) from the lower contact of a dolerite sill was given the same tectonic correction as the dolerite (MS28) determined from measurements on banded agates. The other dolerite samples from sites 43 and 44 were given the same tilt corrections as the tuff they intruded.

Rata Peaks Rhyolite: Samples from sites 45-47 in the Rangitata Gorge, were not given a tectonic tilt. The reason for this was:

1. No indicators of tilt were found in the rhyolite.

2. Rhyolite, overlying andesite on the ridge between Hewson River and the Rangitata Gorge, had an approximately horizontal attitude. The underlying andesite flows contained

agates with bands with variable dips of less than 5°. East of Stew Point the andesite also has agates with approximately horizontal bands and is overlain by flat lying rhyolite at the summit of Stew Point.

3. Although the rhyolite along the gorge is apparently downthrown relative to the rhyolite mentioned in 2, this is possibly a result of collapse (?caldera subsidence), soon after the extrusion, and if so, it probably did not involve tilting.

The evidence for tectonic tilt correction of the Rata Peaks Rhyolite is not entirely satisfactory.

Stew Point Andesite: Samples were collected from, and east of, Stew Point (sites 48-50, 52) and from near Rawtor Stream (site 51).

The andesite from sites 48-50 were given no tectonic correction as adjacent andesite flows to the east contained agate amygdules with approximately horizontal bands. The andesite from Stew Point (site 52) contained large agates from which an accurate tilt correction could be measured. However the NRM inclination after tilt correction was still anomalously low (Table 14). The lava flow sampled was a blocky lava with much secondary chlorite alteration.

Samples of andesite from site 51 contained numerous small agates (<1 cm diameter). A tilt correction was obtained by calculating the true dip of the agate bands from 12 apparent dips.

Malvern Hills Rhyolite: Samples of rhyolite were collected from the Rakaia Gorge (site 53), The Point below Round Top (sites 54-57), and Mt Misery (site 58).

The rhyolitic rock at the Rakaia Gorge (site 53) is a banded ignimbrite. The dip of these bands was inferred to have been originally horizontal, and the present dip of 42°SW was therefore used as a tectonic correction.

The rhyolite from sites 53 and 54 was also determined to be ignimbrite (see section 2.2.5.4) but the dip of the bands in these sites was locally very variable. The dip of the bands at site 53 was 42°SW with a strike of 133° for sample MH2A, while for sample MH2B, less than 10 m distance, the dip was 8°SW with a strike of 145°. Sample MH3 had bands dipping at 35°SW with a strike of 155°. Sample MH5 (site 56) is a pitchstone. The banding in this was very variable, but about 26°N with a strike of 080°. The implication from the variation in the banding directions is that the ignimbrite was tectonically disturbed after deposition. When these measurements were applied as tectonic corrections to the NRMs, the inclinations were found to decrease, resulting in anomalous NRM directions.

The pitchstone could indicate that the ignimbrite below Round Top is made up of at least two volcanic events; the latter ignimbrite sheet being deposited on a cool, or cold, earlier ignimbrite and forming a pitchstone along the contact similar to those at Mt Somers. The upper ignimbrite was in turn overlain by andesite. It could therefore be argued that the deformation in the ignimbrite was either a

pre-cooling, or a post-depositional phenomenon, that took place during, or before, the eruption of the overlying volcanics. Either way it is possible that the ignimbrite was above its curie temperature, or was re-heated, after the deformation, in which case no tectonic correction based on the banding can be applied to the NRM. Zero tectonic corrections to the ignimbrite would give NRMs consistent with those of the other samples of the Mt Somers Volcanics, but because of the uncertainties involved these have not been included in the determinations of pole positions.

The pitchstone (site 56) was the only sample to give a positive NRM direction, indicating a reversed magnetic field (Figure 89). As this is not a dyke, at this locality, it should have the same direction as the ignimbrite. It has been assumed that the pitchstone contains rotated chilled zones (as was also the case at Mt Alford), and it has been rejected from the paleomagnetic pole determinations.

Round Top Andesite: One andesite sample (site 59) was collected from a position above sites 54-58. No indicators of tectonic tilt were found other than an indistinct flow banding with a dip of 25°SE and a strike of 050°. As no correction was applied to the underlying rhyolite, none was applied to this sample. Although the uncorrected NRM gave a direction similar to the other Mt Somers Volcanics samples (Table 14), it was not used for paleomagnetic determinations because of the uncertainty of the tectonic control.

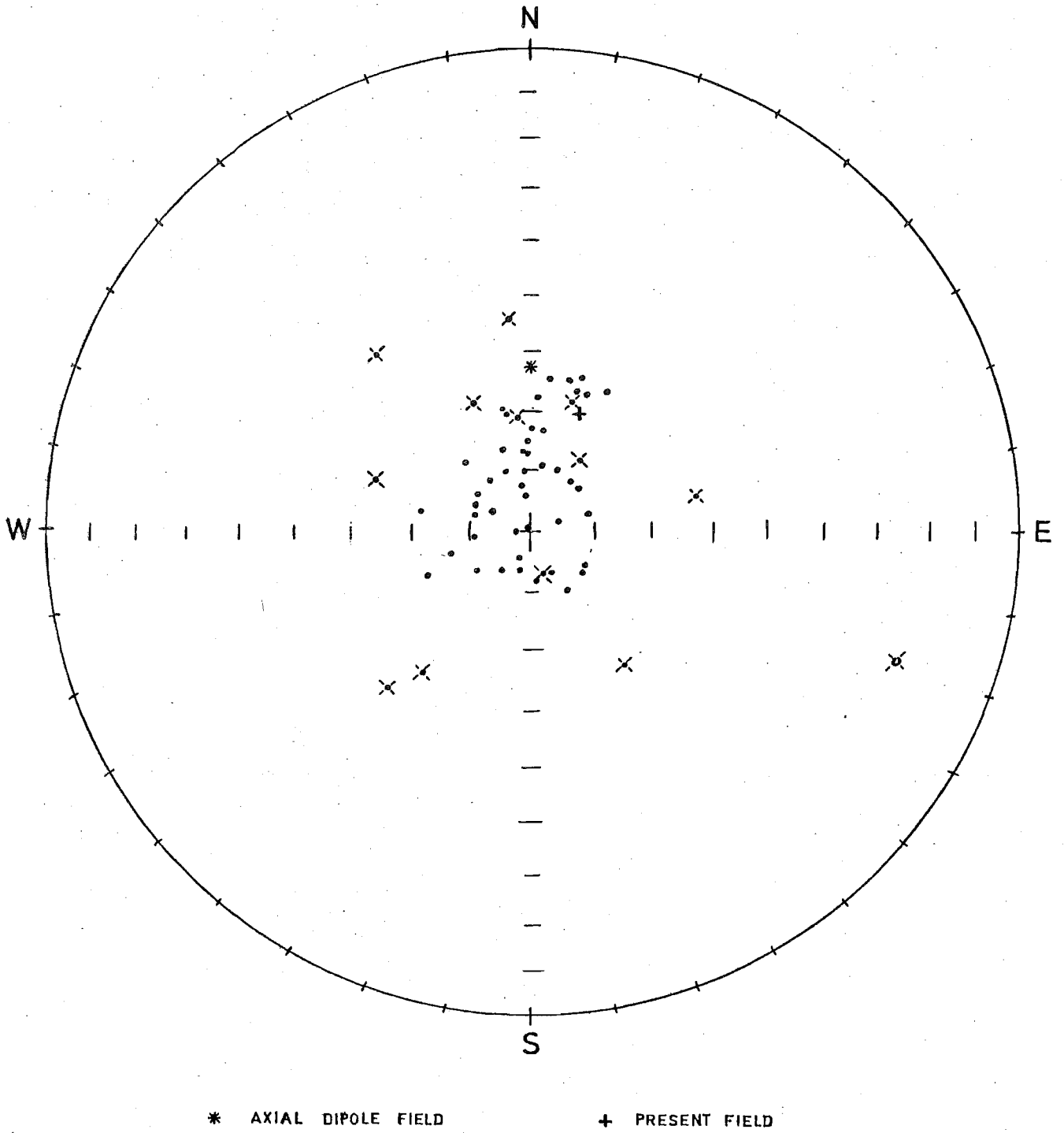

Figure 89. Magnetic directions for Mt.Somers Volcanics (corrected for tectonic tilt). Dots represent normal, and open circles reversed, directions. Sample directions marked with a cross have been rejected in paleomagnetic pole calculations (see text for explanations).

Basalts: A sample of a basalt dike at the contact of the Malvern Hills Rhyolite and the Torlesse Supergroup cropping out on the road to Pullwool Peak (site 60), gave a low NRM inclination. No tectonic correction could be determined from the position of the dike. Subsequent K/Ar dating gave an age of 38 Ma, and so this sample was excluded from the paleomagnetic pole determinations. All the NRMs, corrected for tectonic tilt, are shown in Figure 89.

2.8.5.3 Alternating Field Demagnetisation

Samples were selected, from each rock type, for stepwise alternating field demagnetisation. The variations of intensity with the applied field strength are shown in Figure 90, and the variations in magnetic directions on AF demagnetisation are shown in Figures 91 and 92.

(a) MS10, site 52: This sample of Stew Point Andesite contained secondary chlorite alteration. On demagnetisation the magnetic vector inclination decreased regularly. When the tectonic tilt correction was applied to this sample, the decrease in declination remained anomalous. This sample is not suitable for paleomagnetic pole determinations.

(b) MH1A, site 53: This is an ignimbrite sample of Malvern Hills Rhyolite. The extreme stability of this sample can be seen from the absence of variation in the direction of remanent magnetisation at all stages of demagnetisation (Figure 91). This ignimbrite contains a notable amount of hematite which possibly accounts for its high stability, high

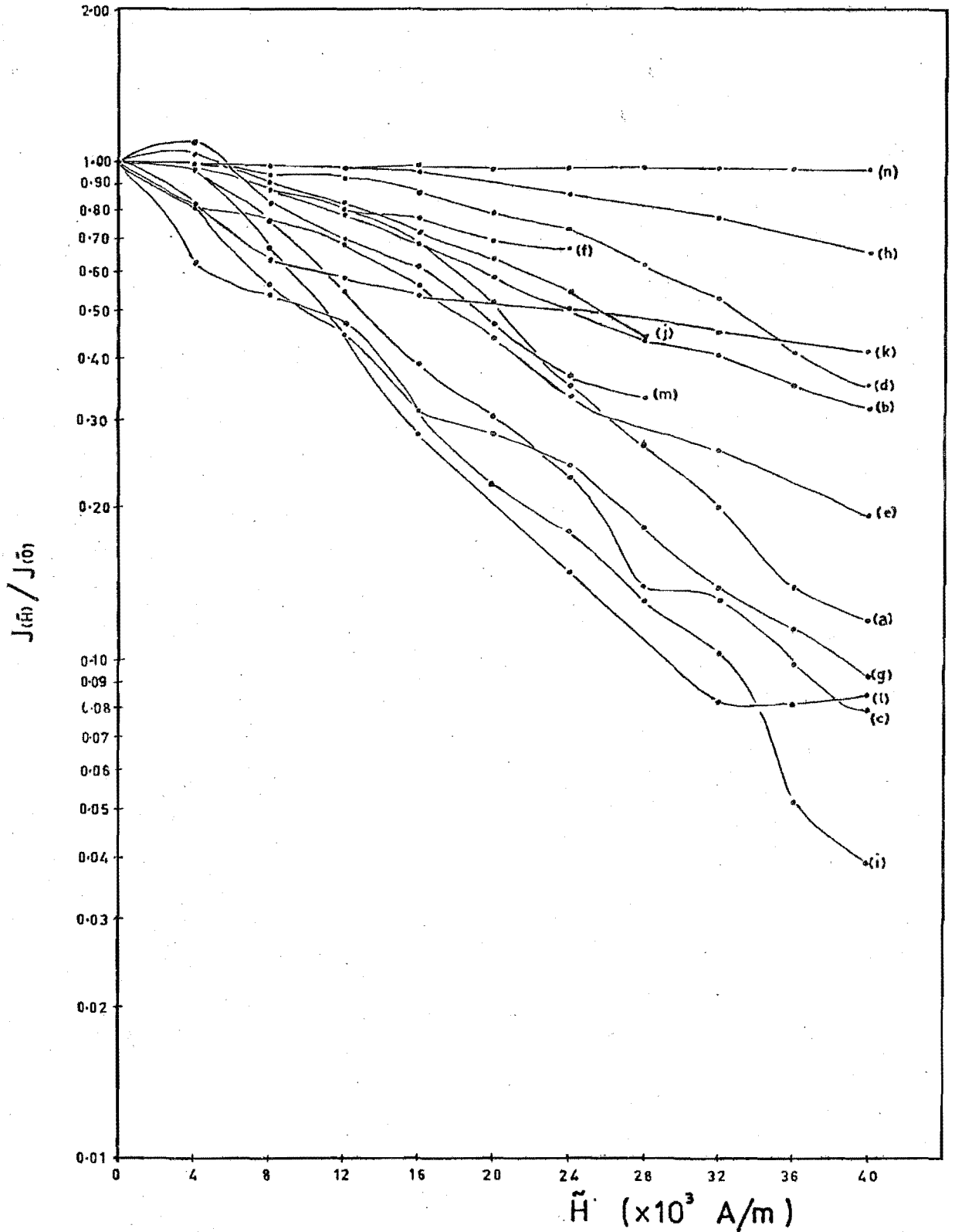

Figure 90. Plot of the ratio $J(\tilde{H})/J(\tilde{O})$ (sample intensity of remanent magnetisation after demagnetisation/initial intensity), against the applied peak demagnetisation field strength (H). (a) MS 10, site 52; (b) MH 1A, site 53; (c) RG 1A, site 48; (d) MS 4B, site 37; (e) MS 30A, site 21; (f) MS 9C, site 51; (g) MS 2C, site 16; (h) MS 30B, site 22; (i) RG 4 site 46; (j) MS 6A, site 30; (k) MS 48, site 13; (l) MS 34 site 44; (m) MS 58, site 29; (n) MS 1, site 1.

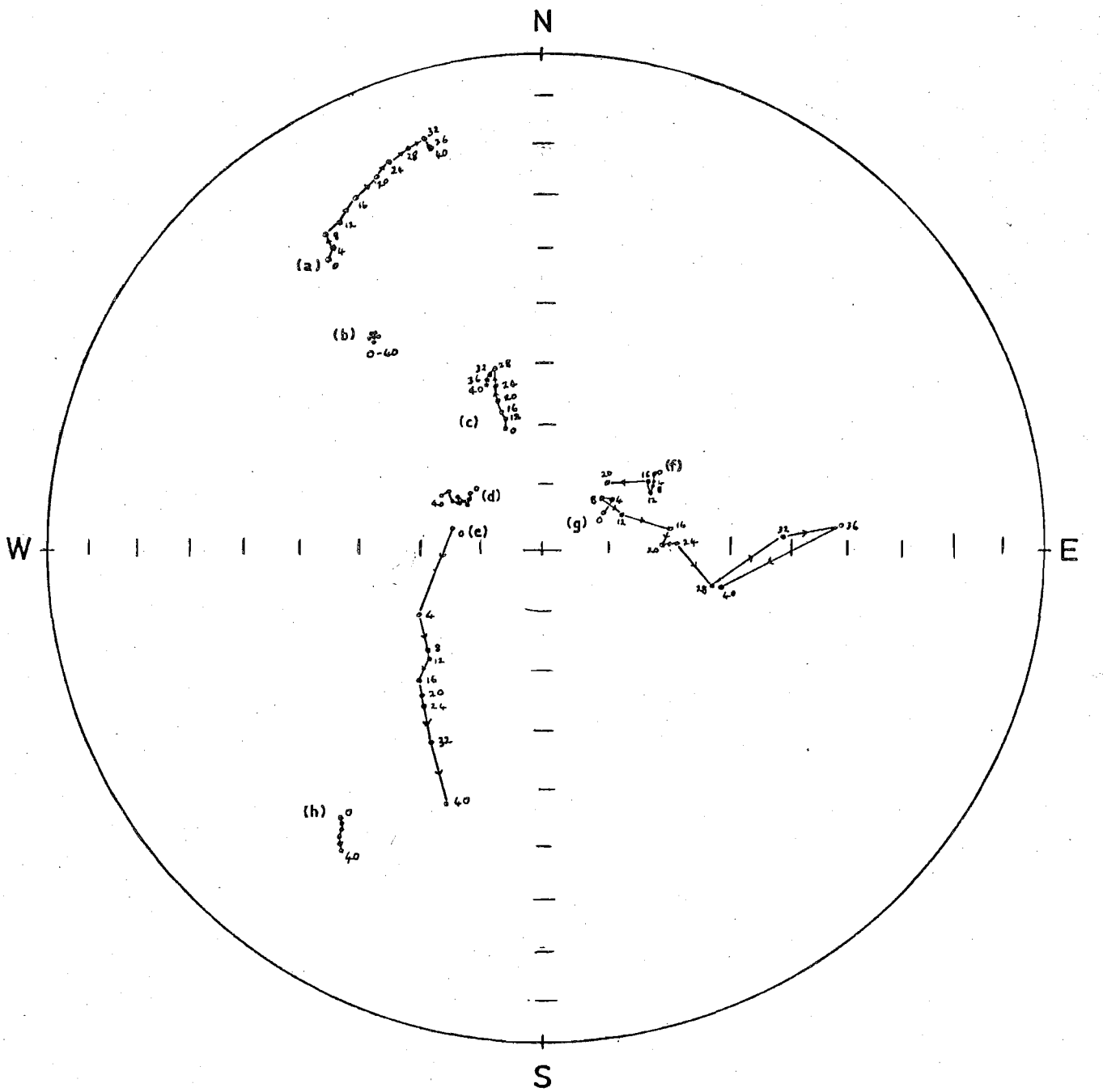

Figure 91. Changes in NRM directions on AF demagnetisation of Mt. Somers Volcanics. All directions normal (represented by dots). No tectonic tilt corrections applied. Numbers , $x10^3$, represent peak demagnetising field (A/m). (a) MS 10, site 52; (b) MH 1A, site 53; (c) RG 1A, site 48; (d) MS 4B, site 37; (e) MS 30A, site 21; (f) MS 9C, site 51; (g) MS 2C, site 16; (h) MS 30B, site 22.

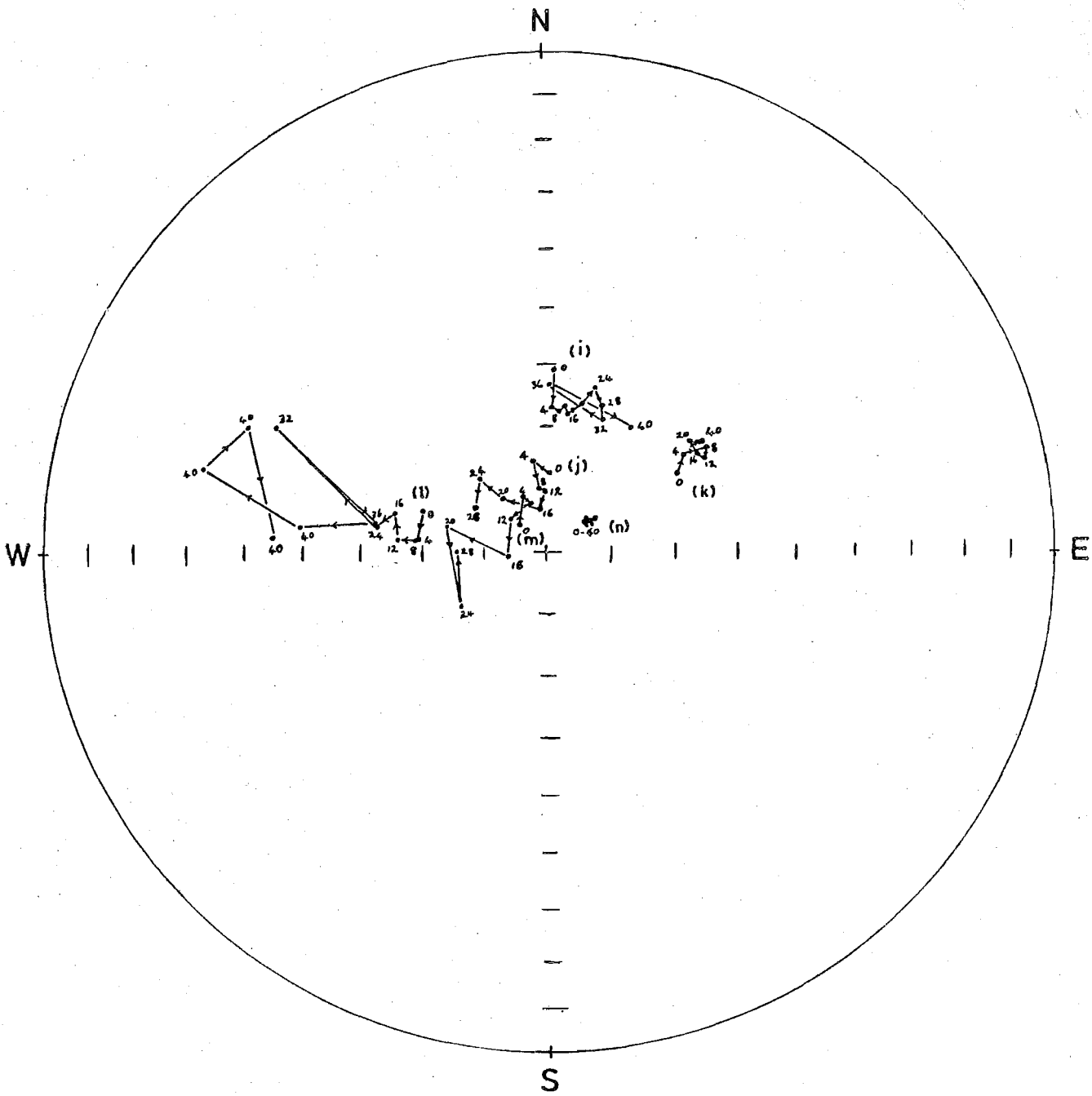

Figure 92. Changes in NRM directions on AF demagnetisation of Mt. Somers Volcanics. All directions normal (represented by dots). No tectonic tilt corrections applied. Numbers, x 10^3, represent peak demagnetising field (A/m). (i) RG 4, site 46; (j) MS 6A, site 30; (k) MS 48, site 13; (l) MS 34, site 44; (m) MS 5B, site 29; (n) MS 1, site 1.

Koenisberger ratio, and relatively strong magnetism (compared to other rhyolites).

(c) RG1A, site 48: This sample of Stew Point Andesite shows a slight decrease in magnetic inclination with increasing A.F. demagnetisation (Figure 91). The affect is not as pronounced as that in MS10 (site 52), and the sample can be regarded as stable. The rate of decrease in relative intensity (Figure 90) levelled off at 28×10^3 A/m followed by a further decrease at higher demagnetising levels. This break in the trend also corresponds to a change in direction of the remanent magnetisation (Figure 91).

(d) MS4B, site 37: A sample of Hinds River Dacite which showed very little movement on demagnetisation (Figure 91) indicating that the sample is very stable.

(e) MS30A, site 21: A sample of Alford Rhyolite which showed a continuous trend of decreasing inclination with increasing AF demagnetisation. The sample contains a significant amount of hematite which is secondary in origin. It would appear from the demagnetisation trends that the primary magnetisation was preferentially removed to the secondary haematite magnetisation.

(f) MS9C, site 51: A sample of Stew Point Andesite which showed a very stable trend on demagnetisation.

(g) MS2C, site 16: A sample of Somers Rhyolite which showed stability up to 12×10^3 A/m, followed by a shift in direction of the remanent magnetisation, then stability again between $16\text{-}24 \times 10^3$ A/m. At even higher fields the sample

became unstable. This relatively weak sample (J = 0.132 A/m) contained iron oxides in fine joints and it is therefore possible the weaker secondary magnetism is more stable than the primary magnetism.

(h) MS30B, site 22: A sample (pitchstone) of Alford Rhyolite which showed a very stable trend on AF demagnetisation. (Figures 90 and 91). The pitchstone has the same mineralogy as the overlying rhyolite (MS30A), the only difference being that the rhyolite is devitrified and contains secondary haematite formed along cooling fractures, whereas the pitchstone does not. A comparison of the two demagnetisation curves shows that the pitchstone has only a minor decreasing inclination trend which is both regular and in the same sense as that of MS30A (see (h) and (e), Figure 91). This is entirely consistent with the trend for MS30A being a result of magnetically stable secondary haematite, and confirms that the NRM measurements are better indicators of the primary magnetism than are the demagnetised measurements for these rhyolites, as if the decreasing inclination trend was of primary origin, it would be expected that the trend for the pitchstone would be in a different direction to that of the rhyolite, because the pitchstone sample was rotated after cooling (see section 2.8.5.2).

(i) RG4, site 46: A sample of Rata Peaks Rhyolite which was stable at low demagnetising fields but tended to be variable at higher fields (Figure 92). This rhyolite contains secondary haematite alteration.

(j) MS6A, site 30: A sample of Surrey Hills Tuff which showed only moderate stability when demagnetised. Some of the apparent instability could be due to errors of measurements caused by the low intensity of the demagnetised samples.

(k) MS48, site 13: A sample of Barrosa Andesite showing slight initial movement of the magnetic vector on demagnetisation but high stability after 8×10^3 A/m (Figure 92). This stability can also be seen in Figure 90 where after an initial decrease in intensity, the curve flattens out.

(l) MS34, site 44: A sample of Graham Dolerite which was moderately stable in low demagnetising field but became unstable at fields higher than 24×10^3 A/m (Figure 92). This instability in direction was not accompanied by a decrease in the intensity of the remanent magnetism (Figure 90). The large size of the ferromagnetic grains in this dolerite has probably resulted in extensive domain structure within the crystals, giving rise to the variation in magnetic directions observed after A.F.-demagnetisation above 24×10^3 A/m had removed the viscous and isothermal remanent magnetisation.

(m) MS5C, site 29: A sample of Surrey Hills Tuff which like MS6A showed relative stability in demagnetising fields of up to 12×10^3 A/m but apparent instability at higher fields. Once again measurement errors caused by the weak magnetic intensity of the sample after demagnetisation could be responsible for the trend seen in Figure 92.

(n) MS1, site 1: A sample of Barrosa Andesite that showed even greater stability than MS48. No change from the

initial NRM or J values were observed, even in the highest demagnetising field, indicating the extreme stability of this sample.

Most of the samples demagnetised were stable up to $12x10^3$ A/m although a small viscous remanent magnetisation component was often removed in the first step of the demagnetising process. The best level to demagnetise the samples at, to obtain a thermoremanent magnetisation (TRM), would be $12x10^3$ A/m. In general the samples demagnetised at this level did not have directions significantly different to their NRMs. Further study of these samples using thermal demagnetisation is necessary to establish the role of the secondary hematite, particularly in the rhyolite.

2.8.5.4 Paleomagnetic Pole Determinations

Virtual geomagnetic pole (VGP) positions for all sites are given in Table 15. These were determined on the NRM results as these gave a better grouping than the demagnetised samples. The sites 7, 22, 36-40, 52, 54-60 were eliminated on the grounds that they have anomalous NRM values, or had a lack of reliable tectonic tilt control. The mean NRM direction after removal of these sites, together with the mean VGP position (i.e. the paleomagnetic pole position), are given in Table 16. From Table 16 it can be seen that the grouping and statistics of the average NRM direction are good, and much better than for the pole position. This is a result

Table 15. Virtual Geomagnetic Pole positions for paleomagnetic sites.

Site No.	J	Dm	Im	V.G.P. Lat (°S)	V.G.P. Long (°E)
1	3.683	348	-83	56	175
2	0.249	215	-82	30	182
3	2.63	70	-86	46	160
4	0.328	233	-78	28	192
5	7.66	150	-78	23	159
6	0.164	177	-82	28	170
7	0.000659	223	-54	2(N)	205
8	0.123	320	-79	58	197
9	0.123	340	-89	56	172
10	1.28	155	-83	31	164
11	9.20	195	-83	30	175
12	3.03	71	-81	47	147
13	2.13	264	-80	62	229
14	4.17	288	-80	47	199
15	2.98	265	-88	43	177
16	0.1197	9	-79	64	165
17	0.138	346	-69	77	216
18	0.0565	14	-64	79	98
19	5.68	37	-80	57	149
20	0.135	358	-75	33	129
21	0.387	341	-85	53	177
22	2.657	218	-60	18(N)	210
23	0.0534	352	-70	24	187
24	7.32	315	-73	59	217
25	0.701	2	-67	84	159
26	0.00390	6	-73	75	159
27	3.68	254	-76	32	202
28	4.56	21	-65	75	102
29	0.00256	280	-71	40	218
30	0.002895	298	-83	49	191
31	0.003245	297	-79	50	201

Table 15 (continued).

Site No.	J	Dm	Im	V.G.P. Lat (^{o}S)	V.G.P. Long (^{o}E)
32	0.142	203	-86	36	175
33	0.00184	246	-71	24	206
34	0.00156	340	-76	67	165
35	0.001040	28	-63	70	93
36	0.004862	*	*	—	—
37	1.71	289	-62	40	235
38	0.0160	319	50	58	259
39	8.87	78	-62	35	100
40	0.00121	146	-63	4	148
41	2.13	21	-79	63	155
61	3.45	122	-80	32	152
42	0.0931	303	-78	52	204
43	3.11	130	-79	28	153
44	3.09	336	-79	62	190
45	0.0433	0	-73	75	172
46	0.879	18	-63	77	91
47	0.420	19	-66	76	108
48	10.034	355	-77	69	175
49	2.82	6	-64	85	108
50	5.18	354	-77	68	178
51	0.2634	349	-70	77	203
52	6.52	354	-53	78	324
53	1.61	46	-80	55	146
54	0.5325	351	-81	59	176
55	—	—	—	—	—
56	3.295	110	+22	22(N)	87
57	0.7031	163	-83	30	167
58	0.00440	18	-67	76	115
59	1.462	32	-76	63	141
60	0.02923	335	-66	72	121

J = Intensity of remanent magnetism (A/m). Dm = Declination of remanent magnetisation for site means (degrees). Im = Inclination of remanent magnetism for site means (degrees). V.G.P. = Virtual Geomagnetic Pole. Lat = Latitude. Long = Longitude. * = inconsistant results. — = not determined.

of the high paleolatitude which results in the VGPs having higher dispersions than do their corresponding directions. Because of the high inclinations of these paleomagnetic directions, small errors in sample orientation made during collection and measurement, or errors in tilt correction applied, can result in very large errors in declination and thus even wider scatter of the VGPs. In spite of these problems all but one of the "valid" NRMs fall within 20° of the mean direction (the circular standard deviation = 13.1), and the "valid" VGPs fall within 40° of the mean value. McElhinny *et al.* (1974) used this for a reliability criteria and rejected all poles that lay greater than 40° from their mean position.

Table 16 Mean NRM direction and Paleo Pole position determined from the Mt Somers Volcanics

Mean NRM direction:					
D	I	N	K	α_{95}	R
350.9°	-82.3°	46	38.4	3.4°	44.83
Pole Position:					
Lat. (°S)	Long (°E)	N	K	α_{95}	R
57°	174°	46	11.9	6.4°	42.23

D = Mean NRM declination
I = Mean NRM inclination.
N = Number of sites.
K = Fisher's precision parameter.
α_{95} = Radius of 95% cone of confidence of mean value.
R = Resultant magnitude of sum of unit vectors.

2.8.6 Significance of Paleomagnetic Results

The location of the Late Cretaceous pole determined from Mt Somers Volcanics indicates that New Zealand's latitude is 33° north of that in late Cretaceous times.

Hayes and Ringis (1973) have shown that ocean-floor magnetic anomalies in the Tasman Sea indicate that New Zealand was separated from Australia between 60 and 80 Ma ago. This coincides with the initial separation of New Zealand from Antarctica which Christoffel and Falconer (1973) considered to have occurred between 63 and 84 Ma ago. Accordingly the late Cretaceous pole position for New Zealand should be at a similar latitude to that obtained from Australia, and at a longitude approximately 20° east of that for the late Cretaceous pole for Australia. Figure 93 shows the pole position obtained from the Mt Somers Volcanics and those of the Cenozoic-Cretaceous polar wander path for Australia (McElhinny *et al.*, 1974). The pole from the Mt Somers Volcanics is in good agreement with the 95 Ma pole for Australia when the opening of the Tasman Sea is allowed for.

The results are consistent with the 450 km dextral movement associated with the Alpine Fault, but not the dextral rotation suggested by Wellman (1973, 1975).

The only other Cretaceous paleomagnetic determination of New Zealand rocks is that of Grindley *et al.* (in press) of the Chatham Islands volcanics. These volcanics are younger and have a lower paleolatitude. The declination of their magnetic directions is however within 13° of the declination of the Mt Somers Volcanics and there is therefore no evidence to support a large rotational shift of the

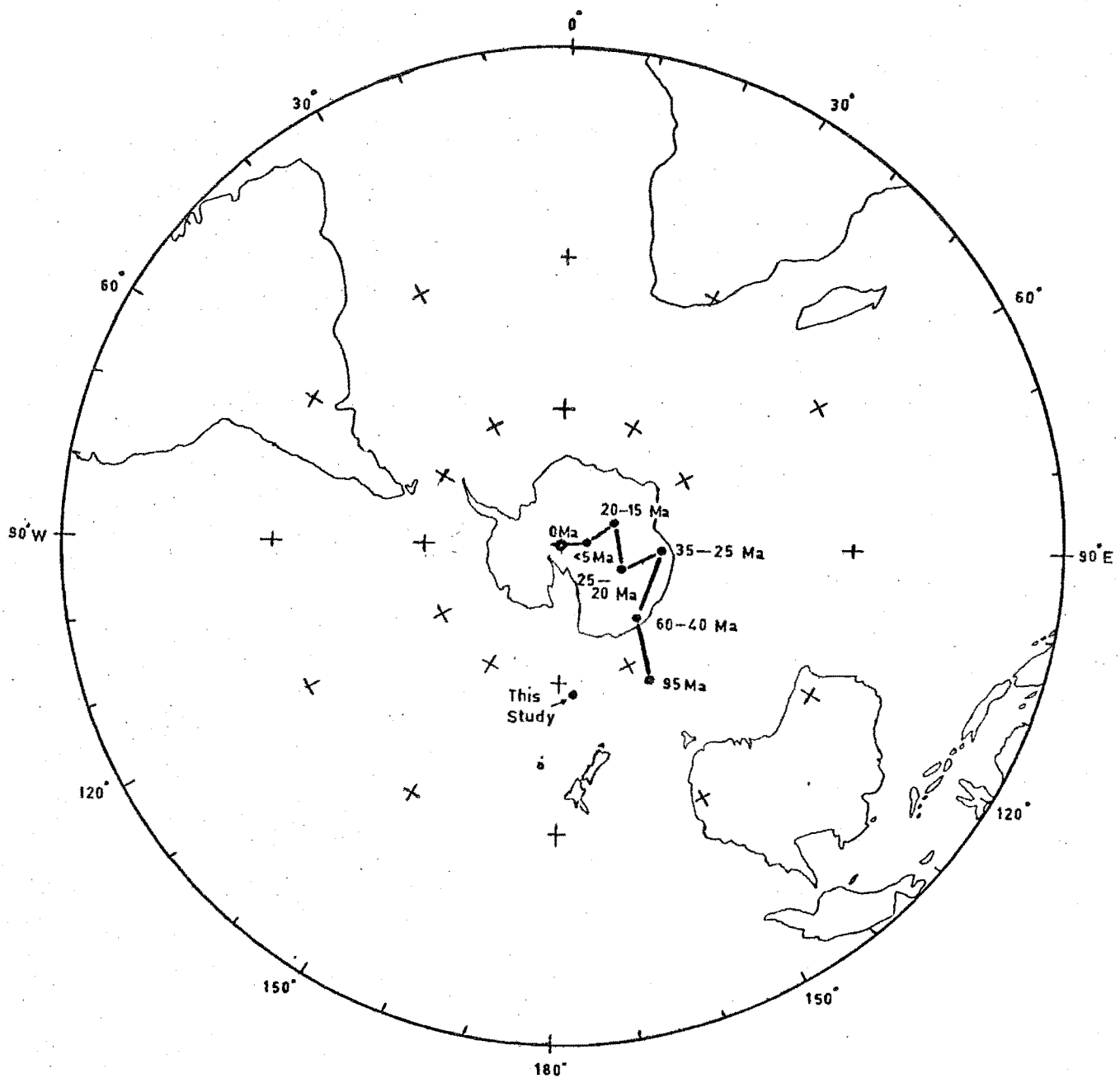

Figure 93. Polar wander path for Australia from mid-Cretaceous to present (after Schmidt and Embleton, 1976), with Cretaceous pole position from the Mt Somers Volcanics. Polar Steriographic projection.

Chatham Islands, relative to the East Coast of the South Island of New Zealand, since late Cretaceous times as used for the plate tectonic reconstructions of Molnar *et al.* (1975).

The Cretaceous paleo pole position determined from the Mt Somers Volcanics is consistent with the Mesozoic pole position of Australia (McElhinny, 1973) when the opening of the Tasman Sea is allowed for, but this Australian Mesozoic pole position has long been inconsistent with the Mesozoic pole positions determined for other Gondwana countries. However, Schmidt (1976) has shown that some Australian Jurassic volcanics give paleomagnetic results similar to the other Gondwana countries, while the Cretaceous results give the "anomalous" position, thus indicating that the Cretaceous results cannot be combined with the Jurassic and Triassic results. This situation is also likely to apply for pre-Cretaceous Mesozoic rocks in New Zealand. The splitup of Gondwanaland in the Cretaceous accounts for this difference in position.

Further paleomagnetic studies on late Cretaceous rocks of New Zealand would enable the result of this present study to be interpreted on a wider level and in more detail.

3. SUMMARY

3.1 Torlesse Supergroup

The Torlesse rocks of the Mt Somers area have been subdivided into the Mt Taylor Group (Middle-Upper Triassic), and the Clent Hills Group (Middle-Upper Jurassic). The Mt Taylor Group consists of two formations; the Fingers Formation (Kaihikuan-Oretian), and the Pudding Hill Formation (?Oretian-Otamitian).

The Fingers Formation consist of thick, coarse-grained, white, micaceous sandstone beds containing black "cannon ball" (calcareous) concretions. These beds are ungraded and contain no visible internal structures. Sole markings are rare. Interbedded siltstone has graded bedding, cross lamination and calcareous concretionary bands. The siltstone is typically sheared and its beds are contorted. Boudin structures, and rare intraformational conglomerate, indicate that some soft-rock deformation occurred. The sandstone beds are probably the proximal deposits of submarine fans with the interbedded, and sometimes interdigitating, siltstone beds representing the distal deposits of adjacent fans. Metamorphism of this Formation is low-grade with only occasional quartz veins present. These veins are the result of diagenesis rather than regional metamorphism. A diverse fossil assemblage was found at two localities. The fossils *Daonella* sp. and *Spiriferina* sp. *abichi* indicate a Kaihikuan-Oretian age range. The depositional environment was most probably shallow

to medium depth continental shelf.

The Pudding Hill Formation consists of thin bedded siltstone and sandstone of turbidite-type origin. The tube fossil *Torlessia mackayi* was the only fossil found in this Formation, but it is moderately abundant both *in situ* and redeposited on bedding planes. Quartz/prehnite veins occur in some areas, but are not ubiquitous. No contact between this Formation and the Fingers Formation was found and the relation between the two formations is not known.

The Clent Hills Group contains marine and probably non-marine formations that are not readily distinguishable in the absence of fossils. The interbedded carbonaceous sandstone and siltstone beds of this formation are generally unsorted and contain no internal structures. Channel conglomerates with boulders up to 1 m diameter and containing lenses of carbonaceous sandstone are common. Red siltstone and zeolite-veined sandstone beds form characteristic marker beds that can be traced through the area. Plant fossils are particularly abundant in the non-marine beds and are concentrated along bedding planes. Fern fronds up to 30 cm in width are well preserved. Plant fragments and tree trunks are also common in the conglomerate of the marine beds. The macro- and microflora fossil assemblages give no better indication of age than that the beds are Jurassic. The marine beds also contain a diverse macrofaunal fossil assemblage, the most significant of which are the *Inoceramus* sp.cf. *gracilis*, and the *Buchia* sp., which together suggest a Puaroan age for these beds. The most common fossil in the

Clent Hills beds is an undescribed bivalve *Tancredia* sp. The depositional environment of the Group ranges from probable non-marine to shallow or marginal-marine conditions. Although paleomagnetic evidence indicates that this area was within 20° of latitude of the South Pole, the fossil evidence from the Mt Somers area supports a temperate climate with distinct seasonality.

Many of the Torlesse rocks of the Mt Somers area are unfossiliferous and in the absence of other positive indicators of age, no subdivision of these has been made. However, lithologic similarities indicate that the rocks of the Peter Range, Moorehouse Range, Trinity Hill, and southern flank of the Clent Hills, are of similar type to the Clent Hills Group, and may also be of Jurassic age. The Torlesse rocks that cap the Winterslow Range, and those of the Dogs Range and Ben McLeod-Coal Hill area have a subschistose appearance, and are of distinctly greater induration than other Torlesse rocks of the Mt Somers area, and may be of Permian age like those found at Mt Peel.

The structure of the Torlesse Rocks in the Mt Somers area is complex and interpretation is complicated by the thick deposits of glacial outwash gravels and moraines. The Jurassic rocks and those of unknown age in the centre of the area, form an arcuate structure, concave to the east. In the region of the Old Man Range and the Mt Somers Range the Jurassic rocks appear to be overthrust, at a low angle, by the mid-Triassic rocks. The Triassic rocks are young and dip to the north at moderate to steep angles. Large scale

folds are not common and in general the beds form a regular bedded sequence. The sub-schistose rocks that cap the Winterslow Range also appear to have been thrust over the Jurassic rocks, at a low angle, from the east. It is probable that the mountain ranges of the area are bounded by block faults, but this is difficult to prove because of the overlying glacial deposits. The thrust faulting occurred in the early Cretaceous during the Rangitata Orogeny, much of the uplift, that has accompanied the block faulting, occurred since the late Tertiary during the Kaikoura Orogeny and is currently active as is shown by recent fault traces.

3.2 Mt Somers Volcanics

The Upper Cretaceous calc-alkaline Mt Somers Volcanics of Canterbury form a single volcanic complex with three main eruptive centres: the Rangitata gorge area, the Clent Hills/ Mt Somers/Mt Alford area, and the Rakaia Gorge/Malvern Hills area. The following volcanic units can be recognised: Somers Rhyolite, Barrosa Andesite, Surrey Hills Tuff, Graham Dolerite, Alford Rhyolite, Hinds River Dacite, Stew Point Andesite, Rata Peaks Rhyolite, and the rhyolite and andesite of the Malvern Hills area.

The Somers Rhyolite is a biotite garnet rhyolite with quartz and sanidine phenocrysts. It predominantly occurs as columnar jointed rhyolite cumulodomes overlain by shallow dipping rhyolitic flows which have been shown to be ignimbrite.

The Barrosa Andesite consists of high-K andesite, andesite, low-Si andesite, and a basic dacite, all with normative quartz and hypersthene. The phenocryst minerals are plagioclase and ortho-pyroxene, with rare clinopyroxene.

The Surrey Hills Tuff consists of poorly welded garnetiferous ignimbrites and water-laid tuffaceous sediments of rhyolitic composition.

The Graham Dolerite is compositionally similar to the low-Si Barrosa Andesite, and intrudes the Surrey Hills Tuff only on the Alford Range.

The Alford Rhyolite contains quartz and sanidine phenocrysts and has a characteristic red colour caused by hematite alteration. Biotite and garnet are absent. The Alford rhyolite occurs as cumulodomes along a fissure and overlies Surrey Hills Tuff, frequently with a pitchstone zone at the contact.

The Hinds River Dacite consists of dacite and rhyodacite and is hypersthene normative. It also typically contains a small corundum component in its normative composition. It is petrographically distinguishable from the andesite by the presence of xenocrystic almandine garnet, together with abundant garnetiferous xenoliths of sedimentary origin.

The Rata Peaks Rhyolite is compositionally similar to the Alford Rhyolite but is readily distinguished by the notable absence of quartz phenocrysts. Like the Alford Rhyolite, garnet and biotite are very rare.

The Stew Point Andesite has a quartz hypersthene normative composition and includes both andesite and andesitic-

dacite compositions. Hypersthene is not always present as a phenocryst phase, but otherwise this andesite is petrographically similar to the Barrosa Andesite.

The rhyolitic rocks of the Malvern Hills area occur as rhyolite domes and ignimbrite and can only be distinguished from the Somers Rhyolite by the greater abundance of garnet and biotite and by its trace element chemistry.

The andesite flows of the Malvern Hills area consist of high-K andesite, andesite, low-Si andesite, and high-Al basalt. They are chemically and mineralogically similar to the Barrosa Andesite.

On the basis of petrology and chemistry, andesite from the J. D. George No.1 well is genetically related to the Mt Somers Volcanics.

There were at least three phases of rhyolitic eruption in the vicinity of Mt Somers, one of which may have been associated with the earliest tuff eruptions (Surrey Hills Tuff). These rhyolitic events alternated with not less than five distinct eruptive phases of more basic lavas. In the Rangitata Gorge area there is evidence for only one phase of andesite eruption followed by rhyolite extrusion. The andesite of the Malvern Hills area definitely overlies younger ignimbrite flows, but there is also the possibility that some rhyolite extrusion post-dates the andesite in this area. All the Mt Somers Volcanics appear to have been erupted from fissures.

Major and trace element geochemistry of the Mt Somers Volcanics has shown that the Volcanics form a continuous

fractionation sequence and that all the volcanics are genetically related. Although the volcanics were derived from a common parent magma, differentiation of separate pulses of magma would account for minor deviations from the main variation trends. The sequence of the eruptions at Mt Somers involved an initial explosive phase depositing tuffs and ignimbrites followed by extrusion of domes, and then major ignimbrite eruptions. The first eruptions were of the most highly fractionated rhyolite with a distinct compositional break occurring at 75% SiO_2; below this composition ignimbrite was erupted. In the Somers Rhyolite the distinction in the field between the youngest ignimbrite and rheo-ignimbrite, and the older rhyolite flows and domes was not always apparent. These ignimbrites could not always be distinguished in thin sections due to the intense welding and devitrification. Chemical analyses showed that the ignimbrites always had a distinctly higher Ba content than the previously erupted rhyolite domes. The ignimbrites have Ba contents greater than 600 ppm (mean Ba content 1089 ppm) and the rhyolite domes less than 600 ppm (mean Ba content 431 ppm).

A small but distinct compositional gap occurred between the rhyolite and the dacite but there is no other evidence to support a separate origin for the rhyolite and the dacite.

The variation trends in the volcanics are consistent with crystal fractionation, of the minerals observed in the volcanics, to produce a normal differentiated sequence of volcanics ranging in composition from high-Al basalt to high-Si

rhyolite. No other alternative petrogenetic mechanism for the derivation of these volcanics was found to be consistent with the data. In particular a fractional crystallisation model is supported by low and constant K/Rb and Ba/Rb ratios; a high Rb/Sr ratio; high abundances of Th, Zr, Ba, Pb, Rb, and K; and low abundances of V and Sr; throughout the compositional range. Fractional crystallisation of plagioclase, orthopyroxene, and minor spinel phases produced the andesite to dacite magmas from high-Al basalt, while the rhyodacite to rhyolite magma fractionation predominantly involved sanidine, plagioclase quartz and almandine garnet, with minor biotite, zircon, apatite and ilmenite. A break in the variation trends of TiO_2 and P_2O_5, at the dacite/rhyolite boundary, is explained by the rhyolitic residual magma being emplaced in a magma chamber at a higher level than that of the dacite, where separate crystal fractionation took place. A rapid rise to a higher magma chamber, with the accompanied change in pressure also explains the dissimilarities in phenocryst and groundmass components of the otherwise compositionally similar rhyolite and dacite members.

The most primitive magma erupted (the high-Al basalt) may have been derived directly from the mantle or may itself be a differentiate of a tholeiitic basalt formed by multistage partial melting processes above a Benioff zone. Only indirect evidence can be gained for a Cretaceous subduction zone under Canterbury. Such a subduction zone would, however, explain the presence of the calc-alkaline Mt Somers Volcanics which are chemically similar to those of other circum-Pacific areas, such

as the Andes, which are known to overlie subduction zones. A calculated depth for magma generation above such a Benioff Zone using Dickinson's (1975) model for "continental" margin arc volcanism gave approximately 190 km for the Mt Somers Volcanics.

The K/Ar dates for the Mt Somers Volcanics give an upper limit to the age of volcanism of 98.1±0.7 Ma. The duration of volcanism cannot be determined with certainty, but it was probably less than 10 Ma. The volcanism coincides with the final stages of the Rangitata Orogeny. Subsequent marine transgression in early Tertiary times resulted in the volcanics being overlain by coal measures, silica sands, limestones, and marine siltstone. Block faulting during the Kaikoura Orogeny has resulted in the present uplifted position of the volcanics. Throughout this later tectonism there has not been much overall tilting of the volcanics. The andesite on the Clent Hills has been tilted less than 15° from its original position and the ignimbrites on Mt Somers suggest that tilting of this block was less than 20°. Excellent tectonic tilt indicators were found in the andesite and dacite throughout the area. These were banded-agate amygdules in the vesicular lavas. The bands were originally laid down horizontally when the rock was still cooling and thus a permanent record of the original attitude of the flows was preserved. This is of particular significance in the paleomagnetic study of these rocks, as accurate tilt corrections were essential for reliable results.

The paleomagnetic measurements of the Mt Somers Volcanics gave consistent normal magnetic directions. The NRM directions were found to give better grouping than the demagnetised measurements. This was found to be the result of the secondary magnetisation (due to hematite) in the rhyolite samples being more stable than the primary magnetism. Thus on progressive alternating field demagnetisation of the rhyolite, only the primary component decreased in intensity, until finally the low-intensity secondary component was dominant. Alternating field demagnetisation of the andesites showed that the NRM directions were almost identical to the demagnetised directions and, as the rhyolite NRM directions were similar to those of the andesite samples, the NRM directions can be taken to represent the primary magnetism. All the NRM directions fall within 20° of the mean direction. This scatter can be accounted for by secular variation. The very steep magnetic vector directions inevitably led to declination errors, but the VGP's calculated fall within the limit of 40° used as a reliability criteria by McElhiney *et al.* (1974). The paleo-pole position determined was 57°S 174°E (α_{95} = 6.4°; K = 11.9; R = 42.2). This pole position is consistent with that determined from the Cretaceous volcanics in Australia, when the opening of the Tasman Sea and movement along the Alpine Fault is allowed for. The results therefore indicate that no significant rotation of the Canterbury Province has occurred since the onset of New Zealand's drift in the late Cretaceous.

REFERENCES

ADAMIAN, A. A., 1966. The Problem of the Genesis of Tuff-Tufflora Formations in Armenia. In "Tufflavas and Ignimbrites". E.F. Cook (Editor) pp. 41-45. Amer. Elsevier Publ. Co., New York.

ADAMS, A. S.; OSMOND, J. K.; and ROGERS, J.J.W. 1959. The Geochemistry of Thorium and Uranium. In "Physics and Chemistry of the Earth". L.H. Ahrens, F. Press, K. Rankama and S. K. Runcorn (Editors), vol. 3, pp.298-348. Pergamon Press, London.

ADAMS, C.J.D. 1970. Geological sampling for K-Ar determinations. Institute of Nuclear Sciences Report No. INS-R-81.

ADAMS, C.J.D. 1975. New Zealand Potassium-Argon Age List-2. N.Z. J. Geol. & Geophys., vol. 18, no.3, pp.443-68.

ANDREWS, P. B. 1974. Deltaic Sediments, Upper Triassic Torlesse Supergroup, Broken River, North Canterbury. N.Z. J. Geol. Geophys. vol. 17, no.4, pp.881-905.

ARBER, E.A.N. 1917. The Early Mesozoic Floras of New Zealand. N.Z. Geol. Survey Palaeo. Bull. no. 6.

BAADSBAARD, H.; LIPSON, J.; and FOLINSBEE, R. E. 1961. The leakage of radiogenic argon from sanidine. Geochimica Cosmochimica Acta vol. 25, pp.147-157.

BAKER, J. 1969. Petrology of the volcanic rocks of St Helena Island, South Atlantic. Bull. Geol. Soc. Amer. vol. 80, p.1283.

BAYER, G. 1969. Thorium. In "Handbook of Geochemistry", K. H. Wedepohl (Editor), vol.II/4. Springer Verlag, Berlin.

BEESO, M. H.; and JACKSON, E. D. 1970. Origin of garnet pyroxenite xenoliths at Salt Lake Crater. Min. Soc. Amer. Spec. Paper 3, pp. 95-112.

BEST, M. G. 1975. Migration of hydrous fluids in the upper mantle and potassium variation in calk-alkaline rocks. Geology, vol. 3, no.8, pp. 429-432.

BLACKETT, P.M.S., 1961. Comparisons of an ancient climate with ancient latitude deduced from rock magnetic measurements. Proc. Roy. Soc. Lond., A, vol. 263, pp. 1-30.

BOETTCHER, A. L. 1973. Volcanism and orogenic belts - the origin of andesites. Tectonophysics, vol. 17, pp. 223-240.

BOTTINGA, Y.; and WEILL, D. F. 1972. The Viscosity of Magmatic Silicate Liquids : A Model for Calculation. American J. of Sci., vol. 272, pp. 438-475.

BOUMA, A. H. 1962. "Sedimentology of some Flysch Deposits" Elsevier Publishing Co., Amsterdam.

BOWEN, N. L. 1928. "The Evolution of the Igneous Rocks." Princeton University Press, Princeton.

BOYD, F. R. 1959. Hydrothermal investigation of amphiboles. In "Researches in Geochemistry" P. H. Abelson (Editor). pp.377-396. John Wiley & Sons, New York.

BRADSHAW, J. D. 1972(a). Stratigraphy and Structure of the Torlesse Supergroup (Triassic-Jurassic) in the foothills of the Southern Alps near Hawarden (S60-61), Canterbury. N.Z. J. Geol. Geophys., vol. 15, no.1, pp. 71-87.

BRAY, J. M. 1942. Spectroscopic distribution of minor elements in igneous rocks from Jamestown, Colorado. Bull. Geol. Soc. Amer. vol. 53, p.765.

BRYAN, W. B.; STICE, G. D.; and EWART, A. 1972. Geology, petrology, and geochemistry of the volcanic islands of Tonga. J. Geophys. Res. vol. 77, pp. 1566-1585.

BURNS, R. G. 1970. "Mineralogical Applications of Crystal Field Theory", Cambridge, London.

BURNS, R. G.; and FYFE, W. S. 1964. Site Preference Energy and Selective Uptake of Transition-metal Ions from a Magma. Science, vol. 144, no. 3621, pp. 1001-1003.

BURNS, R. G. 1973. The partitioning of trace transition elements in crystal structures : a provocative review with applications to mantle geochemistry. Geohim. Cosmochim. Acta, vol. 37, pp.2395-2403.

BURNS, R. G.; and FYFE, W. S. 1966. Behaviour of Nickel during Magmatic Crystallisation. Nature, vol. 210, no. 5041, pp.1147-1148.

CAMPBELL, J. K.; and CAMPBELL, J. D. 1970. Triassic Tube Fossils from Tuapeka Rocks, Akatore, South Otago. N.Z. J. Geol. Geophys. vol. 13, no. 2.

CAMPBELL, J. D.; and COOMBS, D. S. 1966. Murihiku Supergroup (Triassic-Jurassic) of Southland and South Otago, New Zealand. N.Z. J. Geol. Geophys., vol. 9, no.4, pp.393-8.

CAMPBELL, J. D.; COOMBS, D. S.; FLEMING, C. A.; KEAR, D.; McKELLER, I. C.; MUTCH, A. R.; SPEDEN, I. G.; WATERHOUSE, J. B.; WOOD, B. L.; and MARWICK, J. 1960. Note on the Gore-Balfour Series Boundary. N.Z. J. Geol. Geophys., vol.3, no.2, pp. 284-286.

CAMPBELL, J. D.; and WARREN, G. 1965. Fossil Localities of the Torlesse Group in the South Island. Trans. Roy. Soc. N.Z., Geol., vol. 3, no. 8, pp. 99-137.

CARMICHAEL, I.S.E. 1967. The iron-titanium oxides of salic volcanic rocks and their associated ferromagnesian silicates. Contrib. Mineral. & Petrol., vol. 14, pp. 36-64.

CARMICHAEL, I. S.; TURNER, F. J.; and VERHOOGEN, J. 1974. "Igneous Petrology". McGraw-Hill Book Co.

CARPENTER, B. S. 1972(a). Quantitative Applications of the Nuclear Track Technique. Microscope, vol. 20, p. 173-182.

CARPENTER, B. S. 1972(b). Determination of Trace Concentration of Boron and Uranium in Glass by the Nuclear Track Technique. Analytical Chemistry, vol. 44, no. 3, pp.600-602.

CAWTHORN, R. G.; and O'HARA, M. J. 1976. Amphibole Fractionation in Calc-alkaline Magma Genesis. Amer. J. Sci., vol. 276, pp. 309-329.

CHALLIS, G. A. 1968. The K_2O:Na_2O Ratio of Ancient Volcanic Arcs in New Zealand. N.Z. J. Geol. Geophys., vol. 11, no.1, pp.200-211.

CHALLIS, G. A. 1971. Chemical Analyses of New Zealand Rocks and Minerals with CIPW Norms and Petrographic Descriptions 1917-57. Part I: Igneous and Pyroclastic Rocks. N.Z. Geol. Surv. Bulletin n.s.84.

CHALONER, W. G.; and CREBER, G. T. 1973. Growth Rings in Fossil Woods as Evidence of Past Climates. In "Implications of Continental Drift to the Earth Sciences" vol. 1. D. H. Tarling and S. K. Runcorn (Editors). Academic Press, London. pp.425-437.

CHRISTOFFEL, D. A.; and FALCONER, R. F. 1973. Magnetic Measurements in the Macquarie Ridge Region. In "Oceanography of the South Pacific" 1972, comp. R. Fraser. New Zealand National Commission for Unesco, Wellington.

CHURCH, S. E. 1973. Limits of sediment involvement in the genesis of orogenic volcanic rocks. Contr. Mineral. & Petrol., vol. 39, pp. 17-32.

COLLINSON, D. W.; CREER, K. M.; and RUNCORN, S. K. (Editors) 1967. "Methods In Paleomagnetism". Developments in Solid Earth Geophysics, vol. 3, Elsevier Publishing Co., Amsterdam.

COOK, E. F. (Editor) 1966. "Tufflavas and Ignimbrites", Amer. Elsevier Publ. Co., New York.

COTTON, F. A.; and WILKINSON, G. 1966. "Advanced Inorganic Chemistry". Interscience Publishers, London.

COX, P. T. 1926. Geology of the Rakaia Gorge District. Trans. N.Z. Inst. vol. 56, pp.91-111.

COX, S. H. 1877. Report on the Geology of the Mt Somers District. Reports of Geological Exploration during 1876-7, pp.1-10.

COX, S. H. 1884a. On Mount Somers and Malvern Hills District. N.Z. Geol. Surv. Reports of Geological Explorations 1883-1884. vol. 16, pp.22-43.

COX, S. H. 1884b. On the Relations of the Quartz Porphyries and Pitchstones of Mt Somers and Malvern Hills. N.Z. Geol. Surv. Reports of Geological Explorations 1883-1884, pp.107-110.

CREER, K. M. 1970. A Review of Palaeomagnetism. Earth Science Reviews, vol. 6, pp.369-466.

CREER, K. M. 1973. A Discussion of the Arrangement of Palaeomagnetic Poles on the map of Pangea for Epochs in the Phanerozoic. In "Implications of Continental Drift to the Earth Sciences, volume 1". D. H. Tarling and S. K. Runcorn (Editors). Academic Press, London.

CREER, K. M.; and ISPIR, I. 1970. Behaviour of the geomagnetic field during polarity reversals. Phys. Earth Planet. Interiors, vol. 2, pp.283-293.

CURTIS, C. D. 1964. Applications of the crystal-field theory to the inclusion of trace transition elements in minerals during magmatic differentiation. Geochim. Cosmochim. Acta, vol. 28, pp.389-403.

DALRYMPLE, G. B.; and LANPHERE, M. A. 1969. "Potassium-Argon Dating. Principles, Techniques and Applications to Geochronology." W. H. Freeman & Co., San Francisco.

DEER, W. A.; HOWIE, R. A.; and ZUSMAN, J. 1966. "An Introduction to the Rock-Forming Minerals". Longmans, London.

DICKINSON, W. R. 1968. Circum-Pacific andesite types. J. Geophys. Res., vol. 73, pp.2261-2269.

DICKINSON, W. R. 1970. Relation of andesites, granites and derived sandstones to arctrench tectonics. Reviews Geophys. Space Phys. vol. 8, pp.813-860.

DICKINSON, W. R. 1973. Reconstruction of past arch-trench systems from petrotectonic assemblages in the island arcs of the Western Pacific. In "The Western Pacific Island Arcs, Marginal Seas, Geochemistry". P. J. Coleman (Editor), New York, Crare-Russak. pp.569-601.

DICKINSON, W. R. 1975. Potash-depth (K-h) relationships in continental margins and intra-oceanic magmatic arcs. Geology, vol. 3, no.2, pp.53-56.

DICKINSON, W. R.; and HATHERTON, T. 1967. Andesite volcanism and seismicity around the Pacific. Science, vol. 157, pp.801-803.

DOE, B. R.; and TILLING, R. I. 1967. The distribution of lead between co-existing K-feldspar and plagioclase. Amer. Mineralogist, vol. 52, pp.805-816.

DOELL, R. R.; and COX, A. 1965. Measurement of the remanent magnetisation of igneous rocks. Bull. U.S. Geol. Surv. 1203-A, pp.1-32.

DOELL, R. R.; and COX, A. 1967. Palaeomagnetic sampling with a portable coring drill. In "Methods in Palaeomagnetism". D. W. Collinson, K. M. Creer and S. K. Runcorn (Editors). Elsevier Publishing Co., Amsterdam.

DUCHESNE, J. C. 1968. Strontium vs. Calcium and Barium vs. Potassium relations in plagioclases from Southern Rogaland Anorthosites. Ann. Soc. Geol. Belg. Bull. vol. 90, p. 643.

DUNCAN, A. R. 1970. The Petrology and Petrochemistry of Andesite and Dacite Volcanics in Eastern Bay of Plenty, New Zealand. Unpublished Ph.D. Thesis, V.U.W.

DUNCAN, A. R.; and TAYLOR, S. R. 1968. Trace-element Analyses of Magnetites from Andesitic and Dacitic Lavas from Bay of Plenty, New Zealand. Contrib. Mineral & Petrol. vol. 20, pp.30-33.

DUNITZ, J. D.; and ORGEL, L. E. 1957. Electronic properties of transition element oxides - II Cation distribution amongst octahedral and tetrahedral sites. J. Phys. Chem. Solids, vol. 3, pp.318-333.

EDWARDS, W. N. 1934. Jurassic Plants from New Zealand. Ann. Mag. Nat. Hist. Series 10, 13, pp. 81-109.

EICHELBERGER, J. C. 1974. Magma contamination within the volcanic pile; origin of andesite and dacite. Geology, vol. 2,p.29-33.

ETTINGSHAUSEN, C. VON, 1887. On the Fossil Flora of New Zealand. Geol. Mag. decade 3,4, pp.363-7.

ETTINGSHAUSEN, C. VON, 1891. Contributions to the Knowledge of Fossil Flora of New Zealand. Trans. N.Z. Inst., vol. 23, pp.237-310.

EVERNDEN, J. F.; and JAMES, G. T. 1964. Potassium-argon dates and the Tertiary floras of North America. Amer. Jour. Sci., vol.262, p.943-974.

EWART, A.; and BRYAN, W. B., 1973. The Petrology and Geochemistry of the Tongan Islands. In "The Western Pacific Island Arcs Marginal Seas Geochemistry". P. J. Coleman (Editor). University of Western Australia Press. pp.503-522.

EWART, A.; and STIPP, J. J. 1968. Petrogenesis of the volcanic rocks of the Central North Island, New Zealand, as indicated by a study of Sr^{87}/Sr^{86} ratios, and Sr, Rb, K, U and Th abundances. Geochim. Cosmochim. Acta, vol. 32, pp.699-736.

EWART, A.; and TAYLOR, S. R. 1969. Trace element geochemistry of the rhyolitic volcanic rocks, Central North Island, New Zealand. Phenocryst data. Contrib. Mineral. & Petrol., vol. 22, pp.127-146.

EWART, A.; TAYLOR, S. R.; and CAPP, A. C. 1968. Trace and Minor Element Geochemistry of the Rhyolitic Volcanic Rocks, Central North Island, New Zealand. Contrib. Mineral. & Petrol., vol. 18, pp.76-104.

FLANAGAN, F. J. 1973. 1972 values for international geochemical reference samples. Geochim. Cosmochim. Acta, vol. 37, pp.1189-1200.

FLEISCHER, M. 1969. Abundances of Yttrium and Ytterbium in Igneous Rocks. In "Problems of Geochemistry". N. I. Kitarov (Editor). Translated from the Russian by Israel Program for Scientific Translation, Jerusalem, 1969. pp.451-457.

FLEISCHER, R. L.; and HART, H. R. Jr. 1970. Fission-Track Dating : Techniques and Problems. Report No. 70-C-328. General Electric Research and Development Center, Schedectady, New York.

FLEISCHER, R. L.; and PRICE, P. B. 1964. Techniques for geological dating of minerals by chemical etching of fission fragment tracks. Geochim. Cosmochim. Acta, vol. 28, pp.1705-1714.

FLEISCHER, R. L.; PRICE, P. B.; and WALKER, R. M. 1965. Quaternary Dating by the Fission-Track technique. Report No. 65-C-140. General Electric Research and Development Center, Schenectady, New York.

FLEISCHER, R. L.; PRICE, P. B.; and WALKER, R. M. 1969. Fission track dating and processes in the Earth's interior. In "The Application of Modern Physics to the Earth and Planetary Interiors". S. K. Runcorn (Editor). Wiley-Interscience. pp.499-503.

FLEMING, C. A. 1969. The Mesozoic of New Zealand : Chapters in the history of the circum-Pacific mobile belt. Quart. J. Geol. Soc. Lond., vol.125, pp.125-70.

FOLK, R. L.; ANDREWS, P. B.; and LEWIS, D. W. 1970. Detrital sedimentary rock classification and nomenclature for use in New Zealand. N.Z. J. Geol. Geophys., vol. 13, no. 4, pp.937-68.

FOSTER, J. H. 1966. A paleomagnetic spinner magnetometer using a fluxgate gradiometer. Earth Planet. Sci. Letters, vol. 1, pp.463-6.

GAIR, H. S. 1967. Sheet 20, Mt Cook. "Geological Map of New Zealand 1:250,000". Dept. Sci. Industr. Res., Wellington, N.Z.

GAVRILOVA, L. K.; and TURANSKAYA, R. V. 1958. Distribution of Rare Earths in rock-forming and accessory minerals of certain granites. Geochemistry, no.2, pp.163-170.

GAY, P.; and ROY, N. N. 1968. The mineralogy of the potassium-barium feldspar series. III. Subsolidus relations. Mineral. Mag., vol. 35, p. 914.

GIBBON, D. L. 1969. Origin and Development of the Star Mountain Rhyolite. Bull. Volcan. vol.33, pp.438-474.

GIBSON, I. L.; and TAZIEFF, H. 1967. Additional theory of fiamme in ignimbrites. Nature, vol. 215, no. 5109, p.1473-1474.

GILL, J. B. 1974. Role of underthrust oceanic crust in the genesis of a Fijian calc-alkaline suite. Contrib. Mineral. & Petrol., vol.43, pp.29-45.

GILL, J.; and COMPSTON, W. 1973. Strontium Isotopes in Island Arc Volcanic Rocks. In "The Western Pacific Island Arcs Marginal Seas Geochemistry." P. J. Coleman (Editor). University of Western Australia Press. pp.483-496.

GORSHKOV, G. S. 1969. Geophysics and Petrochemistry of Andesite Volcanism of the Circum-Pacific Belt. In "Proceedings of the Andesite Conference". A. R. McBirney (Editor). State of Oregon Department of Geology and Mineral. Industries. pp.91-98.

GREEN, D. H. 1964. The metamorphic aureole of the peridotite at the Lizard, Cornwall. J. Geol. vol. 72, pp.543-563.

GREEN, D. H. 1973. Experimental melting studies on a model upper mantle composition at high pressures under water-saturated and water-undersaturated conditions. Earth Planet. Sci. Letters, vol. 19, pp.37-53.

GREEN, D. H.; and RINGWOOD, A. E. 1967. The Genesis of Basaltic Magmas. Contrib. Min. Pet., vol. 15, pp.103-190.

GREEN, J.; SHORT, N. M. (Editors) 1971. "Volcanic Landforms and Surface Features (a photographic atlas and glossary)". Springer-Verlag, Berlin, Heidlburg, New York.

GREEN, T. H.; and RINGWOOD, A. E. 1968(a). Genesis of the calc-alkaline igneous rock suite. Contrib. Mineral. Petrol. vol. 18, pp.105-162.

GREEN, T. H.; and RINGWOOD, A. E. 1968(b). Origin of garnet phenocrysts in calc-alkaline rocks. Contrib. Mineral. Petrol., vol. 18, pp.163-174.

GREEN, T. H. 1972. Crystallisation of calc-alkaline andesite under controlled high pressure hydrous conditions. Contrib. Min. Petrol., vol. 34, pp.150-166.

GREEN, T. H. 1976. Experimental generation of cordierite - or garnet - bearing granitic liquids from a pelitic composition. Geology, vol. 4, no.2, pp.85-88.

GREEN, T. H.; and RINGWOOD, A. E. 1972. Crystallization of garnet-bearing rhyodacite under controlled high pressure hydrous conditions. J. Geol. Soc. Australia, vol. 19, pp.203-212.

GREGG, D. R. 1964. Sheet 18 Hurunui (1st Ed.) "Geological Map of New Zealand 1:250,000". Dept. Sci. Industr. Res., Wellington, N.Z.

GREGG, D. R. 1965. Geology of the Harper Hills. In "New Zealand Volcanology. South Island". B. N. Thompson and L. O. Kermode (Editors) N.Z. Dep. Sci. Industr. Res. Inf. Ser. No.51.

GRIFFITHS, J. R. 1975. New Zealand and the Southwest Pacific Margin of Gondwanaland. In "Gondwana Geology", K.S.W. Campbell (Editor). A.N.U. Press, Canberra, pp.619-637.

GULSON, B. L. 1972. The high-K diorites and associated rocks of the Yeoval diorite complex, N.S.W. Contrib. Mineral. Petrol., vol. 35, pp.173-192.

HAACK, U. K.; and GRAMSE, M. 1972. Survey of Garnet for Fossil Fission Tracks. Contrib. Mineral. & Petrol., vol. 34, pp.258-260.

HAACK, U. K.; and POTTS, M. J. 1972. Fission Track Annealing in Garnet. Contrib. Mineral. & Petrol. vol. 34, pp.343-345.

HAAST, J. 1862. Notes on the Geology of the Province of Canterbury, New Zealand. N.Z. Gov. Gaz. Prov. Canterbury, vol. 9, no.18, pp.121-31.

HAAST, J. 1864. Report on the Geological Survey of the Province of Canterbury. Proc. prov. Coun. Canterbury. Sess. 22.

HAAST, J. 1872a. Report on the Coal Deposits of the Ashburton District. N.Z. Geol. Surv. Rep. Geol. Explor. 1871-72(7), pp.141-6.

HAAST, J. 1872. Report on the Geology of the Malvern Hills, Canterbury. N.Z. Geol. Surv. Rep. Geol. Explor. 1871-72(7), pp.1-85.

HAAST, J. von, 1877. Geology of the Clent Hills and Mt Somers Districts. N.Z. Geol. Surv. Rep. Geol. Explor. during 1873-74, pp.1-19.

HAAST, J. von, 1879. "Geology of the Provinces of Canterbury and Westland, New Zealand. A Report Comprising the Results of Official Explorations". Times Office, Christchurch.

HAAST, J. von, 1887. "Notes on the age and subdivision of the sedimentary rocks in the Canterbury mountains based upon the palaeontological researches of Professor Dr C. Baron von Ettingshausen, in Gratz (Austria). Trans. N.Z. Inst., vol. 19, pp.449-51.

HASEGAWA, S. 1960. Chemical composition of allanite. Sci. Rep. Tohoku University Ser., vol. 3, no. 6, p.331.

HATCH, F. H.; WELLS, A. K.; and WELLS, M. K. 1972. "Petrology of the Igneous Rocks" (13th Edition). Thomas Murby & Co., London.

HATHERTON, T.; and DICKINSON, W. R. 1969. The Relationship between Andesite Volcanism and Seismicity in Indonesia, the Lesser Antillies, and Other Island Arcs. J. Geophys. Res., vol. 74, no.22, pp.5301-5310.

HAYES, D. E.; and RINGIS, J. 1973. Seafloor Spreading in the Tasman Sea. Nature, vol. 243, no. 5408, pp.454-458.

HECTOR, J. 1870. Catalogue of the Colonial Museum, Wellington, New Zealand. Government Printer, Wellington.

HECTOR, J. 1884. Progress Report, 1883. N.Z. Geol. Surv. Rep. Geol. Explor. 1883-84, vol. 16, pp.ix-xxxviii.

HECTOR, J. 1886. Detailed Catalogue and Guide to the Geological exhibits, New Zealand court, Indian and Colonial Exhibition, London 1886. Wellington Govt. Printer, pp.37-101.

HEIER, K. S.; and ROGERS, J.J.W. 1963. Radiometric determination of thorium, uranium and potassium in basalts and in two magmatic differentiation series. Geochim. Cosmochim. Acta, vol. 27, no. 2, pp.137-154.

HEIR, K. S.; and TAYLOR, S. R. 1959. Distribution of Ca, Sr, Ba in Southern Norwegian pre-cambrian alkali feldspars. Geochim. Cosmochim. Acta, vol. 17, p.286.

HERRMANN, A. G. 1970. Yttrium and lanthanides. In "Handbook of Geochemistry" vol. II/2. K. H. Wedepohl (Editor). Springer-Verlag.

HOLLOWAY, J. R.; and BURNHAM, C. W. 1972. Melting relations of basalt with equilibrium water pressure less than total pressure. J. Petrol. vol. 13, pp. 1-29.

HOLLOWAY, J. R.; and FORD, C. E. 1973. The effect of fluorine on hornblende : Fluid absent melting of F-OH pargasite to 35 kbars (abstract). Eos Trans. A.G.U., vol. 54, p.478.

HULSTON, J. R.; and McCABE, W. J. 1972. New Zealand Potassium-Argon Age List - 1. N.Z. J. Geol. Geophys. vol. 15, pp.406-432.

HUTTON, F. W. 1874. Report on the Geology of the North-east Portion of the South Island, from Cook Straits to the Rakaia. N.Z. Geol. Surv. Rep. geol. Explor. 1872-3, vol. 8a, pp.27-58.

IIYAMA, J. T. 1968. Etude experimentale de la distribution d'element en trace entre deux feldspaths. Feldspath potassique et plagioclase coexistants. I. Distribution de Rb, Cs, Sr et Ba à 600°C. Bull. Soc. Franc. Mineral. Crist. vol. 91, p. 130.

INGERSON, E. 1953. Giant amygdules in andesite from the southern Quitman Mountains, Texas. Amer. Min., vol. 38, pp.1057-1064.

IRVING, E. 1964. Paleomagnetism (and its Application to Geological and Geophysical Problems). John Wiley & Sons, Inc., New York.

ITO, K.; and KENNEDY, G. C. 1967. Melting and phase relations in a matural peridotite to 40 kilobars. Amer. J. Sci. vol. 265, p. 519.

ITO, K.; and KENNEDY, G. C. 1968. Melting and Phase Relationships in the Plane Tholeiite-Lherzolite-Nepheline Basanite to 40 kilobars with Geological Implications. Contrib. Mineral. Petrol., vol. 19, pp.177-211.

JAFFE, H. W. 1951. The role of yttrium and other minor elements in the garnet group. Amer. Mineral. vol. 36, pp.133-155.

JAKES, P.; and WHITE, A.J.R. 1972. Major and Trace Element Abundances in Volcanic Rocks of Orogenic Areas. Geol. Soc. America. Bull., vol. 83, pp.29-40.

JOBBERNS, G. 1926. Geology of Cordy's Flat, Malvern Hills, Canterbury. Trans. N.Z. Inst., vol. 56, pp.214-225.

KELLER, J.; and VILLARI, L. 1973. Rhyolite Ignimbrites in the Region of Afyon (Central Anatolia). Bull. volc. vol. 36, no.2, pp.342-358.

KHOMYAKOV, A. P. 1967. Chemical and Crystallochemical factors in the distribution of rare earths. Geochemistry International, vol. 4, no. 1, pp.127-135.

KRAUSKOPF, K. B. 1967. "Introduction to Geochemistry". McGraw-Hill Inc., New York.

KUNO, H. 1960. High-alumina Basalt. J. Petrol. vol.1, p.121-145.

KUNO, H. 1966. Lateral Variation of Basalt Magma type across continental Margins and Island Arcs. Bull. Volcanologique, vol. 29, pp.195-222.

KUNO, H.1968a. Origin of Andesite its Bearing on the Island Arc Structure. Bull. volc. vol. 32, no.1, pp. 141-176.

KUNO, H. 1968b. Differentiation of Basalt Magmas. In "Basalts : The Poldervaart Treatise on Rocks of Basaltic Composition", vol. 2. H. H. Hess (Editor). Interscience. pp.623-688.

KUSHIRO, I. 1973. Origin of some magmas in oceanic and circum-oceanic regions. Tectonophysics, vol. 17, pp.211-222.

KUSHIRO, I.; and YODER, H. S. 1969. Melting of forsterite and enstatite at high pressures under hydrous conditions. Carnegie Inst. Washington Yearbook, vol. 67, pp.153-158.

KUSHIRO, I.; SHIMAZU, N.; NAKAMURA, Y.; and AKIMOTO, S. 1972. Compositions of coexisting liquid and solid phases formed on melting of natural garnet and spinel lherzolite at high pressures. A preliminary report. Earth Planet. Sci. Letters, vol. 14, no.1, pp.19-25.

KUSHIRO, I.; SYONO, Y.; and AKIMOTO, S. 1968. Melting of a peridotite nodule at high pressure and high water pressures. J. Geophys. Res., vol. 73, p.6023.

LAL, D.; MURALLI, A. V.; RAJAN, R. S.; TAMHANE, A. S.; LORIN, J. C.; and PELLAS, P. 1968. Techniques for proper relevation and viewing of etch-tracks in meteoritic and terrestrial minerals. Earth Plan. Sci. Letters, vol. 5, pp.111-119.

LAMBERT, I. B.; and WYLLIE, P. J. 1968. Stability of hornblende and a model for the lower velocity zone. Nature, London, vol. 219, pp.1240-1241.

LAMBERT, I. B.; and WYLLIE, P. J. 1972. Melting of gabbro (quartz eclogite) with excess water to 35 kilobars with geological applications. J. Geology, vol. 80, pp.693-708.

LAMBERT, I. B.; and WYLLIE, P. J. 1974. Melting of tonalite and crystallisation of andesite liquid with excess water to 30 kilobars. J. Geology, vol. 82, no. 1, pp.88-97.

LAMBERT, R. ST.J.; and HOLLAND, J. G. 1974. Yttrium geochemistry applied to petrogenesis utilizing calcium-yttrium relationships in minerals and rocks. Geochim. Cosmochim. Acta, vol. 38, pp.1393-1414.

LAMBERT, R. ST.J.; HOLLAND, J. G.; and OWEN, P. F. 1974. Chemical petrology of a suite of calc-alkaline lavas from Mount Ararat, Turkey. J. Geol., vol. 82, no. 4, pp.419-438.

LANDERGREN, S. 1974. Vanadium. In "Handbook of Geochemistry". K. H. Wedepohl (Editor), vol. 2. Springer Verlag, Berlin.

LANDIS, C. A.; and BISHOP, D. G. 1972. Plate tectonics and regional stratigraphic-metamorphic relations in the southern part of the New Zealand Geosyncline. Geol. Soc. of Amer. Bull., vol. 83, pp. 2267-84.

LOCARDI, E.; and MITTEMPERGHER, M. 1967. On the Genesis of Ignimbrites. How Ignimbrites and other pyroclastic products originate from a flowing melt. Bull. Volcan., vol. 31, pp.131-152.

LØVLIE, R.1976. The Intensity Pattern of Post-Depositional Remanence acquired in some Marine Sediments deposited during a Reversal of the External Magnetic Field. Earth & Planet. Sci. Letters, vol. 30, pp.209-214.

LUMB, J. T. 1967. A Programme for the Computation of Remanent Magnetism of Small Rock Samples. Geophysics Division Technical Note No.53.

LUMB, J. T.; and ROBERTS, N. L. 1969. A New Spinner Magnetometer. D.S.I.R. Geophysics Div. Technical Note 58.

MACDONALD, G. A. 1972. "Volcanoes". Prentice-Hall, Inc., New Jersey.

MALEYEV, E. F. 1966. Genetic types of Clastolavas and their distinction from Ignimbrites. In "Tufflavas and Ignimbrites." pp.27-31. E. F. Cook (Editor). Amer. Elsevier Publ. Co., New York.

MARSH, B. D.; and CARMICHAEL, I.S.E. 1974. Benioff Zone Magmatism. J. Geophys. Research, vol. 79, pp.1196-1206.

McBIRNEY, A. R. 1973. Factors Governing Intensity of Explosive Andesite Eruptions. Bull. Volc., vol. 37, no.3, pp.443-453.

McCLURE, D. S. 1957. The Distribution of Transition Metal Cations in Spinels. J. Phys. Chem. Solids, vol. 3, pp.311-317.

McELHINNY, M. W. 1973. "Paleomagnetism and Plate Tectonics." Cambridge University Press.

McELHINNY, M. W.; and EMBLETON, B.J.J. 1974. Australian palaeomagnetism and the Phanerozoic plate tectonics of eastern Gondwanaland. Tectonophysics, vol. 22, pp.1-29.

McELHINNY, M. W.; EMBLETON, B.J.J.; and WELLMAN, P. 1974. A Synthesis of Australian Cenozoic paleomagnetic results. Geophys. J., vol. 36, pp. 141-151.

McKAY, A. 1887. On the Geology of the Malvern Hills. N.Z. Geol. Surv. Rep. Geol. Explor. during 1886-87, (18), pp.230-33.

MILDENHALL, D. C. 1970. Checklist of Valid and Invalid Plant Macrofossils from New Zealand. Trans. Roy. Soc. N.Z. Earth Sciences, vol. 8, no. 6, pp.77-89.

MIYASHIRO, A.; and SHIDO, F. 1975. Tholeiitic and calc-alkaline series in relation to the behaviours of Titanium, Vanadium, Chromium and Nickel. Amer. J. Sci. vol. 275, no. 3, pp.265-277.

MOLNAR, P.; ATWATER, T.; HAMMERICKX, J.; and SMITH, S. M. 1975. Magnetic Anomalies, Bathymetry and the Tectonic Evolution of the South Pacific since the Late Cretaceous. Geophys. J. R. Ast. Soc., vol. 40, pp. 383-420.

MYSEN, B. D. 1973. Melting in a hydrous mantle: phase relations of mantle peridotite with controlled water and oxygen fugacities. Carnegie Inst. Wash., Year Book 72, pp.467-478.

MYSEN, B.; and BOETTCHER, A. L. 1976. Melting of a Hydrous Mantle: III. Phase Relations of Garnet Websterite + H_2O at High Pressures and Temperatures. J. Petrology, vol. 17, part 1, pp.1-14.

NICHOLLS, I. A. 1974. Liquids in equilibrium with peridotite mineral assemblages at high water pressures. Contrib. Mineral. Petrol., vol. 45, pp.289-316.

NICHOLLS, I. A.; and RINGWOOD, A. E. 1973. Effect of water on olivine stability in tholeiites and the production of silica-saturated magmas in the island-arc environment. J. Geol. vol. 81, pp.285-300.

NIELSON, D. R.; and STOIBER, R. E. 1973. Relationship of potassium content in andesitic lavas and depth to the seismic zone. J. Geophys. Res., vol. 78, p. 6887.

NOCKOLDS, S. R.; and ALLEN, R. 1953. The Geochemistry of Some Igneous Rock Series. Geochim. Cosmochim. Acta, vol. 4, pp.105-142.

NORRISH, K.; and HUTTON, J. T. 1969. An accurate X-ray spectrographic method for the analysis of a wide range of geological samples. Geochim. Cosmochim. Acta, vol. 33, no. 4, pp.431-453.

OBORN, L. E.; and SUGGATE, R. P. 1959. Sheet 21 Christchurch (1st Ed.) "Geological Map of New Zealand 1:250,000". Dep. Sci. Industr. Res. Wellington, N.Z.

O'HARA, M. J. 1968. The Bearing of Phase Equilibrium Studies in Synthetic and Natural Systems on the Origin and Evolution of Basic and Ultrabasic Rocks. Earth Sci. Rev., vol. 4, pp.69-133.

O'HARA, M. J.; and YODER, H. S. 1967. Formation and fractionation of basic magmas at high pressures. Scot. J. Geol. vol. 3, p. 67.

OSBORN, E. F. 1959. Role of oxygen pressure in the crystallization and differentiation of basaltic magma. Amer. J. Sci., vol. 257, pp. 609-647.

OSBORN, E. F. 1962. Reaction series for subalkaline igneous rocks based on different oxygen pressure conditions. Amer. Mineral., vol. 47, pp. 211-226.

OSBORN, E. F. 1969(a). The complimentariness of Orogenic andesite and alpine peridotite. Geochem. Cosmochim. Acta, vol. 33, pp.307-324.

OSBORN, E. F. 1969(b). Genetic Significance of V and Ni content of andesites : Comments on a paper by Taylor, Kaye, White, Duncan and Ewart. Geochim. Cosmochim. Acta, vol. 33, pp.1553-1554.

OSBORN, E. F.; and ROEDER, P. L., 1960. Effect of oxygen pressure on crystallization in simplified basalt systems. Int. Geol. Congr. XXI Sess. Norden, vol. 13, pp.147-155.

OVERSBY, V. M.; and EWART, A. 1972. Lead isotopic composition of Tonga-Kermadec volcanics and their petrogenetic significance. Contrib. Mineral. & Petrol. vol. 37, pp.181-210.

PAVLENKO, A. S.; VAINSHTEIN, E. E.; and TURANSKAYA, N. V. 1959. Certain regularities in the behaviour of Rare Earths Yttrium in magmatic and postmagmatic processes. Geochemistry, no. 4, pp.357-380.

PETROV, V. P. 1966. Petrologic properties of ignimbrites and tuffaceous lavas and their place among rocks intermediate between lavas and tuffs. In "Tufflavas and Ignimbrites". E. F. Cook (Editor). Amer. Elsevier Publ. Co., New York. pp.16-26.

PHILPOTTS, J. A.; and SCHNETZLER, C. C. 1970. Phenocryst-matrix partition coefficients for K, Rb, Sr, and Ba, with application to anorthosite and basalt genesis. Geochim. Cosmochim. Acta, vol. 34, p.307.

PICHLER, H.; and ZEIL, W. 1972. The Cenozoic rhyolite-andesite association of the Chilean Andes. Bull. Volcanol. vol. 35, pp.424-452.

POLDERVAART, A.; and PARKER, A. B. 1964. The Crystallisation Index as a parameter of Igneous Differentiation in binary variation diagrams. Amer. J. Sci., vol. 262, pp.281-289.

PRICE, P. B.; and WALKER, R. M. 1963. Fossil Tracks of Charged Particles in Mica and the Age of Minerals. J. Geophys. Research, vol. 68, no.16, pp.4847-4861.

REED, J. J. 1957. Petrology of the Lower Mesozoic rocks of the Wellington district, N.Z. N.Z. Geol. Surv. Bull. n.s.57.

REED, J. J. 1958. Regional Metamorphism in South-East Nelson. N.Z. Geol. Surv. Bull. n.s.60.

RINGWOOD, A. E. 1974. The petrological evolution of island arc systems. J. Geol. Soc. Lond., vol. 130, pp.183-204.

RITTMANN, A. 1962. "Volcanoes and their Activity" (Translated from the 2nd German edition by E. A. Vincent). J. Wiley & Sons, New York.

RITTMANN, A. 1971. The probable origin of high-alumina basalts. Bull. Volcanol., vol. 34, pp.414-420.

ROEDER, P. L.; and OSBORN, E. F. 1966. Experimental data for the system $MgO-FeO-Fe_2O_3-CaAl_2Si_2O_8-SiO_2$ and their petrologic implications. Amer. J. Sci., vol. 264, pp.428-480.

ROGERS, J. 1966. Hydrothermal melting of some New Zealand Greywackes and Argillites. Bull. Volcanol., vol. 29, pp.173-175.

RODGERS, J.J.W.; and ADAMS, J.A.S. 1969. Thorium. In "Handbook of Geochemistry". K. H. Wedepohl (Editor), vol. II, 1974. Springer-Verlag, Berlin.

ROSS, C. S.; and SMITH, R. L. 1961. Ash-Flow Tuffs : Their Origin, Geologic Relations and Identification. USGS Prof. Paper 366.

ROY, N. N. 1965. The mineralogy of the potassium-barium feldspar. Series I: The determination of natural members. Mineral. Mag., vol. 35, p.508.

ROY, N. N. 1967. The mineralogy of the potassium-barium feldspar. Series II: Studies on hydrothermally synthesised members. Mineral. Mag., vol. 36, p.43.

SCHEEL , H. J. 1971. Lead feldspar. Z. Kristallogr., vol. 133, p.264.

SCHMIDT, P. W. 1976. A New Palaeomagnetic Investigation of Mesozoic Igneous Rocks in Australia. Tectonophysics, vol. 33, pp.1-13.

SCHMIDT, P. W.; and EMBLETON, B.J.J. 1976. Palaeomagnetic Results from Sediments of the Perth Basin, Western Australia and their Bearing on the Timing of Regional Lateritisation. Palaeogeography, Palaeoclimatology, Palaeoecology, vol. 19, pp.257-273.

SCHNETZLER, C. C.; and PHILPOTTS, J. A. 1970. Partition Coefficients of Rare-Earth Elements between Igneous Matrix Material and Rock-forming Mineral Phenocrysts, Part II. Geochim. Cosmochim. Acta vol. 34, pp.331-340.

SEMENOV, E. I.; and BARINSKII, R. L. 1958. The composition characteristics of the Rare Earths in minerals. Geochemistry, no. 4, pp.398-419.

SHAPIRO, L.; and BRANNOCK, W. W. 1956. Rapid Analysis of Silicate Carbonate and Phosphate Rocks. U.S. Geol. Survey Bulletin 1144-A, pp.A48-A49.

SHAW, D. M. 1968. A review of K-Rb fractionation trends by covariance analysis. Geochim. Cosmochim. Acta, vol. 32, pp.573-602.

SHAW, H. R. 1972. Viscosities of Magmatic Silicate Liquids: An Empirical Method of Prediction. Amer. J. Sci., vol. 272, pp.870-893.

SHIMMER, J. A. 1943. Spectrographic Analysis of New England Granites and Pegmatites. Bull. Geol. Soc. Amer. vol. 54, p.1049.

SHIRINIAN, K. G., 1966. Ignimbrites and tufflavas (principles of classification and origin with especial reference to Armenia). In "Tufflavas and Ignimbrites" E. F. Cook (Editor). pp.32-40. Amer. Elsevier Publ. Co., New York.

SIBLEY, D. F.; VOGEL, T. A.; WALKER, B. M.; and BYERLY, G. 1976. The origin of oscillatory zoning in plagioclase : a diffusion and growth controlled model. Amer. J. Sci., vol. 276, pp.275-284.

SIMPSON, E.S.W. 1954. On the Graphical Representation of Differentiation Trends in Igneous Rocks. Geol. Mag., vol. 91, pp.238-244.

SMITH, J. V. 1974. "Feldspar Minerals. Vol. 2. Chemical and Textural Properties". Springer-Verlag, Berlin.Heidelberg.

SMITH, R. E. 1967. Segregation vesicles in basaltic lava. Amer. J. Sci. vol. 265, pp.696-713.

SORRELL, C. A. 1962. Solid state formation of barium, strontium and lead feldspars in clay-sulphate mixtures. Amer. Mineral. vol. 47, p.291.

SPEDEN, I. G. 1975. Additional Fossil Localities of the Torlesse Rocks of the South Island. Report N.Z.G.S. 69, Dept. Sci. Industr. Res., Wellington.

SPEIGHT, R. 1938. The Geology of Mt Somers District. N.Z. Dep. Sci. Industr. Res. Geol. Memoir 3.

SPORLI, K. B.; STANAWAY, K. J.; and RAMSAY, W.R.H. 1974. Geology of the Torlesse Supergroup in the Southern Liebig and Burnett Ranges, Canterbury, New Zealand. J. Roy. Soc. N.Z., vol. 4, no.2, pp.177-192.

STERN, C. R. 1974. Melting products of olivine tholeiite basalt in subduction zones. Geology, 2, pp.227-230.

STERN, C. R.; and WYLLIE, P. J. 1973. Melting relations of basalt-andesite-rhyolite-water and a pelagic red clay at 30 kb. Contrib. Mineral. Petrol. vol. 42, pp.313-323.

STEVENS, G. R. 1972. Paleontology of the Torlesse Supergroup. N.Z.G.S. Report 54.

STEWART, D. C. 1975. Crystal Clots in Calc-Alkaline Andesites as Breakdown Products of High-Al Amphiboles. Contrib. Mineral. Petrol., vol. 53, pp.195-204.

SUGGATE, R. P. 1961. Rock-stratigraphic names for the South Island schists and undifferentiated sediments of the New Zealand geosyncline. N.Z. J. Geol. Geophys., vol. 4, pp.392-9.

SUGGATE, R. P. 1973. Sheet 21 Christchurch (2nd Ed.) "Geological Map of New Zealand 1:250,000", Dep. Sci. Industr. Res., Wellington, N.Z.

SUGIMURA, A. 1961. Regional variation of the K_2O/Na_2O ratios of volcanic rocks in Japan and environs. Geol. Soc. Japan Jour., vol. 67, pp.292-300.

SUGIMURA, A. 1973. Multiple Correlation Between Composition of Volcanic Rocks and Depth of Earthquake Foci. In "The Western Pacific. Island arcs marginal seas geochemistry." P. J. Coleman (Editor). University of Western Australia Press, pp.471-482.

SUGISAKI, R., 1976. Chemical Characteristics of Volcanic Rocks : Relation to Plate Movements. Lithos., vol. 9, no. 1, pp.17-30.

TARLING, D. H. 1971. "Principles and Applications of Palaeomagnetism" Chapman and Hall, London.

TAUSON, L. V.; KOVALENKO, V. I.; ZNAMENSKAYA, A. S.; PETROC, L. L.; LEGEIDO, V. A.; POPOLITOV, A. I.; and PROKOPENKO, S. R. 1968. Distribution of Rare-Earth Elements (RE), Yttrium, Beryllium, and Tin in Alkaline Granitoides and their Metasomatites. In "Origin and Distribution of the Elements". L. H. Ahrens (Editor). Internat. Ser. of Monographs on Earth Sci., vol. 30, pp.663-667. Pergamon Press, Oxford.

TAYLOR, S. R. 1968. Geochemistry of andesites. In "Origin and Distribution of the Elements". L. H. Ahrens (Editor). Int. Ser. of Monographs on Earth Sci., vol. 30, pp.559-583. Pergamon Press, Oxford.

TAYLOR, S. R. 1969. Trace Element Chemistry of Andesites and Associated Calc-alkaline Rocks. Proc. Andesite Conference Oregon Dept. Geol. Min. Res. Bull. 65, pp.43-63.

TAYLOR, S. R.; KAYE, M.; WHITE, A.J.R.; DUNCAN, A. R.; and EWART, A. 1969(a). Genetic Significance of Co, Cr, Ni, Sc and V content of andesites. Geochim. Cosmochim. Acta, vol. 33, pp.275-286.

TAYLOR, S. R.; KAYE, M.; WHITE, A.J.R.; DUNCAN, A. R.; and EWART, A. 1969(b). Genetic significance of V and Ni content of andesites : Reply to Prof E. F. Osborn. Geochim. Cosmochim. Acta, vol. 33, pp.155-157.

TAYLOR, S. R.; and WHITE, A.J.R. 1966. Trace Element Abundances in Andesites. Bull. Volc., vol. 29, pp.177-194.

THORNTON, C. P.; and TUTTLE, O. F. 1960. Chemistry of Igneous Rocks : Part I Differentiation Index. Amer. J. Sci., vol. 258, pp.664-684.

TOWNROW, J. A. 1967. On Rissikia and Mataia podocarpaceous conifers from the Lower Mesozoic of Southern Lands. Papers Proc. of the Roy. Soc. of Tasmania, vol. 101, pp.103-36.

VITALIANO, C. J. 1968. Petrology and structure of the south-eastern Marlborough Sounds, New Zealand. N.Z.G.S. Bull. n.s.74, Wellington.

VLODAVETZ, V. I. 1966. The problem of tufflavas and ignimbrites. In "Tufflavas and Ignimbrites" E. F. Cook (Editor), p.1-15. Amer. Elsevier Publ. Co., New York.

WALKER, G.P.L. 1962. Tertiary welded tuffs in Eastern Iceland. Geol. Soc. London. Quart. J., vol. 118, pp.275-293.

WALKER, G.P.L. 1973. Lengths of lava flows. Phil. Trans. Roy. Soc. London, A274, pp.107-118.

WARREN, G. 1967. Sheet 17 Hokitika. "Geological Map of New Zealand 1:250,000". N.Z. Dep. Sci. Industr. Res. Wellington. N.Z.

WATERHOUSE, J. B.; and NORRIS, G. 1972. Paleobotanical solution to a granite conundrum : Hawks Crag Breccia of New Zealand and the tectonic evolution of the South-west Pacific. Geoscience and Man, vol. 9, pp.1-15.

WEBBY, B. D. 1967. Tube Fossils from the Triassic of South-west Wellington, N.Z. Trans. Roy. Soc. N.Z. Geol. vol. 5, no. 7, pp.181-191.

WEDEPOHL, K. H. 1960. Spurenanalytische Untersuchungen an Tiefsectonen aus dem Atlantik. Ein Beitrag zur Deutung der Geochemischen Sorderstellung von Pelagischen Tonen. Geochim. Cosmochim. Acta vol. 18, pp.200-231.

WEDEPOHL, K. H. 1972. Zinc. In "Handbook of Geochemistry". K. H. Wedepohl (Editor), vol. II. Springer-Verlag, Berlin.

WEDEPOHL, K. H. 1974. Lead. In "Handbook of Geochemistry", K. H. Wedepohl (Editor), vol. II. Springer-Verlag, Berlin.

WELLMAN, H. W. 1956. Structural Outline of New Zealand. N.Z.G.S. Bull. 121, Wellington.

WELLMAN, H. W. 1973. New Zealand Fault Zones and Sea-floor Spreading. In "The Western Pacific : Island Arcs, Marginal Seas, Geochemistry." P. J. Coleman (Editor), pp.335-48. Univ. Western Australia Press.

WELLMAN, H. W. 1975. New Zealand 60 M.Y. ago. Bull. Aust. Soc. Explor. Geophys., vol. 6, no.2/3, pp.55-56.

WELLMAN, H. W.; DUNN, L.R.L.; and McDOWELL, I. C. 1945. Clays of the Mount Somers District. N.Z. J. Sci. Tech. vol. 6, no.6, pp.311-326.

WHITFIELD, J. M.; ROGERS, J.J.W.; and ADAMS, J.A.S. 1959. The relationship between the petrology and the thorium and uranium contents of some granitic rocks. Geochim. Cosmochim. Acta. vol. 17, pp.248-271.

WHITTAKER, E.J.W.; and MUNTUS, R. 1970. Ionic radii for use in geochemistry. Geochim. Cosmochim. Acta, vol. 34, pp.945-956.

WILKINSON, J.F.G. 1966. Some Aspects of Calc-alkaline Rock Genesis. J. Proc. Roy. Soc. N.S.W., vol. 99, pp.69-77.

WILKINSON, J.F.G. 1971. The petrology of some vitrophysic calc-alkaline volcanics from the carboniferous of New South Wales. J. Petrol. vol. 12, pp.587-619.

WILLIAMS, H.; TURNER, F. J.; and GILBERT, C. M. 1954. "Petrography. An Introduction to the Study of Rocks in Thin Sections" W. H. Freeman & Co., San Fransisco.

WILLIAMS, R.J.P. 1959. Deposition of trace elements in basic magma. Nature, London, vol. 184, p. 44.

WINKLER, H.G.F.; and PLATEN, H. von. 1961. Experimentelle gesteinsmetamorphose-IV Bildung Anateklischer Schmelzen aus Metamorphisierten Grauwacken. Geochim. Cosmochim. Acta, vol. 24, pp.48-69.

WOOD, B. L. 1969. Stratigraphic column of J. D. George No.1, Canterbury N.Z. Unpublished N.Z. Petroleum Co. Report PR 527. Held in N.Z. Geol. Surv. Library.

WOOD, C. P. 1974. Petrogenesis of Garnet-bearing Rhyolites from Canterbury, New Zealand. N.Z.J. Geol. Geophys., vol. 17, no.4, pp.759-787.

WYLLIE, P. J. 1971. "The Dynamic Earth". John Wiley & Sons Inc., New York.

WYLLIE, P. J.; and TUTTLE, O. F. 1961. Hydrothermal melting of shales. Geol. Mag., vol. 98, pp.56-66.

YODER, H. S. 1969. Calc-alkaline Andesites: Experimental Data Bearing on the Origin of their Assumed Characteristics. In "Proceedings of the Andesite Conference". A. R. McBirney (Editor). State of Oregon. Dep. Geol. & Min. Indust., Bull. 65, pp.77-89.

YODER, H. S., Jr.; and KEITH, M. L. 1951. Complete Substitution of the Aluminium for Silicon : the System $3MnO.Al_2O_3.3SiO_3$-$3Y_2O_3.5Al_2O_3$. Amer. Mineral. vol. 36, pp.519-533.

Appendix I. Definitions of cryptocrystalline quartz varieties found in the Mt Somers Volcanics.

The types of cryptocrystalline quartz present as amygdules in andesites of the Mt Somers area are:

1. Chalcedony: Cryptocrystalline quartz, usually massive but may have visible, or microscopic banding parallel to the walls of the cavity or the free surface. Pale grey to white or brown, smokey or greenish colour.
2. Agate: A subvariety of chalcedony in which successive layers differ in colour and degree of translucency. The bands are continuous and follow the shape of the cavity. Agate bands can be horizontal. Often agate nodules have a centre filled with quartz crystals or amethyst.
3. Onyx: A subvariety of agate in which the horizontal bands are alternately milky white and deep brownish-black, or black.
4. Moss agate: Grey to white translucent to subtransparent agate with moss-like green to black inclusions.
5. Plasma: A dark opaque leek-green to apple-green coloured massive chalcedony.
6. Prase: Translucent leek-green massive chalcedony.

Sample localities for analyses given in Appendix II

(Note: All Grid References from S81 unless stated otherwise).

Analysis No.	Sample No.	
1	PO294	Rhyolite tuff, north-east side of Mt Alford. GR 984506.
2	PO440	Rhyolite xenolith in pitchstone. Woolshed Creek. GR 827454.
3	PO184	Pitchstone. Woolshed Creek. GR 826432.
4	PO534	Rhyolite dike in andesite. Morgan Stream. GR 859484.
5	PO459	Rhyolite xenolith in pitchstone. Woolshed Creek. GR 833444.
6	PO163	Rhyolite tuff. Road to Gawler Downs Trig. GR 885309.
7	PO557	Rhyolite. Bowyers Stream. GR 918457.
8	PO355	Rhyolite. Stour River. GR 809464.
9	PO415	Rhyolite. Cox Hills, Mt Somers. GR 905444.
10	PO258	Green cherty rhyolite at contact with andesite. Clent Hills. GR 788475.
11	PO265	Rhyolite (cherty) "Diamond Fields" opposite Diamond Creek. GR 955504.
12	PO286	Rhyolite tuff with Torlesse xenoliths. North-east side of Mt Alford. GR 990501.
13	PO445	Porphyritic rhyolite. Woolshed Creek. GR 828455.
14	PO458	Rhyolite. Woolshed Creek. GR 830450.
15	PO279(a)	Rhyolite.Mt Alford. GR 970493.
16	PO313	Rhyolite (pink). Summit of Alford Range. GR 970522.
17	PO279(b)	Rhyolite. Mt Alford. GR 970493.
18	PO472	Rhyolite near contact with andesite. Morgan Stream. GR 853481.
19	PO393	Flow-banded rhyolite. Staveley Hill, Mt Somers. GR 913441.
20	PO454	Rhyolite. Ridge between Woolshed and Chapman Creeks. GR 834441.
21	PO450	Rhyolite. Ridge between Woolshed and Chapman Creeks. GR 833439.
22	PO559	Rhyolite. Duke Knob. GR 925455.
23	PO245	Rhyolite. Morgan Stream near confluence with Woolshed Creek. GR 848480.
24	PO252	Rhyolite. Between Stour River and Woolshed Creek. GR 835491.

25	PO316	Rhyolite (flow banded). North end of the Alford Range. GR 971526.
26	PO243	Ignimbrite. Top erosion surface of Mt Somers. GR 866466.
27	PO232	Rhyolite tuff. Underlying andesite above Morgan Stream. GR 867486.
28	PO536	Pitchstone. At base of rhyolite and overlying andesite near Morgan Stream. GR 858483.
29	PO535	Rhyolite. Overlying pitchstone near Morgan Stream. GR 858484.
30	PO479	Ignimbrite. Burma Road. GR 834470.
31	PO409	Pitchstone. Bowyers Stream at confluence with Tinstone Creek. GR 922492.
32	PO457	Pitchstone. Woolshed Creek. GR 827451.
33	PO312	Rhyolite (pink). Summit Alford Range. GR 971515.
34	PO457	Pitchstone. Woolshed Creek. GR 827451.
35	PO551	Rhyolite (flow-banded). Summit Mt Somers. GR 890461.
36	PO554	Rhyolite (flow-banded). Ridge east of the summit of Mt Somers. GR 896460.
37	PO528	Ignimbrite. Top erosion surface of Mt Somers. GR 865475.
38	PO553	Rhyolite (flow-banded). Ridge east of the summit of Mt Somers. GR 896460.
39	PO439	Partially welded rhyolite tuff underlying pitchstone and rhyolite dome. Woolshed Creek. GR 827454.
40	PO308	Pitchstone (fused bedded tuff). North-east side Alford Range. GR 977511.
41	PO176	Rhyolite (flow-banded, garnetiferous). Summit Mt Somers. GR 890460.
42	PO187	Ignimbrite. Ridge between Woolshed and Chapman Creeks. GR 829438.
43	PO414	Rhyolite. Above Staveley Hill on south face of Mt Somers. GR 893453.
44	PO270	Pitchstone (flow-banded). Diamond Creek. GR 961512.
45	PO242	Ignimbrite. Top erosion surface of Mt Somers. GR 872458.
46	PO200	Ignimbrite. Top erosion surface Mt Somers. GR 881471.
47	PO199	Ignimbrite. Upper surface on north face of Mt Somers. GR 880470.
48	PO537	Ignimbrite. Between Woolshed Creek and Morgan Stream. GR 848484.
49	PO240	Rhyolite. Top erosion surface of Mt Somers. GR 876459.

50	PO129	Dacite. South of Blands Bluff. GR 809388.
51	PO291	Rhyolite tuff. South-west side of Mt Alford. GR 964503.
52	PO542	Rhyolite. Duke Knob. GR 924456.
53	PO552	Pitchstone. Summit of Mt Somers. GR 889460.
54	PO544	Rhyolite xenolith from rhyodacite dike on north face of Mt Somers. GR 878473.
55	PO241(a)	Rhyodacite ?dike (with hypersthene; rare olivine and quartz phenocrysts). Top erosion surface of Mt Somers. GR 875458.
56	PO549	Rhyodacite dike (with hypersthene and rare quartz phenocrysts). North face of Mt Somers. GR 878472.
57	PO241	Rhyodacite ?dike (with hypersthene; rare olivine and quartz phenocrysts). Top erosion surface of Mt Somers. GR 875458.
58	PO90	Rhyodacite. Bowyers Stream. GR 824451.
59	PO550	Rhyodacite dike. North face Mt Somers. GR 878473.
60	PO346	Dacite. Gawler Downs. GR 874313.
61	PO555	Dacite.Bowyers Stream above Goldsmiths Rapids. GR 920458.
62	PO147	Dacite. South of Blands Bluff. GR 818378.
63	PO467	Dacite. Gawler Downs (Surrey Hills). GR S91/880275.
64	PO343	Dacite. Gawler Downs. GR 874311.
65	PO428	Dacite. Gawler Downs. GR 880307.
66	PO562	Dacite. Gawler Downs (Surrey Hills). GR S91/886298.
67	PO427	Dacite. Track to Trig on Gawler Downs. GR 882306.
68	PO197	Rhyodacite dike. North face Mt Somers. GR 878471.
69	PO405	Dacite. Bowyers Stream. GR 925450.
70	PO403	Dacite. Bowyers Stream. GR 926450.
71	PO261	Dacite. Winterslow track opposite Diamond Creek. GR 954502.
72	PO462	Dacite. Gawler Downs (Surrey Hills). GR S91/875267.
73	PO341	Dacite. Trig Station on Gawler Downs. GR 880313.
74	PO422	Dacite. Track to Trig Station on Gawler Downs. GR 883308.
75	PO359	Dacite. Branch Hinds River. GR 798370.
76	PO62	Andesite. Clent Hills, Ashburton Gorge. GR 755436.
77	PO456	Andesite. Top surface of Clent Hills. GR 748476.
78	PO182	High-K andesite. Near contact below Mt Barrosa. GR 746479.
79	PO360	Dacite. Gorge of North Branch Hinds River. GR 802372.

80	PO482	High-K andesite dike. Near summit of Mt Barrosa (Clent Hills). GR 759458.
81	PO477	High-K andesite (aphyric). Mt Somers near Morgan Stream. GR 853481.
82	PO478	High-K andesite (porphyritic). Mt Somers near Morgan Stream. GR 853481.
83	PO250	Andesite.Spur between Woolshed Creek and Morgan Stream. GR 857495.
84	PO227	High-K andesite. Mt Somers near Morgan Stream. GR 858476.
85	PO354	High-K andesite. At northern contact, Clent Hills. GR 776483.
86	PO218	Andesite. Upper Woolshed Creek. GR 848492.
87	PO227(a)	High-K andesite. Mt Somers near Morgan Stream. GR 858476.
88	PO485	Andesite. Clent Hills above Ashburton Gorge. GR 769449.
89	PO142	Andesite. Blondin Creek. GR 806400.
90	PO283	Dolerite. South-east side Mt Alford. GR 996496.
91	PO195	Low-Si andesite. Coal Reserve, Ashburton Gorge. GR 780414.
92	PO356	Dolerite. Mt Alford. GR 996496.
93	PO484	Low-Si andesite. Clent Hills near Ashburton Gorge. GR 776448.
94	PO538	Dolerite. North end of Alford Range. GR 961534.
95	PO417	Low-Si andesite. Sandrey Stream. GR 762411.
96	PO295(b)	Dolerite. North-east side of Alford Range. GR 985507.
97	PO306(a)	Dolerite. North-east side of Mt Alford. GR 984504.
98	PO306(b)	Dolerite. North-east side of Mt Alford. GR 984504.
99	PO295(a)	Dolerite. North-east side of Mt Alford. GR 985507.
100	PO305	Dolerite. North-east side of Mt Alford. GR 984504.
101	PO298	Dolerite. North-east side of Mt Alford. GR 983504.
102	PO526	Rhyolite. Rata Peaks. GR 619329.
103	PO508	Rhyolite. On Road near Harper Lodge. GR 586356.
104	PO487	Rhyolite. Near Ben McLeod. GR 588348.
105	PO507	Rhyolite. Track to Hewson River. GR 621309.
106	PO516	Rhyolite. Stew Point. GR 636320.
107	PO496	Rhyolite. Stew Point on Zig-zag track. GR 631334.
108	PO502	Andesite. East of RawTor near Ben McLeod. GR 572338.
109	PO523	High-K andesite. Stew Point. GR S91/662288.

110	PO503	Andesite. Power House Stream. GR 599330.
111	PO504	High-K andesite. Rata Peaks; ridge between Rangitata and Hewson Rivers. GR 607316.
112	PO519	Andesite (altered). Stew Point at headwaters of Middle Stream. GR S91/669289.
113	PO488	Andesite (quartz veined). East of Raw Tor near Ben McLeod. GR 581340.
114	PO506	Andesite. Near Hewson River. GR 611303.
115	PO500	Low-Si andesite. East of Raw Tor near Ben McLeod. GR 575347.
116	PO514	Ignimbrite. South of Round Top. GR S72/166608.
117	PC1	Rhyolite. The island lower end of Rakaia Gorge (P. T. Cox, 1926).
118	PO515	Rhyolite. Rakaia Gorge. GR S82/129585.
119	PO509	Rhyolite. Mt Misery above Clay Pits. GR S74/304629.
120	SP3	Pitchstone. Ridge between two branches of Rockwood Creek. (Speight, 1928).
121	SP2	Rhyolite. High Peak. (Speight, 1928).
122	SP1	Rhyolite. Brockley Creek. (Speight, 1928).
123	PC2	Pitchstone. Lower end of Rakaia Gorge, north side. (P. T. Cox, 1926).
124	PO512	Andesite (aphyric). South of Round Top. GR S72/170609.
125	PC3	High-K andesite. Lower end of Rakaia Gorge, south side. (P. T. Cox, 1926).
126	SP5	High-K andesite. Outcrop north-west of Rockwood Homestead. (Speight, 1928).
127	SP4	High-Al andesite. Middle saddle. (Speight, 1928).
128	PO513	High-Al basalt. South of Round Top. GR S72/170609.
129	PO564	Low-Si andesite. J. D. George No.1 well, Ashburton. GR S92/352095.
130	PO273(a)	Basalt (pillow lava). Tertiary. Taylors Stream by old Winterslow Homestead. GR 959487.
131	PO237(b)	Basalt dike. Trig TT; Mt Somers Range. GR 839526.
132	PO511	Basalt dike. Road to Microwave Station, Pullwool Peak. GR S74/277634.
133	PO272	Basalt (pillow lava) Tertiary. Taylors Stream by old Winterslow Homestead. GR 959487.
134	PO179	Basalt dike. Clent Hills near Ashburton Gorge. GR 736476.
135	PO419	Basalt dike. North branch Ashburton River above Cutty Grass Hut. GR 966548.

Appendix II. Chemical analyses, CIPW Norms, Total iron contents, Larsen Indices, AFM and KCN coordinates for the Mt Somers Volcanics.

MAJOR ELEMENTS.

ANALYSIS:	1.	2.	3.	4.	5.	6.	7.	8.	9.	10.	11.	12.	13.	14.	15.
SiO_2	84.66	80.55	79.40	78.86	78.14	77.87	77.18	76.99	76.92	76.90	76.80	76.76	76.62	76.54	76.47
TiO_2	0.16	0.07	0.09	0.12	0.10	0.09	0.16	0.10	0.10	0.08	0.11	0.20	0.11	0.10	0.11
Al_2O_3	8.16	9.16	11.08	11.51	11.75	10.00	12.24	12.78	12.83	10.62	12.29	10.45	12.79	12.64	13.23
Fe_2O_3	≤1.34	0.20	≤0.74	0.49	≤0.65	≤1.06	0.61	0.34	0.28	≤1.05	≤1.82	≤0.94	≤1.39	0.49	0.27
FeO	-	0.18	-	0.20	-	-	0.17	0.37	0.66	-	-	-	-	0.84	0.45
MnO	0.02	0.01	0.01	0.01	0.02	0.01	0.01	0.01	0.01	0.01	0.01	0.01	0.01	0.02	0.00
MgO	0.15	0.07	0.02	0.24	0.29	0.16	0.09	0.00	0.09	0.19	0.02	0.38	0.14	0.17	0.00
CaO	0.22	0.69	0.71	0.55	0.91	0.37	0.13	0.87	0.73	0.44	0.70	1.55	0.91	0.85	0.73
Na_2O	1.19	1.96	2.61	2.38	2.83	0.54	0.06	3.17	2.92	0.69	3.00	1.66	3.17	3.17	3.01
K_2O	4.27	4.02	4.81	5.03	4.75	6.96	5.85	4.99	5.15	7.58	5.48	3.69	5.10	5.07	5.36
P_2O_5	0.05	0.01	0.02	0.02	0.02	0.02	0.04	0.02	0.02	0.01	0.04	0.06	0.03	0.02	0.03
L.O.I.	0.74	3.05	0.74	1.48	0.86	3.09	2.55	0.50	0.62	2.79	0.36	4.26	0.34	0.29	0.39
TOTAL	100.96	99.97	100.23	100.89	100.32	100.17	99.09	100.14	100.33	100.36	100.63	99.96	100.61	100.20	100.04

ANALYSES RECALCULATED TO 100.00% VOLATILE FREE.

SiO_2	84.59	83.13	79.87	79.37	78.62	80.30	80.00	77.30	77.14	78.90	76.73	80.29	76.52	76.65	76.75
TiO_2	0.16	0.07	0.09	0.12	0.10	0.09	0.17	0.10	0.10	0.08	0.11	0.21	0.11	0.10	0.11
Al_2O_3	8.15	9.45	11.15	11.58	11.82	10.31	12.69	12.83	12.87	10.90	12.28	10.93	12.77	12.66	13.28
Fe_2O_3	0.40	0.12	0.22	0.22	0.20	0.33	0.25	0.23	0.28	0.32	0.55	0.30	0.42	0.43	0.23
FeO	0.80	0.25	0.45	0.43	0.39	0.66	0.50	0.45	0.66	0.65	1.09	0.59	0.83	0.86	0.46
MnO	0.02	0.01	0.01	0.01	0.02	0.01	0.01	0.01	0.01	0.01	0.01	0.01	0.01	0.02	0.00
MgO	0.15	0.07	0.02	0.24	0.29	0.17	0.09	0.00	0.09	0.20	0.02	0.40	0.14	0.17	0.00
CaO	0.22	0.71	0.71	0.55	0.92	0.38	0.14	0.87	0.73	0.45	0.70	1.62	0.91	0.85	0.73
Na_2O	1.19	2.02	2.63	2.40	2.85	0.56	0.06	3.18	2.93	0.71	3.00	1.74	3.17	3.17	3.02
K_2O	4.27	4.15	4.84	5.06	4.78	7.18	6.06	5.01	5.17	7.78	5.48	3.86	5.09	5.08	5.38
P_2O_5	0.05	0.01	0.02	0.02	0.02	0.02	0.04	0.02	0.02	0.01	0.04	0.06	0.03	0.02	0.03

ANALYSIS:	1.	2.	3.	4.	5.	6.	7.	8.	9.	10.	11.	12.	13.	14.	15.
C.I.P.W. NORMS.															
Q	60.37	53.77	44.35	44.38	41.23	48.23	55.91	37.57	38.32	43.42	36.30	51.30	36.08	36.24	36.89
C	1.30	-	0.34	1.21	0.35	0.98	5.88	0.63	1.18	0.52	0.25	1.10	0.47	0.44	1.23
or	25.21	24.51	28.59	29.92	28.24	42.41	35.83	29.60	30.52	45.96	32.36	22.81	30.10	30.00	31.79
ab	10.06	17.12	22.22	20.27	24.09	4.71	0.53	26.93	24.78	5.99	25.36	14.69	26.79	26.86	25.56
an	0.76	3.47	3.41	2.62	4.41	1.76	0.40	4.20	3.50	2.17	3.21	7.63	4.31	4.09	3.44
hy fs	0.92	0.25	0.51	0.43	0.43	0.80	0.45	0.50	0.84	0.80	1.29	0.51	1.02	1.09	0.47
hy en	0.37	0.18	0.05	0.60	0.73	0.41	0.23	-	0.23	0.49	0 .05	0.99	0.35	0.42	0.00
mt	0.58	0.18	0.32	0.31	0.28	0.48	0.36	0.33	0.41	0.47	0.79	0.43	0.60	0.62	0.34
il	0.30	0.14	0.17	0.23	0.19	0.18	0.32	0.191	0.19	0.17	0.21	0.40	0.21	0.19	0.21
ap	0.12	0.02	0.05	0.05	0.05	0.05	0.10	0.19	0.05	0.02	0.09	0.15	0.07	0.05	0.07
TOTAL IRON AS-															
%Fe_2O_3	1.29	0.40	0.72	0.69	0.63	1.06	0.80	0.73	1.02	1.04	1.76	0.95	1.34	1.38	0.75
%FeO	1.17	0.36	0.65	0.62	0.57	0.95	0.72	0.66	0.92	0.94	1.58	0.86	1.21	1.24	0.67
LARSEN INDEX-															
	31.26	30.80	30.25	30.27	29.36	32.72	31.98	29.42	0.92	32.76	29.22	27.99	28.69	28.72	29.74
D.I.	95.65	95.40	95.15	94.56	93.56	95.35	92.27	94.10	93.62	95.37	94.01	88.79	92.96	93.10	94.24
C.I.	1.57	3.85	3.52	3.91	5.98	2.64	0.90	4.20	3.99	3.22	3.32	9.77	5.06	5.01	3.44
CO-ORDINATES FOR AFM DIAGRAM															
%Fe_2O_3+FeO															
	17.69	5.62	8.21	7.73	6.92	11.07	10.70	7.65	10.33	10.05	16.15	12.86	12.95	13.22	7.65
%MgO	2.20	1.09	0.25	2.89	3.43	1.86	1.34	0.00	0.99	2.02	0.20	5.78	1.45	1.75	0.00
%Na_2O+K_2O															
	80.11	93.29	91.54	89.38	89.65	87.07	87.96	92.35	88.68	87.93	83.65	81.36	85.60	85.03	92.35
CO-ORDINATES FOR KCN DIAGRAM															
%K_2O	75.18	60.27	59.16	63.19	55.95	88.44	96.85	55.26	58.52	87.03	59.69	53.48	55.56	55.78	58.90
%Na_2O	20.95	29.39	32.10	29.90	33.33	6.86	0.99	35.11	33.18	7.92	32.68	24.06	34.53	34.87	33.08
%CaO	3.87	10.34	8.73	6.91	10.72	4.70	2.15	9.63	8.30	5.05	7.63	22.46	9.91	9.35	8.02

MAJOR ELEMENTS.

ANALYSIS:	16.	17.	18.	19.	20.	21.	22.	23.	24.	25.	26.	27.	28.	29.	30.
SiO_2	76.45	76.45	76.27	76.13	75.99	75.73	75.63	75.22	75.18	74.90	74.83	74.82	74.70	74.64	74.59
TiO_2	0.11	0.12	0.10	0.11	0.10	0.10	0.17	0.13	0.23	0.11	0.18	0.01	0.10	0.18	0.18
Al_2O_3	13.22	13.21	12.05	13.54	12.55	12.89	12.95	13.12	12.21	13.10	14.50	11.64	12.32	14.67	14.36
Fe_2O_3	≤0.94	≤0.85	1.86	0.33	0.88	0.83	≤3.64	≤1.86	≤2.39	≤1.06	≤0.18	≤0.27	0.91	≤0.64	≤0.58
FeO	—	—	0.16	0.54	0.64	0.52	—	—	—	—	—	—	0.49	—	—
MnO	0.00	0.00	0.02	0.01	0.02	0.01	0.02	0.02	0.02	0.00	0.01	0.00	0.02	0.01	0.01
MgO	0.03	0.00	0.06	0.04	0.17	0.05	0.17	0.08	0.40	0.15	0.08	0.13	0.08	0.46	0.09
CaO	0.73	0.75	0.72	0.56	0.56	0.64	0.05	1.04	1.00	0.40	1.05	0.42	0.93	1.11	1.05
Na_2O	3.02	3.27	2.69	2.63	2.40	2.54	0.24	3.34	2.52	2.29	3.04	0.63	4.38	3.15	3.33
K_2O	5.31	5.39	5.36	5.12	5.29	5.73	1.45	5.15	4.50	5.41	5.60	8.54	2.80	5.71	5.78
P_2O_5	0.02	0.03	0.02	0.02	0.02	0.02	0.04	0.04	0.05	0.02	0.04	0.04	0.02	0.05	0.05
L.O.I.	0.33	0.47	1.58	1.73	1.78	1.70	5.85	0.45	1.95	1.34	0.74	4.10	4.13	0.87	0.72
TOTAL	100.40	100.30	100.89	100.76	100.40	100.76	100.21	100.45	100.45	98.78	100.88	100.60	110.88	101.49	100.74

ANALYSES RECALCULATED TO 100.00% VOLATILE FREE.

SiO_2	76.65	76.46	76.94	76.90	77.12	76.51	80.46	75.36	76.51	76.95	75.21	77.56	77.28	74.23	74.62
TiO_2	0.11	0.12	0.10	0.11	0.10	0.10	0.18	0.13	0.23	0.11	0.18	0.01	0.10	0.18	0.18
Al_2O_3	13.26	13.21	12.16	13.68	12.74	13.02	13.78	13.14	12.43	13.46	14.57	12.07	12.75	14.59	14.37
Fe_2O_3	0.28	0.26	0.62	0.28	0.43	0.43	1.16	0.56	0.73	0.33	0.05	0.08	0.45	0.19	0.17
FeO	0.57	0.51	1.23	0.56	0.97	0.85	2.32	1.12	1.46	0.65	0.11	0.17	0.90	0.38	0.35
MnO	0.00	0.00	0.02	0.01	0.02	0.01	0.02	0.02	0.02	0.00	0.01	0.00	0.02	0.01	0.01
MgO	0.03	0.00	0.06	0.04	0.17	0.05	0.18	0.08	0.41	0.15	0.08	0.14	0.08	0.46	0.09
CaO	0.73	0.75	0.73	0.57	0.57	0.65	0.05	1.04	1.02	0.41	1.06	0.44	0.96	1.10	1.05
Na_2O	3.03	3.27	2.71	2.66	2.44	2.57	0.26	3.35	2.57	2.35	3.06	0.65	4.53	3.13	3.33
K_2O	5.32	5.39	5.41	5.17	5.37	5.79	1.54	5.16	4.58	5.56	5.63	8.85	2.90	5.68	5.78
P_2O_5	0.02	0.03	0.02	0.02	0.02	0.02	0.04	0.04	0.05	0.02	0.04	0.04	0.02	0.05	0.05
TOTAL	100.00	100.00	100.00	100.00	100.00	100.00	100.00	100.00	100.00	100.00	100.00	100.00	100.00	100.00	100.00

ANALYSIS:	16.	17.	18.	19.	20.	21.	22.	23.	24.	25.	26.	27.	28.	29.	30.
C.I.P.W. NORMS.															
Q	36.82	35.05	38.14	40.15	40.42	37.54	71.42	33.27	40.64	40.61	33.63	38.76	37.19	31.25	30.77
C	1.23	0.71	0.57	2.73	1.93	1.41	11.69	0.26	1.52	2.87	1.63	0.72	0.46	1.40	0.84
or	31.46	31.86	31.95	30.56	31.73	34.21	9.12	30.49	27.06	32.85	33.26	52.31	17.12	33.56	34.17
ab	25.62	27.67	22.96	22.48	20.61	21.72	2.16	28.32	21.70	19.91	25.86	5.53	38.34	26.51	28.19
an	3.50	3.53	3.47	2.67	2.69	3.08	0.00	4.91	4.72	1.91	4.97	1.89	4.64	5.15	4.88
hy fs	0.62	0.53	1.63	0.64	1.25	1.07	3.05	1.41	1.73	0.74	-	0.22	1.15	0.27	0.22
hy en	0.08	0.00	0.15	0.10	0.43	0.13	0.45	0.20	1.01	0.38	0.20	0.34	0.21	1.14	0.22
mt	0.41	0.37	0.89	0.41	0.70	0.62	1.68	0.81	1.06	0.47	-	0.12	0.65	0.28	0.25
il	0.21	0.23	0.19	0.21	0.19	0.19	0.34	0.25	0.45	0.22	0.25	0.02	0.20	0.34	0.34
ap	0.05	0.07	0.05	0.05	0.05	0.05	0.10	0.09	0.12	0.05	0.09	0.10	0.05	0.12	0.12
hm	-	-	-	-	-	-	-	-	-	-	0.05	-	-	-	-
TOTAL IRON AS-															
%Fe_2O_3	0.91	0.82	1.99	0.91	1.56	1.38	3.74	1.80	2.35	1.05	0.18	0.27	1.46	0.62	0.56
%FeO	0.82	0.74	1.79	0.82	1.41	1.24	3.37	1.62	2.12	0.95	0.16	0.24	1.31	0.55	0.51
LARSEN INDEX-															
	29.52	29.59	29.01	29.61	29.34	29.72	25.78	28.02	27.17	29.97	29.43	33.94	26.68	28.45	29.14
D.I.	93.91	94.58	93.05	93.19	92.76	93.47	82.70	92.07	89.40	93.36	92.75	96.50	92.65	91.31	93.13
C.I.	3.66	3.53	3.08	2.89	3.61	3.35	0.96	5.34	6.90	2.73	5.41	2.61	5.08	7.61	5.37
CO-ORDINATES FOR AFM DIAGRAM															
%Fe_2O_3+FeO															
	9.19	8.12	18.44	9.70	15.41	13.21	63.78	16.34	22.47	10.83	1.82	2.55	15.27	5.82	5.37
%MgO	0.33	0.00	0.60	0.46	1.83	0.52	3.31	0.78	4.18	1.70	0.90	1.36	0.93	4.65	0.93
%Na_2O+K_2O															
	90.49	91.88	80.96	89.84	82.76	86.26	32.91	82.88	73.35	87.46	97.28	96.09	83.79	89.53	93.71
CO-ORDINATES FOR KCN DIAGRAM															
%K_2O	58.61	57.28	61.12	61.61	64.12	64.31	83.33	54.04	56.11	66.79	57.79	89.05	34.53	57.27	56.89
%Na_2O	33.33	34.75	30.67	31.65	29.09	28.51	13.79	35.05	31.42	28.27	31.37	6.57	53.01	31.59	32.78
%CaO	8.06	7.97	8.21	6.74	6.79	7.18	2.87	10.91	12.47	4.94	10.84	4.38	11.47	11.13	10.33

MAJOR ELEMENTS.

ANALYSIS:	31.	32.	33.	34.	35.	36.	37.	38.	39.	40.	41.	42.	43.	44.	45.
SiO_2	74.46	74.40	74.39	74.22	74.20	74.02	73.95	73.92	73.47	73.05	73.03	72.98	72.87	72.83	72.04
TiO_2	0.10	0.10	0.11	0.10	0.17	0.17	0.19	0.18	0.09	0.03	0.19	0.09	0.19	0.11	0.19
Al_2O_3	12.29	12.36	13.13	12.37	14.12	13.52	14.15	14.14	11.22	13.13	13.96	11.82	13.93	12.51	14.17
Fe_2O_3	0.67	0.66	≤ 2.32	0.66	0.40	1.16	0.50	0.47	0.45	≤1.70	1.56	≤1.16	1.58	≤1.80	1.14
FeO	0.83	0.80	—	0.80	0.43	0.79	0.32	0.47	0.19	—	0.50	—	0.70	—	0.31
MnO	0.02	0.02	0.01	0.02	0.01	0.03	0.01	0.01	0.01	0.01	0.02	0.01	0.02	0.01	0.01
MgO	0.05	0.00	0.08	0.03	0.16	0.08	0.16	0.25	0.23	0.03	0.13	0.29	0.06	0.05	0.07
CaO	0.90	0.92	0.32	0.92	1.06	1.22	1.09	1.17	1.24	0.73	1.05	1.04	1.31	0.85	1.16
Na_2O	3.47	3.27	2.02	3.20	2.74	3.14	3.08	3.18	0.93	3.63	3.08	1.02	3.18	3.73	3.29
K_2O	4.24	4.51	5.50	4.50	5.60	5.23	5.51	5.43	5.96	4.32	5.59	5.42	5.35	4.24	5.49
P_2O_5	0.02	0.03	0.02	0.03	0.05	0.04	0.04	0.04	0.01	0.01	0.04	0.01	0.04	0.03	0.05
L.O.I.	3.30	3.62	3.62	2.52	1.46	1.03	1.42	0.85	6.33	4.11	1.40	6.26	1.58	3.87	1.52
TOTAL	100.35	100.69	100.47	100.48	100.49	100.42	100.41	100.11	100.13	100.75	100.54	100.10	100.81	100.03	99.44

ANALYSES RECALCULATED TO 100.00% VOLATILE FREE.

SiO_2	76.78	76.69	76.17	76.70	75.03	74.55	74.74	74.51	78.36	75.72	73.77	77.87	73.55	75.88	73.66
TiO_2	0.10	0.10	0.11	0.10	0.17	0.17	0.19	0.18	0.10	0.03	0.19	0.10	0.19	0.12	0.19
Al_2O_3	12.67	12.78	13.44	12.74	14.28	13.62	14.30	14.25	11.97	13.61	14.10	12.61	14.06	13.03	14.49
Fe_2O_3	0.49	0.48	0.71	0.48	0.27	0.62	0.26	0.30	0.21	0.53	0.64	0.37	0.71	0.56	0.46
FeO	0.99	0.96	1.43	0.96	0.53	1.23	0.52	0.60	0.42	1.06	1.28	0.74	1.43	1.13	0.91
MnO	0.02	0.02	0.01	0.02	0.01	0.03	0.01	0.01	0.01	0.01	0.02	0.01	0.02	0.01	0.01
MgO	0.05	0.03	0.08	0.00	0.16	0.08	0.16	0.25	0.25	0.03	0.13	0.31	0.06	0.05	0.07
CaO	0.93	0.95	0.33	0.95	1.07	1.23	1.10	1.18	1.32	0.76	1.06	1.11	1.32	0.89	1.19
Na_2O	3.58	3.31	2.07	3.37	2.77	3.16	3.11	3.21	0.99	3.76	3.11	1.09	3.21	3.89	3.36
K_2O	4.37	4.65	5.63	4.65	5.66	5.27	5.57	5.47	6.36	4.48	5.65	5.78	5.40	4.42	5.61
P_2O_5	0.02	0.03	0.02	0.03	0.05	0.04	0.04	0.04	0.01	0.01	0.04	0.01	0.04	0.03	0.05
TOTAL	100.00	100.00	100.00	100.00	100.00	100.00	100.00	100.00	100.00	100.00	100.00	100.00	100.00	100.00	100.00

ANALYSIS:	31.	32.	33.	34.	35.	36.	37.	38.	39.	40.	41.	42.	43.	44.	45.
C.I.P.W. NORMS.															
Q	36.65	37.10	40.97	36.79	34.62	32.66	32.63	31.87	44.89	34.39	46.18	30.61	33.83	29.65	29.37
C	0.42	0.66	3.40	0.51	1.76	0.58	1.25	1.01	1.08	1.22	2.57	0.63	0.32	0.84	0.04
or	25.84	27.48	33.28	27.47	33.46	31.13	32.91	32.34	37.57	26.46	34.17	31.91	26.11	33.17	31.70
ab	30.28	27.98	17.50	28.53	23.44	26.76	26.34	27.12	8.39	31.84	9.21	27.16	32.88	28.46	29.31
an	4.47	4.51	1.49	4.50	4.99	5.83	5.20	5.59	6.49	3.69	5.44	6.30	4.19	5.55	6.00
hy fs	1.27	1.23	1.86	1.23	0.49	1.53	0.44	0.57	0.46	1.47	0.92	1.75	1.43	0.99	1.87
hy en	0.13	0.08	0.20	-	0.40	0.20	0.40	0.63	0.61	0.08	0.77	0.51	0.13	0.18	0.15
mt	0.71	0.70	1.03	0.69	0.39	0.84	0.38	0.44	0.31	0.77	0.54	1.04	0.82	0.66	1.08
il	0.20	0.20	0.21	0.20	0.33	0.33	0.37	0.35	0.18	0.06	0.18	0.36	0.22	0.37	0.35
ap	0.05	0.07	0.05	0.07	0.12	0.09	0.09	0.09	0.03	0.02	0.03	0.09	0.07	0.12	0.12
TOTAL IRON AS-															
%Fe_2O_3	1.59	1.55	2.30	1.54	0.86	1.98	0.84	0.97	0.68	1.70	2.07	1.20	2.30	1.81	1.47
%FeO	1.43	1.39	2.07	1.39	0.77	1.79	0.75	0.87	0.61	1.53	1.86	1.08	2.07	1.63	1.32
LARSEN INDEX-															
	27.97	28.24	29.16	28.28	28.88	27.55	28.67	28.25	30.46	27.85	27.74	29.55	27.08	27.62	27.97
D.I.	92.76	92.56	91.75	92.79	91.53	90.55	91.88	91.33	90.84	92.69	90.70	89.56	89.68	92.82	91.29
C.I.	4.75	4.68	1.93	4.50	5.86	6.27	6.07	6.94	7.81	3.85	5.70	7.10	6.62	4.47	5.93
CO-ORDINATES FOR AFM DIAGRAM															
%Fe_2O_3+FeO															
	15.59	15.28	21.53	15.19	8.50	17.85	8.09	9.16	7.71	16.09	17.79	13.43	19.81	16.80	13.11
%MgO	0.54	0.33	0.83	0.00	1.72	0.78	1.68	2.56	2.98	0.32	1.21	3.73	0.56	0.52	0.69
%Na_2O+K_2O															
	83.87	84.39	77.62	84.81	89.77	81.39	90.23	88.28	89.31	83.60	81.00	82.84	79.63	82.68	86.20
CO-ORDINATES FOR KCN DIAGRAM															
%K_2O	49.25	52.20	70.15	51.84	59.57	54.54	56.92	55.52	73.31	49.77	57.51	72.46	54.37	48.07	55.23
%Na_2O	40.30	37.12	25.77	37.59	29.15	32.74	31.82	32.52	11.44	41.82	31.69	13.64	32.32	42.29	33.10
%CaO	10.45	10.67	4.08	10.57	11.28	12.72	11.26	11.96	15.25	8.41	10.80	13.90	13.31	9.64	11.67

MAJOR ELEMENTS.

ANALYSIS:	46.	47.	48.	49.	50.	51.	52.	53.	54.	55.	56.	57.	58.	59.	60.
SiO_2	72.01	71.82	71.57	71.26	71.09	70.78	70.56	70.12	70.09	69.39	69.03	68.98	68.95	67.99	66.80
TiO_2	0.18	0.21	0.17	0.21	0.81	0.02	0.71	0.20	0.32	0.30	0.30	0.29	0.34	0.29	0.83
Al_2O_3	13.45	14.10	14.15	13.97	15.09	11.93	13.71	13.83	14.00	14.30	14.21	14.17	14.31	14.11	15.11
Fe_2O_3	≤2.43	≤2.30	2.10	≤2.93	0.73	≤0.68	≤4.31	0.98	1.75	1.09	2.19	≤4.08	≤3.95	2.12	0.45
FeO	—	—	0.15	—	0.20	—	—	1.37	1.00	2.68	1.34	—	—	0.72	4.16
MnO	0.03	0.01	0.01	0.04	0.02	0.00	0.02	0.04	0.04	0.07	0.04	0.07	0.03	0.03	0.09
MgO	0.06	0.06	0.21	0.09	0.26	0.56	0.21	0.17	0.11	0.17	0.25	0.32	0.19	0.22	1.09
CaO	1.25	1.34	0.35	1.38	2.65	0.93	0.22	1.39	1.76	1.78	1.81	1.81	1.81	1.84	3.03
Na_2O	3.39	3.17	1.74	3.29	3.65	1.74	0.65	3.79	3.46	3.73	3.59	4.73	3.33	3.45	3.65
K_2O	5.25	5.37	5.37	5.32	4.37	4.98	5.87	4.13	4.96	4.24	4.60	4.18	5.02	4.33	3.72
P_2O_5	0.05	0.06	0.04	0.06	0.26	0.01	0.22	0.06	0.10	0.09	0.10	0.10	0.11	0.10	0.26
L.O.I.	1.63	1.43	4.13	1.45	1.31	9.08	3.56	4.13	2.33	2.56	2.99	2.60	0.26	4.88	1.16
TOTAL	99.73	99.86	99.99	100.00	101.33	100.71	100.04	100.21	99.92	100.38	100.45	101.34	98.30	100.07	100.35

ANALYSES RECALCULATED TO 100.00% VOLATILE FREE.

SiO_2	73.59	73.13	74.83	72.52	71.77	77.30	73.46	73.06	71.95	70.92	70.99	70.16	70.61	71.58	67.35
TiO_2	0.18	0.21	0.18	0.21	0.82	0.02	0.74	0.21	0.33	0.31	0.31	0.30	0.35	0.31	0.84
Al_2O_3	13.75	14.36	14.79	14.22	15.23	13.03	14.27	14.41	14.37	14.62	14.61	14.41	14.66	14.86	15.23
Fe_2O_3	0.75	0.70	0.71	0.89	0.29	0.22	1.35	0.78	0.88	1.11	1.14	1.25	1.21	0.92	0.45
FeO	1.49	1.41	1.42	1.79	0.58	0.45	2.69	1.56	1.76	2.74	2.27	2.49	2.43	1.84	4.19
MnO	0.03	0.01	0.01	0.04	0.02	0.00	0.21	0.04	0.04	0.07	0.04	0.07	0.03	0.03	0.09
MgO	0.06	0.06	0.22	0.09	0.26	0.61	0.22	0.18	0.11	0.17	0.26	0.33	0.20	0.23	1.10
CaO	1.28	1.36	0.37	1.40	2.68	1.02	0.23	1.45	1.81	1.82	1.86	1.84	1.85	1.94	3.06
Na_2O	3.46	3.23	1.82	3.35	3.69	1.90	0.68	3.95	3.55	3.81	3.69	4.81	3.41	3.63	3.68
K_2O	5.37	5.47	5.61	5.41	4.41	5.44	6.11	4.30	5.09	4.33	4.73	4.25	5.14	4.56	3.75
P_2O_5	0.05	0.06	0.04	0.06	0.26	0.01	0.23	0.06	0.10	0.09	0.10	0.10	0.11	0.11	0.26
TOTAL	100.00	100.00	100.00	100.00	100.00	100.00	100.00	100.00	100.00	100.00	100.00	100.00	100.00	100.00	100.00

ANALYSIS:	46.	47.	48.	49.	50.	51.	52.	53.	54.	55.	56.	57.	58.	59.	60.
C.I.P.W. NORMS.															
Q	29.37	29.83	40.97	28.32	28.07	42.11	44.76	29.54	27.14	26.56	26.06	21.02	25.82	27.82	21.36
C	0.04	0.79	5.16	0.44	0.16	2.20	6.68	0.77	-	0.57	0.28	-	0.38	0.68	0.19
or	31.70	32.31	33.18	32.00	26.07	32.14	36.12	25.43	30.09	25.61	27.95	25.12	30.38	26.94	22.16
ab	29.31	27.31	15.39	28.33	31.18	16.08	5.73	33.41	30.06	32.26	31.24	40.71	28.86	30.73	31.14
an	6.00	6.37	1.54	6.57	11.56	4.97	-	6.78	8.23	8.43	8.56	5.17	8.46	8.92	13.44
di wo	-	-	-	-	-	-	-	-	0.03	-	-	1.38	-	-	-
di fs	-	-	-	-	-	-	-	-	0.02	-	-	1.17	-	-	-
di en	-	-	-	-	-	-	-	-	-	-	-	0.30	-	-	-
hy fs	1.87	1.67	1.75	2.27	-	0.60	2.65	1.96	2.02	3.74	2.80	2.02	2.94	2.18	6.11
hy en	0.15	0.15	0.55	0.23	0.65	1.52	0.55	0.44	0.28	0.43	0.64	0.51	0.49	0.58	2.74
mt	1.08	1.02	1.03	1.30	-	0.32	1.95	1.13	1.28	1.62	1.65	1.80	1.76	1.34	0.66
il	0.35	0.41	0.34	0.41	1.26	0.04	1.40	0.40	0.62	0.58	0.59	0.56	0.66	0.58	1.59
ap	0.12	0.14	0.10	0.14	0.61	0.03	0.53	0.15	0.24	0.21	0.24	0.24	0.26	0.24	0.61
hm	-	-	-	-	0.29	-	-	-	-	-	-	-	-	-	-
TOTAL IRON AS-															
%$Fe0_2O_3$	2.40	2.26	2.29	2.88	0.93	0.72	4.34	2.52	2.84	4.16	3.66	4.01	3.91	2.97	5.11
%FeO	2.16	2.04	2.06	2.59	0.84	0.65	3.90	2.27	2.56	3.74	3.29	3.61	3.52	2.67	4.60
LARSEN INDEX-															
	27.04	26.99	28.52	26.28	24.80	29.11	27.44	25.44	25.37	23.22	23.98	22.96	24.18	24.38	17.83
D.I.	90.39	89.45	89.54	88.65	85.32	90.33	86.60	88.38	87.28	84.43	85.25	86.85	85.06	85.49	74.66
C.I.	6.33	6.70	2.72	7.06	12.97	8.25	0.81	7.73	8.83	9.36	9.94	6.28	9.51	10.17	19.35
CO-ORDINATES FOR AFM DIAGRAM															
%Fe_2O_3+FeO															
	20.09	19.40	21.79	23.26	9.38	7.75	36.56	21.77	23.19	31.65	28.17	28.46	29.39	24.72	35.27
%MgO	0.55	0.56	2.24	0.79	2.85	7.10	1.98	1.64	0.99	1.43	2.13	2.48	1.57	2.07	8.34
%Na_2O+K_2O															
	79.36	80.04	75.96	75.95	87.78	85.15	61.46	76.58	75.82	66.92	69.70	69.06	69.04	73.21	56.39
CO-ORDINATES FOR KCN DIAGRAM															
%K_2O	53.08	54.35	71.98	53.25	40.96	65.10	87.09	44.36	48.72	43.49	46.00	38.99	49.41	45.01	35.77
%Na_2O	34.28	32.09	23.32	32.93	34.21	22.75	9.64	40.71	33.99	38.26	35.90	44.12	32.78	35.86	35.10
%CaO	12.64	13.56	4.69	13.81	24.84	12.16	3.26	14.93	17.29	18.26	18.10	16.88	17.81	19.13	29.13

MAJOR ELEMENTS.

ANALYSIS:	61.	62.	63.	64.	65.	66.	67.	68.	69.	70.	71.	72.	73.	74.	75.
SiO_2	66.78	66.63	66.50	66.41	66.16	65.66	65.63	65.59	65.33	64.44	63.92	63.22	62.92	62.79	62.67
TiO_2	0.79	0.84	1.00	0.83	0.84	0.92	0.94	0.32	0.81	0.88	1.06	1.16	1.10	0.97	1.12
Al_2O_3	15.28	15.14	17.09	14.99	15.17	15.42	15.53	14.12	15.31	15.36	15.46	15.73	15.50	16.54	15.62
Fe_2O_3	0.86	0.85	0.95	2.30	1.24	0.77	1.83	≤ 4.07	1.07	0.50	2.74	1.88	1.65	0.91	0.64
FeO	1.63	3.56	0.75	2.18	2.65	3.68	1.90	—	3.29	4.78	2.93	3.98	4.42	0.72	5.38
MnO	0.04	0.08	0.03	0.05	0.08	0.08	0.05	0.05	0.07	0.11	0.09	0.10	0.11	0.03	0.11
MgO	0.60	0.97	0.70	0.99	0.94	1.37	0.87	0.39	1.02	1.23	1.80	2.26	1.55	0.97	2.19
CaO	2.19	3.07	3.19	2.95	3.06	3.12	3.01	2.01	3.28	3.51	3.53	4.15	3.72	3.80	4.15
Na_2O	1.43	3.60	3.37	3.13	3.33	3.77	3.36	3.44	3.73	3.68	3.92	3.25	3.38	2.66	3.40
K_2O	4.28	3.57	3.91	3.91	3.34	3.09	3.78	4.25	3.14	3.10	3.36	3.19	3.15	2.56	2.77
P_2O_5	0.25	0.28	0.28	0.27	0.26	0.27	0.26	0.11	0.24	0.28	0.27	0.29	0.29	0.24	0.26
L.O.I.	5.89	2.53	2.95	1.51	3.35	2.42	2.89	4.87	2.98	2.27	2.02	1.91	2.77	8.52	2.03
TOTAL	100.02	101.12	100.73	99.54	100.41	100.57	100.03	99.22	100.28	100.14	101.08	101.11	100.54	100.71	100.34

ANALYSES RECALCULATED TO 100.00% VOLATILE FREE.

SiO_2	71.01	67.58	68.08	67.92	68.16	66.90	67.68	69.82	67.15	65.84	64.69	63.72	64.34	68.18	63.75
TiO_2	0.84	0.85	1.02	0.85	0.87	0.94	0.97	0.34	0.83	0.90	1.07	1.17	1.13	1.05	1.14
Al_2O_3	16.25	15.36	17.50	15.33	15.63	15.71	16.01	15.03	15.74	15.69	15.65	15.86	15.85	17.96	15.89
Fe_2O_3	0.85	0.86	0.55	1.45	1.28	0.79	1.22	1.30	1.10	0.51	1.82	1.90	1.67	0.56	0.65
FeO	1.70	3.61	1.10	2.90	2.73	3.75	2.44	2.50	3.38	4.88	3.64	4.01	4.52	1.11	5.47
MnO	0.04	0.08	0.03	0.05	0.08	0.08	0.05	0.05	0.07	0.11	0.09	0.10	0.11	0.03	0.11
MgO	0.64	0.98	0.72	1.01	0.97	1.40	0.90	0.42	1.05	1.26	1.82	2.28	1.59	1.05	2.23
CaO	2.33	3.11	3.27	3.02	3.15	3.18	3.10	2.14	3.37	3.57	3.57	4.18	3.80	4.13	4.22
Na_2O	1.52	3.65	3.45	3.20	3.43	3.84	3.47	3.66	3.83	3.76	3.97	3.28	3.46	2.89	3.46
K_2O	4.55	3.62	4.00	4.00	3.44	3.15	3.90	4.52	3.23	3.17	3.40	3.22	3.22	2.78	2.82
P_2O_5	0.27	0.28	0.29	0.28	0.27	0.28	0.27	0.12	0.25	0.29	0.27	0.29	0.30	0.26	0.26
TOTAL	100.00	100.00	100.00	100.00	100.00	100.00	100.00	100.00	100.00	100.00	100.00	100.00	100.00	100.00	100.00

ANALYSIS:	61.	62.	63.	64.	65.	66.	67.	68.	69.	70.	71.	72.	73.	74.	75.
C.I.P.W. NORMS.															
Q	39.05	23.05	25.44	25.52	26.37	22.19	24.48	24.86	22.56	19.79	17.61	18.98	19.84	31.06	17.66
C	5.22	0.45	2.24	0.91	1.17	0.86	1.09	0.50	0.40	0.24	-	0.08	0.47	3.32	0.11
or	26.89	21.40	23.66	23.63	20.33	18.60	23.03	26.73	19.07	18.72	20.10	19.00	19.04	16.43	16.65
ab	12.87	30.90	29.20	27.09	29.03	32.50	29.32	30.99	32.44	31.82	33.57	27.72	29.25	24.44	29.27
an	9.82	13.59	14.33	13.16	13.89	13.97	13.65	9.85	15.11	15.92	14.84	18.84	16.94	18.77	19.21
di wo	-	-	-	-	-	-	-	-	-	-	0.46	-	-	-	-
di fs	-	-	-	-	-	-	-	-	-	-	0.20	-	-	-	-
di en	-	-	-	-	-	-	-	-	-	-	0.25	-	-	-	-
hy fs	1.12	4.66	-	2.82	2.68	4.84	1.97	3.24	4.06	7.27	3.38	4.06	5.26	-	7.84
hy en	1.59	2.45	1.80	2.52	2.41	3.48	2.24	1.03	2.61	3.13	4.29	5.67	3.95	2.62	5.55
mt	1.24	1.25	0.66	2.10	1.85	1.14	1.77	1.88	1.60	0.74	2.64	2.75	2.45	0.64	0.94
il	1.60	1.62	1.94	1.61	1.64	1.78	1.84	0.65	1.58	1.71	2.04	2.22	2.14	2.00	2.16
ap	0.62	0.66	0.66	0.64	0.62	0.64	0.62	0.27	0.57	0.66	0.63	0.68	.69	0.60	0.61
hm	-	-	-	-	-	-	-	-	-	-	-	-	-	-	-
TOTAL IRON AS-															
%Fe_2O_3	2.75	4.88	1.77	4.67	4.31	4.95	3.93	4.19	4.86	5.94	5.87	6.35	6.71	1.80	6.73
%FeO	2.47	4.39	1.59	4.20	3.88	4.46	3.54	3.77	4.37	5.34	5.28	5.72	6.04	1.62	6.06
LARSEN INDEX-															
	23.53	18.42	21.60	19.69	19.29	17.10	20.00	22.62	17.79	15 37	15.91	13.96	14.74	19.19	12.12
D.I.	78.81	75.32	78.29	76.23	75.73	73.29	76.83	82.58	74.07	70.32	71.28	65.70	68.12	71.93	63.57
C.I.	13.24	18.88	18.18	18.60	19.09	21.47	18.47	12.08	20.75	22.68	24.10	31.08	25.46	24.43	31.18
CO-ORDINATES FOR AFM DIAGRAM															
%Fe_2O_3+FeO															
	27.59	35.14	16.74	34.61	33.83	35.09	30.69	31.19	35.59	39.73	37.27	40.25	42.90	19.91	41.86
%MgO	6.89	7.73	7.30	8.06	8.17	10.80	7.53	3.32	8.33	9.26	12.43	15.52	10.95	12.55	15.23
%Na_2O+K_2O															
	65.53	57.13	75.95	57.33	58.00	54.10	61.78	65.49	56.08	51.06	50.29	44.23	46.15	67.54	42.91
CO-ORDINATES FOR KCN DIAGRAM															
%K_2O	54.18	34.86	37.34	39.14	34.33	30.96	37.24	43.81	30.94	30.13	31.08	30.12	30.73	28.38	26.84
%Na_2O	18.10	35.16	32.19	31.33	34.22	37.78	33.10	35.46	36.75	35.76	36.26	30.69	32.98	29.49	32.95
%CaO	27.72	29.98	30.47	29.53	31.45	31.26	29.66	20.72	32.32	34.11	32.65	39.19	36.29	42.13	40.21

MAJOR ELEMENTS.

ANALYSIS:	76.	77.	78.	79.	80.	81.	82.	83.	84.	85.	86.	87.	88.	89.	90.
SiO_2	62.33	61.80	61.63	61.46	61.17	60.96	60.34	59.99	59.25	59.18	59.13	58.46	58.01	56.97	56.18
TiO_2	1.17	1.21	1.18	1.21	1.25	1.25	1.11	1.28	1.32	1.13	1.41	1.30	1.20	1.20	1.25
Al_2O_3	15.52	15.53	15.51	16.13	15.51	15.40	15.75	15.93	15.99	16.03	15.37	15.85	15.67	16.40	16.86
Fe_2O_3	0.59	0.57	0.75	3.41	0.85	2.27	2.30	1.54	≤8.02	1.99	0.95	2.47	2.35	3.62	1.53
FeO	5.42	5.77	5.23	1.94	5.52	4.41	4.14	5.58	-	4.60	6.16	4.98	4.51	3.69	5.73
MnO	0.11	0.11	0.12	0.06	0.12	0.11	0.11	0.16	0.12	0.13	0.14	0.12	0.13	0.13	0.13
MgO	2.10	2.16	2.18	1.89	2.40	1.72	3.24	2.92	3.15	4.17	2.36	3.02	4.89	4.79	5.01
CaO	4.43	4.78	4.51	4.17	4.79	4.66	5.30	5.13	5.54	5.22	5.58	5.59	6.21	7.06	8.02
Na_2O	3.77	3.66	4.35	3.52	3.11	3.31	3.15	4.35	3.35	2.40	4.19	4.20	2.96	3.66	3.01
K_2O	2.30	2.20	2.58	3.27	2.80	3.10	2.82	1.94	2.56	3.36	1.32	2.54	2.13	2.02	1.76
P_2O_5	0.27	0.28	0.28	0.28	0.28	0.28	00.25	0.27	0.29	0.23	0.30	0.29	0.24	0.22	0.26
L.O.I.	2.79	2.11	1.96	1.53	2.41	1.31	1.87	2.53	1.85	1.53	1.96	1.93	1.78	1.89	0.64
TOTAL	1oo.81	100.18	100.28	98.86	100.19	98.77	100.39	101.61	101.44	99.96	98.88	100.74	100.07	101.65	100.38

ANALYSES RECALCULATED TO 100.00% VOLATILE FREE.

SiO_2	63.60	63.02	62.68	63.36	62.55	62.69	61.40	60.54	59.98	60.12	61.02	59.16	59.16	57.32	56.33
TiO_2	1.19	1.23	1.20	1.25	1.28	1.29	1.13	1.29	1.34	1.15	1.46	1.32	1.22	1.21	1.25
Al_2O_3	15.84	15.84	15.78	16.63	15.86	15.84	16.03	16.08	16.19	16.28	15.86	16.04	15.98	16.50	16.90
Fe_2O_3	0.60	0.58	0.76	1.72	0.87	2.21	2.11	1.55	2.44	2.02	0.98	2.50	2.25	2.33	1.53
FeO	5.53	5.88	5.32	3.44	5.64	4.42	4.21	5.63	4.87	4.67	6.36	5.04	4.50	4.66	5.75
MnO	0.11	0.11	0.12	0.06	0.12	0.11	0.11	0.16	0.12	0.13	0.14	0.12	0.13	0.13	0.13
MgO	2.14	2.20	2.22	1.95	2.45	1.77	3.30	2.95	3.19	4.24	2.44	3.06	4.99	4.82	5.02
CaO	4.52	4.87	4.59	4.30	4.90	4.79	5.39	5.18	5.61	5.30	5.76	5.66	6.33	7.10	8.04
Na_2O	3.85	3.73	4.42	3.63	3.18	3.40	3.21	4.39	3.39	2.44	4.32	4.25	3.02	3.68	3.02
K_2O	2.35	2.24	2.62	3.37	2.86	3.19	2.87	1.96	2.59	3.41	1.36	2.57	2.17	2.03	1.77
P_2O_5	0.28	0.29	0.29	0.29	0.29	0.29	0.25	0.27	0.29	0.23	0.31	0.29	0.25	0.22	0.26

ANALYSIS:	76.	77.	78.	79.	80.	81.	82.	83.	84.	85.	86.	87.	88.	89.	90.
C.I.P.W. NORMS.															
Q	16.89	16.47	12.39	16.77	16.62	17.33	14.96	10.70	13.13	13.76	13.03	8.32	12.20	6.56	6.98
or	13.87	13.26	15.51	19.92	16.92	18.84	16.96	11.57	15.31	20.17	8.05	15.19	12.84	12.01	10.43
ab	32.55	31.58	37.44	30.71	26.91	28.80	27.12	37.15	28.70	20.63	36.59	35.96	25.54	31.16	25.54
an	19,01	19.83	15.43	19.13	20.54	18.52	20.87	18.38	21.29	23.41	19.85	17.10	23.64	22.49	27.37
di wo	0.67	1.04	2.28	0.13	0.79	1.41	1.77	2.31	1.93	0.57	2.80	3.78	2.58	4.72	4.52
di fs	0.41	0.64	1.31	0.05	0.44	0.69	0.58	1.12	0.70	0.18	1.66	1.48	0.65	1.27	1.60
di en	0.27	0.41	0.98	0.08	0.35	0.69	1.09	1.14	1.13	0.36	1.15	2.14	1.74	3.12	2.69
hy fs	7.49	7.86	6.08	2.91	7.32	3.69	3.76	6.10	4.24	5.08	7.07	3.77	3.99	3.61	5.85
hy en	5.06	5.07	4.55	4.78	5.77	3.71	7.12	6.20	6.81	10.19	4.91	5.47	10.68	8.89	9.82
mt	0.87	0.84	1.11	2.50	1.26	3.21	3.05	2.25	3.53	2.93	1.42	3.62	3.27	3.38	2.22
il	2.27	2.34	2.28	2.37	2.43	2.44	2.15	2.45	2.54	2.18	2.76	2.50	2.32	2.29	2.38
ap	0.64	0.66	0.66	0.67	0.66	0.67	0.59	0.63	0.68	0.54	0.72	0.68	0.57	0.51	0.60
TOTAL IRON AS-															
%Fe_2O_3	6.75	7.12	6.67	5.55	7.14	7.13	6.79	7.81	7.85	7.22	8.04	8.10	7.26	7.51	7.92
%FeO	6.07	6.41	6.01	4.99	6.43	6.41	6.11	7.03	7.06	6.49	7.24	7.29	6.53	6.76	7.13
LARSEN INDEX-															
	11.33	10.27	11.37	14.78	10.70	13.08	10.41	8.36	8.90	9.22	7.13	8.52	6.05	4.54	1.71
D.I.	63.31	61.31	65.34	67.40	60.45	64.97	59.03	59.42	57.14	54.56	57.66	59.47	50.57	49.73	42.94
C.I.	29.93	30.78	25.24	29.43	32.98	26.53	36.23	31.75	35.99	45.39	30.44	28.8?	46.68	41.66	48.56
CO-ORDINATED FOR AFM DIAGRAM															
%Fe_2O_3+FeO															
	42.38	44.15	39.63	36.59	43.39	44.25	40.27	43.60	44.34	39.89	47.46	43.29	39.89	39.89	42.61
%MgO	14.81	15.04	14.45	13.81	16.35	11.80	21.01	17.88	19.35	25.24	15.75	17.55	29.45	27.50	29.40
%Na_2O+K_2O															
	42.81	40.81	45.92	49.60	40.26	43.96	38.72	38.52	36.31	34.87	36.78	39.16	30.65	32.61	27.99
CO-ORDINATES FOR KCN DIAGRAM															
%K_2O	21.90	20.68	22.55	29.84	26.17	28.00	25.02	16.99	22.36	30.60	11.90	20.60	18.85	15.86	13.76
%Na_2O	35.90	34.40	38.02	32.12	29.07	29.90	27.95	38.09	29.26	21.86	37.78	34.06	26.19	28.73	23.53
%CaO	42.19	44.92	39.42	38.05	44.77	42.10	47.03	44.92	48.38	47.54	50.32	45.34	54.96	55.42	62.71

MAJOR ELEMENTS.

ANALYSIS:	91.	92.	93.	94.	95.	96.	97.	98.	99.	100.	101.
SiO_2	56.02	55.56	55.23	55.00	54.90	54.87	54.78	54.59	54.26	53.66	48.92
TiO_2	1.23	1.22	1.07	1.22	1.06	1.25	1.22	1.22	1.25	1.26	1.21
Al_2O_3	16.50	16.50	15.74	16.41	15.74	16.58	16.51	16.43	16.39	16.21	15.74
Fe_2O_3	1.96	2.22	2.78	1.93	2.67	≤8.17	2.38	2.33	≤8.49	2.44	1.09
FeO	5.41	5.58	4.80	5.42	4.88	-	5.55	5.69	-	5.89	6.53
MnO	0.15	0.14	0.13	0.15	0.16	0.14	0.16	0.16	0.13	0.16	0.18
MgO	4.33	5.19	6.35	5.33	6.48	5.10	5.41	5.22	4.88	5.11	2.95
CaO	7.32	7.74	7.51	8.05	7.52	8.24	8.42	8.44	8.20	7.88	7.98
Na_2O	3.22	2.88	2.56	3.00	2.92	3.15	2.83	3.51	3.25	2.87	2.48
K_2O	1.61	1.73	1.41	1.38	1.41	1.24	1.31	1.31	1.24	1.18	1.31
P_2O_5	0.23	0.25	0.01	0.26	0.20	0.27	0.25	0.25	0.25	0.26	0.25
L.O.I.	2.30	1.46	2.43	2.01	2.73	1.77	1.80	1.87	1.79	2.75	11.26
TOTAL	100.28	100.46	100.02	100.15	100.67	100.78	100.63	101.01	100.14	99.66	99.90

ANALYSES RECALCULATED TO 100.00% VOLATILE FREE

SiO_2	57.18	56.12	56.76	56.04	56.21	55.88	55.43	55.06	55.65	55.37	55.19
TiO_2	1.26	1.23	1.10	1.24	1.09	1.27	1.24	1.23	1.28	1.30	1.37
Al_2O_3	16.84	16.67	16.18	16.72	16.12	16.89	16.71	16.57	16.81	16.73	17.76
Fe_2O_3	2.00	2.24	2.50	1.97	2.49	2.50	2.41	2.35	2.61	2.52	1.23
FeO	5.52	5.64	5.00	5.52	4.97	4.99	5.62	5.74	5.22	6.08	7.37
MnO	0.15	0.14	0.13	0.15	1.64	0.14	0.16	0.16	0.13	0.17	0.20
MgO	4.42	5.24	6.53	5.43	6.63	5.19	5.48	5.27	5.01	5.27	3.33
CaO	7.47	7.82	7.72	8.20	7.70	8.39	8.52	8.51	8.41	8.13	9.00
Na_2O	3.29	2.91	2.63	3.06	2.99	3.21	2.86	3.54	3.33	2.96	2.80
K_2O	1.64	1.75	1.45	1.41	1.44	1.26	1.33	1.32	1.27	1.22	1.48
P_2O_5	0.24	0.25	0.01	0.27	0.21	0.28	0.25	0.25	0.26	0.27	0.28

ANALYSIS:	91.	92.	93.	94.	95.	96.	97.	98.	99.	100.	101.
C.I.P.W. NORMS.											
Q	8.77	7.73	9.34	7.30	7.22	7.61	7.55	4.18	6.89	7.78	7.40
or	9.71	10.33	8.56	8.31	8.53	7.46	7.83	7.81	7.52	7.20	8.73
ab	27.81	24.61	22.26	25.86	25.30	27.15	24.23	29.96	28.21	25.06	23.68
an	26.35	27.25	28.05	27.75	26.29	27.94	28.82	25.42	27.15	28.75	31.53
di wo	3.84	4.13	4.25	4.68	4.41	4.97	4.93	6.33	5.39	4.11	4.72
di fs	1.38	1.32	1.00	1.46	1.03	1.33	1.50	2.05	1.55	1.38	2.65
di en	2.27	2.56	2.91	2.93	3.03	3.28	3.11	3.91	3.48	2.50	2.06
hy fs	5.32	5.41	4.56	5.28	4.56	3.93	5.08	4.82	4.02	5.86	7.99
hy en	8.74	10.50	13.34	10.59	13.49	9.66	10.52	9.20	8.99	10.63	6.23
mt	2.90	3.25	3.63	2.85	3.60	3.62	3.49	3.41	3.79	3.65	1.78
il	2.38	2.34	2.09	2.36	2.06	2.42	2.35	2.34	2.44	2.47	2.59
ap	0.54	0.59	0.02	0.61	0.47	0.64	0.59	0.58	0.59	0.62	0.65
TOTAL IRON AS-											
%Fe_2O_3	8.14	8.51	8.06	8.10	8.01	8.04	8.65	8.73	8.42	9.29	9.42
%FeO	7.32	7.65	7.25	7.29	7.21	7.24	7.78	7.85	7.58	8.34	8.47
LARSEN INDEX-											
	3.27	1.74	1.10	0.91	0.86	1.29	0.17	0.14	1.17	0.17	0.16
D.I.	46.29	42.67	40.16	41.48	41.05	42.22	39.61	41.94	42.61	40.04	39.81
C.I.	45.20	49.89	56.82	50.60	55.39	48.78	51.51	45.27	46.55	51.68	44.96
CO-ORDINATES FOR AFM DIAGRAM											
%Fe_2O_3+FeO	44.59	44.32	41.43	43.08	40.25	43.65	45.37	44.41	44.91	47.63	53.06
%MgO	26.19	29.49	36.04	31.24	35.82	30.28	30.95	28.90	28.69	29.22	20.54
%Na_2O+K_2O	29.22	26.19	22.53	25.67	23.93	26.07	23.68	26.69	26.40	23.16	26.39
CO-ORDINATES FOR KCN DIAGRAM											
%K_2O	13.25	14.01	12.28	11.10	11.90	9.82	10.43	9.88	9.77	9.89	11.13
%Na_2O	26.50	23.32	22.30	24.14	24.64	24.94	22.53	26.47	25.61	24.06	21.07
%CaO	60.25	62.67	65.42	64.76	63.46	65.24	67.04	63.65	64.62	66.05	67.80

MAJOR ELEMENTS.

ANALYSIS:	102.	103.	104.	105.	106.	107.	108.	109.	110.	111.	112.	113.	114.	115.
SiO_2	74.26	73.31	73.06	71.89	71.78	71.23	61.96	60.74	60.55	60.38	57.54	57.53	56.03	55.61
TiO_2	0.24	0.26	0.25	0.24	0.24	0.24	1.21	1.27	15.73	1.17	1.08	1.16	1.11	1.17
Al_2O_3	13.78	14.26	14.68	14.28	14.37	14.20	15.64	15.87	1.23	14.20	15.91	16.30	15.88	16.10
Fe_2O_3	≤1.26	0.87	0.66	1.80	2.14	2.63	0.62	0.57	0.53	4.78	2.73	2.25	2.19	2.33
FeO	-	0.34	0.35	0.34	0.60	0.42	5.47	5.85	6.37	2.05	4.01	5.04	4.95	4.55
MnO	0.02	0.05	0.05	0.01	0.05	0.03	0.12	0.13	0.12	0.13	0.12	0.14	0.16	0.14
MgO	0.19	0.19	0.21	0.29	0.15	0.24	2.42	2.79	2.31	1.32	5.67	4.51	5.78	4.55
CaO	0.28	1.25	1.28	1.19	1.08	0.71	5.13	5.02	4.52	2.88	6.65	6.95	7.10	7.69
Na_2O	3.44	3.38	3.43	3.07	3.34	3.84	3.46	3.39	3.73	3.69	3.06	2.64	2.89	2.89
K_2O	6.19	5.24	5.42	5.38	5.91	5.52	2.01	2.81	2.05	4.74	2.12	1.40	1.55	1.48
P_2O_5	0.07	0.07	0.07	0.07	0.06	0.07	0.29	0.29	0.30	0.31	0.22	0.23	0.22	0.24
L.O.I.	0.62	1.05	1.10	1.72	0.57	1.48	2.40	1.96	2.88	1.93	1.60	2.40	2.66	3.58
TOTAL	100.34	100.27	100.56	100.28	100.29	100.61	100.72	100.69	100.33	97.58	100.71	100.55	100.52	100.32

ANALYSES RECALCULATED TO 100.00% VOLATILE FREE.

SiO_2	74.56	73.95	73.51	73.07	72.14	72.05	63.01	61.52	62.14	63.44	58.22	58.61	57.26	57.62
TiO_2	0.24	0.26	0.25	0.24	0.24	0.24	1.23	1.29	1.26	1.23	1.09	1.18	1.13	1.21
Al_2O_3	13.84	14.39	14.77	14.52	14.44	14.36	15.91	16.07	16.14	14.92	16.10	16.61	16.23	16.68
Fe_2O_3	0.38	0.38	0.32	0.66	0.85	0.94	0.63	0.58	0.54	2.22	2.18	2.29	2.24	2.30
FeO	0.76	0.76	0.63	1.33	1.69	1.88	5.56	5.93	6.34	4.45	4.36	5.14	5.06	4.59
MnO	0.02	0.05	0.50	0.01	0.05	0.03	0.12	0.13	0.12	0.14	0.12	0.14	0.16	0.15
MgO	0.19	0.19	0.21	0.30	0.15	0.24	2.46	2.83	2.37	1.39	5.74	4.60	5.91	4.71
CaO	0.28	1.26	1.29	1.21	1.09	0.72	5.22	5.09	4.64	3.03	6.73	7.08	7.26	7.97
Na_2O	3.45	3.41	3.45	3.12	3.36	3.88	3.52	3.43	3.83	3.88	3.10	2.69	2.95	2.99
K_2O	6.22	5.29	5.45	5.47	5.94	5.58	2.04	2.85	2.10	4.98	2.15	1.43	1.58	1.53
P_2O_5	0.07	0.07	0.07	0.07	0.06	0.07	0.30	0.29	0.31	0.33	0.22	0.23	0.23	0.25

ANALYSIS:	102.	103.	104.	105.	106.	107.	108.	109.	110.	111.	112.	113.	114.	115.
C.I.P.W. NORMS.														
Q	29.67	30.77	29.42	30.48	26.54	25.33	17.63	13.20	14.88	13.05	9.33	14.47	9.39	10.98
C	1.08	0.93	1.02	1.43	0.66	0.79	-	-	-	-	-	-	-	-
or	36.72	31.24	32.22	32.32	35.10	32.99	12.08	16.82	12.43	29.43	12.68	8.43	9.36	9.06
ab	29.22	28.85	29.20	26.41	28.40	32.87	29.78	29.05	32.39	32.81	26.20	22.76	24.99	25.34
an	0.94	5.79	5.93	5.54	4.99	3.10	21.57	20.04	20.65	8.50	23.69	29.03	26.34	27.55
di wo	-	-	-	-	-	-	1.00	1.36	0.15	1.79	3.44	1.91	3.42	4.32
di fs	-	-	-	-	-	-	0.56	0.74	0.09	1.02	0.77	0.61	0.90	1.17
di en	-	-	-	-	-	-	0.44	0.61	0.06	0.77	2.38	1.19	2.27	2.85
hy fs	0.72	0.74	0.58	1.51	2.10	2.33	7.33	7.78	9.61	3.54	3.86	5.24	4.97	3.64
hy en	0.48	0.48	0.53	0.73	0.38	0.61	5.70	6.43	5.85	2.68	11.91	10.26	12.45	8.89
mt	0.55	0.55	0.46	0.96	1.23	1.36	9.14	0.84	0.79	3.23	3.16	3.32	3.25	3.33
il	0.46	0.50	0.48	0.46	0.46	0.46	2.34	2.44	2.40	2.34	2.08	2.25	2.15	2.30
ap	0.16	0.16	0.16	0.17	0.14	0.16	0.68	0.68	0.71	0.76	0.52	0.54	0.52	0.58
TOTAL IRON AS-														
%Fe_2O_3	1.22	1.22	1.02	2.14	2.73	3.03	6.81	7.16	7.81	7.17	7.03	8.00	7.86	7.40
%FeO	1.10	1.10	0.92	1.93	2.45	2.72	6.13	6.45	7.03	6.45	6.32	7.20	7.07	6.66
LARSEN INDEX-														
	29.81	27.70	27.80	26.97	27.03	26.74	9.79	9.50	9.25	17.25	4.71	4.13	2.43	3.45
D.I.	95.62	90.85	90.85	89.20	90.05	91.19	59.48	59,07	59.70	75.29	48.20	45.66	43.74	45.38
C.I.	1.96	6.82	7.06	7.12	5.80	4.40	33.85	33.90	33.27	14.38	49.37	51.15	53.19	46.73
CO-ORDINATES FOR AFM DIAGRAM														
%Fe_2O_3+FeO														
	10.35	11.30	9.44	18.32	21.18	22.50	43.56	41.66	46.03	39.45	37.34	46.02	41.13	42.70
%MgO	1.73	1.91	2.10	2.71	1.26	1.94	17.31	18.11	15.41	8.20	32.74	28.47	33.29	29.23
%Na_2O+K_2O														
	87.91	86.78	88.47	78.97	77.56	75.57	39.13	40.23	38.56	52.36	29.91	25.51	25.58	28.07
CO-ORDINATES FOR KCN DIAGRAM														
%K_2O	62.46	53.09	53.50	55.81	57.21	54.82	18.96	25.04	19.90	41.91	17.92	12.74	13.43	12.27
%Na_2O	34.71	34.25	33.86	31.85	32.33	38.13	32.64	30.21	36.21	32.63	25.87	24.02	25.04	23.96
%CaO	2.83	12.66	12.64	12.34	10.45	7.05	48.40	44.74	43.88	25.46	56.21	63.24	61.53	63.76

MAJOR ELEMENTS.

ANALYSIS:	116.	117.	118.	119.	120.	121.	122.	123.	124.	125.	126.	127.	128.	129.
SiO_2	75.91	75.68	73.08	71.69	71.42	71.25	71.24	69.54	59.39	58.57	56.24	52.04	51.35	55.89
TiO_2	0.20	0.19	0.28	0.43	0.21	0.34	0.59	0.21	1.37	1.38	1.57	1.65	1.24	1.41
Al_2O_3	13.24	12.45	13.53	15.75	12.93	13.88	14.50	13.18	15.85	17.03	15.34	16.46	16.45	15.94
Fe_2O_3	0.17	0.44	0.67	0.26	0.92	1.66	0.58	1.04	2.00	4.85	2.58	5.63	3.30	≤8.52
FeO	0.52	0.40	1.20	0.66	0.77	0.68	0.58	0.94	5.54	1.33	5.33	2.66	6.17	-
MnO	0.01	0.01	0.01	0.02	0.02	0.02	0.02	0.02	0.15	0.11	0.17	0.17	0.17	0.11
MgO	0.69	0.07	0.32	0.21	0.12	0.31	0.11	0.31	2.75	1.17	1.92	3.58	6.20	4.15
CaO	0.74	0.66	1.21	1.38	1.04	1.03	1.56	1.06	5.20	5.45	4.61	6.36	8.65	7.56
Na_2O	2.60	2.14	3.12	3.50	3.89	3.17	2.49	4.16	4.08	3.20	3.29	3.31	2.63	3.10
K_2O	5.51	6.41	5.13	5.20	3.30	4.89	4.70	2.25	1.36	2.70	2.57	2.31	0.97	2.20
P_2O_5	0.09	0.20	0.13	0.16	0.13	0.24	0.17	0.11	0.30	0.32	0.43	0.42	0.26	0.23
L.O.I.	0.95	1.24	1.54	1.16	5.03	2.18	2.98	7.14	1.64	3.83	3.35	5.24	3.02	5.12
TOTAL	100.63	100.07	100.22	100.42	99.96	99.84	99.75	99.96	99.66	100.11	99.79	99.95	100.40	104.23

ANALYSES RECALCULATED TO 100.00% VOLATILE FREE.

SiO_2	76.15	76.75	74.11	72.22	75.45	73.22	73.84	75.02	60.61	61.25	59.80	55.35	52.91	56.88
TiO_2	0.20	0.19	0.28	0.43	0.22	0.35	0.61	0.23	1.40	1.44	1.67	1.76	1.28	1.44
Al_2O_3	13.28	12.63	13.72	15.87	13.66	14.27	15.03	14.22	16.18	17.81	16.31	17.51	16.95	16.22
Fe_2O_3	0.17	0.27	0.61	0.26	0.56	0.75	0.38	0.67	2.04	1.99	2.74	2.74	3.14	2.60
FeO	0.52	0.54	1.22	0.67	1.13	1.49	0.76	1.34	5.65	3.97	5.67	5.48	6.28	5.20
MnO	0.01	0.01	0.01	0.02	0.02	0.02	0.02	0.02	0.15	0.12	0.18	0.18	0.18	0.11
MgO	2.69	0.07	0.33	0.21	0.13	0.32	0.11	0.33	2.81	1.22	2.04	3.81	6.39	4.22
CaO	0.74	0.67	1.23	1.39	1.10	1.06	1.62	1.14	5.31	5.70	4.90	6.76	8.91	7.69
Na_2O	2.61	2.17	3.16	3.53	4.11	3.26	2.58	4.49	4.16	3.35	3.50	3.52	2.71	3.16
K_2O	5.53	6.50	5.20	5.24	3.49	5.03	4.87	2.43	1.39	2.82	2.73	2.46	1.00	2.24
P_2O_5	0.09	0.20	0.13	0.16	0.14	0.25	0.18	0.12	0.31	0.34	0.46	0.45	0.27	0.23

ANALYSIS:	116.	117.	118.	119.	120.	121.	122.	123.	124.	125.	126.	127.	128.	129.
C.I.P.W. NORMS.														
Q	37.23	38.07	32.47	28.68	35.47	32.28	37.00	36.30	13.99	16.49	14.26	19.73	4.65	8.29
C	1.88	1.29	0.97	2.25	1.46	2.13	2.99	2.41	-	-	-	-	-	-
or	32.67	38.41	30.74	30.96	20.60	29.70	28.79	14.34	8.20	16.69	15.15	5.67	5.91	13.23
ab	22.07	18.36	26.77	29.84	34.77	27.57	21.84	37.98	35.23	28.32	29.60	12.34	22.93	26.70
an	3.09	2.00	5.23	5.84	4.55	3.64	6.87	4.90	21.35	25.23	20.73	19.30	31.13	23.49
di wo	-	-	-	-	-	-	-	-	1.24	0.36	0.25	4.63	4.73	5.49
di fs	-	-	-	-	-	-	-	-	0.50	0.19	0.13	1.37	1.37	1.71
di en	-	-	-	-	-	-	-	-	0.62	0.17	0.12	3.26	3.05	3.44
hy fs	0.50	0.47	1.28	0.33	1.27	1.58	0.11	1.57	6.08	3.29	5.59	7.25	5.78	3.53
hy en	1.72	0.18	0.81	0.53	0.32	0.79	0.28	0.83	6.37	2.88	4.97	17.27	12.86	7.08
mt	0.25	0.39	0.88	0.38	0.82	1.08	0.55	0.97	2.96	2.88	3.98	3.73	4.55	3. 7
il	.38	0.37	0.54	0.82	0.42	0.66	1.16	0.43	2.66	2.74	3.17	4.77	2.43	2.73
ap	0.21	0.47	0.31	0.37	0.32	0.57	0.41	0.28	0.71	0.78	1.06	0.68	0.62	0.54
TOTAL IRON AS-														
%Fe_2O_3	0.75	0.87	1.96	1.00	1.81	2.40	1.23	2.151	8.32	6.40	9.04	8.83	10.11	8.38
%FeO	0.68	0.78	1.77	0.90	1.63	2.16	1.10	1.94	7.49	5.76	8.14	7.94	9.10	7.54
LARSEN INDEX-														
	28.93	30.78	27.11	27.02	26.26	26.54	26.97	24.60	7.80	12.33	10.04	4.84	-2.96	4.06
D.I.	91.97	94.85	89.98	89.47	90.84	89.54	87.62	88.62	57.43	61.49	60.01	49.76	33.48	48.22
C.I.	6.81	2.38	6.97	6.98	5.23	5.35	7.48	6.69	35.08	31.45	31.45	41.91	58.88	38.76
CO-ORDINATES FOR AFM DIAGRAM														
%Fe_2O_3+FeO														
	7.27	8.45	17.38	9.36	17.94	20.62	13.11	21.64	47.93	44.61	50.41	45.65	48.25	44.79
%MgO	7.27	0 74	3.08	2.14	1.35	2.94	1.31	3.61	17.48	9.17	12.24	21.15	32.74	24.25
%Na_2O_3+K_2O														
	85.46	90.80	79.54	88.50	80.72	76.44	85.58	74.74	34.58	46.22	37.35	33.20	19.01	30.96
CO-ORDINATES FOR KCN DIAGRAM														
%K_2O	62.26	69.60	54.23	51.59	40.10	53.80	53.71	30.12	12.78	23.79	24.55	19.28	7.92	17.11
%Na_2O	29.38	23.24	32.98	34.72	47.27	34.87	28.46	55.69	38.35	28.19	31.42	27.63	21.47	24.11
%CaO	8.36	7.17	12.79	13.69	12.64	11.33	17.83	14.19	48.87	48.02	44.03	53.09	70.61	58.79

MAJOR ELEMENTS.

ANALYSIS:	130.	131.	132.	133.	134.	135.
SiO_2	50.32	49.68	48.98	47.90	44.86	42.41
TiO_2	2.16	1.70	1.42	2.06	2.82	2.35
Al_2O_3	13.99	13.04	11.88	13.25	14.75	12.33
Fe_2O_3	2.63	4.92	2.35	3.58	6.09	3.59
FeO	7.42	6.44	7.64	6.62	4.40	7.91
MnO	0.16	0.17	0.16	0.17	0.19	0.13
MgO	5.90	9.44	11.48	6.39	2.23	7.88
CaO	11.10	8.88	9.22	11.83	10.29	8.18
Na_2O	2.80	2.41	2.45	3.36	3.45	2.66
K_2O	0.88	0.41	0.77	0.58	0.62	1.20
P_2O_5	0.33	0.26	0.23	0.39	0.35	0.49
L.O.I.	3.19	3.48	3.57	4.90	10.19	10.13
TOTAL	100.88	100.82	100.14	101.03	100.23	99.27

ANALYSES RECALCULATED TO 100.00% VOLATILE FREE.

SiO_2	51.51	51.29	50.71	50.02	50.16	47.58
TiO_2	2.21	1.76	1.47	2.15	3.15	2.64
Al_2O_3	14.32	13.46	12.30	13.84	16.49	13.83
Fe_2O_3	2.69	3.74	2.43	3.43	3.68	4.03
FeO	7.60	7.48	7.91	6.85	7.36	8.88
MnO	0.16	0.18	0.17	0.18	0.21	0.15
MgO	6.04	9.75	11.89	6.67	2.49	8.84
CaO	11.36	9.17	9.55	12.35	11.51	9.18
Na_2O	2.87	2.49	2.54	3.51	3.86	2.98
K_2O	0.90	0.42	0.80	0.61	0.69	1.35
P_2O_5	0.34	0.27	0.24	0.41	0.39	0.55

ANALYSIS		130.	131.	132.	133.	134.	135.
C.I.P.W. NORMS.							
Q		1.79	2.30	-	-	1.46	
or		5.32	2.50	4.71	3.58	4.10	7.96
ab		24.25	21.06	21.47	28.94	32.64	25.25
an		23.55	24.32	19.82	20.21	25.64	20.37
ne		-	-	-	0.40	-	-
di	wo	12.78	8.11	10.85	16.04	12.06	9.00
	fs	4.32	1.86	2.60	4.19	5.61	2.40
	en	7.76	5.59	7.40	10.67	6.15	5.95
hy	fs	4.06	6.21	4.35	-	0.06	0.69
	en	7.28	18.69	12.40	-	0.06	1.72
fo		-	-	6.87	4.17	-	10.06
fa		-	-	2.66	1.80	-	4.47
mt		3.90	5.42	3.53	4.97	5.34	5.84
il		4.20	3.33	2.79	4.09	5.99	5.01
ap		0.78	0.62	0.55	0.94	0.91	1.27
TOTAL IRON AS-							
%Fe_2O_3		11.13	12.05	11.22	11.04	11.87	13.89
%FeO		10.12	10.85	10.10	9.93	10.68	12.50
LARSEN INDEX		-6.94	-8.89	-11.66	-8.61	-3.97	-9.70
D.I.		31.37	25.85	26.18	32.92	38.19	33.21
C.I.		39.26	64.62	53.44	24.38	25.17	34.13
CO-ORDINATES FOR AFM DIAGRAM							
%Fe_2O_3+FeO		51.20	46.99	40.46	48.79	61.06	49.48
%MgO		30.06	40.82	46.50	31.68	13.78	33.91
%Na_2O+K_2O		18.75	12.19	13.04	19.53	25.16	16.61
CO-ORDINATES FOR KCN DIAGRAM							
%K_2O		5.95	3.50	6.19	3.68	4.32	9.97
%Na_2O		18.94	20.60	19.69	21.31	24.03	22.09
%CaO		75.10	75.90	74.12	75.02	71.66	67.94

Appendix III. Calculated viscosities of samples of Mt Somers Volcanics.

Sample No.	Analysis No.*	Calculated viscosities ($\ln \eta$)					X_{SiO_2}
		1200°C	1250°C	1300°C	1350°C	1400°C	
P0355	8	14.2206	13.3670	12.5186	11.7014	10.9598	0.8453
P0415	9	14.1801	13.3253	12.4870	11.6701	10.9294	0.8462
P0458	14	14.1084	13.3056	12.4490	11.6429	10.9076	0.8368
P0279a	15	14.2600	13.3845	12.5490	11.7258	10.9815	0.8442
P0514	116	14.0568	13.2225	12.3531	11.5341	10.7888	0.8387
P0457	34	14.1070	13.2957	12.4542	11.6479	10.9152	0.8385
P0551	35	14.1617	13.2836	12.4516	11.6227	10.8787	0.8355
P0553	38	14.1372	13.2988	12.4437	11.6215	10.8793	0.8258
P0508	103	14.1050	13.2794	12.427	11.6081	10.8689	0.8206
P0537	48	14.0009	13.0648	12.3336	11.4991	10.7625	0.8464
P0496	107	14.0406	13.3048	12.4643	11.6671	10.9410	0.7973
P0550	59	13.7578	13.0265	12.1922	11.3940	10.6773	0.8007
P0562	66	12.9142	12.3811	11.4955	10.7316	10.0425	0.7578
P0261	71	9.9204	9.1926	8.5541	8.2915	7.6844	0.7298
P0341	73	10.0029	9.2757	8.6326	8.3242	7.7053	0.7354
P0502	108	9.6681	8.9126	8.3054	7.947	7.3283	0.7181
P0360	79	9.8904	9.1563	8.5074	8.2104	7.5966	0.7248
P0482	80	9.6112	8.8667	8.2683	7.9299	7.3158	0.7140
P0477	81	9.6689	8.9103	8.3026	8.0069	7.4009	0.7154
P0478	82	9.3180	8.5714	8.0029	7.6674	7.0601	0.6969
P0512	124	9.2498	8.5067	7.9513	7.6287	7.0251	0.6915
P0142	89	8.4877	7.7156	7.2336	6.9124	6.3283	0.6469
P0506	114	8.4098	7.6613	7.2007	6.7918	6.1902	0.6478
P0564	129	8.4626	7.1863	7.6608	6.8531	6.2701	0.6464
P0356	92	8.3507	7.5760	7.1159	6.7248	6.1294	0.6413
P0484	93	8.2098	7.461	7.0286	6.5917	5.9889	0.6383
P0417	95	8.1014	7.3499	6.9275	6.5227	5.9292	0.6310
P0513	128	7.7147	6.9406	6.5634	6.1396	5.5508	0.6057
P0237a	130	6.6457	5.8911	5.5836	5.2646	4.7058	0.5594
P0511	132	6.2117	5.4557	5.2985	4.9027	4.3604	0.5386
P0272	133	6.6713	5.7283	5.4699	5.1759	4.6583	0.5505
P0179	134	7.5039	6.5495	6.1663	5.9028	5.3713	0.5824

* see Appendix II for corresponding analyses.

$\ln \eta$: natural log of the coefficient of viscosity.

X_{SiO_2}: mole fraction of SiO_2 in sample.

Appendix IV. List of University of Canterbury Sample Numbers with corresponding numbers used in the text.

University of Canterbury No.	Author's Sample No.	University of Canterbury No.	Author's Sample No.	University of Canterbury No.	Author's Sample No.
UC8000	PO62	UC8034	PO286	UC8068	PO452
UC8001	PO90	UC8035	PO291	UC8069	PO454
UC8002	PO129	UC8036	PO294	UC8070	PO456
UC8003	PO142	UC8037	PO295	UC8071	PO457
UC8004	PO147	UC8038	PO298	UC8072	PO458
UC8005	PO163	UC8039	PO305	UC8073	PO459
UC8006	PO176	UC8040	PO306	UC8074	PO462
UC8007	PO179	UC8041	PO308	UC8075	PO467
UC8008	PO182	UC8042	PO312	UC8076	PO472
UC8009	PO184	UC8043	PO313	UC8077	PO477
UC8010	PO187	UC8044	PO316	UC8078	PO478
UC8011	PO195	UC8045	PO341	UC8079	PO479
UC8012	PO197	UC8046	PO343	UC8080	PO482
UC8013	PO199	UC8047	PO346	UC8081	PO484
UC8014	PO200	UC8048	PO354	UC8082	PO485
UC8015	PO218	UC8049	PO355	UC8083	PO487
UC8016	PO227	UC8050	PO356	UC8084	PO488
UC8017	PO232	UC8051	PO359	UC8085	PO496
UC8018	PO237	UC8052	PO360	UC8086	PO500
UC8019	PO240	UC8053	PO393	UC8087	PO502
UC8020	PO241	UC8054	PO403	UC8088	PO503
UC8021	PO242c	UC8055	PO405	UC8089	PO504
UC8022	PO243	UC8056	PO409	UC8090	PO506
UC8023	PO245	UC8057	PO414	UC8091	PO507
UC8024	PO250	UC8058	PO415	UC8092	PO508
UC8025	PO252	UC8059	PO417	UC8093	PO509
UC8026	PO258	UC8060	PO419	UC8094	PO511
UC8027	PO261	UC8061	PO422	UC8095	PO512
UC8028	PO265	UC8062	PO427	UC8096	PO513
UC8029	PO270	UC8063	PO428	UC8097	PO514
UC8030	PO272	UC8064	PO439	UC8098	PO515
UC8031	PO273	UC8065	PO440	UC8099	PO516
UC8032	PO279	UC8066	PO445	UC8100	PO519
UC8033	PO283	UC8067	PO450	UC8101	PO523

Appendix IV (continued)

University of Canterbury No.	Author's Sample No.
UC8102	PO526
UC8103	PO528
UC8104	PO534
UC8105	PO535
UC8106	PO536
UC8107	PO537
UC8108	PO538
UC8109	PO542
UC8110	PO544
UC8111	PO549
UC8112	PO550
UC8113	PO551
UC8114	PO552
UC8115	PO553
UC8116	PO554
UC8117	PO555
UC8118	PO557
UC8119	PO559
UC8120	PO562
UC8121	PO564